Synthesis and Study of Dinuclear Cobalt(III)-Platinum(II) Complexes as Potential Anti-cancer Pro-drugs

---

A thesis submitted in partial fulfilment of the requirements for the

degree of

Doctoral of Philosophy in Chemistry

at the

University of Canterbury

by

Fatemeh Tavakolinia

2016

Acknowledgment

First and foremost, I would like to express my gratitude to my senior supervisor, Associate Professor Richard Hartshorn, for the patient guidance, encouragement, support and wealth of knowledge throughout my time as his student. I have been extremely lucky to have a supervisor who cared so much about my work, and who responded to my questions and queries promptly.

I would also extend my sincere thanks to my co-supervisor, Dr Jan Wikaira, for her guidance and precise review. My special thanks go to Dr. Matthew Polson for X-Ray crystallography and his expert technical support, and Dr. Marie Fitchett for NMR and mass spectrometric analysis. I also appreciate committee members, especially Professor Bryce Williamson, for their valuable advice and comments. I would also like to acknowledge the technical and administrative staff of the Department of Chemistry for their assistance and cooperation throughout my PhD research project.

I must express my gratitude to Dr Anna Renfrew at the University of Sydney for doing the cytotoxicity evaluation.

University of Canterbury (UC) Doctoral and Departmental Scholarships as well as other funding from New Zealand Institute of Chemistry (NZIC) are gratefully acknowledged.

I would also like to thank present and past members of Hartshorn's research group, especially Janadari, Gurpreet, Maria, Sally and Samantha as well as Marzieh and Davey Lim from other groups.

I must express my greatest gratitude to Dr Maryam Nejat and Dr Majeed Safa for their true friendship, support and generous care.

I especially thank my mom, dad, and sisters for their unconditional love and care. I love them so much, and I would not have made it this far without them.

Last but not least, I would like to thank my lovely husband, Seyed Ardalan, for his continued and unfailing love. This thesis would have never been possible without him.

This Thesis is dedicated to those suffering from Cancer…

Contents

Abbreviations

Å	Angstrom
chda	Cyclohexane-1,2-diamine
COSY	Correlation spectroscopy
DEPT	Distortionless enhancement of polarisation transfer
DNA	Deoxyribonucleic acic
en	Ethane-1,2-diamine
g	Gram
ESI-MS	Electron spray ionisation mass spectroscopy
EtOH	Ethanol
HMBC	Heteronuclear multiple-bond correlation spectroscopy
HSQC	Heteronuclear single-quantum correlation spectroscopy
Hz	Hertz
M	Molar
MeOH	Methanol
mg	Milligram
NMR	Nuclear magnetic resonance
nta	Nitrilotriacetate
ottp	4'-(2"'-Toluyl)-2,2':6',2"-terpyridine
pttp	4'-(4"'-Toluyl)-2,2':6',2"-terpyridine
m/z	Mass to charge ratio
tren	Tris(2-aminoethyl)amine
TMPS	Sodium 3-(trimethylsilyl)-1-propane sulfonate

Abstract

The aim of this project was to develop [Co(μ-OH)$_2$Pt] prodrugs that can undergo bio-reduction in hypoxic cells within solid tumours. This thesis describes synthetic methods to produce heterodinuclear [Co(μ-OH)$_2$Pt] complexes. Purification methods and characterisation of this class of complexes are also discussed.

The formation of [{Co(μ-OH)$_n$M}$_m$] complexes (M = transition metals) by reaction between equilibrium mixtures of *cis*- and *trans*-[Co(en)$_2$(OH)(OH$_2$)]$^{2+}$ and different metal ions was studied using ^{13}C NMR spectroscopy, in order to gain a better understanding of the reactions that may be occurring in solution. This involved monitoring the effect of the added metal ions on the position of the *cis*-*trans* equilibrium of the Co complex. This work is described in chapter 2.

In chapter 3, the synthesis and characterisation of [Co(μ-OH)$_2$Pt] complexes is discussed. Formation of [Co(μ-OH)$_2$Pt] complexes has been confirmed, following separations on ion exchange resins. These complexes proved to be rather labile and this led to insurmountable difficulties when attempting to isolate these complexes in pure form.

Problems associated with purification of [(en)$_2$Co(μ-OH)Pt(L)] and [(tren)Co(μ-OH)Pt(L)] (L = chda, (NH$_3$)$_2$) complexes led us to synthesise a new class of [Co(μ-OH)$_2$Pt] complexes, bearing a nitrilotriacetate ligand, as many reported anticancer drugs in literature are neutral (chapter 4). Both characterisation and biological assessment of these complexes was hindered by their low solubility. However, NMR studies at high temperature in DMSO again demonstrated the lability of these complexes.

In summary, [Co(μ-OH)$_2$Pt] complexes can be made, but they proved to be very labile and they do decompose. The direction of this research should be changed in future in order to

produce a less labile [Co(μ-OH)$_2$Pt] system. We speculate that this may be possible by incorporating a bulky group to reduce ligand exchange on platinum.

In chapter 5, a conclusion for synthesis of dinuclear [Co(μ-OH)$_2$Pt] complexes and the future work for this study are discussed.

Chapter 6 describes the synthesis and characterisation of organotin complexes which can be potential anticancer drugs.

The experimental work of the thesis is explained in chapter 7.

Chapter 1

Introduction

Chapter 1. Introduction

1.1 Cancer

Cancer is a class of diseases characterised by out-of-control cell growth. In 2012, the New Zealand Cancer Registry received 21,814 new cancer registrations. This was a rate of 337.5 new cases of cancer per 100,000 people[1]. There are over 100 different types of cancer, and each is classified by the type of cell that is initially affected[2]. All cancers begin in cells. The human body is made up of more than a hundred billion cells. Cancer starts with changes in one cell or a small group of cells. Cells produce signals to control how much and how often the cells divide. If any of these signals are faulty or missing, a cell and its daughters may start to grow and multiply too often and form a lump or mass called a tumour (except in the case of leukaemia where cancer prohibits normal blood function by abnormal cell division in the blood stream). The place where the cancer starts is called the primary tumour.

Tumours can grow and interfere with the digestive, nervous and circulatory systems and they can release hormones altering body function. Tumours that stay in one spot and demonstrate limited growth are generally considered to be benign. More dangerous, or malignant, tumours form when two conditions occur:

1. A cancerous cell manages to spread throughout the body using the blood or lymph systems, destroying healthy tissues in a process called invasion.
2. A cancerous cell divides and grows in a new location, making new blood vessels to feed itself in a process called angiogenesis.

Once a tumour successfully spreads to other parts of the body and grows, invading and destroying other healthy tissues, it is said to have metastasised. This process itself is called metastasis, and the result is a serious condition which is very difficult to treat[3].

1.2 Chemotherapy

Chemotherapy works by stopping or slowing the growth of cancer cells, which grow and divide quickly. Many of these treatments target rapidly dividing cells (not necessarily just cancer cells), but normal cells usually can recover from any chemical-induced damage while cancer cells cannot. Chemotherapy is generally used to treat cancer that has spread or metastasised, because the medicines travel throughout the entire body. It is a necessary treatment for some forms of leukaemia and lymphoma[4].

Chemotherapy treatment often occurs in cycles, so the body has time to heal between doses. Chemotherapy treatment uses medicine to weaken and destroy cancer cells in the body, including cells at the original cancer site and any cancer cells that may have spread to another part of the body. Chemotherapy medicines prevent cancer cells from growing and spreading by destroying the cells or stopping them from dividing[5].

Due to the rapid proliferation of cancer cells, sometimes they break away from the original tumour and travel to other places in the body. Chemotherapy weakens and destroys cancer cells at the original tumour site and throughout the body.

Normal cells usually grow and divide in a precise, orderly way. However, some normal cells do divide quickly, including cells in hair follicles, nails, the mouth, digestive tract, and bone marrow (bone marrow makes blood cells). Chemotherapy also can unintentionally harm

these other types of rapidly dividing cells, possibly causing chemotherapy side effects. This unintentional targeting of non-cancerous cells leads to side effects such as hair loss, nausea, fatigue, and vomiting. Combination therapies often include multiple types of chemotherapy or chemotherapy combined with other treatment options[5].

1.1.1 Classes of Chemotherapy Drugs

1.1.1.1 Alkylating Agents

The oldest class of anticancer drugs are alkylating, nitrogen mustard compounds, showing remarkable chemotherapeutic activity in cancer treatment. Nitrogen mustard compounds are poisonous and initially developed for military purpose.

Nitrogen mustard compounds attack at the nucleophilic centre of DNA, mainly the guanine N7 and O6[6]. Alkylation of the DNA, leads to DNA strand breaks and DNA strand cross-linking, which stops the cellular activity and the cell will die.

1.1.1.2 Antimetabolites

The first effective chemotherapeutic agents based on antimetabolite drugs are folic acid, pyrimidine or purine analogues. They are characterised by low molecular weights. They have similar structures as naturally occurring molecules used in nucleic acid (DNA and RNA) synthesis. Antimetabolites are similar to chemicals needed for normal biochemical activity, but differ enough so that they interfere with normal cell function. Generally, antimetabolites induce cell death during the S phase of cell growth when incorporated into RNA and DNA or inhibit enzymes needed for nucleic acid production. These agents are used

for a variety of cancer therapies including leukaemia, breast, ovarian and gastro-intestinal cancers.

1.1.1.3 Anthracyclines

Anthracyclines work by the formation of oxygen free radicals. These oxygen free radicals lead to breaking of DNA strands and this inhibits DNA synthesis and function. The enzyme topoisomerase is also inhibited as a complex is formed by the enzyme and DNA. Many of the effective anti-cancer drugs in this class come from natural products.

1.1.1.4 Taxanes

Another class of chemotherapeutics are the taxanes, these are specific for the M phase of the cell cycle. They bind to microtubules and inhibit their normal function. This class of drugs has a broad range of applications in cancer treatment.

1.1.1.5 Platinum agents

Platinum agents operate by DNA cross-linking. The cross-link inhibits DNA synthesis, transcription and function. The platinum compounds are not cell cycle specific. The most important platinum drugs bare a large similarity to cisplatin because of its high anti-cancer activity.

1.3 Cisplatin, the first platinum anticancer drug

Cis-diamminedichloridoplatinum or cisplatin (*cis*-$[PtCl_2(NH_3)_2]$) was the first inorganic cancer chemotherapeutic agent (**Figure 1-1**). It was first prepared by an Italian chemist Michele Peyrone, a Professor of Chemistry at the University of Genoa, in 1845 [7] . This compound,

originally known as 'Peyrone's chloride', was of fundamental interest in the development of the 'coordination theory', for which Alfred Werner earned the Nobel Prize in 1913.

1.1 1.2

Figure 1-1. Structure of the antitumour drug, cisplatin(**1.1**), and its inactive *trans* isomer, transplatin(**1.2**)

In the mid-1960s, Barnett Rosenberg and his co-workers serendipitously discovered that cisplatin exhibited antitumour activity, whereas the *trans* isomer, *trans*-$[PtCl_2(NH_3)_2]$ did not [8]. In 1972, *cis*-$[PtCl_2(NH_3)_2]$ was first tested in clinical trials in human patients [9]. Cisplatin is active against a wide spectrum of solid neoplasms, including ovarian, testicular, bladder, colorectal, lung and head and neck cancers[10],[11]. It was approved by the U.S. Food and Drug Administration as an anti-cancer treatment in 1979 [12]. Currently, *cis*-$[PtCl_2(NH_3)_2]$ is one of the most widely used anti-cancer agents.

The drug often leads to an initial therapeutic response associated with complete disease remission, partial response or disease stabilisation. However, cisplatin therapy requires additional medication and is accompanied by severe side effects including dose-limiting nephrotoxicity (renal toxicity), ototoxicity (ear poisoning) due to irreversible damage of the hair cells in Corti organ, myelosuppression (bone marrow suppression) as well as nausea and vomiting.

These toxic side effects limit the therapeutic efficacy of cisplatin [13],[14],[15]. In addition to the serious side effects, inherent or treatment-induced resistant tumour cell sub-populations

also restrict the therapeutic efficacy of cisplatin[16],[17]. These toxic side effects of cisplatin limit the dose that can be administered to patients.

1.4 New platinum drugs

Due to the fact that *cis*-[$PtCl_2(NH_3)_2$] exhibits severe renal toxicity and has narrow applicability to a few tumour types, the search has continued for less toxic and a wider variety of platinum-containing anti-cancer agents. Consequently, new platinum complexes such as carboplatin, nedaplatin, oxaliplatin (Figure 1-2), and thousands of other platinum compounds have been synthesised and studied for clinical usage [18].

The toxicity of cisplatin can be decreased by exchanging the labile chloride ligands for comparatively more stable bidentate leaving groups, thereby slowing down the hydrolytic activation of the drugs[19]. The diaqua form of cisplatin is highly toxic, and that toxicity can possibly be decreased by reducing the lability of the leaving ligand, while more stable bidentate leaving ligands can still produce active complexes, and activity is only lost when very tightly bound ligands are used[20]. Once the chloride leaving groups are substituted by more stable ligands, such as 1,1-cyclobutanedicarboxylate, the renal effects are decreased, while the antitumour activity remains[21]. Three of the "*second-generation*" platinum drugs, fulfilling the requirements mentioned above, are currently used in cancer chemotherapy: carboplatin, nedaplatin and oxaliplatin, **Figure 1-2**[19].

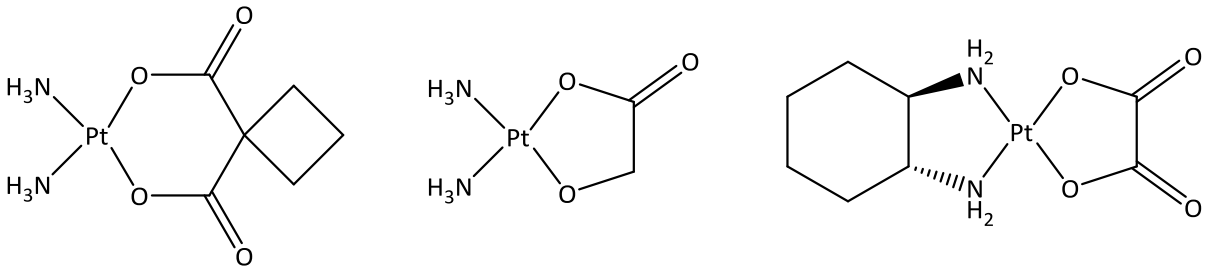

1.3 **1.4** **1.5**

Figure 1-2 Structures of clinically used antitumour drugs: carboplatin (**1.3**), nedaplatin (**1.4**) and oxaliplatin (**1.5**)

Carboplatin, the most successful complex of these second-generation platinum complexes[22], and nedaplatin[23] are cisplatin derivatives that show less nephrotoxicity, gastrointestinal toxicity, neurotoxicity and vomiting[22],[23],[24],[25]. Carboplatin has achieved worldwide approval and steadily increasing acceptance as a less toxic alternative to cisplatin, while nedaplatin has received only limited approval[19]. Oxaliplatin exhibits a safe toxicity profile, and in various clinical situations is superior to cisplatin by being less toxic and retaining activity against cisplatin-resistant tumours [26], [27], [28].

1.5 Mechanism of Cisplatin Antitumour Activity

The most recent review of the mechanism of cisplatin was discussed as follows[29],[30]. The mechanism of action of cisplatin and the classical platinum drugs analogous to cisplatin are very similar. Compounds analogous to cisplatin are complexes that are neutral, square-planar including two cis amine and two cis anionic ligands[31]. The amine groups which can be chelating or non-chelating ligands are referred to as non-leaving groups because they stay bound to the Pt metal centre throughout the course of intercellular transformation. In

contrast, the leaving groups which can be monodentate or chelating ligands leave the Pt coordination sphere.

The general mechanism of action contains four key steps: 1) cellular uptake 2) aquation or activation of the Pt drugs, 3) DNA interaction, and 4) cellular processing of DNA lesions leading to the cell death[31].

There are different cellular events which appear to contribute to the cytotoxic effect of cisplatin, although binding of platinum to DNA is found as a crucial step. Drug resistance can be generated by abnormality in any of the following effects. The mechanisms of cisplatin resistance have been classified as pre-target (i.e., those interfering with cisplatin transport prior to DNA binding), on-target (repair of Pt-DNA lesions), post-target (cellular events taking place after DNA platination) and off-target (alterations in signalling pathways not directly engaged by cisplatin but interfering with cisplatin induced proapoptotic events)[32].

Before any reaction can take place between cisplatin and DNA, the platinum drug must enter the cell. However, cisplatin is vulnerable to attack by proteins found in blood plasma, particularly those that contain thiol groups, such as human serum albumin. The cisplatin that remains intact can enter tumour cells; previously it was believed to be mainly by diffusing through the cell membrane because of the concentration dependence of cisplatin [33],[34],[35]. Recent studies demonstrate that the copper transporter 1 (CTR1) plays an important role in the uptake of cisplatin as well as other ATPase's extrude copper[36]. Active transport mediated by membrane proteins is the predominant mechanism of action. For instance, cisplatin efficacy has been linked to the level of expression of the copper transporters[37],[38],[39]. In a similar way, oxaliplatin uptake has been linked to expression of organic cation transporters[40].

The square-planar geometry of cisplatin facilitates ligand substitution which is the crucial step for formation of DNA lesions. Cisplatin undergoes a ligand substitution even prior to DNA binding in which a chloride ligand is replaced by a water molecule. This aquation is more likely to occur in the cytoplasm, where the chloride ion concentration drops below 20 mM[41]. In the presence of these lower salt concentrations *vs* bloodstream (~100 mM), the half-life of the aquation reaction, producing *cis*-$[Pt(NH_3)_2Cl(H_2O)]^+$, is approximately 2 h. The positively charged aquated cisplatin can enter the nucleus, and can be substituted by DNA bases.

The ultimate target for cisplatin inside the cell is DNA. Platinum ions react preferably with nitrogen atom donors in ligands rather than O atoms. In fact, the preferred binding site in DNA is the N7 atom of purines nucleobases[42],[43],[44],[45],. At physiological pH, the N3 atom of thymine is protonated, while the N3 of purines are sterically hindered[45] and aromatic nitrogen atoms without a σ lone pair are not available for platinum coordination. The N1 of adenine and the N3 atom of cytosine are appropriate positions for platinum binding. The potential platinum binding sites on DNA bases are represented with arrows in **Figure 1-3.**

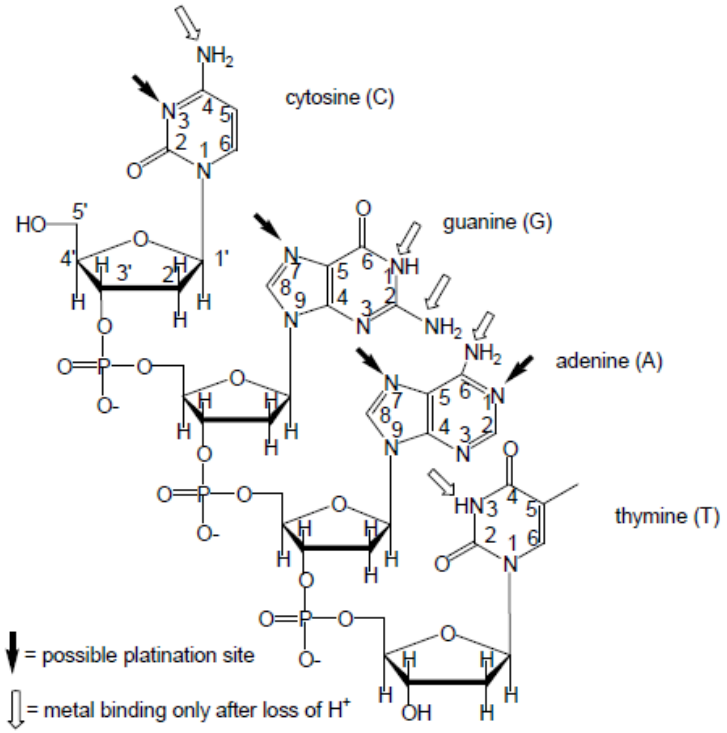

Figure 1-3 Available binding sites for platinum. Guanine-N(7) is the preferred site for initial binding of the platinum(II) complex, since guanine is the most nucleophilic DNA base

All four presented positions can be coordinated to platinum, but the preferred binding site is the N7 atom of guanine, showing a strong kinetic preference[46],[43]. This tendency results from the strong basicity of that position, and from hydrogen bonding interactions between amine protons of cisplatin with O6 in guanine and their accessibility for the platinum complexes[47].

In vitro studies have shown that this monoaquated platinum species is responsible for at least 98% of the platinum binding to DNA within the cell nucleus[48]. Cisplatin reacts with one of the DNA bases, usually guanine, forming a monofunctional DNA adduct [48-49], [50]. Ring closure to form a bifunctional adduct may occur either directly from the

monofunctional adduct or may involve aquation of the second chloride ligand followed by rapid ring closure [51], [52].

The reaction of cisplatin with DNA results in the formation of six major categories of Pt-DNA adducts. The most important ones are schematically depicted in **Figure 1-4**. The major adduct formed by cisplatin, was found to be the 1,2-intrastrand d(GpG) cross-links on adjacent purine bases, followed by 1,2-intrastrand d(ApG)[53] cross-links between an adjacent adenine and guanine, 1,3-intrastrand d(GXG) and 1,4-intrastrand d(GXXG) cross-links between purines separated by one or two intervening bases, respectively.

A small percentage of cisplatin was found to be involved in interstrand cross-links, linking the two strands of the DNA double helix, or in monofunctional adducts coordinated to a single purine and protein-DNA cross-link, in which cisplatin coordinates a protein molecule and a nucleobases[54], [55].

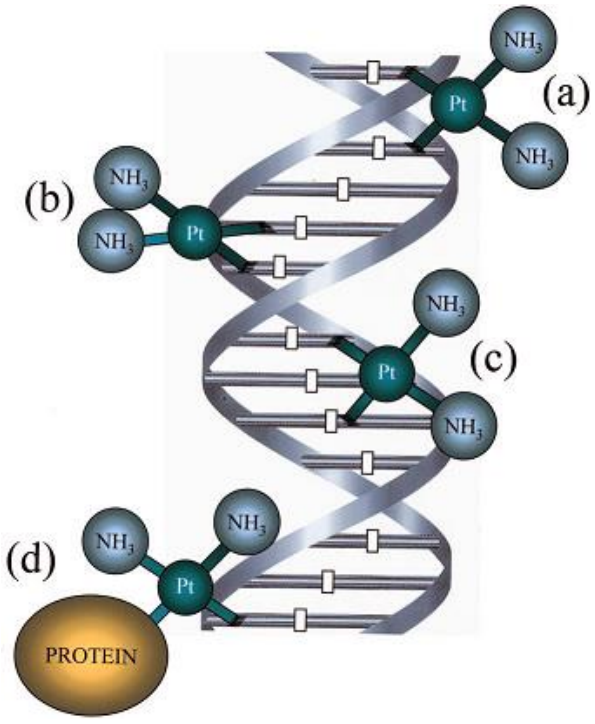

Figure 1-4 Main adducts formed in the interaction of cisplatin with DNA. (a) interstrand cross-link; (b) 1,2-intrastrand cross-link; (c) 1,3-intrastrand cross-link; (d) protein-DNA cross-link[55]

Cisplatin-DNA adducts result in distortion of the DNA that can be recognised by one or more DNA binding proteins. These proteins can either initiate a DNA damage repair (**Figure 1-5**, path b) or signal for apoptosis (cell death) to be initiated (**Figure 1-5**, path a) [51], [52], [56], [57]. However, some cancer cells can develop overactive DNA repair systems to compensate[48].

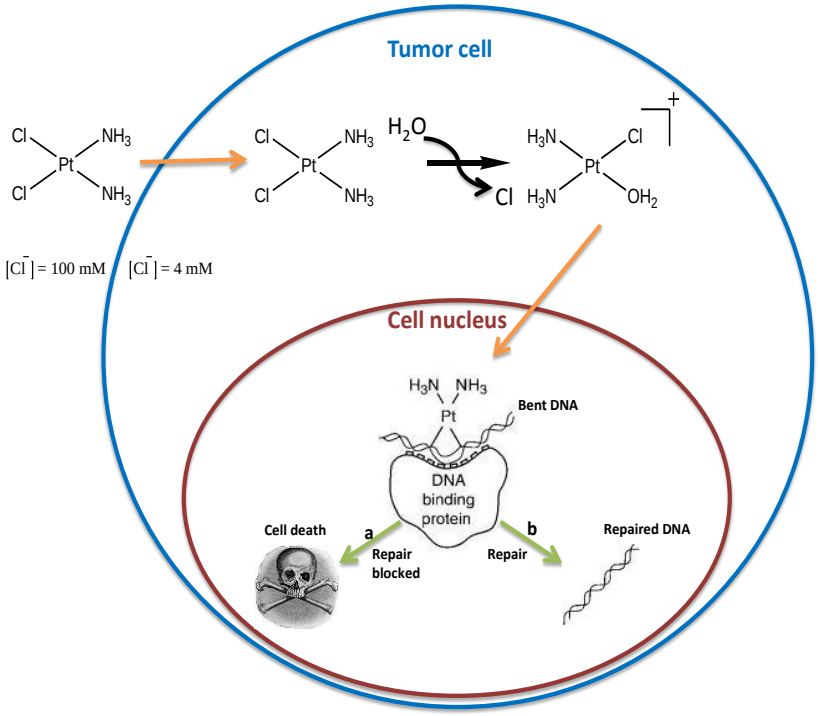

Figure 1-5 Schematic depiction of the cytotoxic pathway for cisplatin. After entering the cell, cisplatin is aquated, and then binds to cellular DNA. If the DNA lesion is not repaired by the cell (path a), then cell death (apoptosis) can occur [48].

1.6 Tumour Microenvironment

Solid tumours are associated with multiple cell types and altered extracellular matrix[58],[59],[60],[61]. The abnormal architecture of tumours leads to a unique microenvironment which is different from normal tissue[60],[62]. One major difference

between many solid tumours and surrounding normal tissue is the nutritional and metabolic environment.

The functional vasculature of tumours is often insufficient to supply the nutritional needs of the expanding population of tumour cells, resulting in deficiency of oxygen and many other nutrients. Hydrolysis of adenosine triphosphate (ATP) in an energy-deficient environment under anaerobic metabolism produces lactic acid [63]. The protons generated by this process, are not subsequently consumed by ATP re-synthesis, and instead accumulated in the extracellular space[64].

Wike-Hooley and his colleagues have provided a complete review of several thousand microelectrode measurements of pH in human and animal tumours[65]. Their results are summarised as follows: determination of pH in subcutaneous tissue and muscle ranged from 7.00 to 8.06, with mean values of 7.52 for human subcutaneous tissue, and 7.32 and 7.43 for muscle in dogs and rats, respectively. There is a wider range of pH values in malignant tissue, from about 5.8 to 7.6 in both human and rodent tumours. There is considerable variation within different regions of the same tumour but in general; tumours are more acidic than normal tissues with median pH values of about 7.0 in tumours and 7.5 in normal tissues.

Accumulative distributions of pH obtained in tumours and normal tissues by Wike-Hooley and his colleagues are presented in **Figure 1-6**[65].

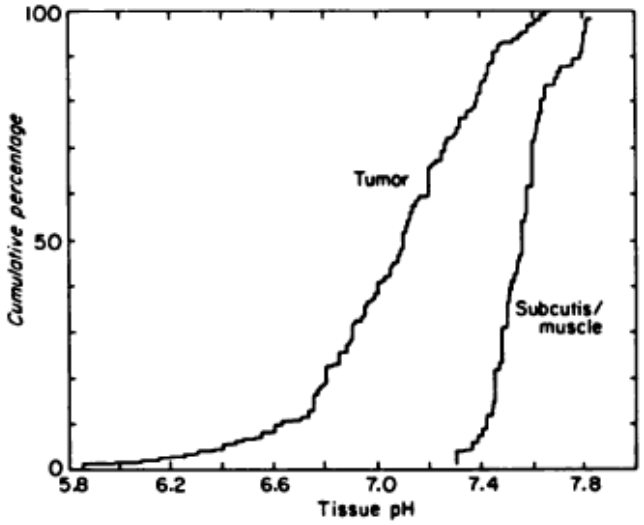

Figure 1-6 Accumulative distribution of extracellular pH rates measured by electrode, in normal and tumours tissues[63]

1.7 Tumour hypoxia

Tissue oxygen levels are not uniformly distributed in the same organ. Levels of oxygenation depend on diffusion of oxygen from blood vessels and the distance from a functional blood vessel; therefore distant areas from blood vessels are more hypoxic [66],[67].

Human solid tumours are invariably less well-oxygenated than the normal tissues. Due to the aggressive proliferation of tumour cells, oxygen demand is high in tumours. In addition, disorganised blood vessel formation in tumours makes blood flow sluggish, and therefore oxygen supply can be lower in some parts of the tumour[68],[69]. Moreover, the tightly packed interface between tumour cells prevents oxygen diffusion to the inside of tumour tissue [69],[62].

Most solid tumours contain hypoxic regions. Hypoxic cells are relatively resistant to radiotherapy[70] and chemotherapy[71] due to the low concentration of oxygen. Often the

proliferation rate in hypoxic tumour cells is lower than normoxic cells, limiting the impacts of anticancer drugs which target the cell cycle and/or rapid proliferating cells. Thus, efficient delivery of drugs to hypoxic regions of solid tumours is another consideration in the chemotherapeutic treatment of cancer[62].

There are at least three potential reasons why cells, which are distant from blood vessels, might be resistant to chemotherapy: first, most anticancer drugs exert selective toxicity on cycling cells, so that non proliferating or slowly proliferating cells are resistant[72]; second, some drugs might be less active in hypoxic, acidic or nutrient deprived microenvironments[73],[63]; and third, cells distant from blood vessels might be exposed to low concentrations of the drug due to its limited access.

Diffusion of fluorescent Pt-based compounds into multicellular tumour spheroids has demonstrated that the outer layers of the spheroid receive or accumulate very much higher doses of drug than the central cells[74]. This has little effect on the population of hypoxic cells in the central part of the spheroid that potentially do not receive an adequate dose of the anticancer drug.

Traditional hypoxia-activated prodrugs (based on nitroimidazoles, quinones, or aromatic N-oxides) rely on reoxidation of the active form to the inert form in normal cells, but not in cancer cells[75]. Healthy tissues, however, can also be highly hypoxic under certain conditions. Thus to completely avoid toxic side effects, it is essential for prodrugs to have high activation thresholds[76]. Cobalt(III) complexes can have their redox potential fine-tuned by ligand choice to coincide with the cytoplasmic environment in cancer cells rather than normal cells[77]. Thus such agents offer a feasible route to develop selective prodrugs.

1.8 Application of cobalt complexes in hypoxia selectivity

As detailed in the previous section, hypoxic cells limit the response of tumours to radiation therapy[78],[79] and perhaps chemotherapy[73]. Hypoxia, however, can be turned into an advantage for selective cancer therapy because it is much more severe in tumours than in normal tissues[76],[80].

Prodrugs are inert agents that can be activated by external stimulation such as light, ionising radiation, or reducing environments[81]. Due to resistance of hypoxic cancer cells to conventional radiotherapy and chemotherapy, hypoxia-activated prodrugs are highly sought-after.

Bioreductive activation is a process by which an inert agent undergoes reduction upon cell entry, releasing one or more bioactive agents (**Figure 1-7**)[82]. Cobalt(III) complexes are relatively inert and usually adopt octahedral geometries and, owing to the high crystal field stabilisation energy of Cobalt (III) (d^6, low spin). Co(II) complexes (d^7, high-spin) on the other hand are more labile and susceptible to ligand substitution[77]. The active Co(II) form is thought to undergo re-oxidation back to the inert Co(III) form in normoxic cells[77].

Cobalt(III) prodrugs can potentially be converted to an active form through the intracellular reduction by xanthine and NADPH oxidase, or cytochrome P450[83],[84],[85]. Co(II) can be reoxidised to the parent prodrug by the molecular oxygen present in normal tissues, but in the absence of oxygen it can be further converted or fragmented to toxic species[85],[86].

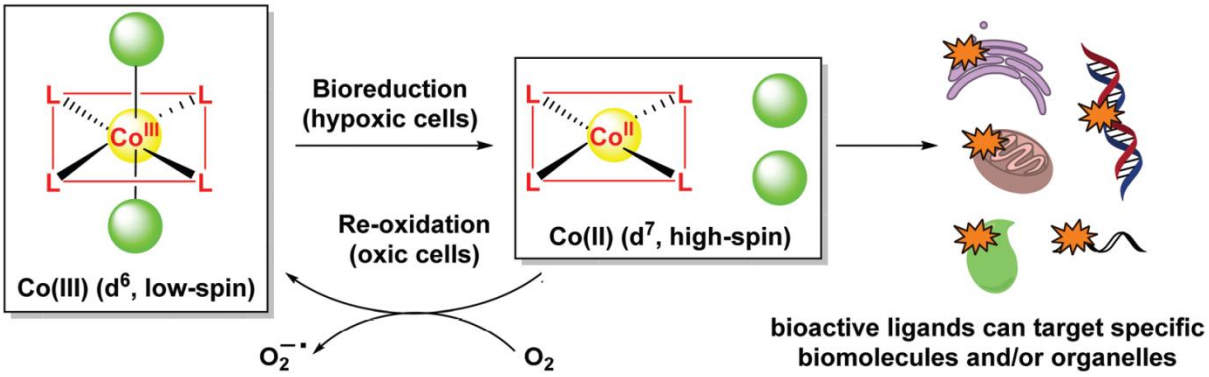

Figure 1-7 The proposed mechanism of action for Co(III) prodrugs in a hypoxic region. Co(III) complexes are hypothesised to undergo a bio-reduction within the hypoxic region in solid tumours. Reducing Co(III) to Co(II) results in rapid ligand exchange and consequently releasing the bioactive ligand[77]

1.9 Cobalt(III)-mustard agents

Nitrogen mustard agents are a class of clinically approved anticancer chemotherapy drugs,[87] that induce their therapeutic effect by alkylating purine DNA bases[88]. The mechanism of action of nitrogen mustards for alkylating DNA is shown in **Figure 1-8**.

Using a hypoxia activated Co(III) inert metal centre, is one of the strategies to target their cytotoxicity. This is achieved by complexing the Co(III) metal centre to the nitrogen mustards[89]. Coordination of the nitrogen lone pair of the nitrogen mustard to Co(III) can supress its toxicity due to the fact that the electron pair is no longer available to activate the nitrogen mustard by making an aziridinum ion. Co(III) complexes are kinetically inert[90]. The nitrogen mustard ligand can then be released by reduction of Co(III) to labile Co(II). The cytotoxic nitrogen mustard might be released by rapid ligand exchange with surrounding water molecules.

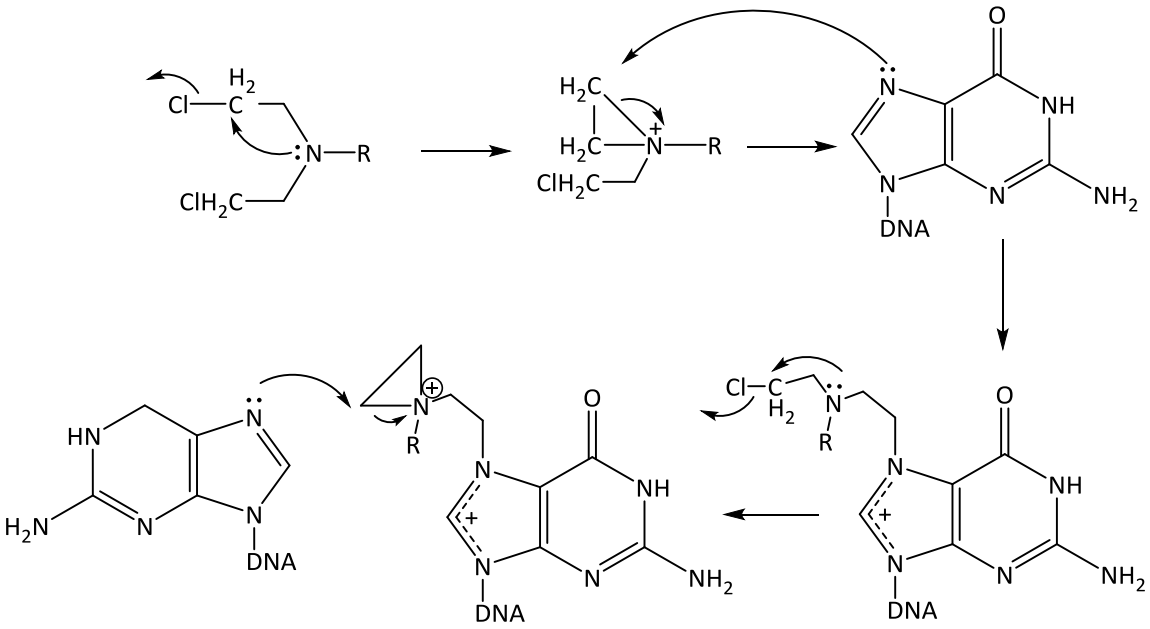

Figure 1-8 A mechanism of nitrogen mustards for the alkylation of DNA

The ancillary ligands present on the Co(III) metal centre are important to tune the physiologically and chemically important properties of the complex such as Co(III)/Co(II) reduction potential, overall charge, solubility and lipophilicity. These factors play a major role for entry of the prodrug into the biological system and also release of the active nitrogen mustard to the target sites.

Co(III) complexes containing amine and nitrido ligands are very effective radiation sensitisers for hypoxic mammary carcinoma cells (EMT6)[91]. Among Co(III)-nitrido complexes, those containing acetylacetonate (acac) and nitrogen mustard ligands, such as bis(2-chloroethyl)amine, were especially effective against cultured murine tumour cells[92] (**Figure 1-9**).

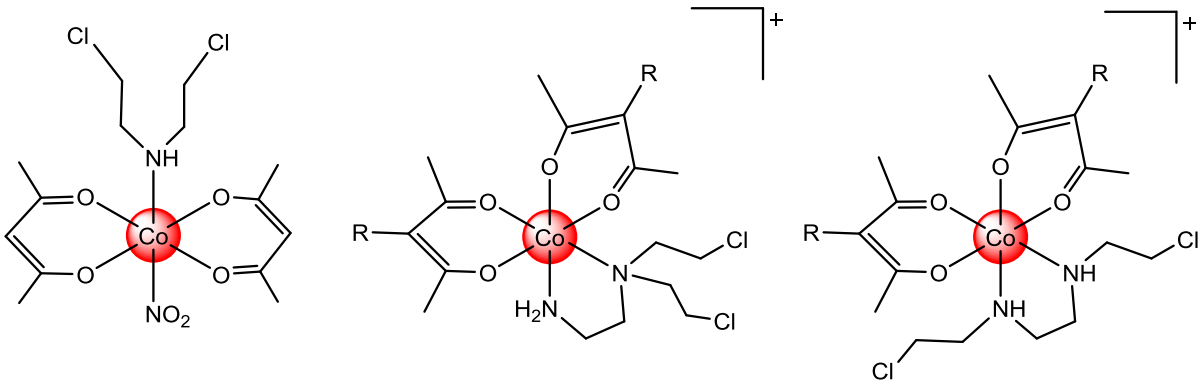

Co(III)-BCA **1.6**

Co(III)-DCE
R = H **1.7**
Me **1.8**
Et **1.9**

Co(III)-BCE
R = H **1.10**
Me **1.11**
Et **1.12**

Figure 1-9 Structures of hypoxia activated Co(III) prodrugs with monodentate and bidentate nitrogen mustard ligands

Compound **1.6** (**Figure 1-9**) in its oxidised state is inert, and the nitrogen lone pair of the BCA component is involved in coordination to cobalt and unavailable for intramolecular formation of an aziridinium ion, which is a perquisite for DNA alkylation. In the reduced state, BCA released from the resulting Co(II) complex, produces a cytotoxic effect. Cytotoxicity studies showed that **1.6** displays strong radio-sensitisation of hypoxic mammary carcinoma cells (EMT6) and exhibited higher toxicity towards oxygenated cells than hypoxic cells[92].

The Ware research group used the same rational design employed for compound **1.6** to develop Co(III)–nitrido complexes with alkylating aziridine groups, to release the bioactive ligands under hypoxic conditions[93]. Unfortunately, testing of complexes in a hypoxic cell culture indicated that the complexes underwent facile reduction, leading to uncontrolled release of the aziridine groups. Bidentate mustard ligands, BCE and DCE, were used to synthesise a new class of Co(III)–acetylacetonate complexes (**1.7-9** and **1.10–12**). Biological

results from these complexes revealed that metal complexes of nitrogen mustards have significant hypoxia-selective cytotoxicity toward mammalian cells in cell culture, and are a new series of hypoxia-selective cytotoxins[94],[90],[95].

Matching the cytotoxicity trend of the Co(III)-BCE and Co(III)-DCE complexes with the free mustard agents, implied that the toxicity was due to the release of the mustard agents. Complex **1.8**, was 6-fold more cytotoxic towards Chinese hamster ovary fibroblast cells (AA8 and UV4) grown in hypoxic conditions than the same cells cultured in aerobic conditions[87]. This complex also exhibited high activity against mammary carcinoma cells (EMT6) in intact spheroids. Spheroids have hypoxic centres, therefore **1.8** induced toxicity is believed to be caused by DCE release within the core followed by back-diffusion to the outer areas[94]. Structure activity relationship studies found that the nature of the ancillary ligand, acetylacetonate, was crucial to hypoxic selectivity. While Co(III)-DCE complexes with unsubstituted acetylacetonate displayed no hypoxic selectivity, methyl and ethyl analogues showed considerable selectivity[94].

Replacement of acetylacetonate with bis-troplonate yielded complexes that are structurally similar to related complexes with acac ancillary ligands (**Figure 1-10**). Tropolonates are flat molecules when they coordinated to the Co(III) centre. Formation of complexes of this kind with bulky tertiary amine nitrogen mustard ligands can minimise the steric hinderance.

The tropolonato complexes have significantly higher reduction potentials than the corresponding acac complexes due to their electron withdrawing nature[96]. The tropolonato ligands therefore facilitate the cellular reduction of the coordinated Co(III) centres and accordingly release of the mustard ligand.

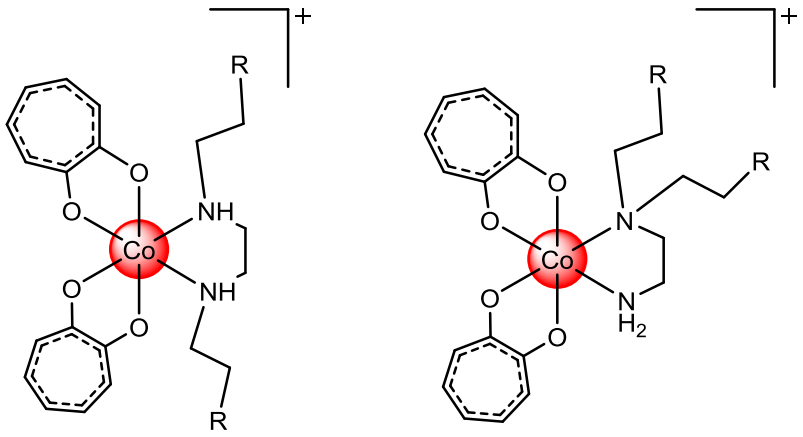

Co(III)BCE, R = Cl **1.13**
Co(III)BEE, R = H **1.14**

Co(III)DCE, R = Cl **1.15**
Co(III)DEE, R = H **1.16**

Figure 1-10 Chemical structure of bis-tropolonato dervatives of Co(III) as potential hypoxia selective cytotoxins

Biological results showed that complexes **1.13** and **1.15**, have cytotoxicity similar to the free mustard in cell culture under oxic and hypoxic conditions. For this reason, unsubstituted bis-tropolonate was deemed to be an unsuitable ancillary ligand for generating hypoxic selective Co(III) complexes. The two non-mustard complexes, **1.14** and **1.16**, where the ligands are incapable of forming DNA adducts, showed much lower AA8/UV4 IC50 ratios.

The ancillary ligands present on the Co(III) centre are also important to tune the physiologically and chemically important properties of the complex such as Co(III) to Co(II) reduction potential, overall charge, solubility and hydrophilicity or lipophilicity. These factors play a major role for entering the prodrug into the biological system and also in releasing the active nitrogen mustard into the target sites.

In order to develop physiologically stable Co(III)-prodrugs with enhanced hypoxic selectivity, tridentate mustard agents were synthesised (**Figure 1-11**)[89]. Introducing electron withdrawing groups into the tropolone ring could generate hypoxia-selective complexes.

Replacement of acetylacetonate with carbonato and oxalato ligands afforded Co(III)-DCE complexes (**1.17** and **1.18**) with reasonable hypoxic selectivity (2–4-fold against UV4 cells) (**Figure 1-11**)[97]. Nevertheless, the hypoxic selectivity of **1.8** was still superior to that of **1.17** and **1.18** under the same conditions.

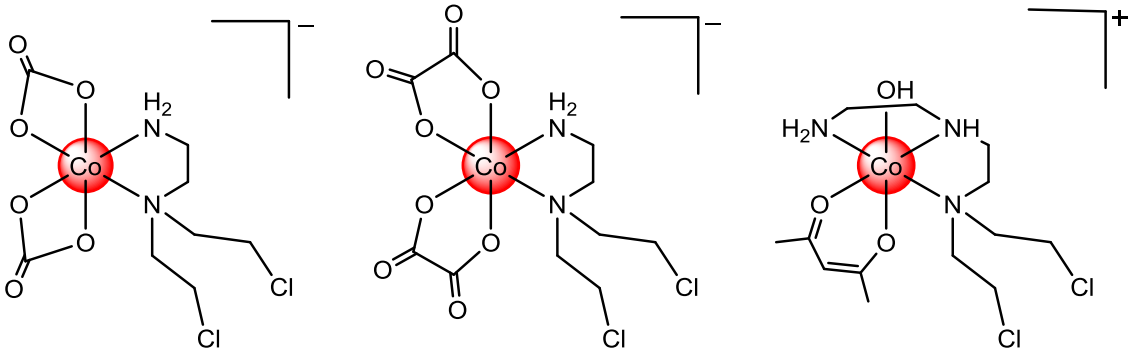

Co(III)-DCE-bis-carbonato **1.17** Co(III)-DCE-oxalato **1.18** Co(III)-DCD **1.19**

Figure 1-11 Hypoxia active Co(III) prodrugs

Co(III)–acetylacetonate complexes containing DCD (**1.19**) proved to be much less cytotoxic than the corresponding bidentate analogue DCE used previously. The reason for this is not known; while both would be expected to have similar chemical reactivity, the tridentate analogue DCD may have slower kinetics of cell uptake. However, both had similar AA8/UV4 IC50 ratios (19- vs. 26-fold), suggesting that DNA crosslinking is the major mode of cytotoxicity in both cases[89].

1.10 Cobalt(III) complexes as carrier for bioactive ligands

New approaches to cancer therapy have involved the selective inhibition of enzymes involved in the process of tumour metastasis. The development of potent inhibitors of these

enzymes has resulted in a new class of drugs that have antimetastatic and cytostatic action[98].

One such therapy involves combating the action of specific matrix metalloproteinases (MMPs). Hambley and co-workers utilised the electrochemical properties of Co(III) complexes to selectively deliver matrix metalloproteinase (MMP) inhibitors to target tumour sites[99]. MMPs are a family of zinc-dependent peptidases which have been implicated in cancer progression and other diseases[99].

MMPs decompose the extracellular matrix (ECM) of cancer cells in primary tumour sites, providing cancer cell migration and metastasis[100]. Despite the fact that several exogenous MMP inhibitors have been developed to restrain metastasis in cancer patients, none have been clinically approved (the only FDA-approved MMP inhibitor is doxycycline (**Figure 1-12**), which is used as a periodontitis (gum disease) treatment)[101].

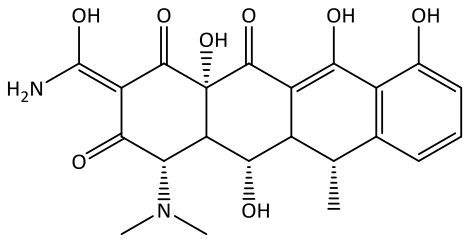

1.19

Figure 1-12 Structure of doxycycline

A major deficiency in the structural design of some of the MMP inhibitors developed to date (like marimastat and batimastat (**Figure 1-13**) is the exposed hydroxamate acid group.

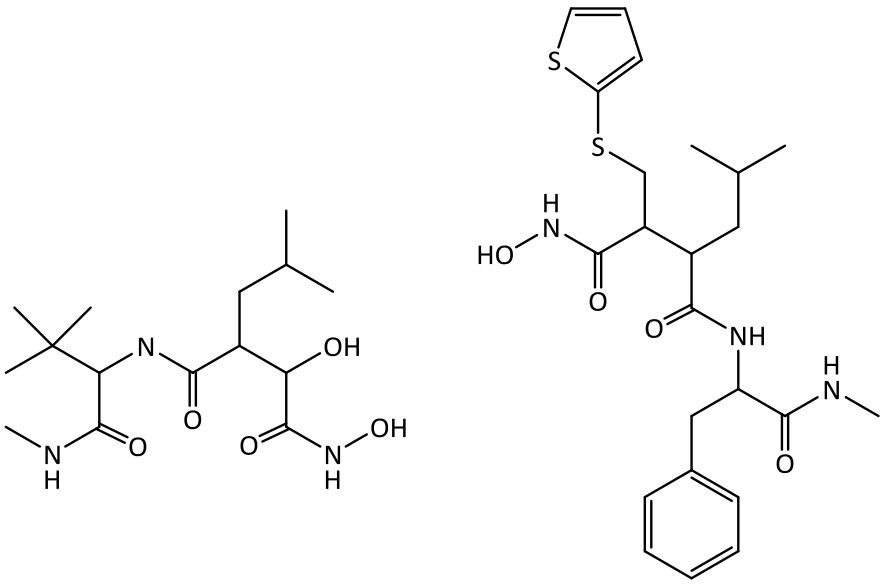

Marimastat

1.21

Batimastat

1.22

Figure 1-13 Marimastat and Batimastat chemical structure

Indeed, the poor oral bioavailability of these inhibitors in clinical trials is thought to result from non-specific reactions between the hydroxamate acid group and biomolecules[102]. Hambley's research group linked MMP inhibitors to Co(III)-TPA *via* the hydroxamate acid moiety (**Figure 1-14**) to overcome this problem [99].

The result was deactivation of the MMP inhibitors in normoxic sites, and selective release in hypoxic regions (upon reduction of the inert Co(III) complex to the more reactive Co(II) complex).

Initial electrochemical studies with prototypical systems containing simple alkyl and aryl hydroxamate acid ligands (**1.23**-**25**), established that Co(III)-TPA was a suitable transporter of hydroxamate acid-containing compounds to hypoxic sites[103]. Having obtained these results, marimastat, a potent MMP inhibitor, was attached to Co(III)-TPA *via* the two oxygen atoms on the hydroxamate acid moiety (**1.26**) (**Figure 1-14**).

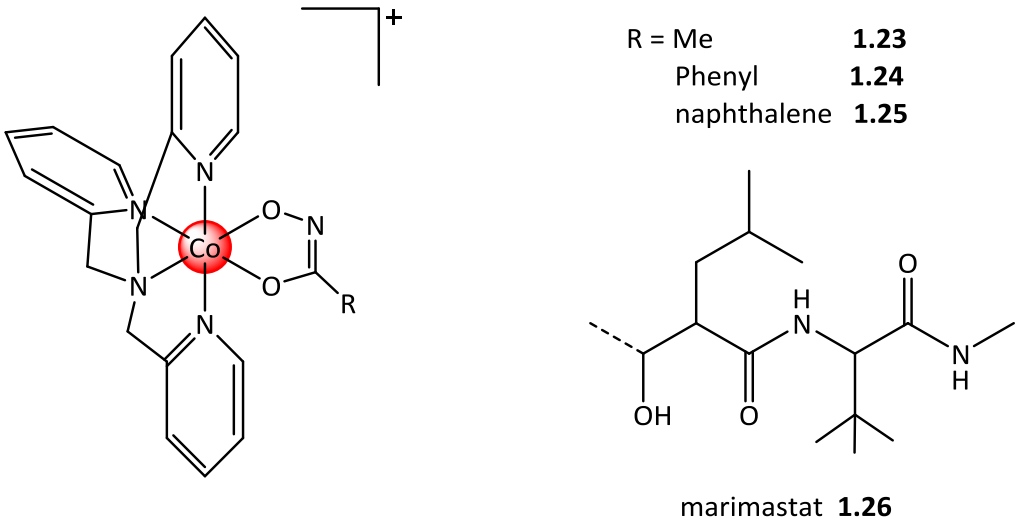

Figure 1-14 Chemical structure of Co(III)-TPA with different hydroxamate acid ligands

Complex **1.26** suppressed 4T1.2 tumour growth in mice more effectively than free marimastat. This was tentatively attributed to the failure of primary tumours in the control group to reach an appropriate size[99]. In light of this seemingly conflicting *in vivo* data, the authors suggested that further experiments with longer administration times were needed to calculate the true efficacy of **1.26**. More recent studies involving Co(III)-TPA complexes, **1.23-125** showed that both the hydroxamate and hydroximate forms (**Figure 1-15**) could be isolated[104].

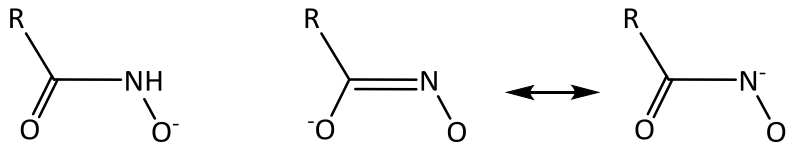

hydroxamate **1.27** hydroximate forms **1.28**

Figure 1-15 Hydroxamate and hydroximate acid structures

The reduction potential of the two protonated states was notably different, and thus the ability of the complexes to release the bound ligand was also different. The differing electrochemical properties of the hydroxamate and hydroximate forms could be modified to develop Co(III) systems capable of delivering bioactive ligands (containing hydroxamate acids) to acidic regions.

Other tetradentate ligand systems, aside from TPA have also been used to prepare Co(III) carriers for biologically active ligands (**Figure 1-17**). Ware et al. showed that Co(III)-1,4,7,10-tetraazacyclododecane (cyclen) complexes were effective carriers for cytotoxins such as 8-hydroxyquinoline (8-HQ) and azaCBI[83],[105],[106]. Detailed mechanistic studies revealed that these systems (**1.27** and **1.28**) underwent efficient reduction (and cytotoxin release) in hypoxic cells through radiolytic and non-radiolytic pathways, upon exposure to ionising radiation. Moreover, **1.28** displayed selective potency (20-fold) towards colorectal adenocarcinoma cells (HT29) grown in hypoxic conditions over the same cells cultured in oxic conditions[83]. Systematic modification of the azaCBI backbone yielded analogues with greater hypoxic selectivity[107].

To improve solubility and stability, 1,7-substituted cyclen ligands containing anionic sulfonato, phosphinato and carboxylato groups were employed (**1.30, 1.31 and 1.32**)[108]. Biological studies of **1.30**, **1.31**, **1.32**, **1.33**, **1.34** and **1.35**, demonstrated that although solubility was slightly improved, their stability (in cell culture media) and hypoxic selectivity were commensurate to the parent complexes (**1.28** and **1.28**)

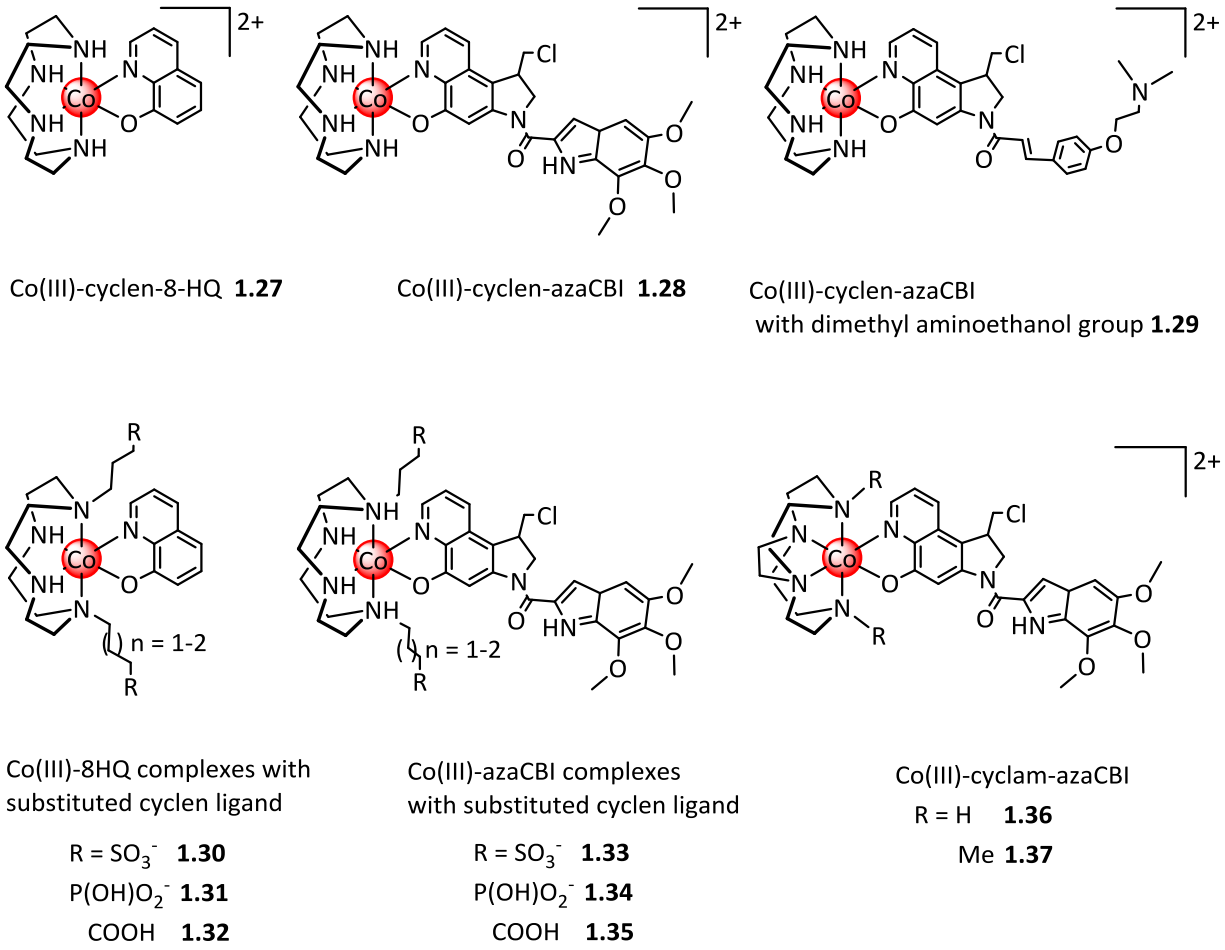

Figure 1-16 Chemical structures of Co(III) carriers with tetradentate ligand systems

Larger macrocyclic ligands such as 1,4,8,11-tetraazacyclotetradecane (cyclam), with cross-bridged nitrogen atoms have been used as well (**1.36** and **1.37**)[109]. The bridging of opposing nitrogen atoms within cyclam was proposed to force the nitrogen lone pairs to align better with the cobalt d-orbitals, preorganising the host site and ensuring formation of only complexes with cis geometry. This potentially allows a better fit around the Co(III) centre, thereby stabilising Co(III) relative to Co(II) and lowering the reduction potential of the Co(III) complexes. The most effective complex in this series, **1.36,** showed 81–212-fold higher toxicity under hypoxia than 20% oxygen against a panel of human cancer cell lines[109]. Interestingly, the cytotoxicity of this complex was not increased in cell lines

overexpressing reduction which is known as a initiator of other hypoxia-activated prodrugs (based on nitroaromatics and quinones)[110]. A similar trend was observed for the cyclen bearing derivative, **1.28**. Given these results, the identity of the reductase or non-enzymatic reductant reducing these complexes, remains unknown. There is speculation that the lipophilicity of these complexes facilitates mitochondrial accumulation, resulting in reduction by the mitochondrial electron transport chain[83]. However, there is no experimental evidence for this mechanism reported.

1.11 Thesis Coverage

As mentioned in earlier sections, Lack of discrimination between cancer cells and normal tissue is the main problem of cytotoxic anti-cancer drugs. Commonly, anti-cancer drugs act on cells that divide rapidly, one of the main properties of cancer cells. Therefore, damage can be expected in particular in rapidly dividing normal cells, like bone marrow, gastrointestinal mucosa and hair follicles. This results in the most common side effects of chemotherapy like myelosuppression (decreased production of blood cells), mucositis (inflammation of the lining of the digestive tract) and alopecia (hair loss) [111].

Another problem in cancer therapy is the existence of hypoxia in solid tumours and that low oxygenation can accelerate malignant progression and metastasis, thereby creating a poorer prognosis irrespective of which cancer treatment is used[112].

The presence of hypoxic cells in human tumours provides an important target for selective cancer therapy. The main goal of this project is to synthesise smart targeted drug delivery systems that deliver drugs to cancer cells with better efficacy and lower toxicity levels. Therefore, we are going to develop synthetic routes to achieve novel heterodinuclear

[Co(μ-OH)$_2$Pt] complexes. This will be done within the context of developing an entirely new approach to delivering platinum anti-cancer drugs to targeted sites in the body.

The Co(III) ion is kinetically inert, that is, it exchanges ligands only very slowly, but when reduced to Co(II) (by bioreduction after entering to hypoxic cells) the ligands will be exchanged rapidly. This results in release of the platinum component which will be an anti-cancer drug.

In chapter 2, the formation of [{Co(μ-OH)$_n$M}$_m$] complexes ((M= metal ion) by reaction between equilibrium mixtures of *cis*- and *trans*-[Co(en)$_2$(OH)(OH$_2$)]$^{2+}$ and different metal ions is studied using ^{13}C NMR spectroscopy, in order to gain a better understanding of the reactions that may be occurring in solution.

In chapter 3, the synthesis, characterisation and purification of dinuclear [Co(μ-OH)$_2$Pt] complexes are discussed.

In chapter 4, the synthesis and characterisation of a new class of dinuclear [Co(μ-OH)$_2$Pt] complexes bearing a nitrilotriacetate (nta) ligand are discussed. The scope of this chapter is to produce neutral [Co(μ-OH)$_2$Pt] complexes in order to facilitate the isolation of the dinuclear complexes.

In chapter 5, the conclusion and future prospects of this research are discussed.

In chapter 6, the syntheses and characterisation of organotin complexes with pttp and ottp ligands (**Figure 1-17**) are explained.

In chapter 7, the experimental work relevant to this thesis is described in detail.

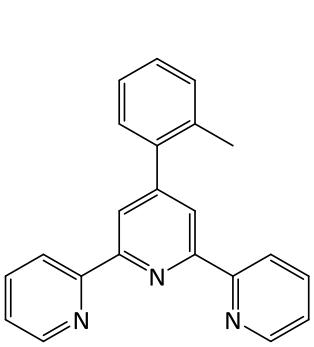

ottp

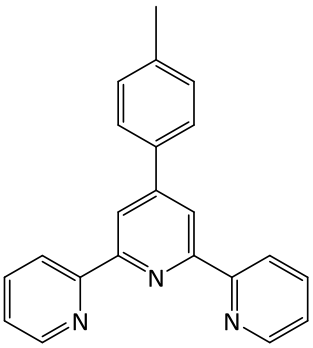

pttp

1-17 Terpyridine derived ligands employed in chapter 6.

Chapter 2

Exploring Formation of Dinuclear Complexes in Solution by NMR

Chapter 2. Exploring Formation of Dinuclear Complexes in Solution by NMR

2.1 Introduction

Syntheses of [{Co(μ-OH)$_n$M}$_m$] complexes (M= transition metals) have been studied previously[113],[114],[115],[116] and the products have been characterised by X-ray crystallography and spectroscopically. Here we summarise the structures of some dinuclear and polynuclear [{Co(μ-OH)$_n$M}$_m$] type complexes.

In 1888, Jørgensen reported the synthesis of a compound containing a cation which he described as being dinuclear[117]. In 1907, Werner provided the final piece of evidence of his theory of octahedral coordination by demonstrating the optical activity of species containing bidentate inorganic "ligands" for the cluster cations of composition [Co{(OH)$_2$Co(NH$_3$)$_4$}$_3$]$^{6+}$ (**Figure 2-1**)[118]. Alfred Werner was awarded the Nobel Prize in 1913 for coordination theory.

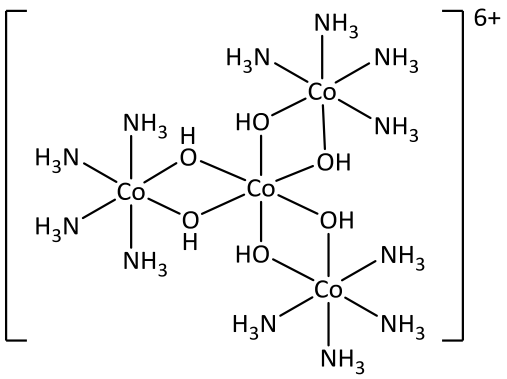

Figure 2-1 Werner's hexol ([Co{(OH)$_2$Co(NH$_3$)$_4$}$_3$]$^{6+}$)

Another complex, believed by Werner to be a hexol (Werner's supposed hexol, **Figure 2-2**), was synthesised by Jackson *et al* [119] according to Werner's procedure [118],[120] but the ^{1}H NMR study did not agree with Werner's original formulation. The expected singlet for the 18 equivalent NH_3 protons, and another singlet for the six equivalent OH protons at very high field (well above SiMe4), were not observed. Instead, a lower symmetry complex was apparent, but one clearly bearing the high field bridging OH protons.

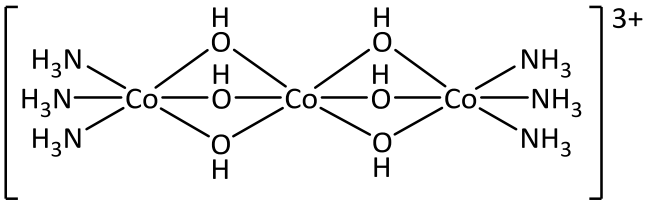

Figure 2-2. The structure proposed by Werner for his second hexol

The product was purified by ion-exchange chromatography and the single crystal X-ray structural analysis was performed on a crystal which proved to be a double salt of composition $[NH_4]_2[Co_6(NH_3)_{14}(OH)_8(O)_2](ZnCl_4)_2$]. The complex cation is shown in **Figure 2-3**.

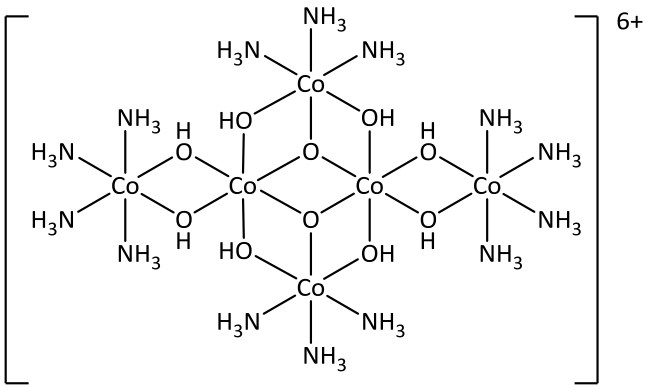

Figure 2-3. The structure of Werner's second hexol

Tetranuclear complexes with the general formula of $[M^{II}((OH)_2M^{III}A_4)_3]^{5+}$ (where M^{II} is Mg, Zn, Co, Mn or Ni and M^{III} is Co or Cr, and A_4 is either four monodentate ammonia ligands,

two bidentate ethane-1,2-diamine (en) ligands, or one tetradentate N,N'-bis(2-methylpyridyl)propane-l,3-diamine (bispictn) ligand) have similar structures to each other[113]. The inner coordination spheres around the metal centres in the $[Co\{(OH)_2Cr(bispictn)\}_3]^{5+}$ cation are depicted in **Figure 2-4**.

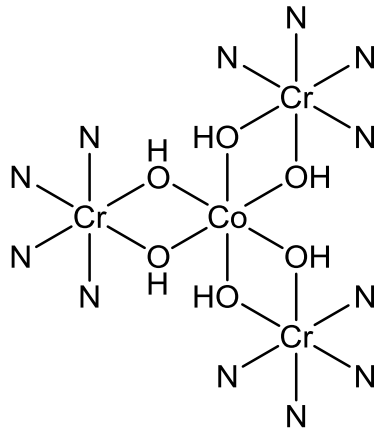

Figure 2-4. Inner coordination spheres around the cobalt and chromium atoms in the $[Co\{(OH)_2Cr(bispictn)\}_3]^{5+}$ cation[113].

X-ray diffraction studies showed that metal ions such as Mn^{3+}, Ni^{2+}, Zn^{2+} and Mg^{2+} bind to $[(en)_2Co(H_2O)_2]^{2+}$ to give the structure shown in **Figure 2-5 a**. The complexes of the form $[\{(en)_2Co(\mu\text{-}OH)_2\}_2M(H_2O)_2]^{3+}$ containing $Cu^{2+}$and Co^{2+} metal ions have the structure illustrated in **Figure 2-5 b**[115]. The complexes containing Pd^{2+} and Pt^{2+} metal ions have the structure shown in **Figure 2-5 c**[116].

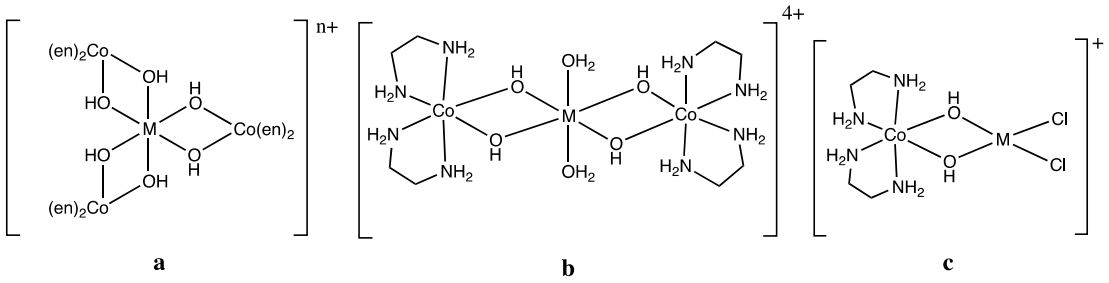

Figure 2-5 Structures of the Co complex $[(en)_2Co(H_2O)_2]^{3+}$) in association with **a)** Mn^{3+}, Ni^{2+}, Zn^{2+}, Mg^{2+} [121] **b)** Cu^{2+}, Co^{2+} [115], **c)** Pd^{2+} and Pt^{2+} metal ions[116]

This chapter examines the formation of products of this kind in the solution state. [Co(μ-$OH)_n$-M] (M= metal ions) heterodinuclear (and polynuclear) complexes were synthesised *via* reaction between $[Co(en)_2(OH)(OH_2)](ClO_4)_2$ and different metal ions (M= Zn^{2+}, Mg^{2+}, Ni^{2+}, Cu^{2+}, Co^{2+}, Mn^{3+}, Pd^{2+} and Pt^{2+}).

2.2 Using NMR spectroscopic techniques to explore dinuclear complex formation in solution

The complexes described above, were studied in the solid state by X-ray crystallography, but the nature of the chemistry that occurs in solution may be different. It is important to explore how the chemistry in solution relates to the data from the solid state. NMR spectroscopy is the best technique to study the behaviour of such systems in solution, at least for diamagnetic metal ions, and under some circumstances for paramagnetic metal ions.

The progress of reactions which will be explained in the following part, were monitored by ^{13}C NMR spectroscopy. Before dealing into any detail, there are certain details that are needed to bear in mind regarding ^{13}C NMR spectroscopy. This is important to remember

that ^{13}C is only present as 1.1 % of the total carbon content of any organic compound. This, in combination with an inherently less sensitive nucleus, means that signal to noise issues will always be a major consideration in the acquisition of ^{13}C spectra. So it takes a great deal longer to acquire ^{13}C NMR spectra than it does ^{1}H NMR spectra.

Another important aspect of ^{13}C NMR spectroscopy is that the signals are not normally integrated. The reason for this is that some carbon signals have quite long relaxation times. In order to make NMR signals quantitative, and therefore more suitable for integration, acquisition must allow for a relaxation delay (delay period between acquisition pulses) of at least five times the duration of the slowest relaxing nuclei in the compound being considered. However, on the assumption that chemically similar carbon atoms have similar relaxation times, reasonably reliable integrations can be obtained without such long delays being necessary.

The standard is usually added directly to the NMR solvent and is thus referred to as an internal standard. It is also possible to insert a small tube containing standard in solvent into the bulk of the sample so that the standard does not come into direct contact with the sample. This would be referred to as an external standard. We used an internal standard in our research for reasons of convenience. In the present research, the usage of an internal standard helped to follow changes in chemical shifts. In some cases, an internal standard was used to compare the integration of a signal with the internal standard's integration and also to be able to compare integrations between spectra.

2.3 Data analysis

^{13}C NMR was used to monitor the formation of $[(en)_2Co(\mu\text{-}OH)_n\text{-}M]$ (M = Zn^{2+}, Mg^{2+}, Ni^{2+}, Cu^{2+}, Co^{2+}, Mn^{3+}, Pd^{2+} and Pt^{2+}) complexes. The reaction progress was monitored by ^{13}C NMR spectroscopy. TMPS was used as an internal standard when diamagnetic metal ions were present.

Experimental data could be conveniently presented by plotting graphs of *cis* to *trans* ratio *vs* molar equivalent and chemical shift *vs* molar equivalent. The *cis* to *trans* ratio was obtained by addition of the integrations of the two *cis* signals and dividing by the integration of the *trans* signal.

For the *cis* to *trans* ratio *vs* molar equivalent graphs, the standard error for each signal integration was calculated using the equations presented in **Appendix 1,** and error bars were drawn. In cases where the *cis* signals were broadened through interactions with paramagnetic metal ions, dioxane was added as an internal standard to allow absolute integration of the remaining signal.

In some cases, the standard errors associated with a data point were too small to be plotted.

2.4 Results and Discussion

The ^{13}C-NMR spectrum of $[Co(en)_2(OH)(OH_2)](ClO_4)_2$ in D_2O contains three signals at 46.19, 46.98 and 47.71 ppm with relative integrations of 0.68, 1 and 0.70 at 25° C (**Figure 2-6**).

Results from isotopic analysis described in the literature show that the *cis* and *trans* isomers are in equilibrium with each other in an aqueous medium (**Figure 2-7**)[122]. The half-life ($t_{1/2}$)

for formation of the equilibrium is approximately 3 minutes for this facile *cis-trans* isomerisation[122],[123] .

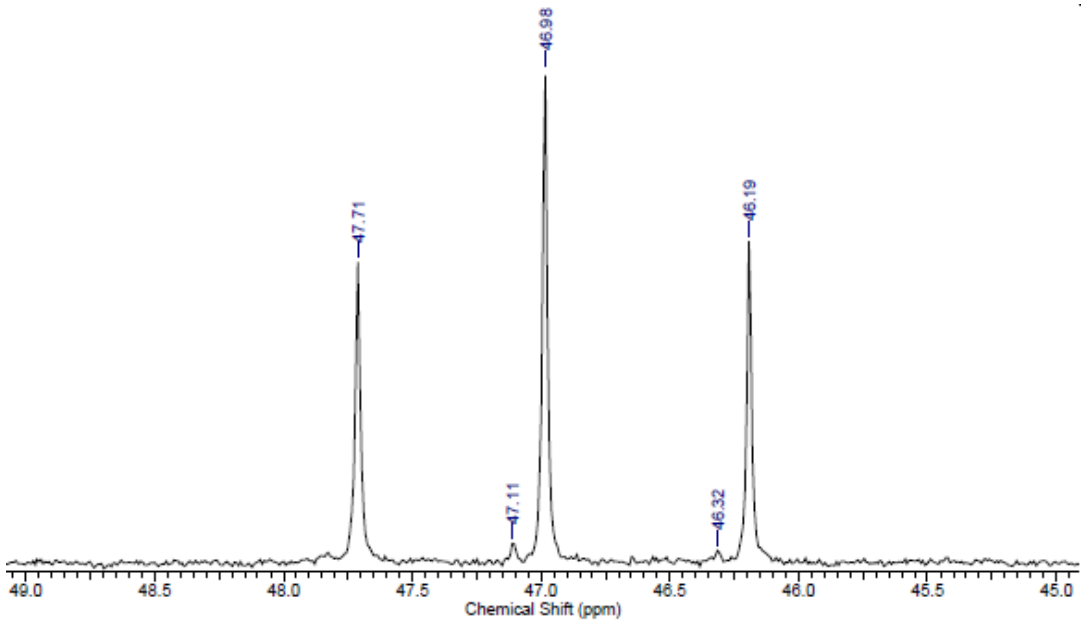

Figure 2-6. The ^{13}C NMR spectrum of $[Co(en)_2(OH)(OH_2)]^{2+}$ in D_2O in presence of TMPS internal standard

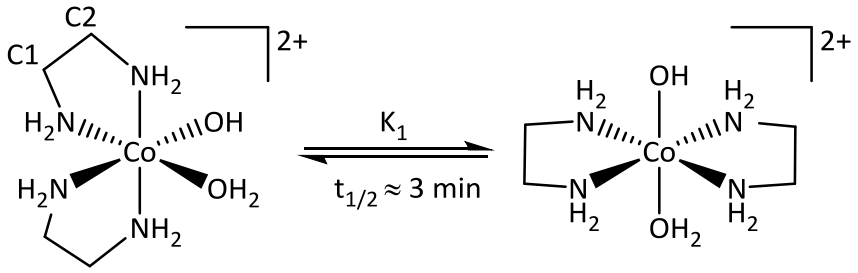

Figure 2-7. *Cis* to *trans* facile isomerisation of $[Co(en)_2(OH)(OH_2)]^{2+}$

There are two kinds of carbon atoms in the *cis* isomer but when it converts to the *trans* isomer, there is only one kind of carbon atom (**Figure 2-7**). Therefore, it is expected to see two signals for *cis*-$[Co(en)_2(OH)(OH_2)]^{2+}$ and one signal for its *trans* isomer. Consequently, two signals, which are marked A and B, at 46.2 and 47.7 ppm, in **Figure 2-6** are assigned to

the *cis* isomer and the single signal at 46.9 ppm to the *trans*- isomer. The *cis* to *trans* ratio can be obtained by adding the integrations of the two *cis* signals together and dividing by the integration of the *trans* signal. The *cis* to *trans* ratio value for $[Co(en)_2(OH)(OH_2)]^{2+}$ under our conditions is 1.4.

Apart from *cis* and *trans* peaks in ^{13}C NMR spectra, some small peaks were observed at longer reactions times which may be related to deuterium exchange. Deuterium isotope exchange on the amine group has already reported[124]. Deuterium isotope exchange results in having $-CH_2-NH_2$, $-CH_2-NHD$, and $-CH_2-ND_2$ in the NMR sample. As a result, small signals appear next to main signals. Two closely spaced signals in the ^{13}C NMR spectrum might be assigned to the carbon atoms affected by deuterium isotope exchange on their neighboring amine group.

2.4.1 Studies with diamagnetic metal ions

NMR titrations of $[Co(en)_2(OH)(OH_2)](ClO_4)_2$ with different metal ions were analysed in order to find out the interaction between them in the solution state and also to find out the progress of the reaction. Each titration was carried out inside a NMR tube, with $[Co(en)_2(OH)(OH_2)](ClO_4)_2$ (0.0860 g, 1 eq) and different molar equivalents of M (M= $Li(NO_3)$, $K(NO_3)$, $Mg(NO_3)_2$, $Ag(NO_3)$, $Zn(ClO_4)_2$, $Zn(NO_3)_2$, $Cd(NO_3)_2$, $K_2[PdCl_4]$ and $K_2[PtCl_4]$) in 1 ml D_2O). TMPS (3-(trimethylsilyl)-1-propane-sulfonic acid) was added inside the tube as an internal reference. The ^{13}C-NMR spectrum was taken at least 30 minutes (>10 $t_{1/2}$) after addition of the metal ion to the cobalt complex solution.

The ^{13}C NMR spectra of $[Co(en)_2(OH)(OH_2)]^{2+}$ were taken after addition of 0.1, 0.3, 0.5, 1, 2, 4 and 8 equivalents of $Zn(ClO_4)_2$. Spectral changes were observed in both the *cis* to *trans*

ratio and chemical shifts. In addition, different peak heights can be seen compared to those seen in **Figure 2-7**. The *cis* peak height increased while the *trans* peak height decreased. The spectra presented here are those obtained with 0.5, 1 and 2 equivalents of Zn^{2+} (**Figure 2-8**), and should be compared to **Figure 2-6**.

The value of the *cis* to *trans* ratio changed from 1.37±0.00 to 5.02±0.00 after addition of 0.50 equivalents of Zn^{2+}. This shows that the *cis* isomers are becoming more stable than the *trans*- isomer as Zn^{2+} is added. In addition, there is an alteration of chemical shift of about 0.29 ppm for the *cis*(A) signal relative to *cis*(A) in **Figure 2-7**, which is significant in comparison to the changes of 0.05 ppm for *cis*(B) and 0.03 ppm for the trans signal. These spectral changes can be understood using the equilibria presented in **Figure 2-9**. The changes in *cis* to *trans* ratio imply that K_c is significantly larger than K_t. Having had one set of signals for each isomer **in Figure 2-9**, may suggest the fast addition and loss of Zn^{2+} species to the Co complex.

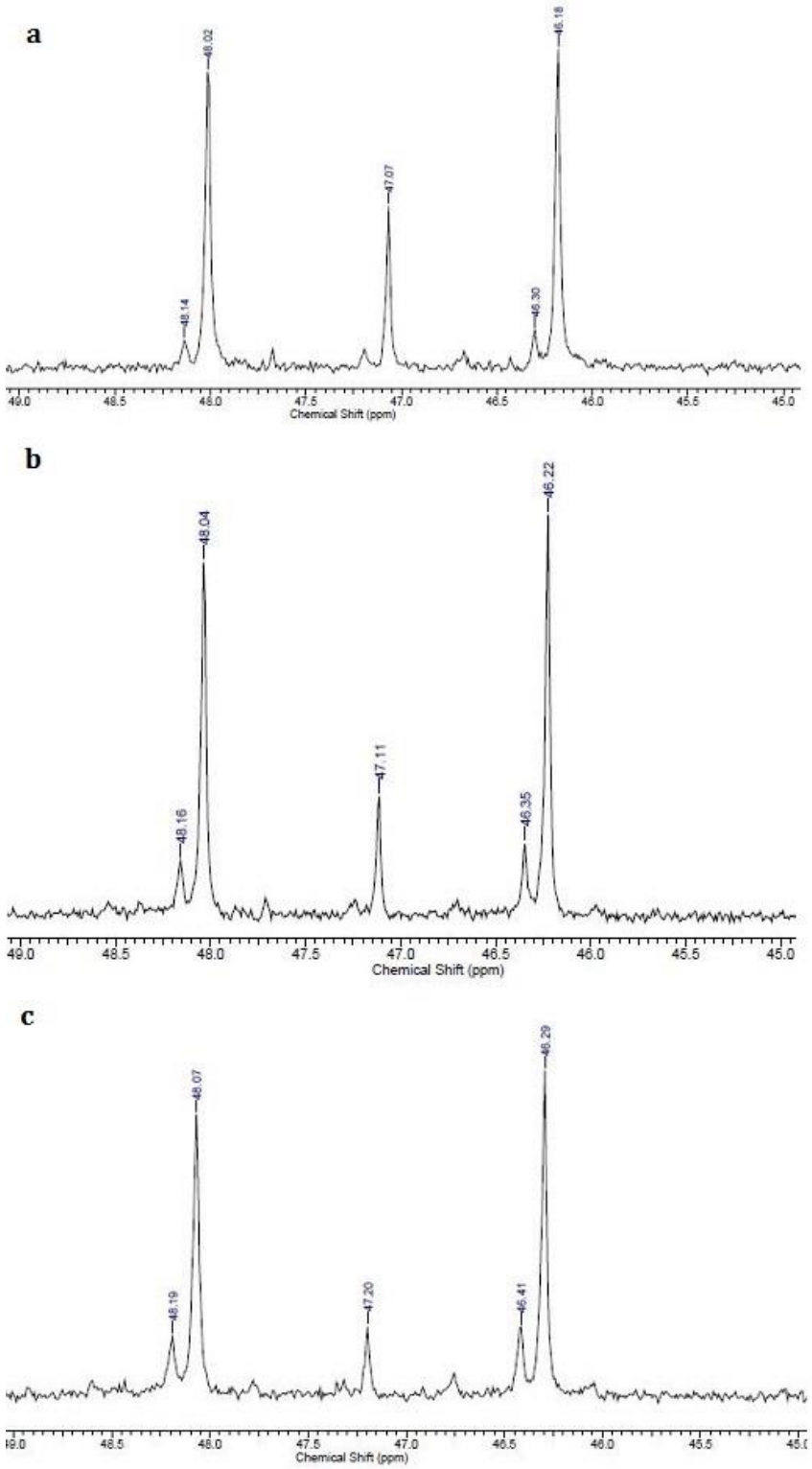

Figure 2-8 a) The ^{13}C NMR spectrum of $[Co(en)_2(OH)(OH_2)]^{2+}$ after addition of 0.5 equivalent Zn^{2+} in D_2O in presence of TMPS internal standard **b)** The ^{13}C NMR spectrum of $[Co(en)_2(OH)(OH_2)]^{2+}$ after addition of 1 equivalent Zn^{2+} in D_2O in presence of TMPS internal standard **c)** The ^{13}C NMR spectrum of $[Co(en)_2(OH)(OH_2)]^{2+}$ after addition of 2 equivalent Zn^{2+} in D_2O in presence of TMPS internal standard

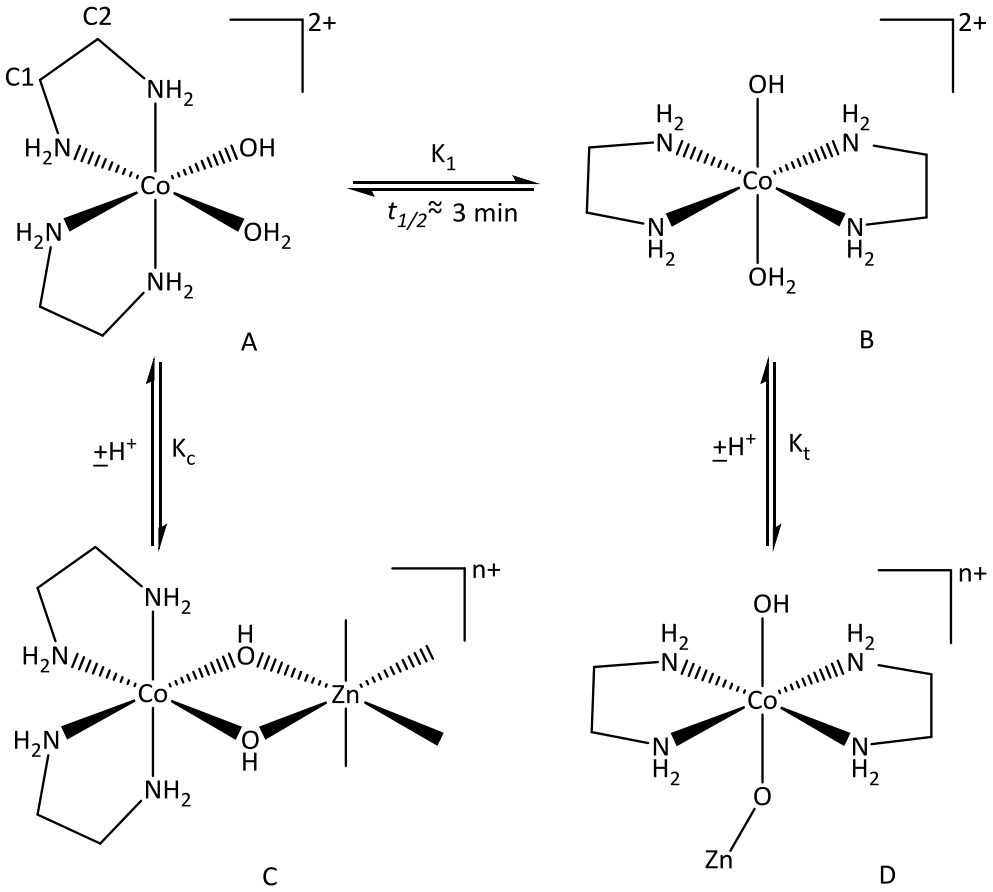

Figure 2-9 Reaction scheme for $[Co(en)_2(OH)(OH_2)]^{2+}$ with zinc metal ions.

K1=[B]/[A], Kc=[C]/[A] and Kt=[D]/[B]

Although, the two *cis* signals are differently affected by addition of the zinc ion (**Figure 2-8**), this cannot clearly be said which of the carbon atoms might be more affected by coordinating to the new metal ion. There are two possible interpretations. Firstly, it could be due to the inductive effect through binding of the hydroxide ligands to the Zn^{2+} ion. In this situation, the carbon atoms (C1) on amines in position *trans* to the hydroxide ligands may be affected more (**Figure2-7**).

Alternatively, there is a possibility of hydrogen bonding between hydrogen atoms of the zinc complex and the hydrogen atoms on amines in *cis* positions relative to the hydroxide ligands of the cobalt complex possibly mediated by a water molecule as is shown below (**Figure 2-10**). In the latter case, the chemical environment of C2 (**Figure 2-7**) may experience a greater effect, which results in chemical shift changes.

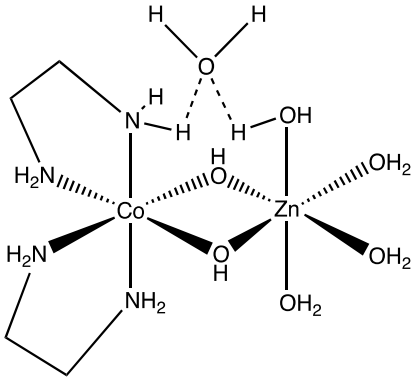

Figure 2-10. Possible hydrogen bonding between Co(μ-OH)$_2$Zn complex

In a separate experiment, 8 equivalents of Zn^{2+} were added in one aliquot. Results showed that even with a large excess addition of metal ion there was still some *trans* isomer. The value of the *cis* to *trans* ratio after a single addition of 8 equivalents of Zn^{2+} is 14.00±0.05 and this value for the sequential addition of Zn^{2+} is 13.85±0.10 which is very similar, indeed just barely within the experimental error of each other. After a single addition of 8 equivalents of Zn^{2+}, the small *cis* peaks next to the large *cis* peaks, assigned to deuterium exchange, were still observed but they were of lower intensity, which is consistent with assignments of those peaks.

The reaction between $[Co(en)_2(OH)(OH_2)]^{2+}$ and $Zn(ClO_4)_2$ was repeated with $Zn(NO_3)_2$. Since similar results were obtained with the $Zn(NO_3)_2$ salt, we can conclude that this kind of

reaction appears to be independent of the anion, at least when the anion is relatively non-coordinating.

Similar results were obtained for the $Cd(NO_3)_2$ salt. However, the change in *cis*:*trans* ratio for Cd^{2+} is less than Zn^{2+}. Changes in chemical shifts and *cis*:*trans* ratio with addition of different equivalents of Zn^{2+}/Cd^{2+} are illustrated in **graphs 2-1**, **2-2** and **2-3**.

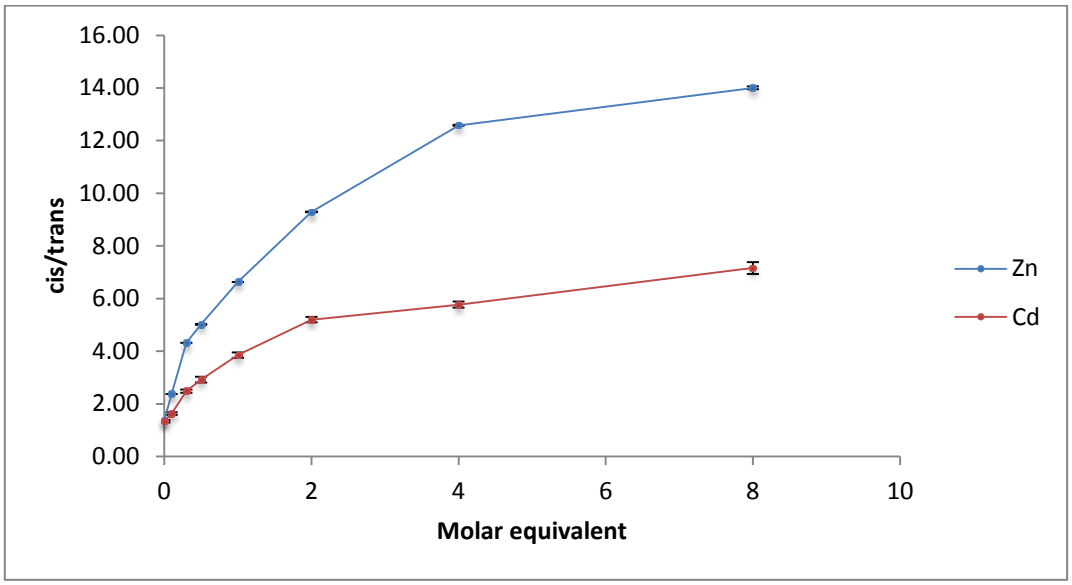

Graph 2-1 *Cis*:*trans* ratio of $[Co(en)_2(OH)(OH_2)]^{2+}$ as a function of added molar equivalents of Zn^{2+}/Cd^{2+}. The lines joining the data points are merely for clarity

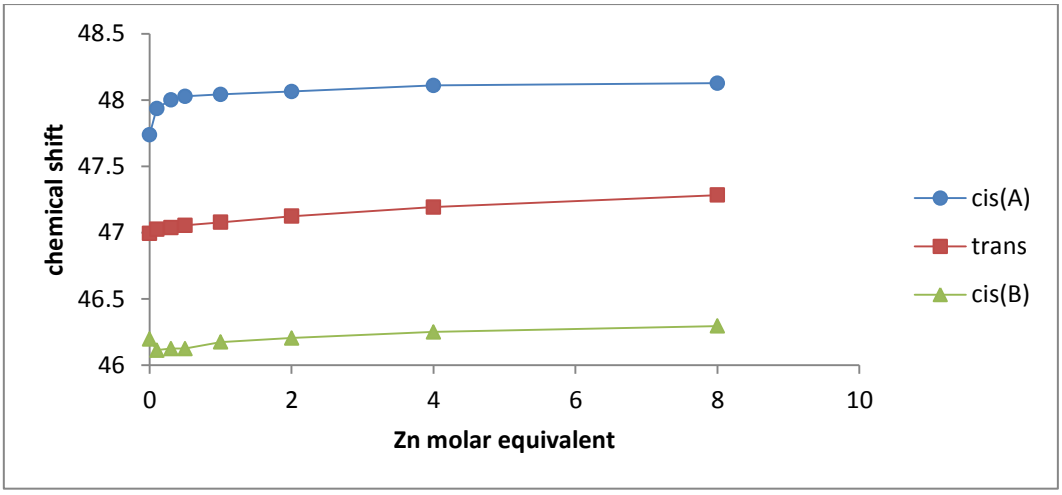

Graph 2-2 Chemical shift of $[Co(en)_2(OH)(OH_2)]^{2+}$ as a function of added molar equivalents of to Zn^2. Standard errors on this graph's data points and the succeeding ones are too small to be plotted. Chemical shifts were measured relative TMPS internal standard.

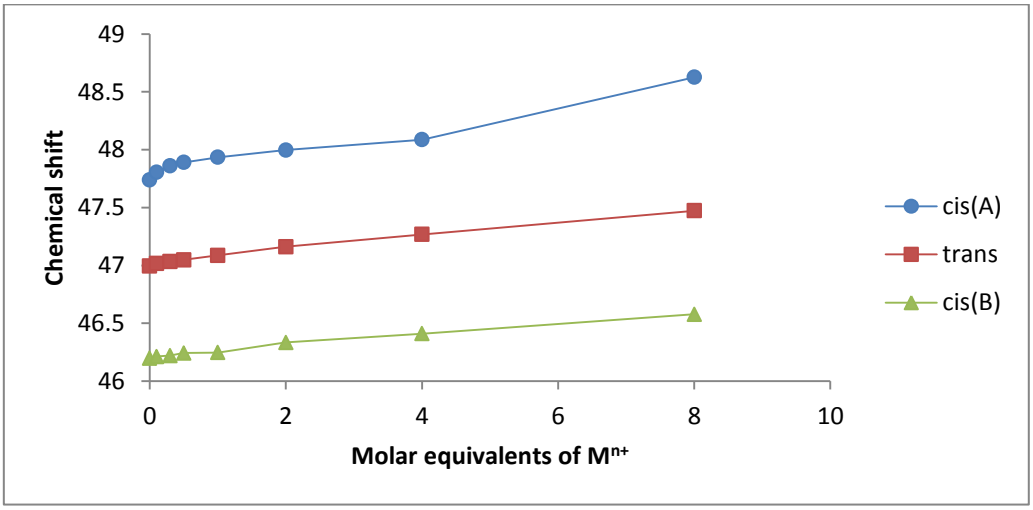

Graph 2-3 Chemical shift of $[Co(en)_2(OH)(OH_2)]^{2+}$ as a function of added molar equivalents of Cd^{2+}. Chemical shifts were measured relative TMPS internal standard.

The ^{13}C NMR titration was repeated for four other diamagnetic metal ions (using the nitrate salts: $LiNO_3$, $AgNO_3$, KNO_3 and $Mg(NO_3)_2$). Results obtained from ^{13}C NMR spectra of these metals are illustrated **Graphs 2-4**, **2-5**, **2-6**, **2-7** and **2-8**. The graphs show there are not

significant changes in *cis*/*trans* ratio and chemical shifts after addition of Li^+, Ag^+, K^+ and Mg^{2+} metal ions to the Co complex.

After addition of Li^+ very small changes were seen in the ^{13}C NMR spectrum. The ratio of *cis* to *trans* isomers only changed from 1.32±0.00 to 1.50±0.00. Even the addition of a large excess did not change the *cis* to *trans* ratio. The chemical shift of the *cis* signals and the *trans* signal were changed equally, about 0.11 ppm as 8 equivalents of Li^+ added.

By addition of K^+, very slight changes were seen in the ^{13}C NMR spectrum of cobalt complex. The ratio of *cis* to *trans* isomers only changed from 1.32±0.00 to 1.49±0.01. After addition of 8 equivalents of K^+, chemical shifts of cis(A) and cis(B) were changed equally (0.08), and more than the trans signal (0.07).

Considering chemical shifts, *cis* to *trans* ratio and equilibria (**Figure 2-9**), K_C is bigger than K_t for these metal ions. However, the difference is not large, so we conclude that these metal ions do not change the equilibrium between *cis* and *trans* significantly and there is less significant interaction between cobalt complex and K^+/Li^+ metal ions than others.

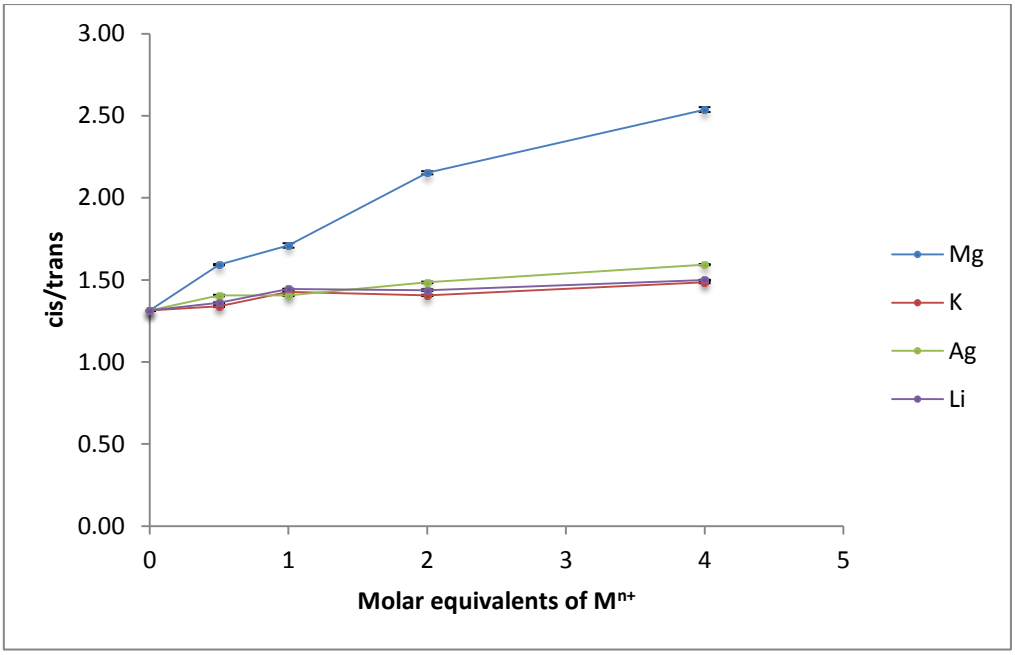

Graph 2-4. *Cis*:*trans* ratio of $[Co(en)_2(OH)(OH_2)]^{2+}$ as a function of molar equivalents of $Li^+/K^+/Mg^{2+}/Ag^+$. The lines joining the data points are merely for clarity

After addition of Mg^{2+} and Ag^+ to $[Co(en)_2(OH)(OH_2)]^{2+}$, the *cis* to *trans* ratio value was changed from 1.32±0.01 to 2.54±0.05 and 1.59±0.01, respectively. The chemical shift of the *cis*(A) signal for both Mg^{2+} (0.25 ppm) and Ag^+ (0.32 ppm) metal ions was changed more than that of Li^+ and K^+. Mg^{2+} metal ion has the biggest K_c in comparison with K^+, Li^+ and Ag^+ and it can be said that Mg^{2+} perturbs the equilibrium more. It might be because 2+ metal ions are better Lewis acids than 1+ charged ones. Having said that, among metal ions with a 1+ charge, the silver ion changes the equilibrium more than other ions, presumably because it has stronger interactions with the cobalt complex.

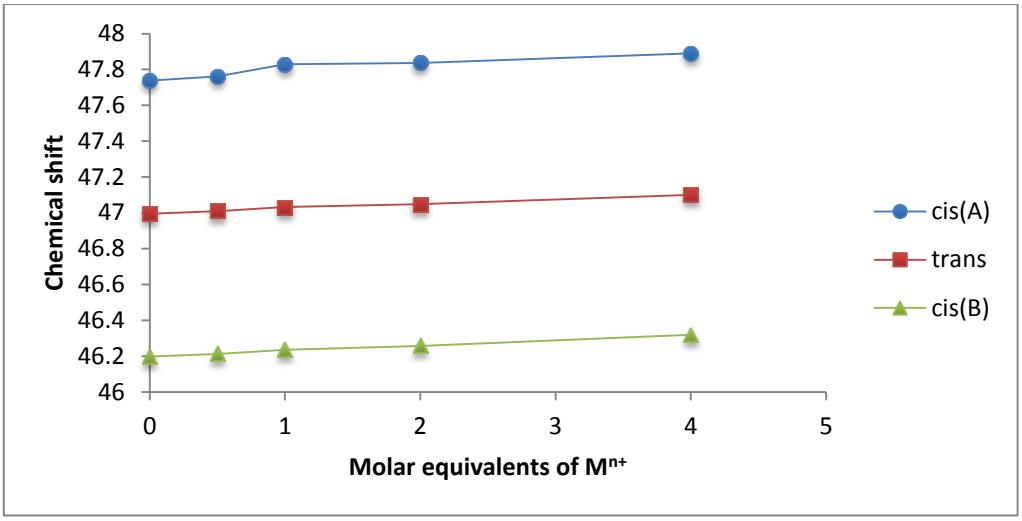

Graph 2-5. Chemical shift of $[Co(en)_2(OH)(OH_2)]^{2+}$ as a function of added molar equivalents of Li^+. Chemical shifts were measured relative TMPS internal standard

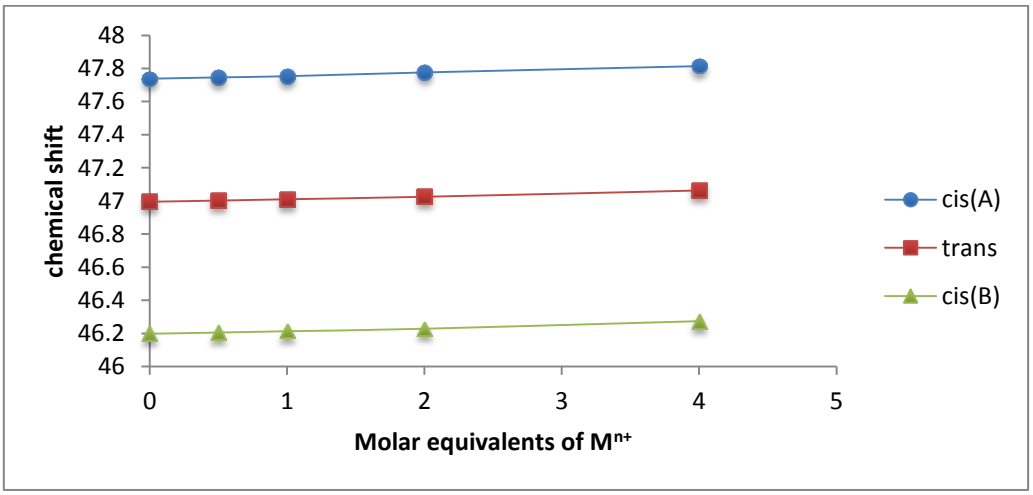

Graph 2-6. Chemical shift of $[Co(en)_2(OH)(OH_2)]^{2+}$ as a function of added molar equivalents of K^+. Chemical shifts were measured relative TMPS internal standard

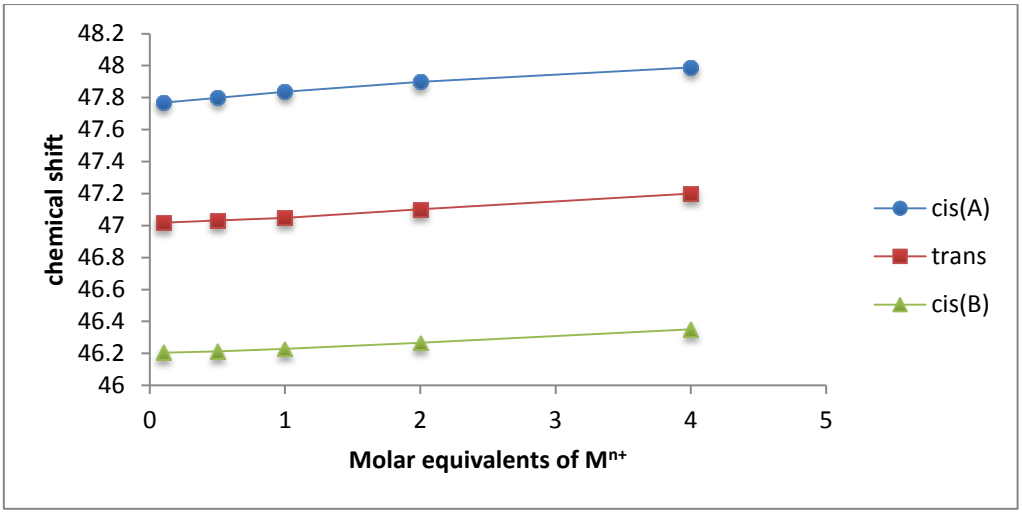

Graph 2-7. Chemical shift of $[Co(en)_2(OH)(OH_2)]^{2+}$ as a function of added molar equivalents of Mg^{2+}. Chemical shifts were measured relative TMPS internal standard

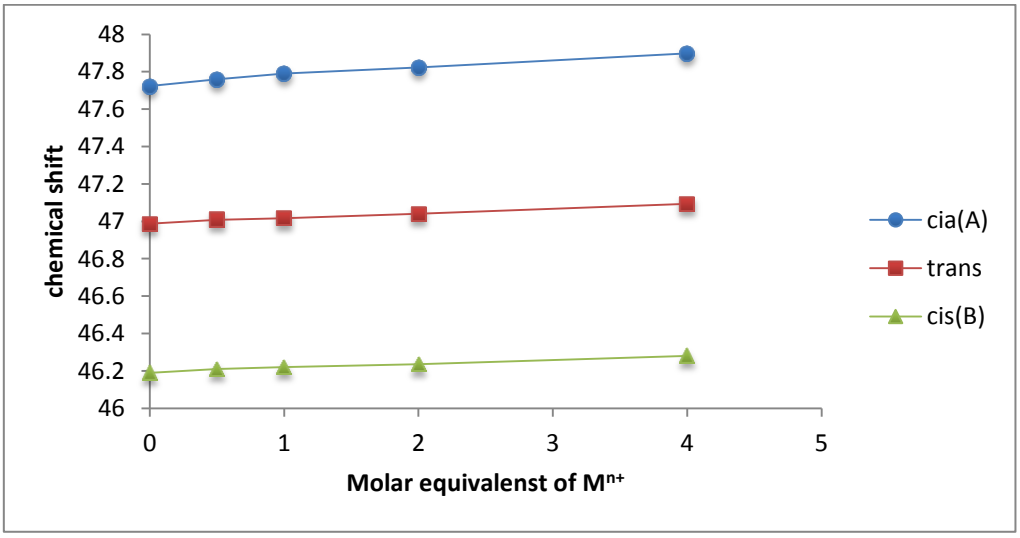

Graph 2-8. Chemical shift of $[Co(en)_2(OH)(OH_2)]^{2+}$ as a function of added molar equivalents of Ag^{+}. Chemical shifts were measured relative TMPS internal standard

2.4.2 Studies with labile paramagnetic metal ions

Since the NMR technique can still be usefully applied to solutions containing low concentrations of paramagnetic samples, we have also monitored the progress of reactions

between $[Co(en)_2(OH)(OH_2)]^{2+}$ and paramagnetic metal ions Cu^{2+}, Ni^{2+} and Fe^{2+} (as their NO_3^- salts) using ^{13}C NMR spectroscopy.

The ^{13}C NMR spectrum of $[Co(en)_2(OH)(OH_2)]^{2+}$ and the ^{13}C NMR spectrum of this complex after addition of 0.1 equivalents of Cu^{2+} in the presence of 1,4-dioxane as an internal standard are shown in **Figure 2-11**.

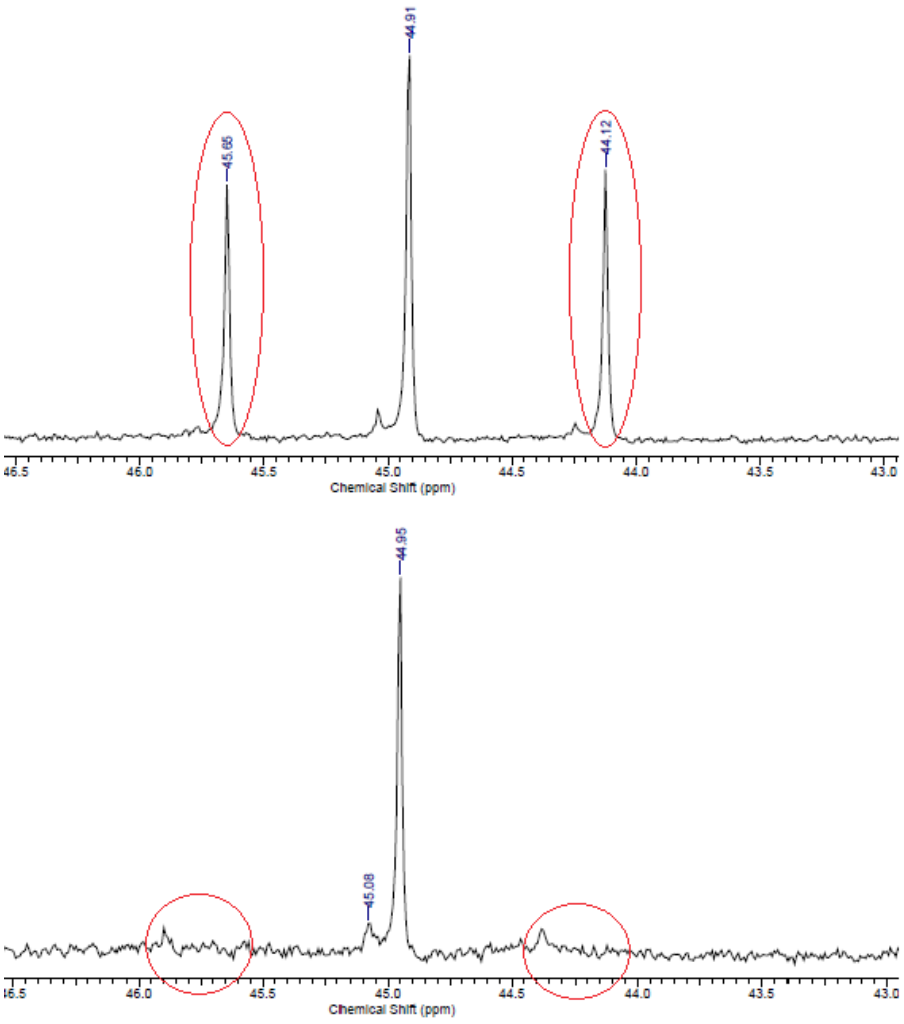

Figure 2-11. Top: The ^{13}C NMR spectrum of $[Co(en)_2(OH)(OH_2)]^{2+}$ in D_2O with 1,4-dioxane added as an internal standard for comparison of chemical shift, set at 66.66 ppm, and to determine chemical shifts and for comparison of integrations. **Bottom**: The ^{13}C NMR spectrum of $[Co(en)_2(OH)(OH_2)]^{2+}$ after addition of 0.1 equivalent Cu^{2+} in D_2O.The broadened signals are circled.

As shown in **Figure 2-11b**, after addition of 0.1 equivalents of Cu^{2+}, the *cis* signals of $[Co(en)_2(OH)(OH_2)]^{2+}$ have been significantly broadened, to the point that they are barely observable above the baseline. This provides strong evidence of a close association of the Cu^{2+} ions with the *cis* isomer. It can be said that there must be a rapid exchange, as only a small amount of Cu^{2+} affects all of the *cis* isomer. Having said that, the *trans* signal appears to be largely unaffected, from which we can infer that little, if any, Cu^{2+} can be bound to *trans*-$[Co(en)_2(OH)(OH_2)]^{2+}$.

The results obtained from the ^{13}C NMR spectrum of $[Co(en)_2(OH)(OH_2)]^{2+}$ after successive addition of Cu^{2+} are shown in **Table 2-1**.

Cu^{2+} equivalent	*Trans*:dioxane integration ratio	FWHM of *trans* signal	FWHM of dioxane
0	5.00	2.153	1.485
0.1	3.48	2.058	1.249
0.2	1.32	2.8035	2.120
0.3	0.59	3.1505	2.818

Table 2-1 The ^{13}C NMR spectral data of $[Co(en)_2(OH)(OH_2)]^{2+}$ after addition of Cu^{2+} in presence of dioxane to determine chemical shifts and allow us to compare integrations.

The presence of the internal standard allows monitoring of the position of the *cis* to *trans* equilibrium, even though the *cis* signals could not be integrated, because the amount of the *cis* isomer can be inferred using the integrations of the *trans* isomer and the internal standard before and after addition of the paramagnetic ions. Another expectation was that if binding between *trans*-$[Co(en)_2(OH)(OH_2)]^{2+}$ and paramagnetic metal ions does occur, broadening of the *trans* signal would be observed. For this reason, the full width at half

maximum (FWHM) was measured. However, due to the fact that width at the half height of *trans* and dioxane signals change consistently with each other, the possibility of binding to the *trans* isomer cannot be evaluated.

The integration of the *trans* to dioxane signal decreased from 5.00 to 0.59 as 0.3 equivalents of Cu^{2+} added. After addition of more than 0.3 equivalents of Cu^{2+}, the signal to noise ratio decreased to an extent that integration became impossible. Thus, in order to get a better signal to noise ratio we increased the collection time from 10 min to 1 hr. In addition, we changed some parameters for the NMR experiment, in an effort to improve the appearance of the spectrum. Relaxation delay and acquisition time were decreased accordingly, from 1 to 0.5 which enabled us to compare the spectra with earlier spectra.

Unlike Cu^{2+}, after addition of Ni^{2+}, *cis* signals were seen in ^{13}C NMR spectrum. This may mean that at low addition ratios the Ni^{2+} ions are square planar and therefore diamagnetic, but that addition of more than 0.5 eq might lead to paramagnetic octahedral Ni^{2+} species being present in solution. The progress of the reaction was monitored by the *cis* to *trans* ratio and also by following the change in chemical shifts (**Figures 2-12a and 2-12b**).

The presence of additional signals in **Figure 2-12b** may be because of the formation of different stereoisomers, which will be explained later in the chapter, in the section that addresses the Pt^{2+} and Pd^{2+} metal ions.

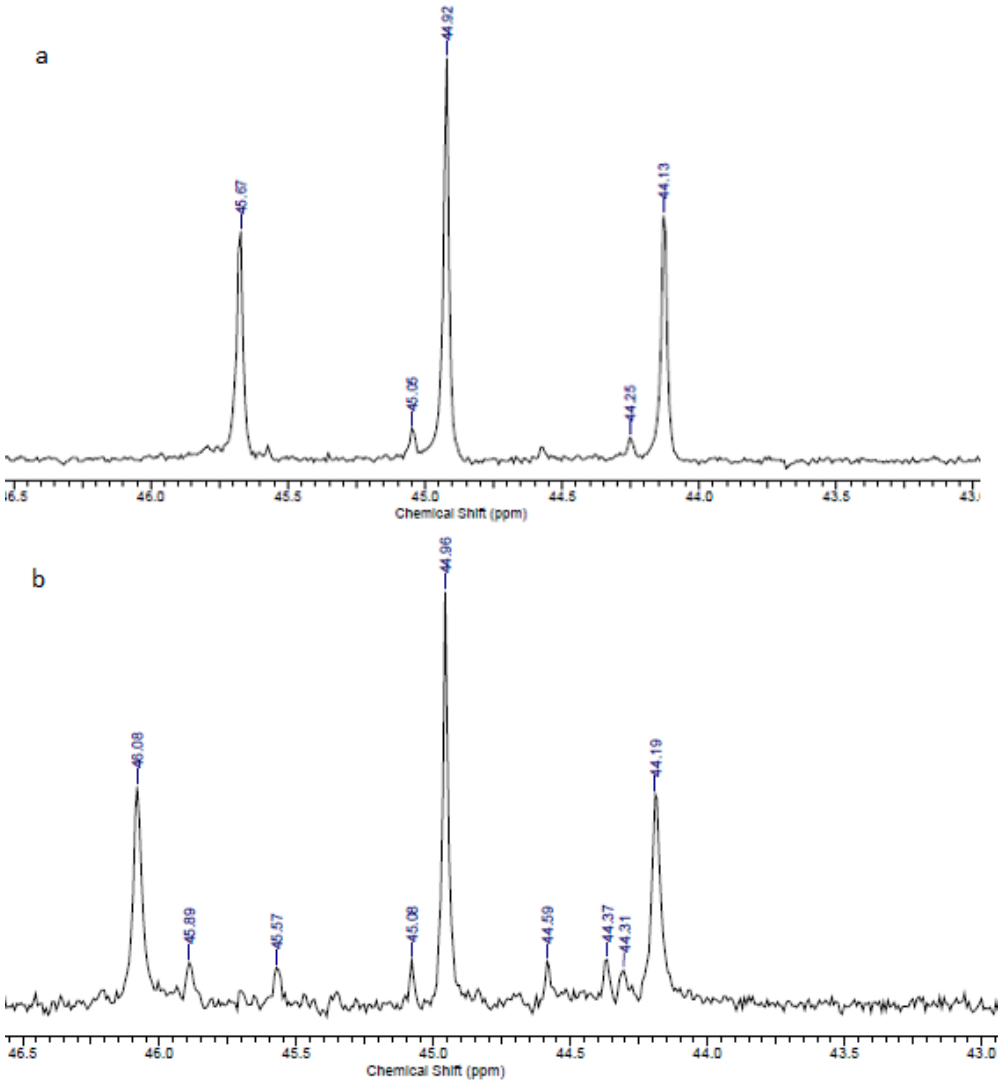

Figure 2-12. a) The ^{13}C NMR spectrum of $[Co(en)_2(OH)(OH_2)]^{2+}$ in D_2O before addition of Ni^{2+} in D_2O in presence of 1,4-dioxane **b)** The ^{13}C NMR spectrum of $[Co(en)_2(OH)(OH_2)]^{2+}$ after addition of 0.1 equivalents of Ni^{2+} in D_2O in presence of 1,4-dioxane to determine chemical shifts for comparison of integrations.

As illustrated in **Figure 2-13** and **Graph 2-10**, the chemical shift of the *cis*(A) changed significantly after addition of 0.1 equivalents of Ni^{2+}.

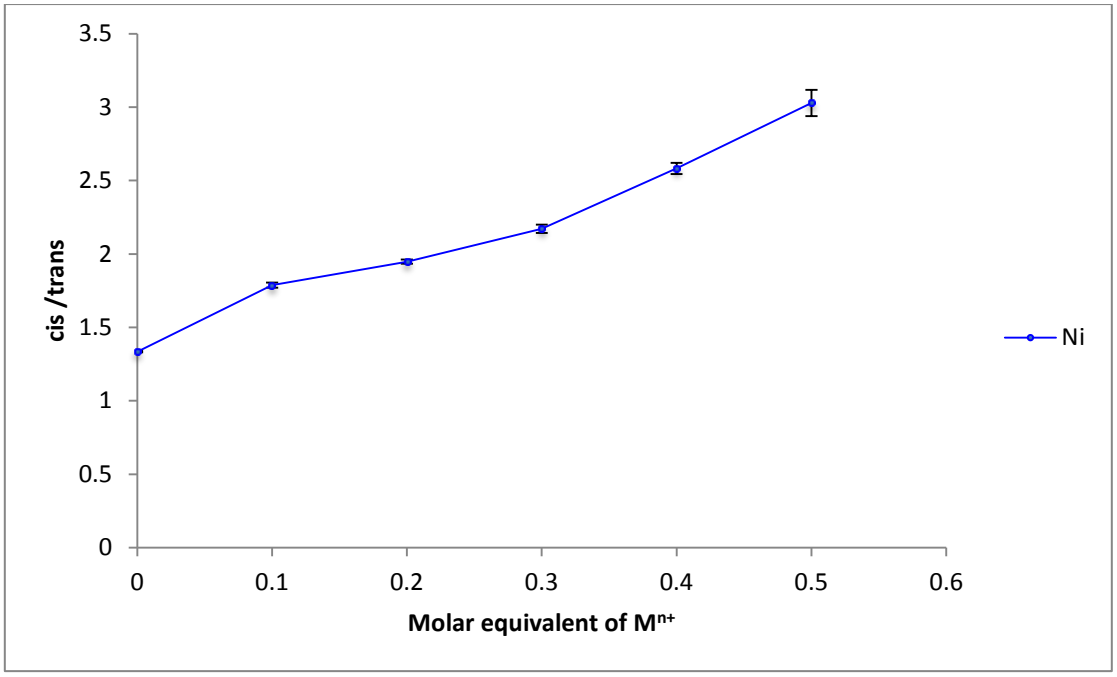

Graph 2-9. *Cis*:*trans* ratio of $[Co(en)_2(OH)(OH_2)]^{2+}$ as a function of added molar equivalents of Ni^{2+} .

The lines joining the data points are merely for clarity

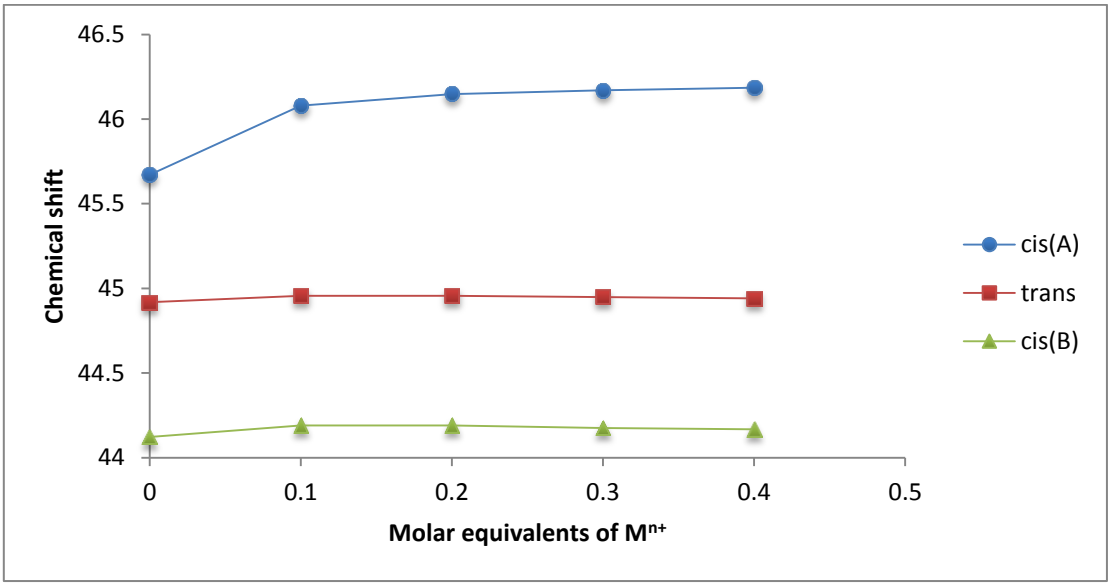

Graph 2-10. Chemical shift of $[Co(en)_2(OH)(OH_2)]^{2+}$ as a function of added molar equivalents of Ni^{2+}

Similar to ^{13}C NMR spectra of $[Co(en)_2(OH)(OH_2)]^{2+}$ with Ni^{2+}, *cis* signals can be seen after addition of Fe^{3+}. Due to having both *cis* and *trans* signals, the progress of reaction was followed by *cis* to *trans* ratio and change in chemical shift.

The colour of the reaction mixture changed from red to brownish orange after addition of Fe^{3+}. We were not able to take NMR spectra for more than 0.2 equivalents of Fe^{3+} due to the error response of the NMR machine, possibly because of the presence of paramagnetic metal ions. Results obtained from addition of 0.1 and 0.2 equivalent Fe^{3+} are shown below (**Graph 2-11** and **Graph 2-12**).

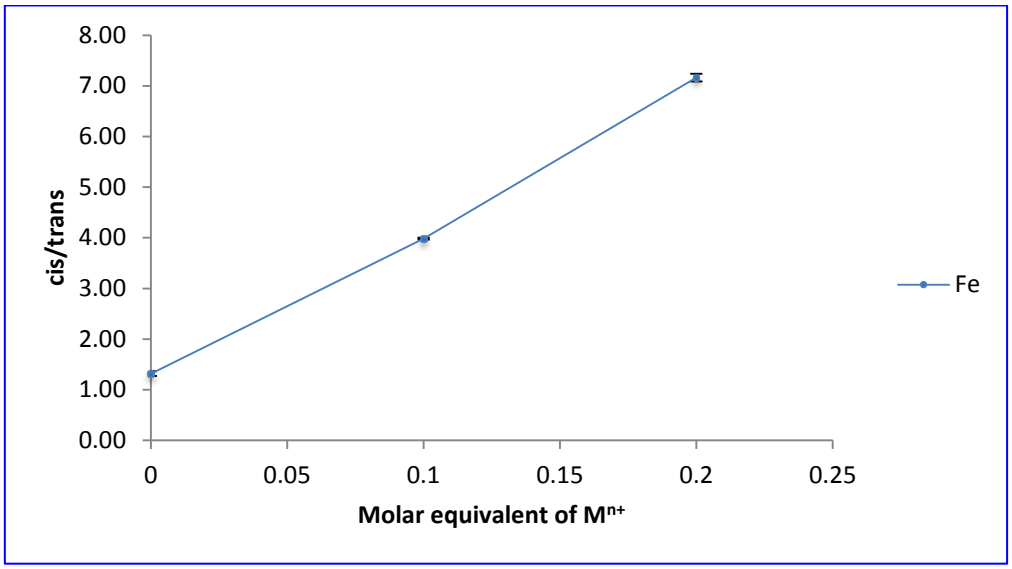

Graph 2-11. *Cis*:*trans* ratio of $[Co(en)_2(OH)(OH_2)]^{2+}$ as a function of added molar equivalents of Fe^{3+}. The lines joining the data points are merely for clarity

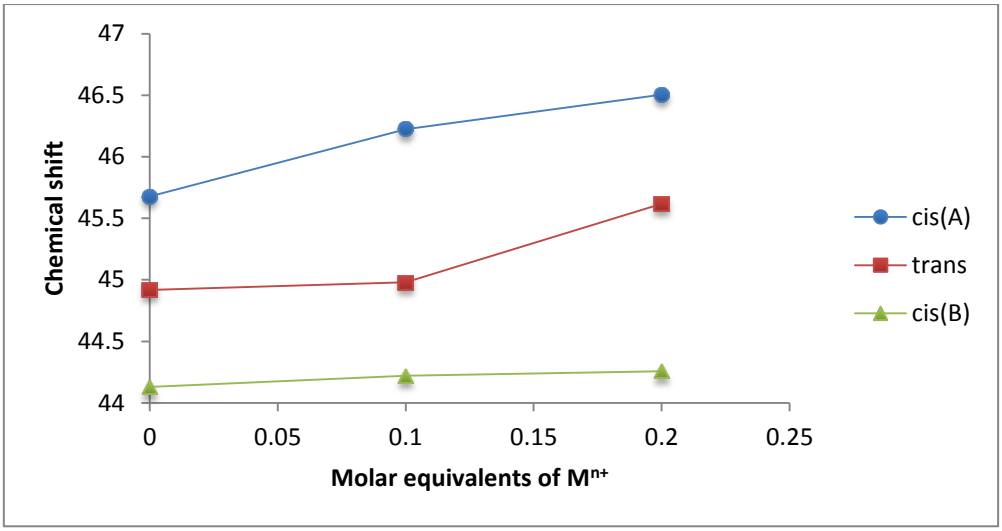

Graph 2-12. Chemical shift of $[Co(en)_2(OH)(OH_2)]^{2+}$ as a function of added molar equivalents of Fe^{3+}. Chemical shifts were measured raltive 1,4-dioxane internal standard

From **Graph 2-11** we can see that the *cis* to *trans* value increased remarkably from 1.32±0.04 to 7.16±0.07 after addition of 0.2 equivalent of Fe^{3+}. In addition, a significant change can be seen for *cis*(A) and *trans* signals in **Graph 2-12**. These two observations are strong enough for us to infer association of Co^{2+} and Fe^{3+} through hydroxido bridging ligands.

2.4.3 Studies with Pt^{2+} and Pd^{2+} metal ions

After addition of 0.2 equivalents of $K_2[PtCl_4]$ to an aqueous solution of $[Co(en)_2(OH)(OH_2)]^{2+}$ and removal of any resulting precipitate ($(Co(\mu\text{-}OH)_2Pt)$ complex), a small signal appeared at 39.23 ppm. As more equivalents of Pt^{2+} were added, the intensity of this signal increased. From the chemical shift of the new signal, we suspected loss of ethane-1,2-diamine as Pt^{2+} was added and to confirm this, some ethane-1,2-diamine was added and the intensity of the peak increased. Another observation was extra signals in the region where the *cis* and *trans*

peaks of the starting material would normally be observed. **Figure 2-13** shows the ^{13}C NMR spectrum of Co^{2+} complex after addition of 1 equivalent of the Pt^{2+} metal ion.

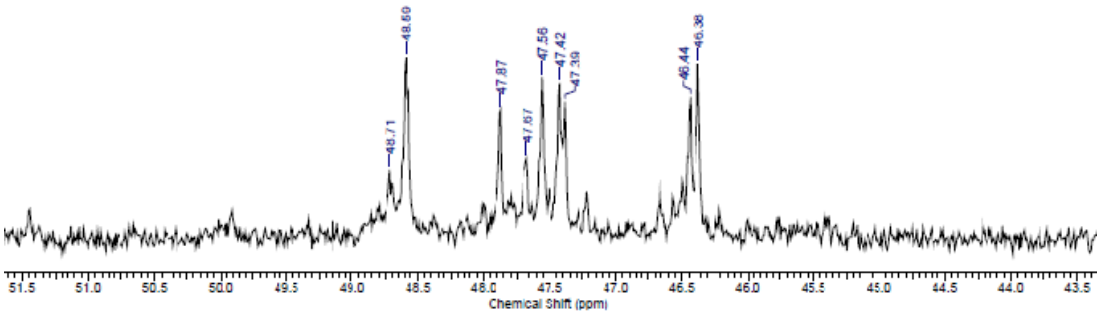

Figure 2-13. The ^{13}C NMR spectrum of $[Co(en)_2(OH)(OH_2)]^{2+}$ solutions after addition of 1 equivalent of Pt^{2+} in D_2O in presence of TMPS internal standard.

The reaction between $K_2[PdCl_4]$ and $[Co(en)_2(OH)(OH_2)]^{2+}$ showed similar results to that of Pt^{2+}. As illustrated in **Figure 2-14**, there are extra signals, similar to those observed in the case of Pt^{2+}. According to the intensity of the signals and also the chemical shifts that they appear at, they may not be related to the deuterium isotope exchange phenomenon.

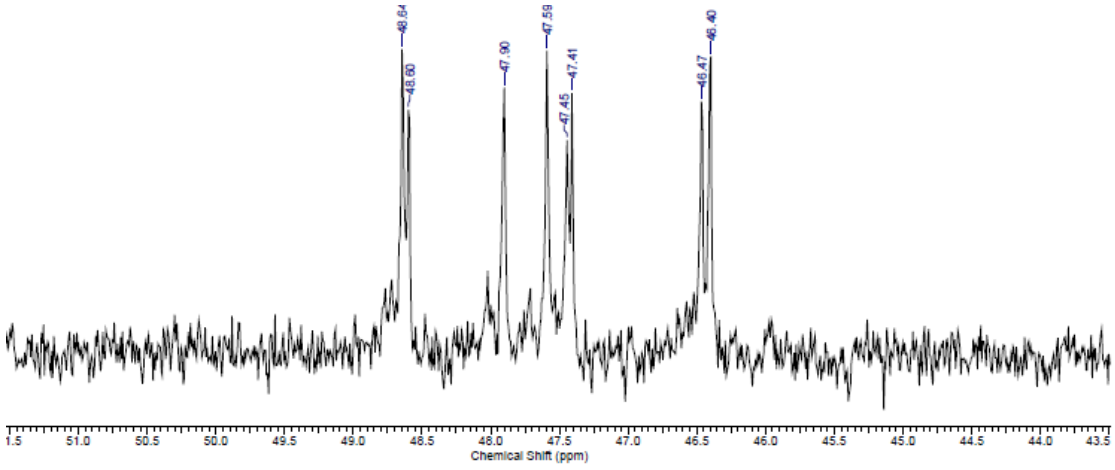

Figure 2-14. The ^{13}C NMR spectrum of $[Co(en)_2(OH)(OH_2)]^{2+}$ after addition of 1 equivalent of Pd^{2+} in D_2O in presence of TMPS internal standard.

Addition of $K_2[PtCl_4]$ or $K_2[PdCl_4]$ results in the formation of precipitates in solution. To see if the obtained powders are the same as the crystals reported in the literature (**Figure 2-15**) [116], X-ray powder diffraction experiments were performed. Results presented in **Figure 2-16** show that the powders are the same as the dinuclear complex, $[(en)_2Co(\mu\text{-}OH)_2MCl_2]^+$ (M = Pd, Pt), found by X-ray diffraction (**Figure 2-15**) [116].

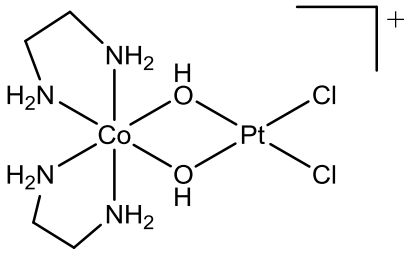

Figure 2-15 Structure of $[(en)_2Co(\mu\text{-}OH)_2PtCl_2]^{+1}$, found by X-ray diffraction[116]

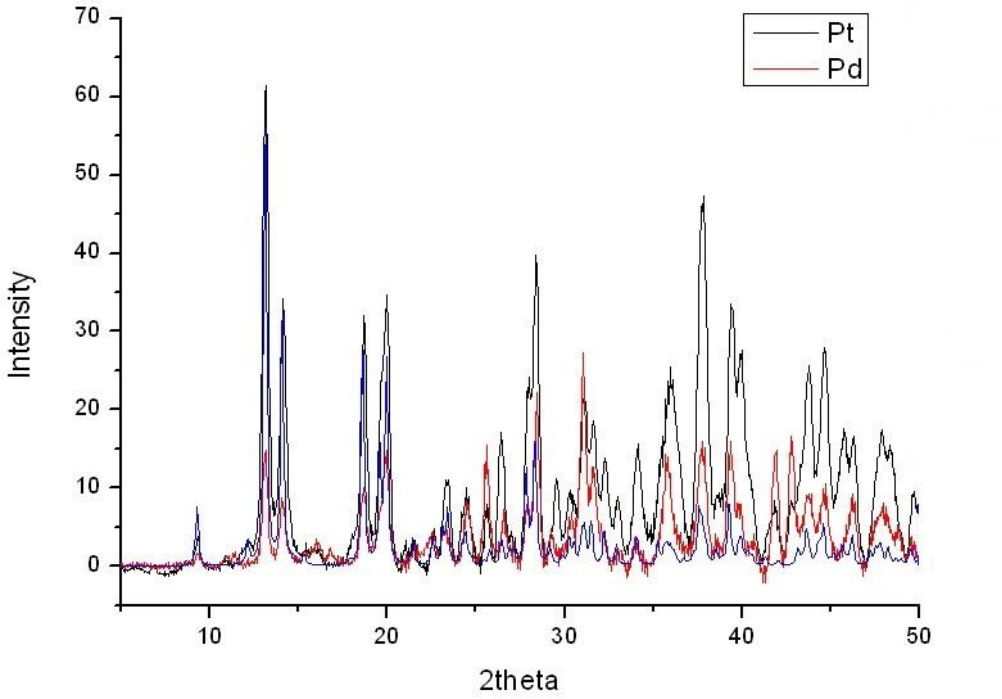

Figure 2-16. Powder diffraction of Co-Pt and Co-Pd complexes compared with calculated powder diffraction of the crystal reported in literature (**Figure 2-15**) [116]. Blue, red and black lines refer to powder diffraction patterns of Co-Pt crystal, Co-Pd complex and Co-Pt complex.

If we suppose that a complex with four bridging hydroxide ligands (**Figure 2-17**) is formed in solution, there is the possibility of having several stereoisomers.

If complexes such as that shown in **Figure 2-17** are formed, there might be ΔΔ-, ΛΛ- and ΔΛ-configurations for two the cobalt centres and additional signals will be observed in the NMR spectra.

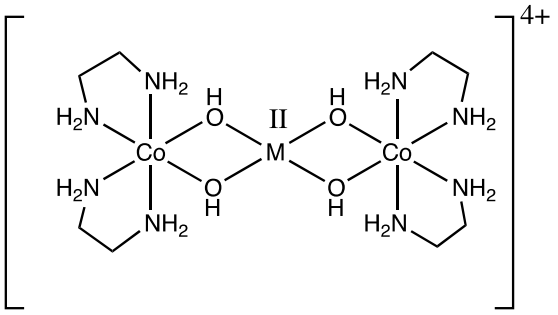

Figure 2-17. Proposed structure for Pd^{2+} and Pt^{2+} metal ions in solution when they react with $[Co(en)_2(OH)(OH_2)]^{2+}$.

2.5 Conclusion

In this work, we presented NMR studies of the formation of diamagnetic and paramagnetic $[\{Co(\mu\text{-}OH)_n\text{-}M\}_m]$ complexes (M=Li, K, Mg, Ag, Cd, Zn, Pt, Pd, Cu, Ni and Fe) in solution.

The ^{13}C NMR study showed that there is an equilibrium between the *cis* and *trans* $[Co(en)_2(OH)(OH_2)]^{2+}$ complexes. In the case of diamagnetic metal ions, the equilibrium between the *cis* and *trans* isomer of the Co complex shifts toward the cis isomer after addition of metal ions. In addition, the elimination of cis peaks in the ^{13}C NMR after the addition of paramagnetic metal ions, showed the association of metal ions with the cis isomer of the Co complex.

Formation of $[Co(\mu\text{-}OH)_2\text{-}M]$ (M=Pd and Pt) complexes have been demonstrated by X-ray crystallography[116]. However, ^{13}C NMR spectroscopy shows that the reaction of

$[Co(en)_2(OH)(OH_2)]^{2+}$ complex with Pt^{2+} and Pd^{2+} species produces several other complexes in addition to the dinuclear complexes observed in the solid state.

Chapter 3

Dinuclear Amine-Cobalt(III)-Platinum(II)

Complexes

Chapter 3. Dinuclear Amine-Cobalt(III)-Platinum(II) Complexes

3.1 Introduction

There is not much literature precedent for the synthesis of heterodinuclear cobalt-platinum complexes with hydroxido bridging ligands. To our knowledge, the molecule shown in **Figure 3-1** is the only [Co(μ-OH)$_2$Pt] complex reported in the literature. Although this molecule does not involve a cisplatin derivative, it does show that such a synthesis should be possible. This cobalt-platinum heterodinuclear complex was synthesised *via* a reaction between [(en)$_2$Co(H$_2$O)$_2$](ClO$_4$)$_3$ and K$_2$[PtCl$_4$] [121]. As it is shown in **Figure 3-1**, two metal centres are bound to each other by di-hydroxido bridging ligands.

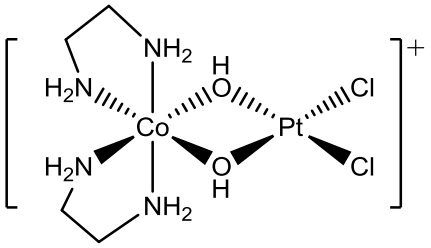

Figure 3-1 The structure of [Cl$_2$Pt(μ-OH)$_2$Co(en)$_2$]$^+$, drawn from the crystal structure. [121]

3.2 Results and Discussion

3.1.1 Dinuclear Cobalt-platinum Complexes

The aim of this study was to produce novel heterodinuclear Co(III)(μ-OH)Pt(II) metal complexes within the context of delivering platinum anti-cancer drugs to targeted sites in the body

3.1.1.1 $[(en)_2Co(\mu\text{-}OH)_2Pt(chda)]^{3+}$ (3.2)

The synthetic route to produce the title complex is presented in **Scheme 3-1**. (cyclohexane-1,2-diamine)diiodidoplatinum(II) ($[Pt(chda)I_2]$ was treated with silver nitrate for 2 days[125]. The silver iodide precipitate was removed by centrifugation and the supernatant was reacted with $[Co(en)_2(OH)(OH_2)]^{2+}$. The reaction mixture was stirred for 3 days.

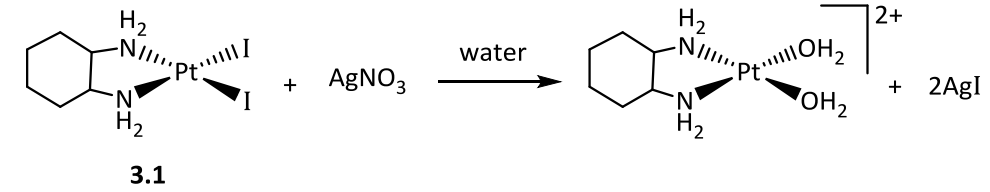

3.1

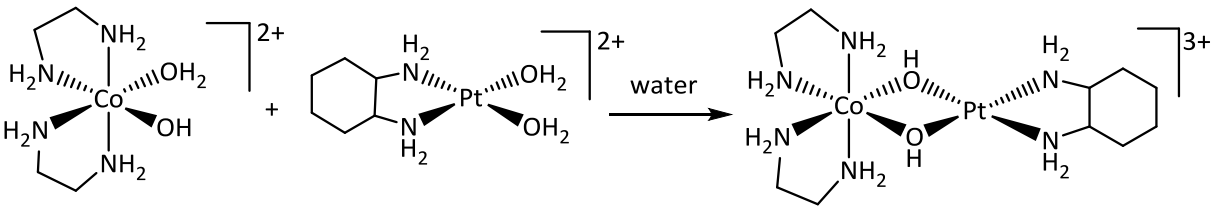

2.1 **3.2**

Scheme 3-1 Synthetic route to obtain the $[(en)_2Co(\mu\text{-}OH)_2Pt(chda)]^{3+}$ complex

The crude compound was purified using cation exchange chromatography on CM Sephadex. The column was eluted with $NaNO_3$ solutions. The first band was collected and then desalted by using size exclusion column chromatography on Sephadex G10. Ultimately, the first band from the CM Sephadex column was isolated as a pink powder. Crystals from the first fraction were obtained by vapour diffusion of ethanol into an aqueous solution of the complex. They were characterised by NMR and X-ray crystallography.

X-ray crystallography determined the structure to be $[Co(CO_3)(en)_2](NO_3)$ (**3.3**) as shown in **Figure 3-2**. This compound crystallises with two formula units in the asymmetric unit. Co(III) is octahedrally coordinated to the four N atoms of two en ligands and two O atoms of the carbonato group.

The packing structure of **3.3** is presented in **Figure 3-3**. There is hydrogen bonding observed between O6 of the carbonate ligand and the hydrogen atom on N4, and between O7 and O10 of the nitrate ions and hydrogen atoms on N8 and N3 respectively.

The bond lengths of H4-O6 and H8-O7 are 2.034(4) and 2.059(4) Å respectively. Selected bond lengths and bond angles of **3.3** are shown in **Tables 3-1** and **3-2**.

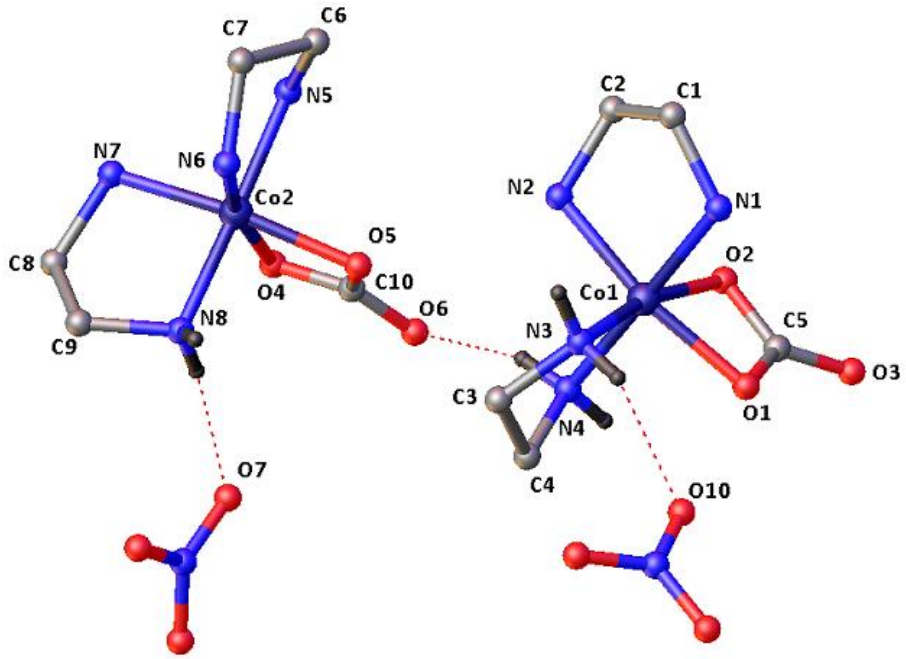

Figure 3-2 The molecular structure of complex **3.3**, hydrogen atoms omitted for clarity.

Selected bond lengths for Co1 [Å]		Selected bond lengths for Co2 [Å]	
Co1-O2	1.926(3)	Co2-O4	1.919(3)
Co1-O1	1.935(4)	Co2-O5	1.926(4)
Co1-N3	1.959(4)	Co2-N5	1.942(4)
Co1-N4	1.944(3)	Co2-N8	1.948(4)
Co1-N1	1.970(5)	Co2-N6	1.948(4)
Co1-N2	1.947(4)	Co2-N7	1.952(5)

Table 3-1 Selected bond lengths [Å] of complex **3.2**

Selected bond angles for Co1 [°]		Selected bond angles for Co2 [°]	
O2-Co1-O1	68.85(15)	O4-Co2-O5	69.02(15)
O2-Co1-N3	167.46(18)	O4-Co2-N5	91.91(16)
O2-Co1-N4	92.77(16)	O4-Co2-N8	90.77(16)
O2-Co1-N2	96.98(16)	O4-Co2-N6	167.25(17)
O1-Co1-N1	89.20(17)	O4-Co2-N7	96.45(17)
O2-Co1-N2	96.98(16)	O5-Co2-N5	90.72(17)
O1-Co1-N3	98.68(17)	O5-Co2-N8	90.68(18)
O1-Co1-N4	90.01(18)	O5-Co2-N6	98.45(17)
O1-Co1-N1	90.80(18)	O5-Co2-N7	165.23(17)
O1-Co1-N2	165.57(16)	N5-Co2-N6	85.69(17)
N3-Co1-N1	92.38	N5-Co2-N7	92.47(19)
N4-Co1-N3	85.72(18)	N8-Co2-N5	177.28(18)
N4-Co1-N1	178.03(16)	N8-Co2-N6	91.79(17)
N4-Co1-N2	93.5(2)	N8-Co2-N7	86.75(19)
N2-Co1-N3	95.54(17)	N6-Co2-N7	96.17(18)

Table 3-2 Selected bond angles [°] of complex **3.3**

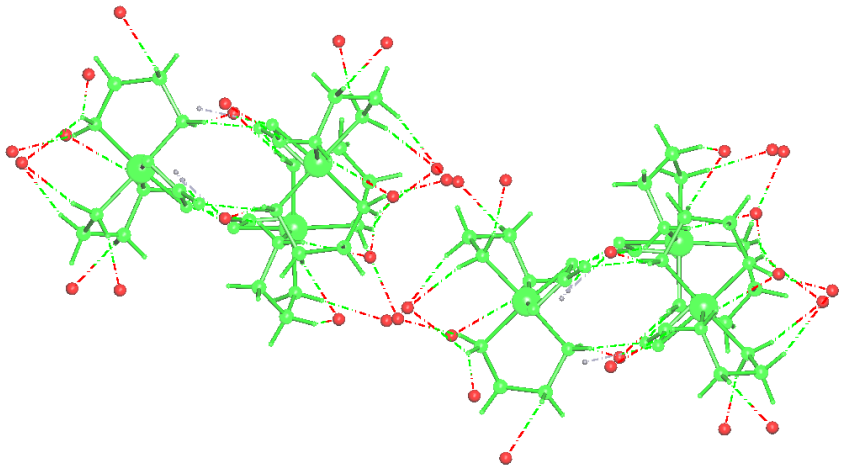

Figure 3-3 Hydrogen bonding network within the crystal lattice of the complex **3.3**. only the oxygen atoms (red) involved in hydrogen bonding are shown.

The crystal structure of $[Co(CO_3)(en)_2](NO_3)\cdot H_2O$ has been published before[126]. The published crystal structure has a water molecule in the structure while our crystal does not. This results in the two structures having different unit cells and space groups. The crystal

data for our crystal and those of the published structure are presented for comparison in **Table 3-3**.

$[Co(CO_3)(en)_2](NO_3)\cdot H_2O$	$[Co(CO_3)(en)_2](NO_3)$
a = 9.407 (2)	a = 11.3918 (7)
b = 23.121 (4)	b = 8.4058 (5)
c = 11.604 (2)	c = 23.4969 (12)
Monoclinic, $P2_1/n$	Monoclinic, $P2_1/c$
α = 90	α = 90
β = 107.315 (3)	β = 96.826 (5)
γ = 90	γ = 90

Table 3-3. Crystal data comparison of $[Co(CO_3)(en)_2](NO_3).H_2O$ and $[Co(CO_3)(en)_2](NO_3)$

The ^{13}C NMR data are consistent with the crystal structure (**Figure 3-4**). The two signals at 43.87 and 44.87 ppm are assigned to the two kinds of carbon atoms of the en ligands. The peak at 166.82 ppm is assigned to the carbon atom of the carbonate ligand. A peak at m/z 239.05 corresponding to $[Co(en)_2CO_3]^+$ was also observed in the mass spectrum.

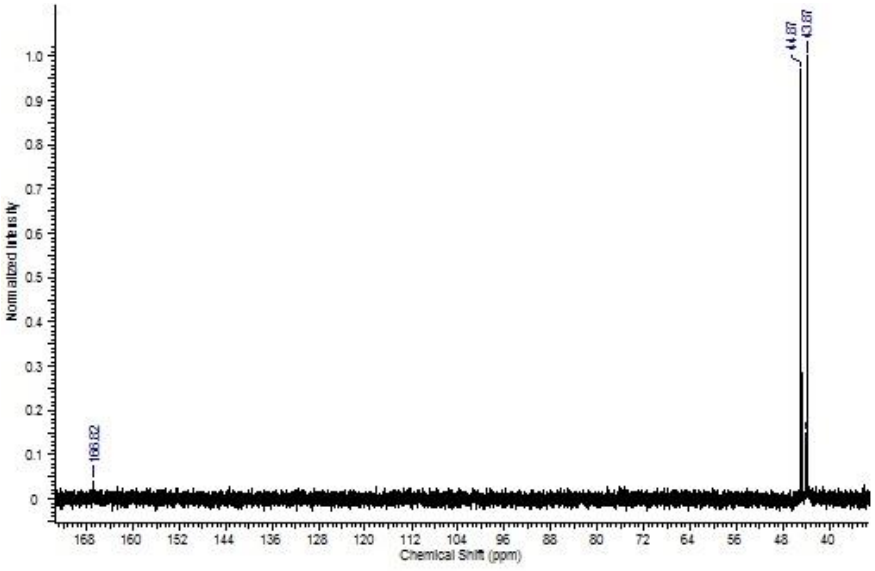

Figure 3-4 The ^{13}C NMR spectrum of **3.3** in D_2O

The desired product, $[(en)_2Co(\mu\text{-}OH)_2Pt(chda)]^{3+}$ (**3.2**), was the principal component of the third band, eluted with 0.3 M $NaNO_3$. The band was collected in fractions of ~50 mL. Each

fraction was desalted by evaporation and then extraction of the complex from the residue by methanol. A desalting procedure, using acetone extraction and then size exclusion column chromatography on Sephadex G10 ultimately gave the complex product as a red slurry. Even after several desalting cycles, some salt remained with the product. This prevented obtaining elemental analysis results for the complex.

The complex was characterised by NMR and mass spectrometry techniques. The isotope pattern at m/z 523.07 is a good match with $([M - 2H)]^+$ (**Figure 3-5**). It is speculated that the ion being detected is $[(en)_2Co(\mu\text{-}O)_2Pt(chda)]^{1+}$; but clearly deprotonation from other sites may be possible.

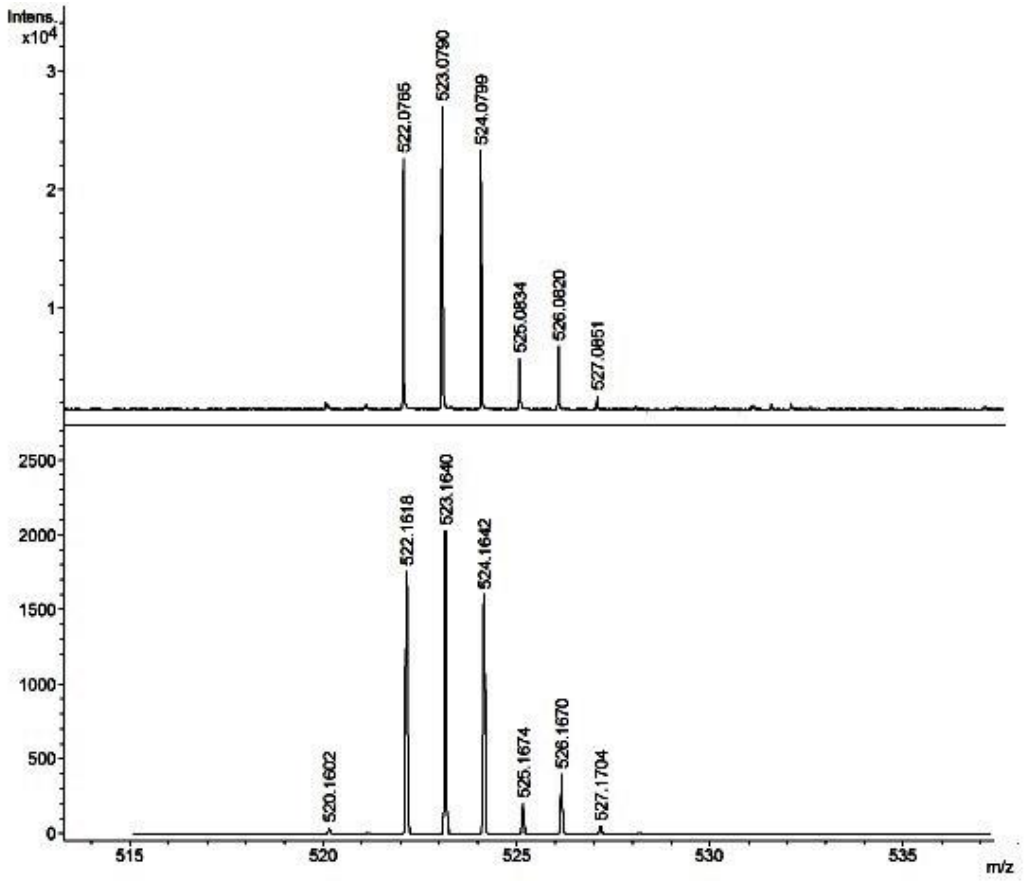

Figure 3-5 Experimental (top) and simulated isotope patterns for the 8.5% abundance mass peak of $[(en)_2Co(\mu\text{-}OH)_2Pt(chda)\text{-}2H^+]^{1+}$ ion

The ^{1}H and ^{13}C NMR Spectra of complex **3.2** were assigned using COSY and HSQC techniques (**Figures 3-6**, **3-7**, **3-8** and **3-9**). The integration value for the en ligands on Co vs chda ligand on Pt is 8 to 10 which is consistent with the compound being the dinuclear Co-Pt complex.

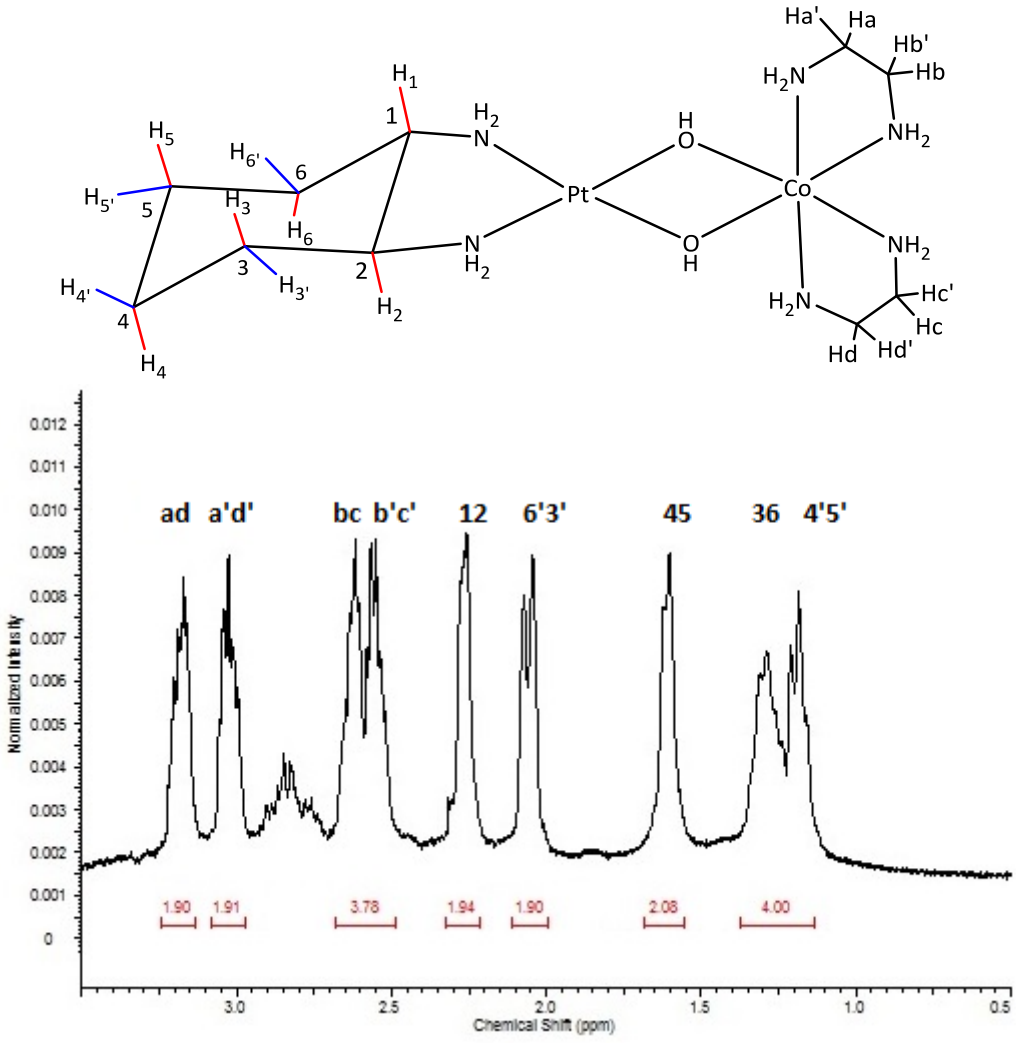

Figure 3-6 The ^{1}H NMR spectrum of $[(en)_2Co(\mu\text{-}OH)_2Pt(chda)]^{3+}$ in D_2O. The multiple peaks at 2.7 ppm are due to impurities (which are discussed later).

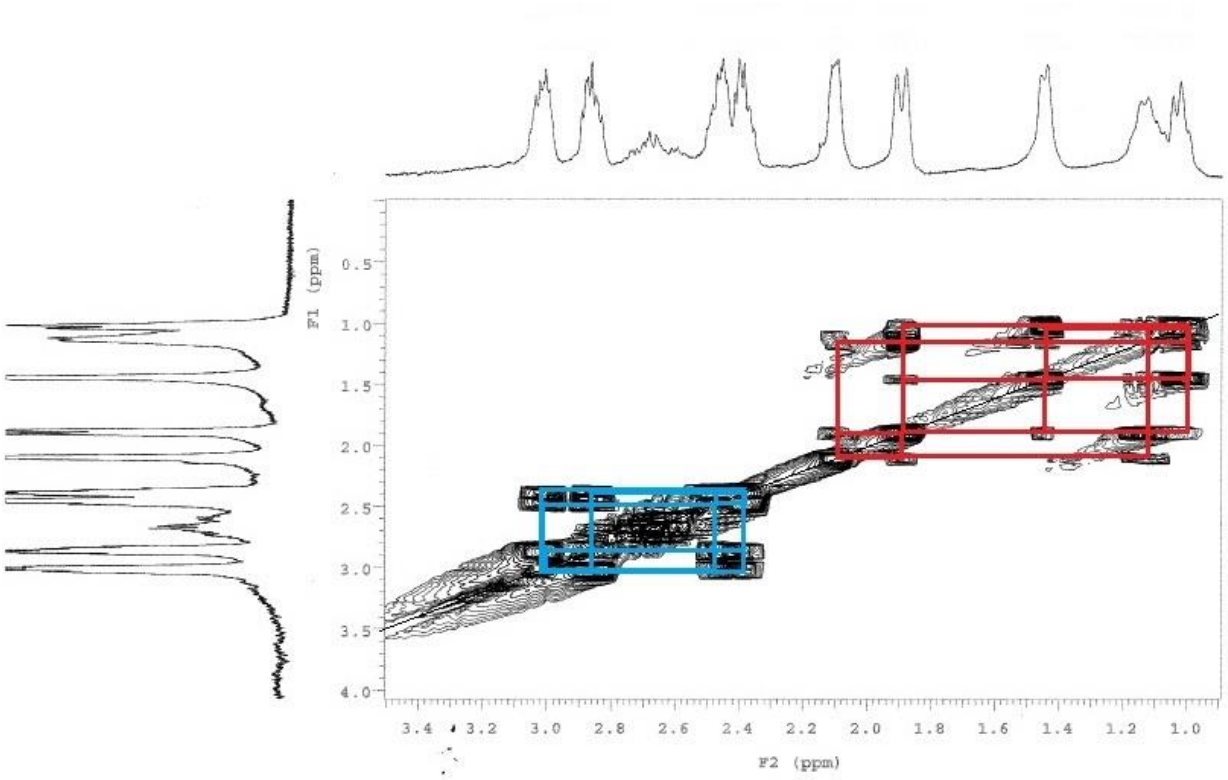

Figure 3-7 ^{1}H-^{1}H COSY of $[(en)_2Co(\mu\text{-}OH)_2Pt(chda)]^{3+}$ in D_2O. The blue lines represent the en region and the red lines indicate the chda region.

The two peaks at 44.69 and 43.65 ppm are assigned to the two kinds of carbon atoms of the en ligands on Co. Due to the use of *RR*,*SS*-cyclohexane-1,2-diamine, it is expected that the chda ligand configuration to be *trans* in the complex. The two carbon atoms on the cyclohexane ring next to the amine groups have the same absolute configurations. The Pt(chda) precursor exists as two enantiomers. Because the Co centre in the final complex has three chelate rings, it is also a stereogenic centre (with Δ and Λ configurations), which means that there are four stereoisomers – two sets of enantiomeric pairs. And the sets will have different spectra from each other, although they may be very similar. There are two very close sets of peaks were observed for C1,2 and C3,6 of the cyclohexane ring as well as en carbon atoms. This would support the existence of isomers within the sample. C4,5

carbon atoms came as one peak, presumably because they are too far from at least one of the stereocentres to be affected (probably the Co centre).

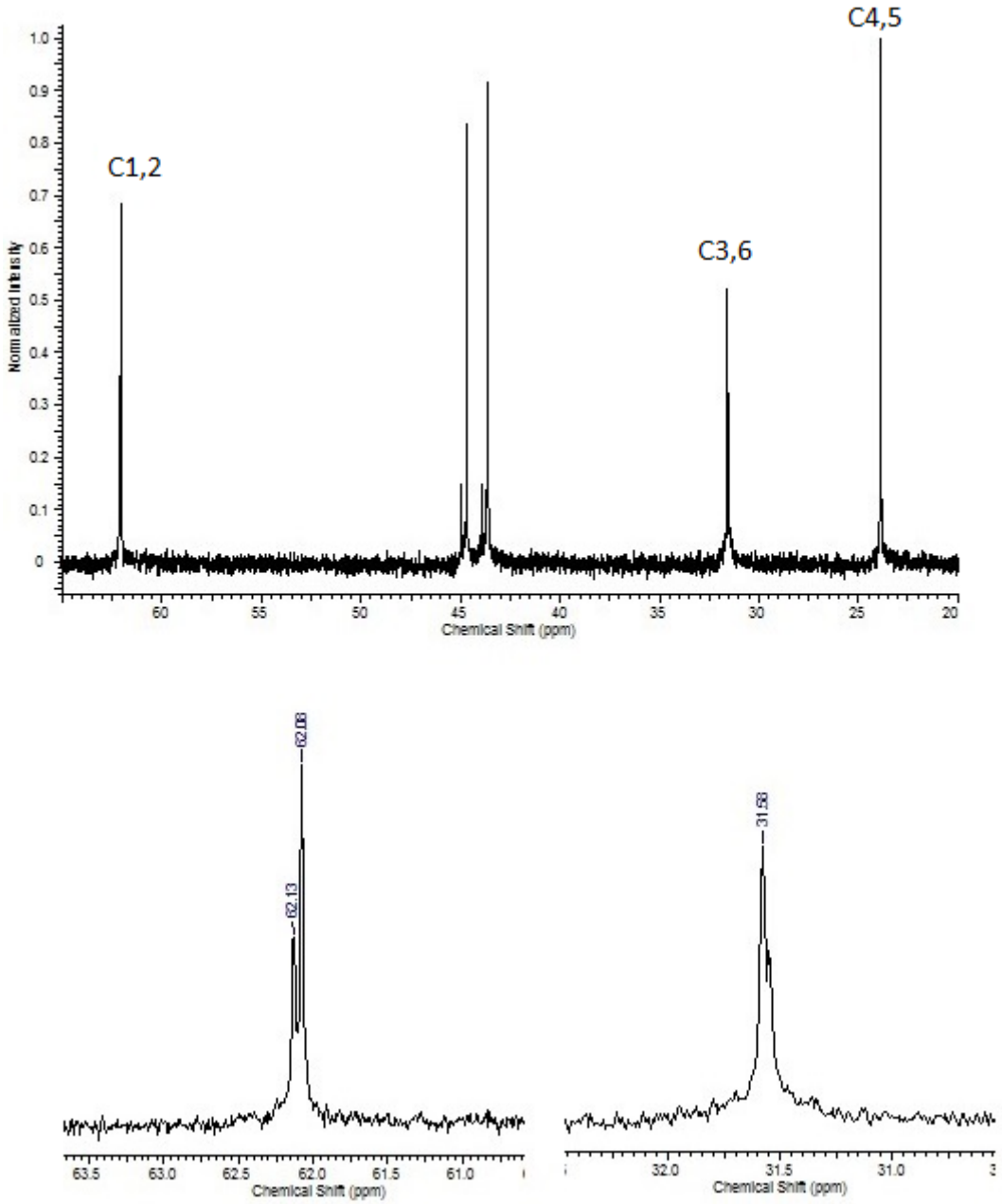

Figure 3-8 Top: The ^{13}C NMR spectrum of $[(en)_2Co(\mu\text{-}OH)_2Pt(chda)]^{3+}$ in D_2O. Bottom: Enlargement of the ^{13}C NMR spectrum of complex **3.2**. The small peaks in the en region may be due to the existence of another isomer or impurity.

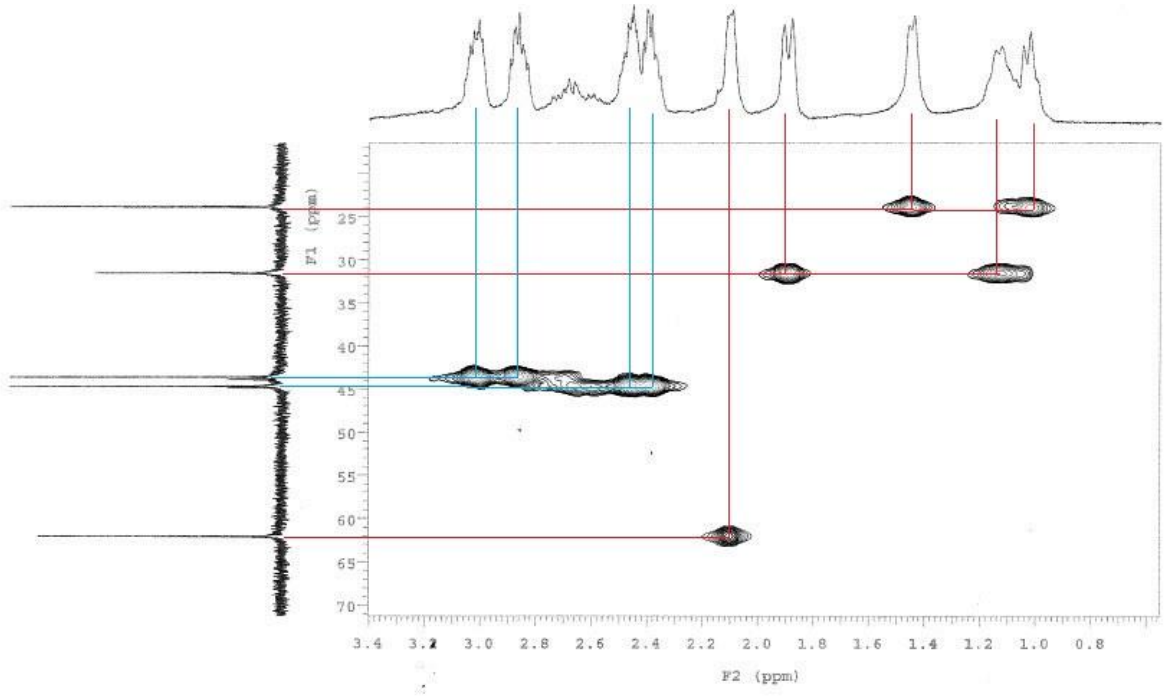

Figure 3-9 ^{1}H-^{13}C HSQC of $[(en)_2Co(\mu\text{-}OH)_2Pt(chda)]^{3+}$ in D_2O. The cross peaks for the impurity indicate they are en type carbon atoms and may be related to another isomer of the complex

On one occasion, very few red crystals were obtained on standing (and by slow evaporation) of a water/methanol solution of a fraction from the third band of the column.

The structure of the crystals which was determined by X-ray crystallography showed a trinuclear Pt-Co-Pt complex, $([(en)_2Co(\mu\text{-}OH)_2(\mu\text{-}O)\{Pt(chda)\}_2]^{2+}$ (**3.4**), in which the metal ions are linked through oxygen bridges (**Figure 3-10**). Complex **3.4** crystallised in the monoclinic space group $P2_1/c$. The geometry of Co is octahedral, with two bidentate en ligands and two oxido bridges, each to different platinum centres. The geometries of platinum can be described as distorted square planar; with two amine groups and two oxido bridges, one to Co and another to the other platinum. The cyclohexane rings in the structure are disordered, each with different absolute configurations with the ratio of 60/40. One of the configurations is shown in pink. The pink stereocentres have the *SS* configurations and the grey stereocentres have the *RR* configurations (**Figure 3-11**). The $CoPt_2O_3$ has adopted a twisted half boat configuration (**Figure 3-13**).

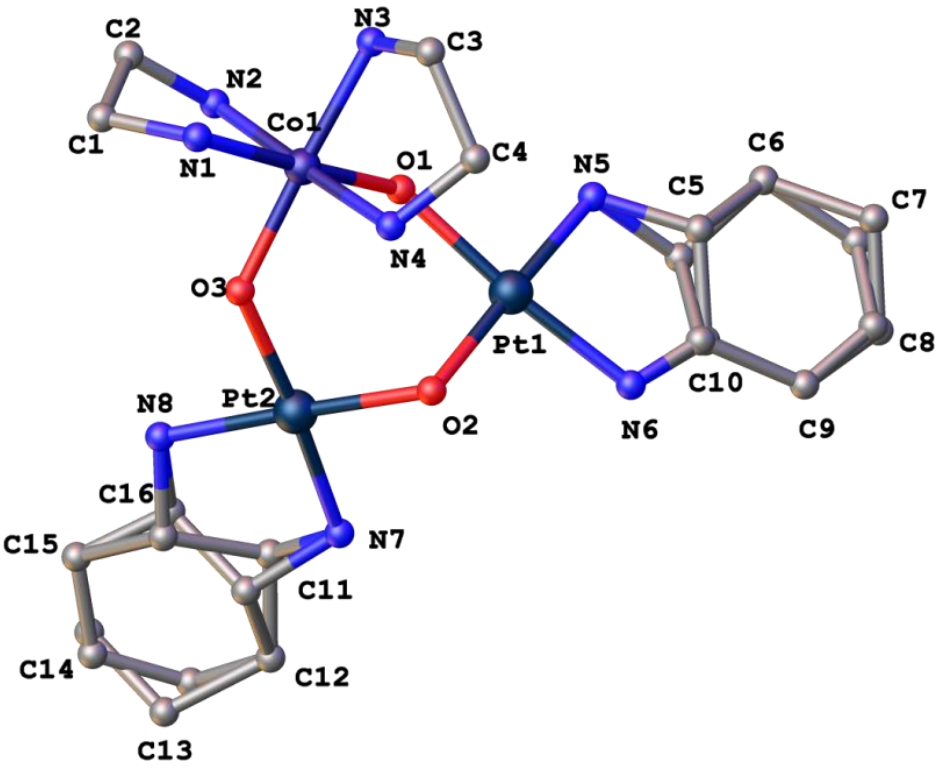

Figure 3-10 The molecular structure of complex **3.4**. The three nitrate anions and four water molecules omitted are for clarity. The cyclohexane rings exhibited different configurations

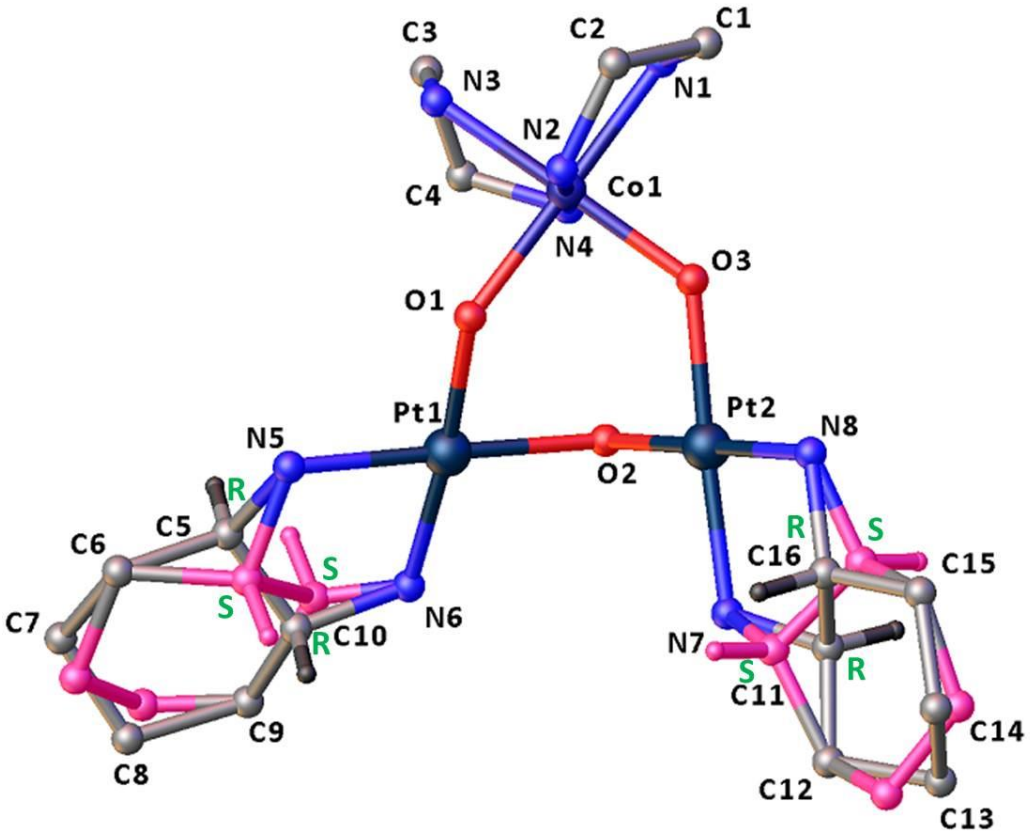

Figure 3-11 RR and SS configurations of the cyclohexane ring in compound **3.4**

There is hydrogen bonding between O2 of the central six-membered ring, O8 of nitrate ion, O13 and O14 of the water molecules and the hydrogen atoms on N4, N1, N5 and N7. The bond length of H4-O2, H14-O1, H5-O13 and H7-O14 are 2.034(4), 2.175(2), 2.12(3) and 2.177(17) Å respectively (**Figure 3-12**).

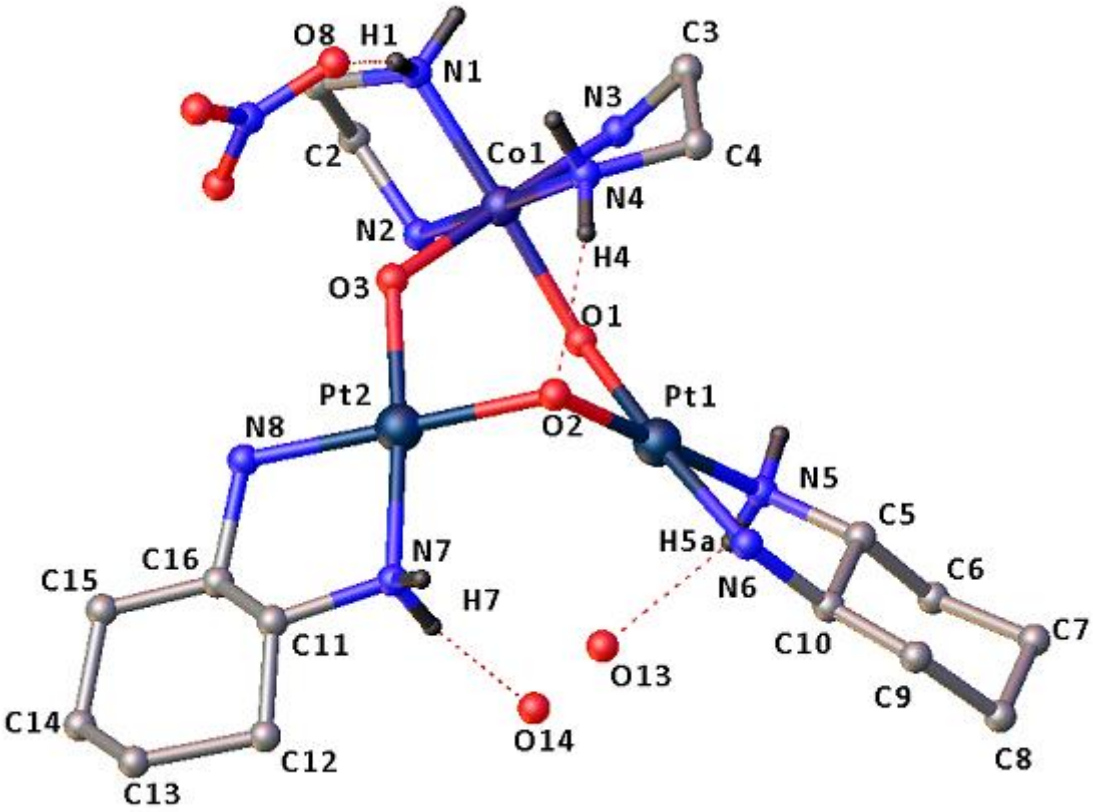

Figure 3-12 Molecular structure of **3.4** with three nitrate anions and four water molecule omitted for clarity in one configuration of disorder. Hydrogen bond lengths [Å]: O2-H4 2.055, O14-H7 2.047, O13-H5 2.134, O8-H1 2.175. Selected bond lengths [Å] and angles [°]: Pt1-O2 2.051(7); Pt1-O1 2.022(8); Pt1-N5 2.039(10); Pt1-N6 2.037(9); Pt2-O2 2.054(9); Pt2-O3 2.031(8); Pt2-N8 2.032(11); Pt2-N7 2.042(10); Co1-O1 1.936(8); Co1-O3 1.890(8); Co1-N4 1.953(10); Co1-N2 1.955(10); Co1-N1 1.947(10); Co1-N3 1.944(10); O1-Pt1-O2 90.2(3); O1-Pt1-N5 91.2(4); O1-Pt1-N6 174.6(4); N5-Pt1-O2 178.6(4); N6-Pt1-N5 83.8(4); O3-Pt2-O2 89.8(3); O3-Pt2-N8 90.8(4); O3-Pt2-N7 174.7(4); N8-Pt2-O2 178.0(4); N8-Pt2-N7 84.0(5); N7-Pt2-O2 95.4(4); O1-Co1-N4 91.2(4); O1-Co1-N2 89.3(4); O1-Co1-N1 175.3(4); O1-Co1-N3 87.9(4); O3-Co1-O1 91.5(4); O3-Co1-N4 92.2(4); O3-Co1-N2 89.2(4); O3-Co1-N1 89.0(4); O3-Co1-N3 177.4(4); N4-Co1-N2 178.5(5); N1-Co1-N4 93.5(4); N1-Co1-N2 86.0(4); N3-Co1-N4 85.3(4); N3-Co1-N2 93.3(4); N3-Co1-N1 91.8(4); Pt1-O2-Pt2 106.9(4); Co1-O1-Pt1 132.1(4); Co1-O3-Pt2 128.8(4)

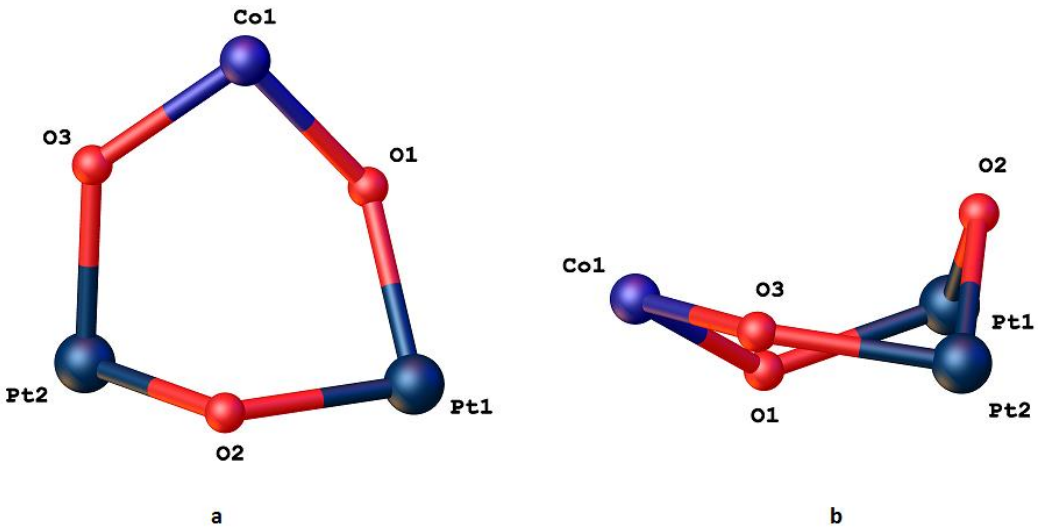

Figure 3-13 a) The front and **b)** the side view of **3.4** of six membered $CoPt_2O_3$ unit; showing deviations [in Å] of the atoms from the plane (33, -12, 6): Co1 0.412, O1 -0.504, O3 0.004, Pt2 -0.573, Pt1 0.132 and O2 0.800

The packing structure of **3.4** is presented in **Figure 3-14**.

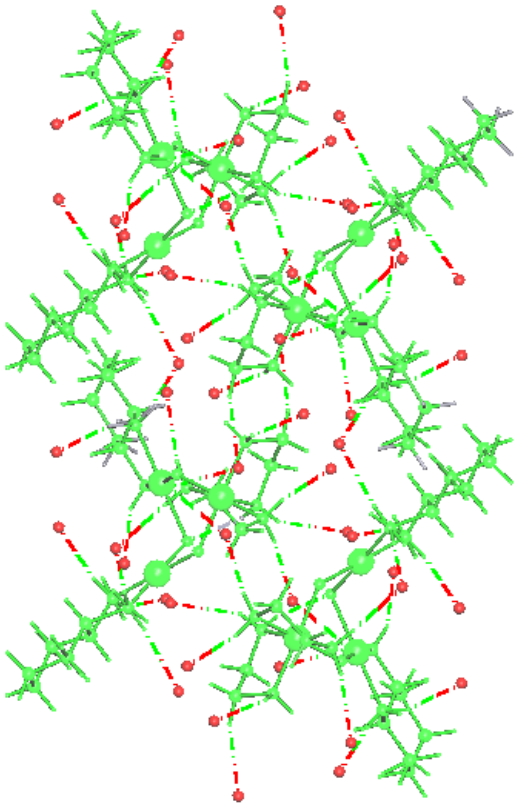

Figure 3-14 Hydrogen bonding network within the crystal lattice of the complex **3.4**

Although structures of numerous oxido bridged M_3 (M: any metal) complexes have been studied, very few feature a six-membered metal-oxo ring where different metals are present in the ring.

The crystal structures of $[((TPA)Fe)_2(\mu\text{-}MoO_4)(\mu\text{-}O)](OTf)_2$ (TPA = tris(2-pyridylmethyl)-amine)[127], $Co(bpe)_2(V_4O_{12})$ (bpe = (bis(4-pyridyl)ethylene))[128] and $[Pt_3(\mu\text{-}OH)_3(dpk{\cdot}H_2O)_2(dpk)](NO_3)_3{\cdot}4.5H_2O$ (dpk = 2,2'-Dipyridylketone)[129] are shown in Figure **3-15**, **3-16** and **3-17** respectively. The $MoFe_2O_3$ unit forms a twisted conformation and the CoV_2O_3 and Pt_3O_3 units form half chair and chair configurations respectively. The CoV_2O_3 system is most similar to our structure.

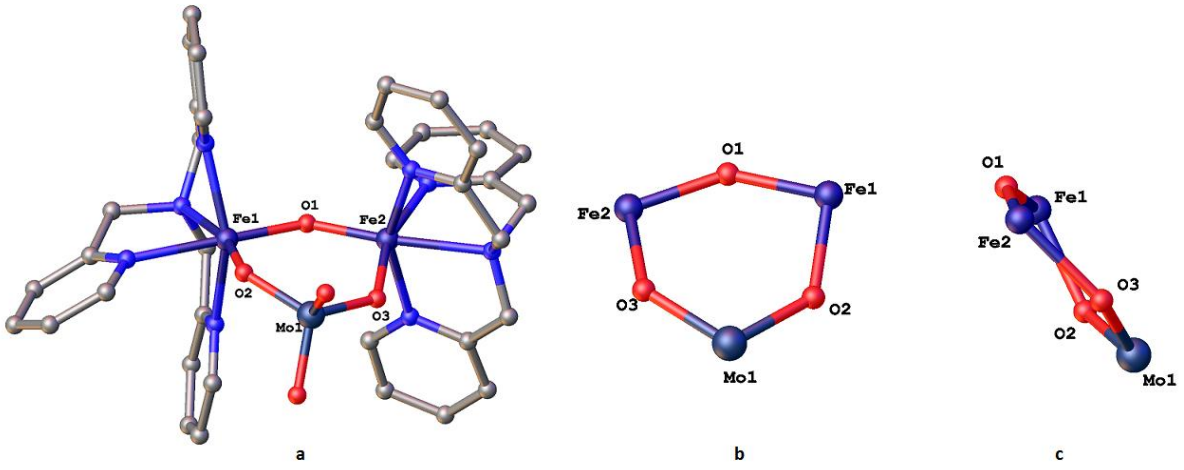

Figure 3-15 a) The molecular structure of $[((TPA)Fe_2(\mu\text{-}MoO_4)(\mu\text{-}O)](OTf)_2$ **b)** The front view and **c)** the side view of the six membered $MoFe_2O_3$ unit. The six member unit forms a twisted configuration

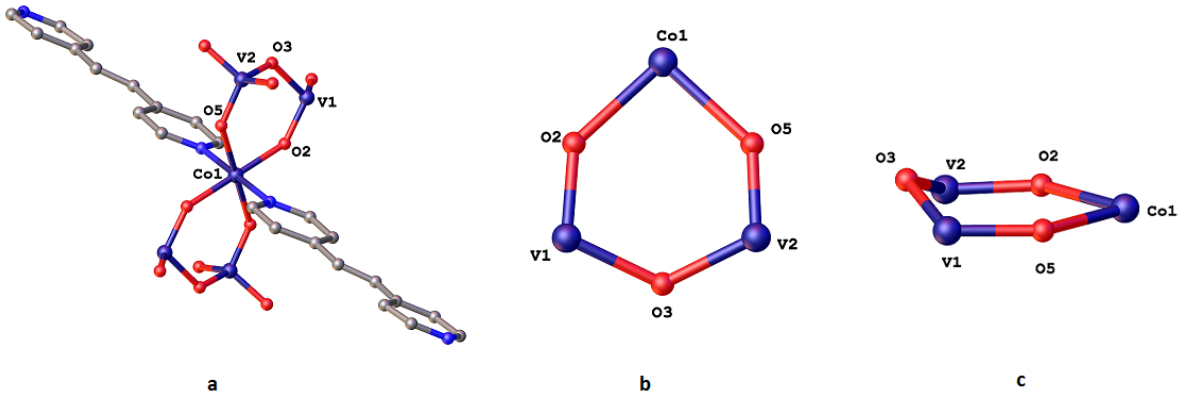

Figure 3-16 a) The molecular structure of $Co(bpe)_2(V_4O_{12})$ **b)** The front view and **c)** the side view of six membered CoV_2O_3 unit. The six member unit forms a half-chair configuration

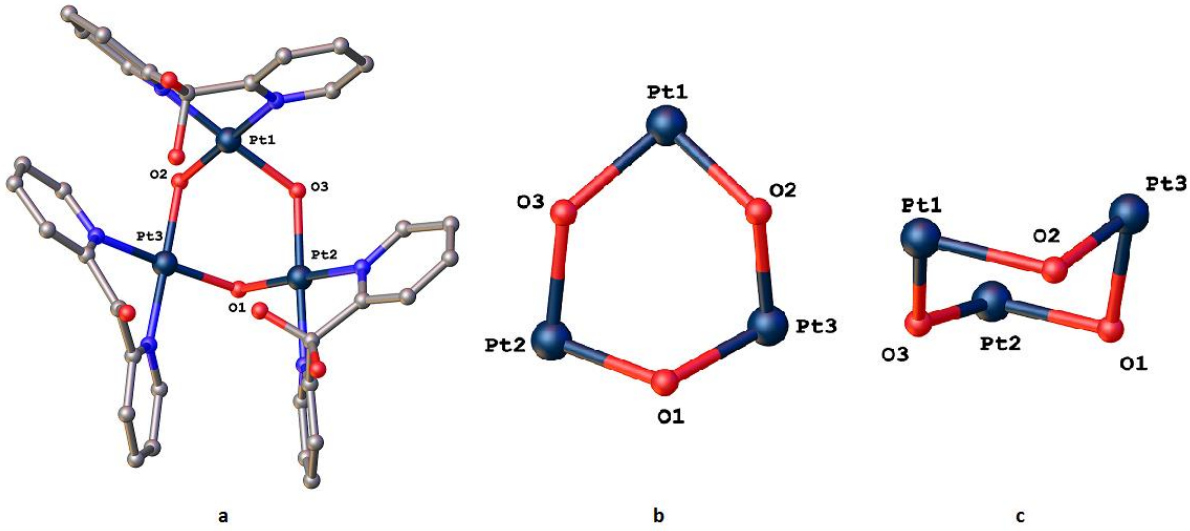

Figure 3-17 a) The molecular structure of $[Pt_3(\mu\text{-}OH)_3(dpk\cdot H_2O)_2(dpk)]$ **b)** The front view and **c)** the side view of six membered Pt_3O_3 unit. The six membered unit forms a chair configuration.

This crystal structure is clearly different from that proposed for the bulk material of the third band based on NMR and mass spectrometry studies. Those studies are consistent with the formation of a dinuclear Co-Pt complex, while the X-ray study determined a trinuclear Pt-Co-Pt complex with the formula of $[(en)_2Co(\mu\text{-}OH)_2(\mu\text{-}O)\{(Pt(chda)\}_2](NO_3)_3\cdot 3H_2O$ (**3.4**).

The ^1H NMR spectrum of crystals (**3.4**) is shown in **Figure 3-18** (bottom). The NMR data are consistent with the crystal structure, but importantly is different from that obtained for the complete fraction, as described above. The integrations in NMR spectrum of the bulk

crystals (**Figure 3-18** (bottom)) show 1:2 molar ratios of en ligand *vs* chda ligand from which a ratio of one cobalt *vs* two platinum is inferred.

The signals assigned to the en groups in the crystals may be responsible for at least some of the impurity signal in the spectra of the bulk sample. Formation of the trinuclear species from two equivalents of the dinuclear complex would also produce a mononuclear Co species, which could also contribute to the impurity signals.

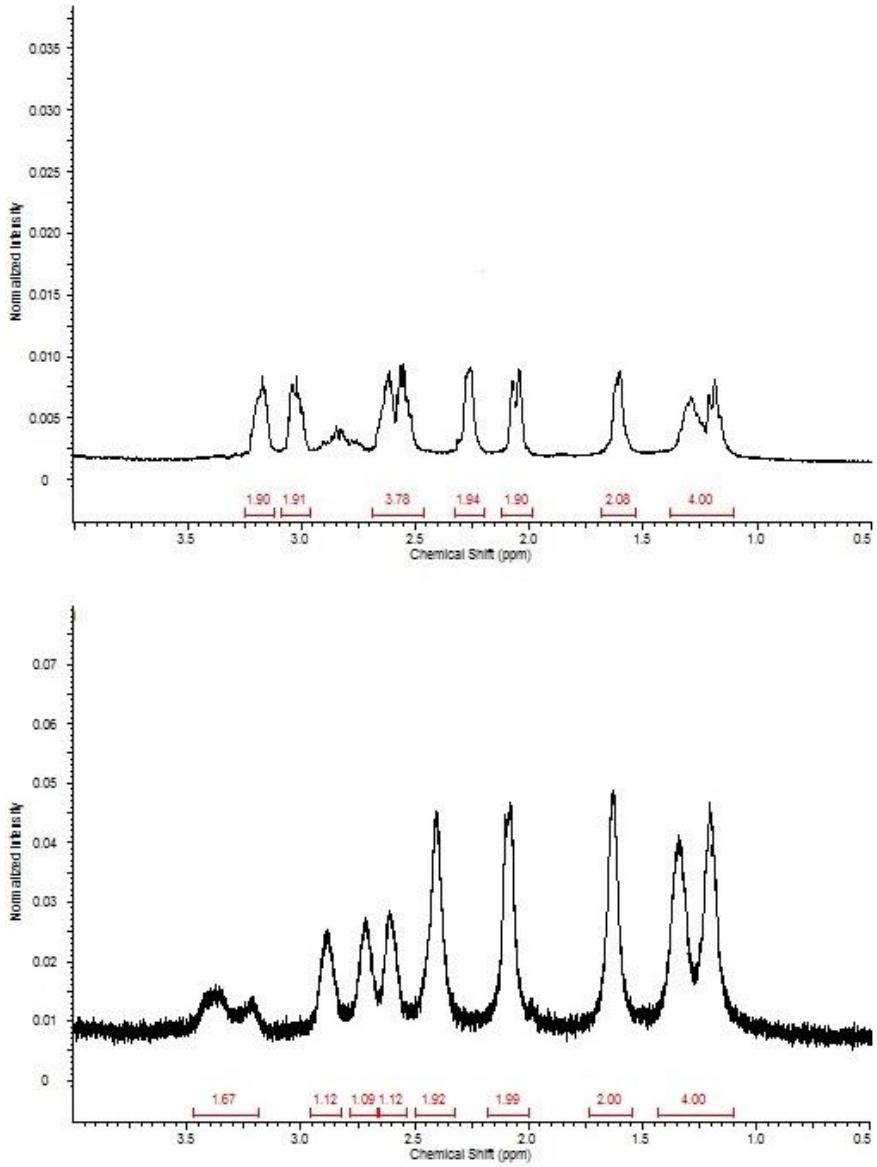

Figure 3-18 Comparison of ^{1}H NMR spectra of the third fraction of the column, **3.2** (top), and the obtained crystals from the same fraction, **3.4**, (bottom) in D_2O

The mass spectrum taken from crystals (**3.4**) contained peaks at m/z = 393.07 and 326.08, which are assigned to the $[(en)Co(\mu\text{-}OH)_3\{Pt(chda)\}_2\text{-}2H^+]^{2+}$ and $[(chda)Pt(\mu\text{-}OH)_2Pt(chda)]^{2+}$ ions (**Figures 3-19, 3-20** and **3-21**).

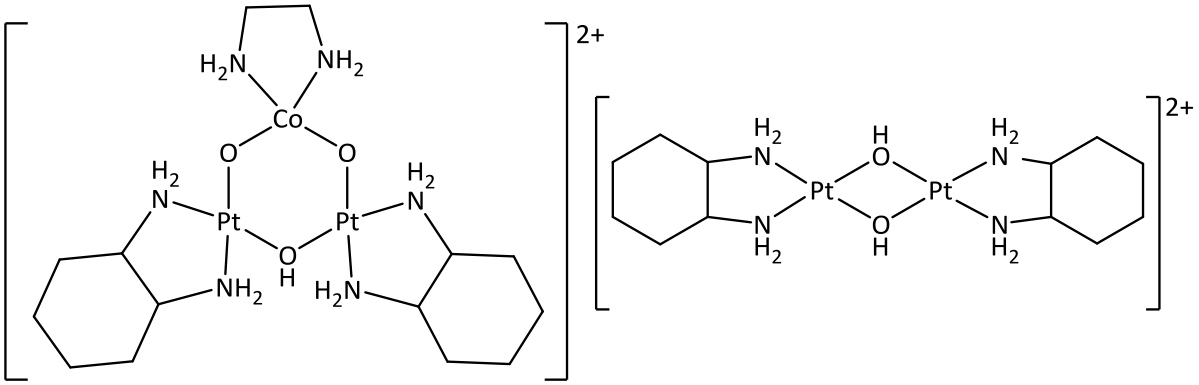

Figure 3-19 Proposed structures of the molecules for which the masses were found by Mass Spectrometry (Figures 3-20 and 3-21)

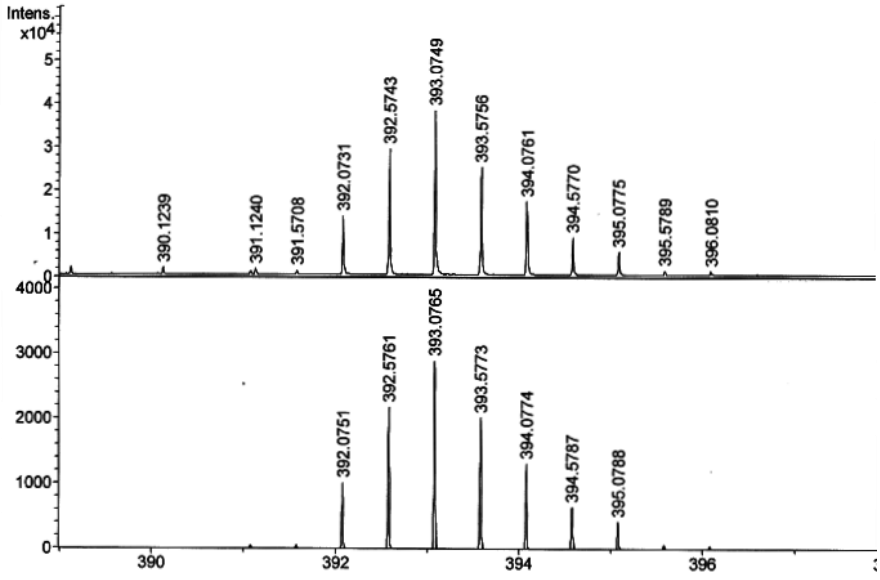

Figure 3-20 Experimental (top) and simulated isotope patterns for the highest abundance mass peak of the $[(en)Co(\mu\text{-}OH)_3\{Pt(chda)\}_2\text{-}2H^+]^{2+}$ ion

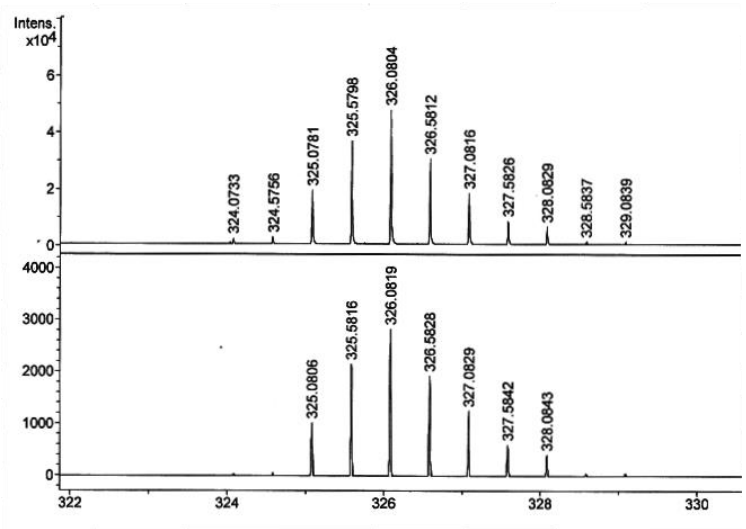

Figure 3-21 Experimental (top) and simulated isotope patterns for the highest abundance mass peak of the $[(chda)Pt(\mu\text{-}OH)_2Pt(chda)]^{2+}$ ion

3.1.1.2 $[(en)_2Co(\mu\text{-}OH)_2Pt(NH_3)_2]^{3+}$ (3.5)

The synthetic chemistry used to prepare complex **3.5** is presented in **Scheme 3-2**. Cisplatin $[PtCl_2(NH_3)_2]$ was treated with silver nitrate for 2 days[125]. The silver chloride precipitate was centrifuged and the supernatant was reacted with $[(en)_2Co(OH)(OH_2)]^{2+}$. The reaction mixture was stirred for 3 days. The purification of the crude compound by size exclusion column chromatography on Sephadex G10 resin was not useful as no bands separated.

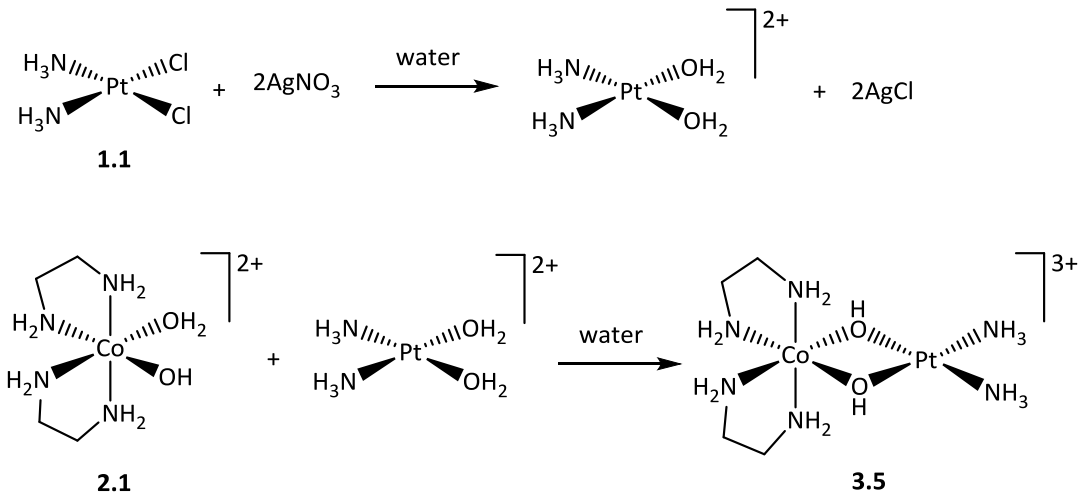

Scheme 3-2 Synthetic route to obtain $[(en)_2Co(\mu\text{-}OH)_2Pt(NH_3)]^{3+}$ complex

In the **Figure 3-22** the signals at 43.71 and 45.79 ppm are assigned to the desired *cis*-dinuclear Co-Pt complex in the ^{13}C NMR spectrum of the crude sample. The small signals marked with circles are assigned to a small amount of an equilibrium mixture of *cis* and *trans* isomers of $[(en)_2Co(OH)(OH_2)]^{2+}$ (see chapter 2). The single signal at 44.48 ppm is therefore assigned to a *trans*-dinuclear Co-Pt complex, since there is only one signal and the only alternatives would seem to involve coordination of poor ligands such as nitrate.

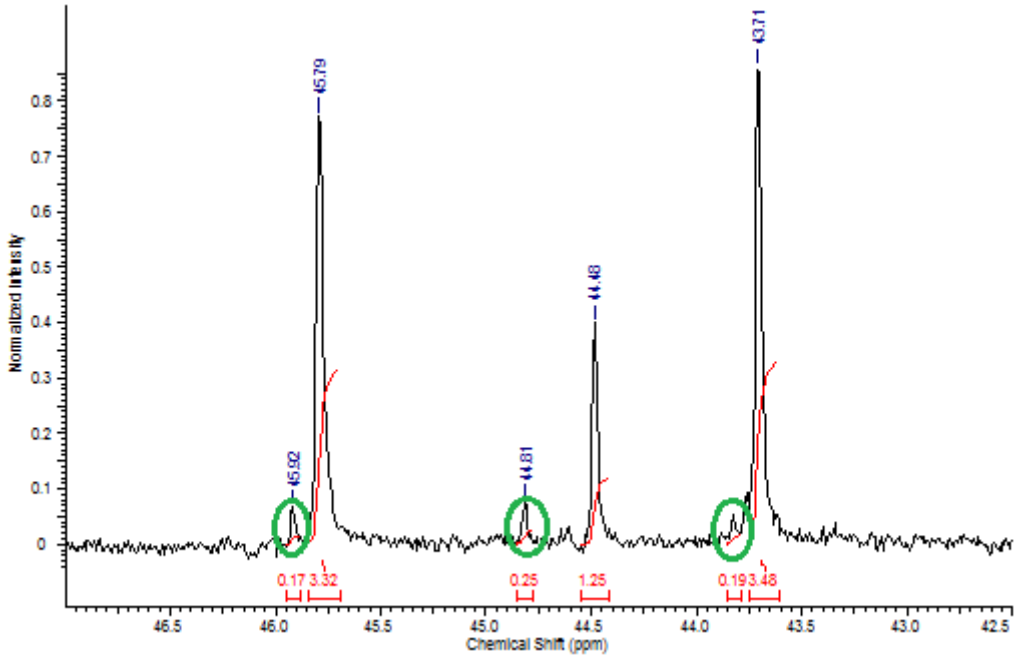

Figure 3-22 The ^{13}C NMR spectrum of $[(en)_2Co(OH)_2Pt(NH_3)_2]^{3+}$ in D_2O, 6 h after starting the reaction. The small peaks marked by green circles are assigned to an equilibrium mixture of the *cis* and *trans* isomers of $[Co(en)_2(OH)(OH_2)]^{2+}$

The ^{13}C NMR spectrum presented in **Figure 3-23** was taken 3 days after starting the reaction. The value of the *cis* to *trans* ratio was changed from 9.49 to 14.12 for the large set of peaks. As discussed in chapter 2, the *cis* complex is always more likely, than the *trans,* to form dinuclear complexes. It presumably takes time for the *trans* complex to convert to the *cis* and form the chelated dinuclear complex.

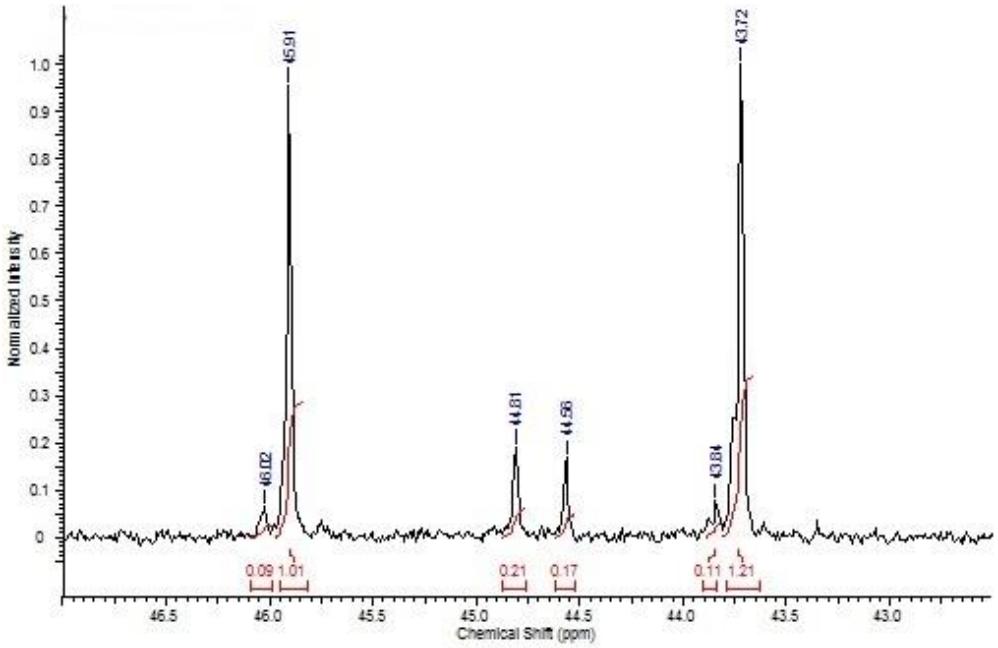

Figure 3-23 The ^{13}C NMR spectrum of $[(en)_2Co(\mu\text{-}OH)_2Pt(NH_3)]^{3+}$,3 days after starting the reaction

Signals were observed at m/z = 220.54 in the mass spectrum and the isotopic pattern simulation with $\{[(en)_2Co(\mu\text{-}OH)_2Pt(NH_3)_2]^{3+}\text{-}H^+\}^{2+}$ is shown in **Figure 3-24**.

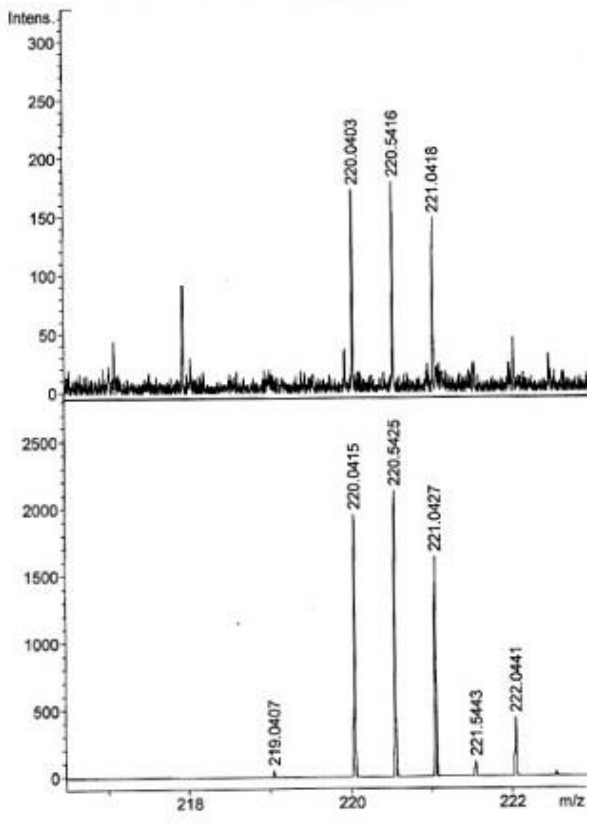

Figure 3-24 Experimental (top) and simulated isotope patterns for the highest abundance mass peak of the $\{[(en)_2Co(\mu\text{-}OH)_2Pt(NH_3)_2]^{3+}\text{-}H^+\}^{2+}$ ion

3.1.1.3 $[(tren)Co(\mu\text{-}OH)_2Pt(NH_3)_2]^{3+}$ (3.6)

The synthetic chemistry used to prepare complex **3.6** is presented in **Scheme 3-3**. Cisplatin, $[PtCl_2(NH_3)_2]$, was treated with silver nitrate for 2 days[125]. The silver chloride precipitate was centrifuged and the supernatant was reacted with $[Co(tren)(OH)(OH_2)](ClO_4)_2$.

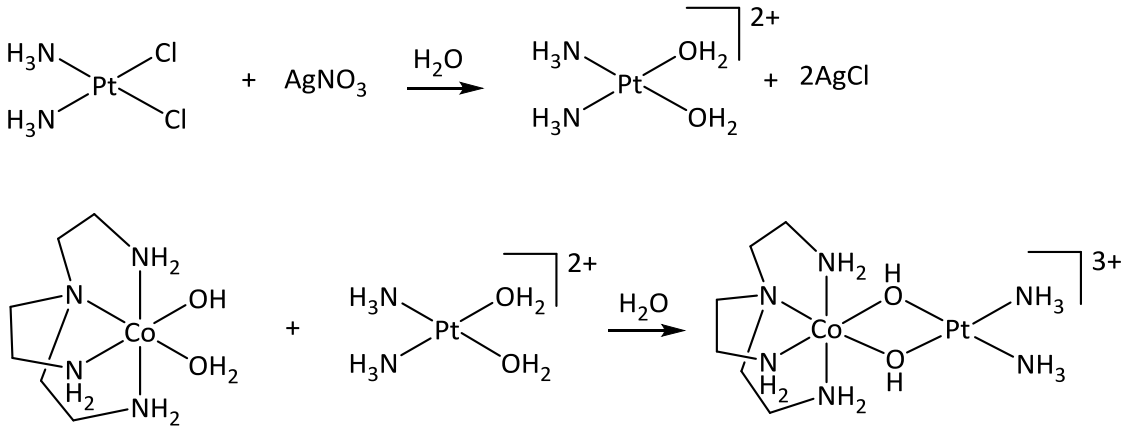

3.6

Scheme 3-3 Synthetic route to obtain $[(tren)Co(\mu\text{-}OH)_2Pt(NH_3)_2]^{3+}$ complex

Although the reaction of $[Co(tren)(OH)(OH_2)]^{2+}$ and $[Pt(chda)(OH_2)_2]$ is very similar to those discussed above, it was very soon clear that reactions of the Co(tren) system were much slower than those of the $Co(en)_2$ system. Ultimately, it was found that the reaction could be conducted in two hours, but only if microwave heating was employed. Without microwave heating the reaction took weeks.

The ^{13}C NMR spectrum of $[Co(tren)(OH)(OH_2)]^{2+}$ is presented in **Figure 3-24 a**, and contains 4 signals at 62.10, 60.96, 44.48 and 43.64 ppm. The two former and the two latter signals are assigned to the carbon atoms next to tertiary amine and the carbon atoms next to primary amines, respectively.

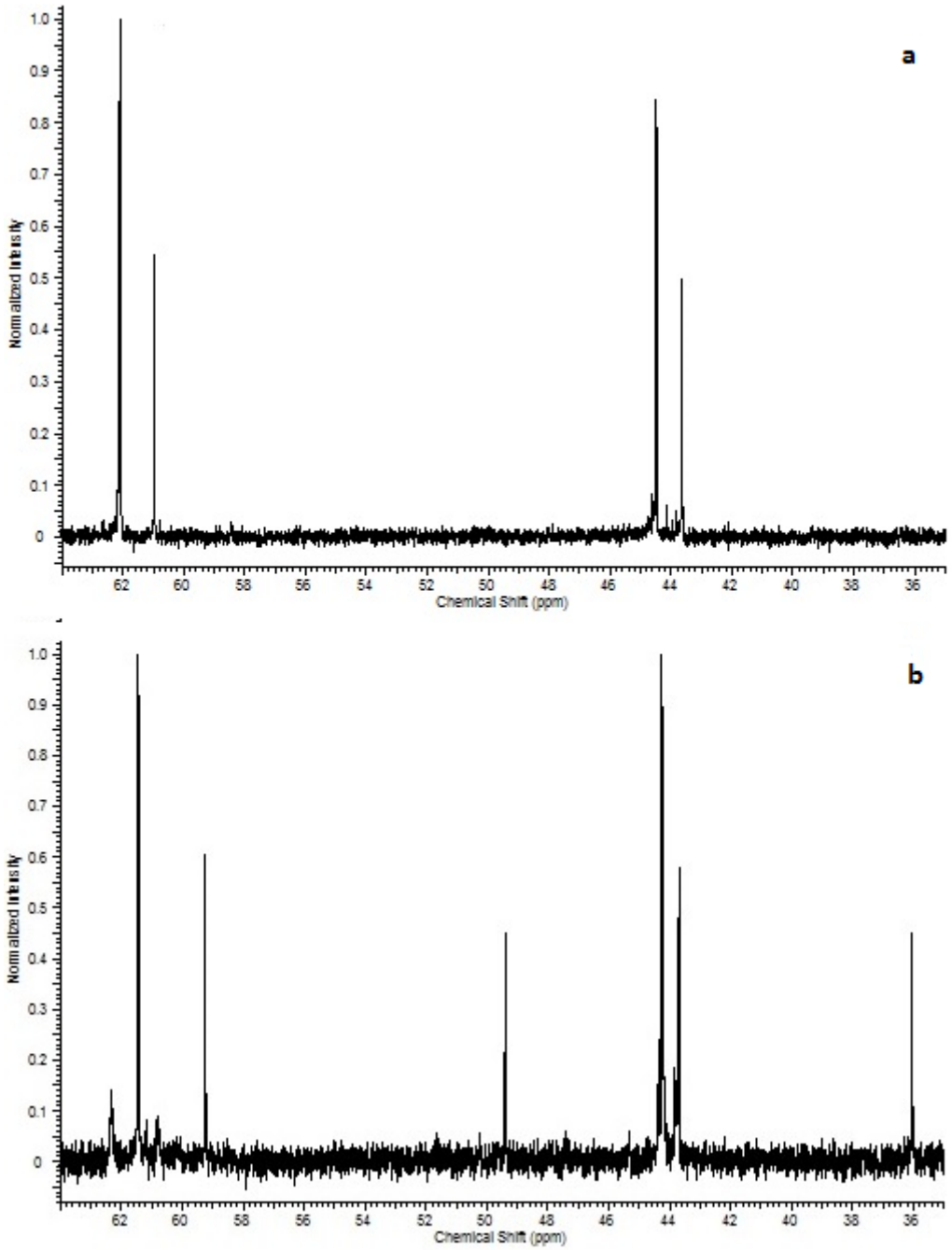

Figure 3-25 a) The ^{13}C NMR spectrum of $[Co(tren)(OH)(OH_2)]^{2+}$ in D_2O **b)** The ^{13}C NMR spectrum of the reaction mixture of $[Co(tren)(OH)(OH_2)]^{2+}$ and $[Pt(NH_3)_2(OH_2)_2]^{2+}$ in D_2O after 2 hours of microwave heating

The ^{13}C NMR spectrum of $[Co(tren)(OH)(OH_2)]^{2+}$ and cisplatin reaction after 2 hours under microwave heating is shown in **Figure 3-25 b**. The signals of $[Co(tren)(OH)(OH_2)]^{2+}$ have decreased significantly and substantial new signals have appeared. The new peaks at 61.21,

59.01, 44.01 and 43.46 ppm are assigned to the dinuclear complex. There are very small signals due to unreacted $[Co(tren)(OH)(OH_2)]^{2+}$ present in the spectrum. Moreover, there are a further two new signals at 49.86 and 36.52 ppm. To confirm these two signals belong to free tren, a small amount of free tren was added. Subsequently, the integration of signals increased.

To follow the reaction more conveniently, an integration *vs* time graph is drawn (**Graph 3-1**). The integration of unreacted $[Co(tren)(OH)(OH_2)]^{2+}$, product and free tren were plotted *vs* time. The integration of product and unreacted materials are obtained by addition of the integration of two signals of carbon atoms next to tertiary amines dividing by the sum of all signal integrations. Similarly, the integration of free tren is obtained by addition of two signals of free tren dividing by the overall integration. The standard error for signal integration was calculated using the equations in **Appendix 1**, and error bars were drawn.

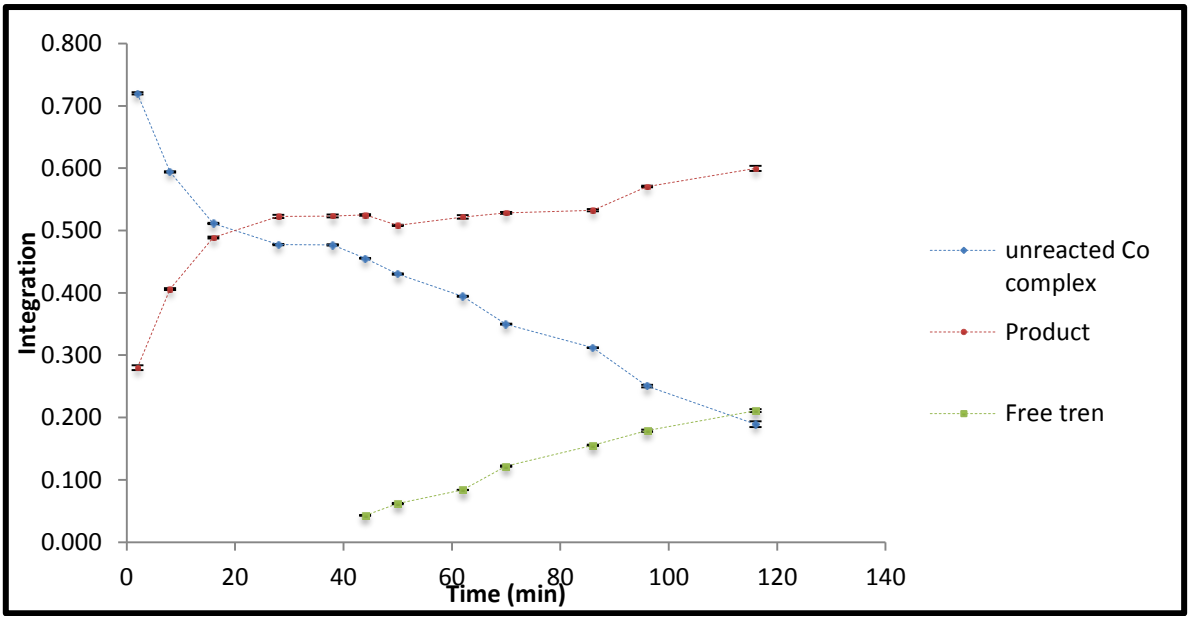

Graph 3-1 Integration of unreacted $[Co(tren)(OH)(OH_2)]^{2+}$, the product ($[(tren)Co(\mu\text{-}OH)_2Pt(NH_3)]^{3+}$) and free tren *vs* time in reaction between $[Co(tren)(OH)(OH_2)]^{2+}$ and cisplatin under microwave conditions.

Graph 3-1 shows that most of the product formed after 40 minutes heating in a microwave and after that, the trend seems linear. The integration of free tren started to increase after 40 minutes. The formation of dinuclear Co-Pt complex did not go any further after 40 minutes. This could be due to loss of platinum species in the primary step of reaction.

The crude compound was purified by size exclusion column chromatography on Sephadex G10 resin.

The first band was taken from the column and evaporated to dryness and gave yellowish oil. The ^{1}H NMR data allowed us to identify this material as free tren. The second and third bands were collected and evaporated to give reddish oils. The oily residue obtained from the second and third bands were characterised using mass spectrometry and NMR techniques. The ^{13}C NMR spectrum of the third band is shown in **Figure 3-26**.

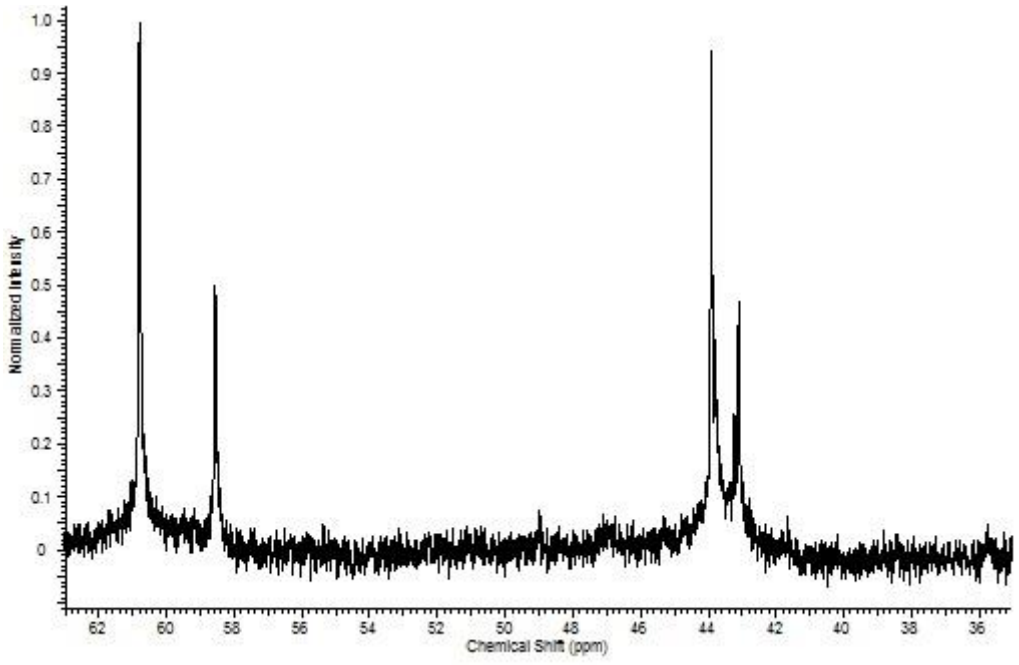

Figure 3-26 The ^{13}C NMR spectrum of $[(tren)Co(\mu\text{-}OH)_2Pt(NH_3)]^{3+}$ after purification by size exclusion column chromatography on Sephadex G10

Mass spectrometry results showed that both the second and the third fractions contain $[(tren)Co(\mu\text{-}OH)_2Pt(NH_3)]^{3+}$; but based the mass spectra (see below), we believe the second fraction is the nitrate salt of the complex and the third fraction is the perchlorate salt. (**Figures 3-27 and 3-28**).

In the mass spectrum of the second fraction, the peaks at m/z = 158.03, 233.54 and 466.09 are assigned to $([(tren)Co(\mu\text{-}OH)_2Pt(NH_3)_2]^{3+}$ (**Figure 3-27 b**), $[(tren)Co(\mu\text{-}OH)_2Pt(NH_3)_2\text{-}H^+]^{2+}$ (**Figure 3-27 c**) and $([(tren)Co(\mu\text{-}OH)_2Pt(NH_3)_2\text{-}2H^+]^+$ (**Figure 3-27 d**) ions respectively. The simulation of each isotopic pattern is shown below the enlargement of each signal. The mass peak and the simulation of the isotopic pattern of the nitrate salt of the complex ($\{[(tren)Co(\mu\text{-}OH)_2Pt(NH_3)_2\text{-}H^+](NO_3)\}^+$) is shown in **Figure 3-27 e**.

Mass spectrum of the third fraction of $[(tren)Co(\mu\text{-}OH)_2Pt(NH_3)]^{3+}$ from size exclusion column chromatography on Sephadex G10 is shown in Figure **3-28 a**. The found peaks at m/z = 158.03 and 233.54 are assigned to $([(tren)Co(\mu\text{-}OH)_2Pt(NH_3)_2]^{3+}$ (**Figure 3-28 b**) and $[(tren)Co(\mu\text{-}OH)_2Pt(NH_3)_2\text{-}H^+]^{2+}$ (**Figure 3-28 c**). The isotopic pattern simulations of the found peaks are shown below the enlargement of each peak. The mass peak and the simulation of the isotopic pattern of the perchlorate salts of the complex ($\{[(tren)Co(\mu\text{-}OH)_2 Pt(NH_3)_2](ClO_4)_2\}^+$ and $\{[(tren)Co(\mu\text{-}OH)_2Pt(NH_3)_2\text{-}H^+](ClO_4)\}^+$) are shown in **Figures 3-27 d and 3-27 e**.

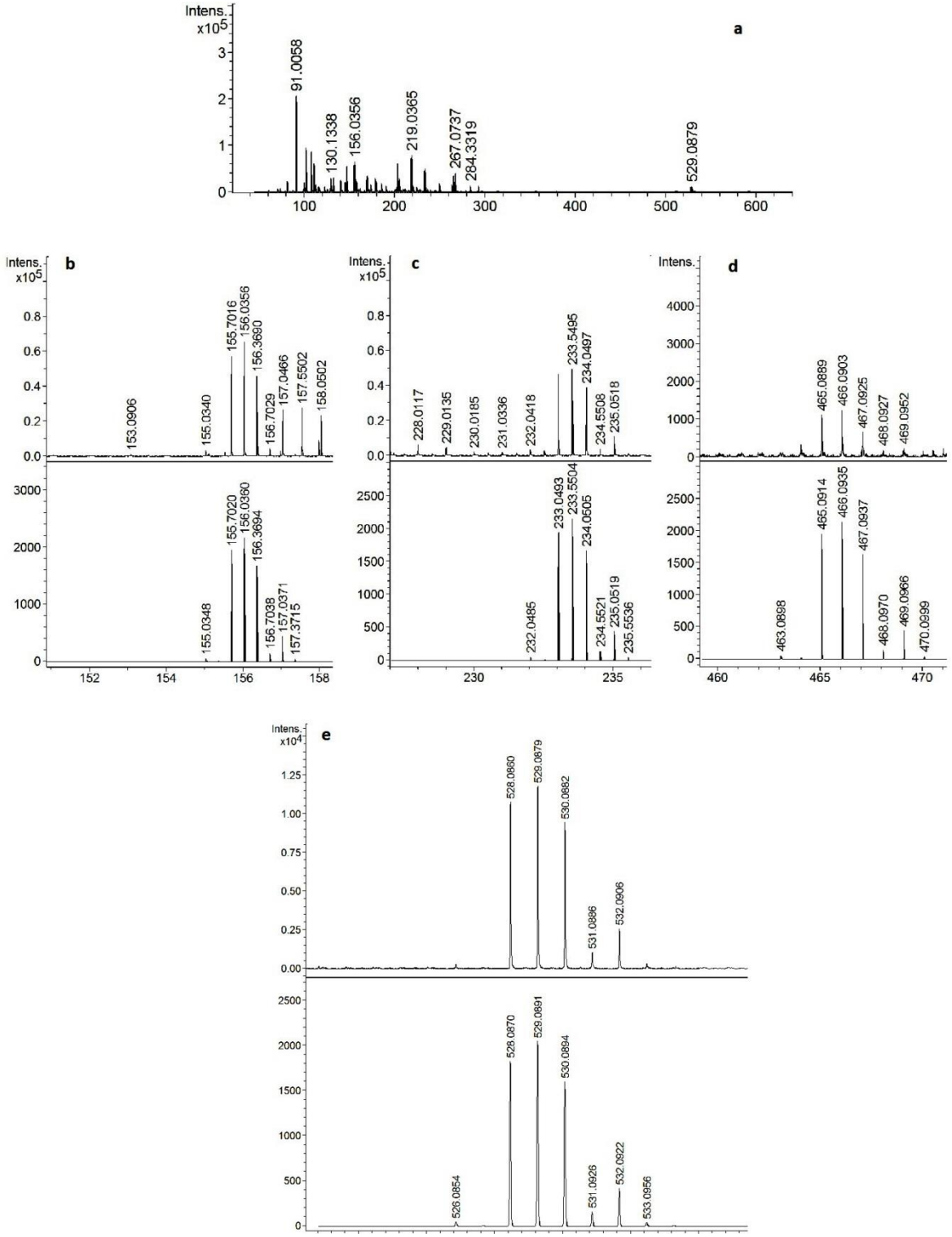

Figure 3-27 a) Mass spectrum of the second fraction of [(tren) Co(μ-OH)$_2$Pt(NH$_3$)]$^{3+}$ on size exclusion column chromatography on Sephadex G10. The rest of spectra are the enlargement of the found peaks: experimental (top) and simulated isotope patterns (bottom) for the highest abundance mass peak of **b)** [(tren)Co(μ-OH)$_2$Pt(NH$_3$)$_2$]$^{3+}$ ion **c)** [(tren)Co(μ-OH)$_2$Pt(NH$_3$)$_2$-H$^+$]$^{2+}$ ion, **d)** [(tren)Co(μ-OH)$_2$Pt(NH$_3$)$_2$-2H$^+$]$^+$ ion and **e)** {[(tren)Co(μ-OH)$_2$Pt(NH$_3$)$_2$-H$^+$](NO$_3$)}$^+$ ion

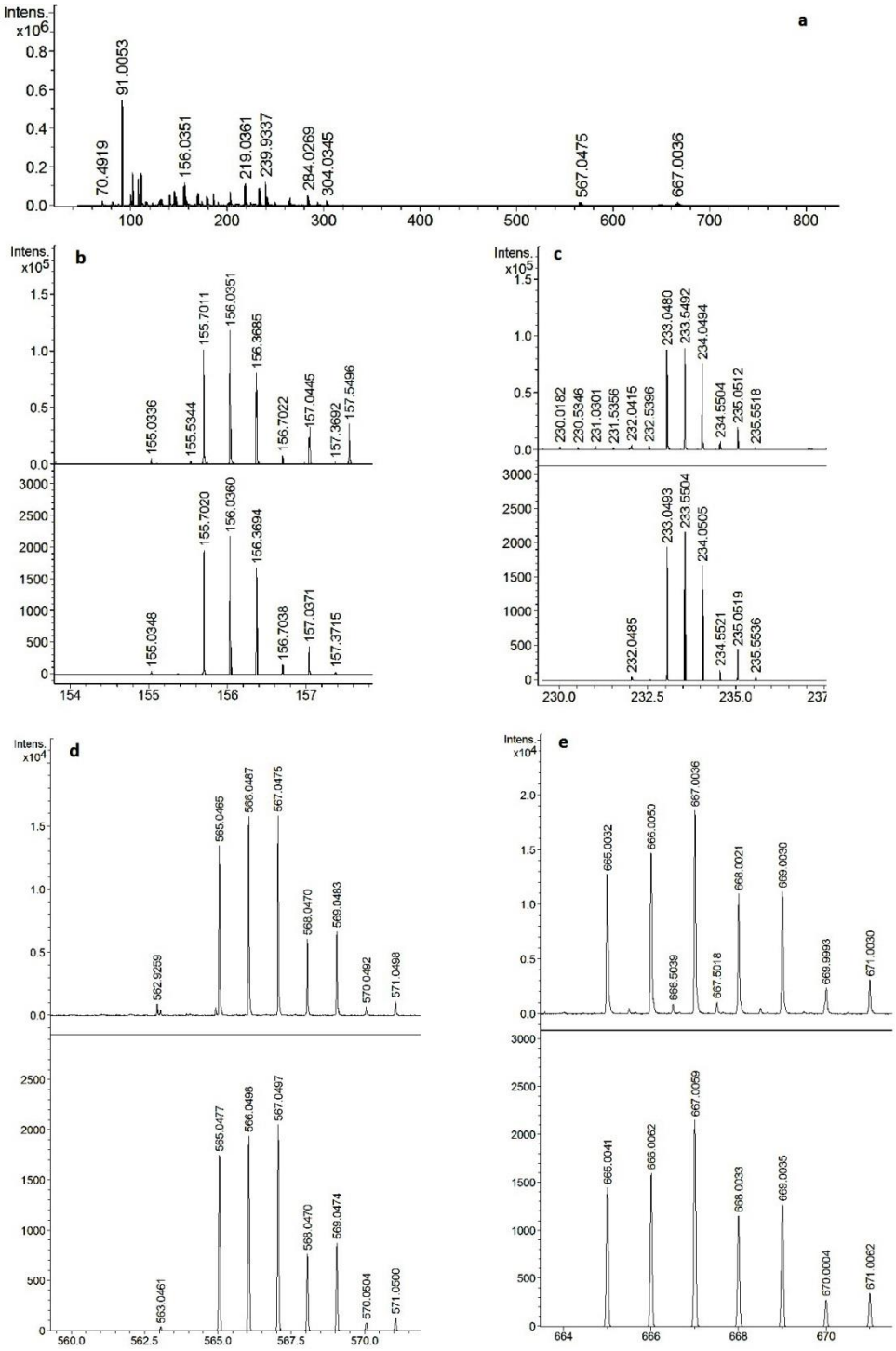

Figure 3-28 a) Mass spectrum of the third fraction of [(tren) Co(μ-OH)$_2$Pt(NH$_3$)]$^{3+}$ on size exclusion column chromatography on Sephadex G10. The rest of spectra are the enlargement of the found peaks: experimental (top) and simulated isotope patterns (bottom) for the highest abundance mass peak of **b)** [(tren)Co(μ-OH)$_2$Pt(NH$_3$)$_2$]$^{3+}$ ion, **c)** [(tren)Co(μ-OH)$_2$Pt(NH$_3$)$_2$-H$^+$]$^{2+}$ ion **d)** {[(tren)Co(μ-OH)$_2$Pt(NH$_3$)$_2$](ClO$_4$)$_2$}$^+$ ion and **e)** {[(tren)Co(μ-OH)$_2$Pt(NH$_3$)$_2$-H$^+$](ClO$_4$)}$^+$ ion

3.1.1.4 $[(tren)Co(\mu\text{-}OH)_2Pt(chda)]^{3+}$ (3.7)

The synthetic route for preparing the title complex is presented in **Scheme 3-4**. $[PtI_2(chda)]$ was treated with silver nitrate for 2 days[125]. The silver iodide precipitate was centrifuged and the supernatant was reacted with $[Co(tren)(OH)(OH_2)](ClO_4)_2$. The reaction mixture was heated in over the 2 hour period of 90 sec bursts in a microwave.

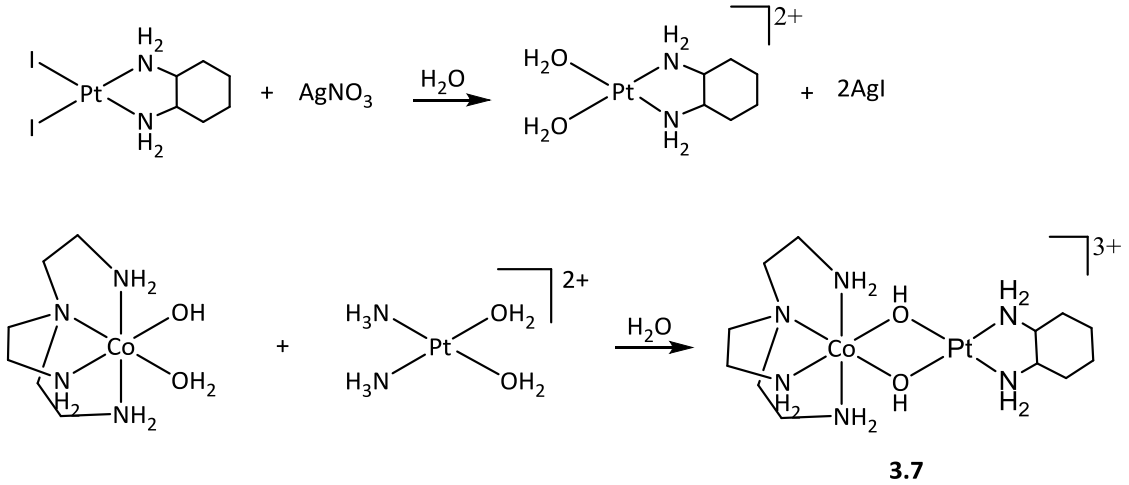

3.7

Scheme 3-4 Synthetic route to obtain $[(tren)Co(\mu\text{-}OH)_2Pt(chda)]^{3+}$, complex **3.7.**

The product was purified using cation exchange chromatography on CM Sephadex. The column was eluted with $NaNO_3$ solutions. The first band was collected, evaporated and gave a pink powder. The product collected from the second and third bands gave a reddish slurry after evaporation of the solvent. The compounds obtained from second and third bands were characterised using mass spectrometry and NMR techniques. Crystals from the first band were obtained by slow evaporation of a water-methanol solution of the fraction. They were also characterised by NMR and X-ray crystallography.

X-ray crystallography determined the first fraction to be $[Co(tren)(OH_2)(ONO_2)](NO_3)_2$ (**3.8**), as shown in **Figure 3-29**.

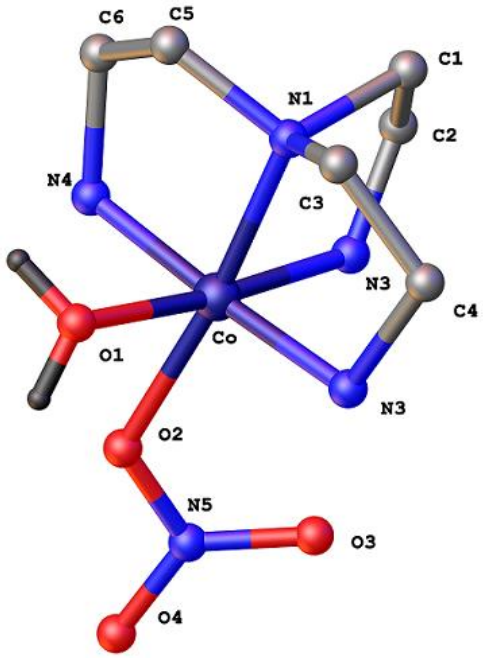

Figure 3-29 The molecular structure of **3.8**, with two nitrate anions omitted for clarity. Hydrogen atoms are omitted for clarity, except those on the water ligand

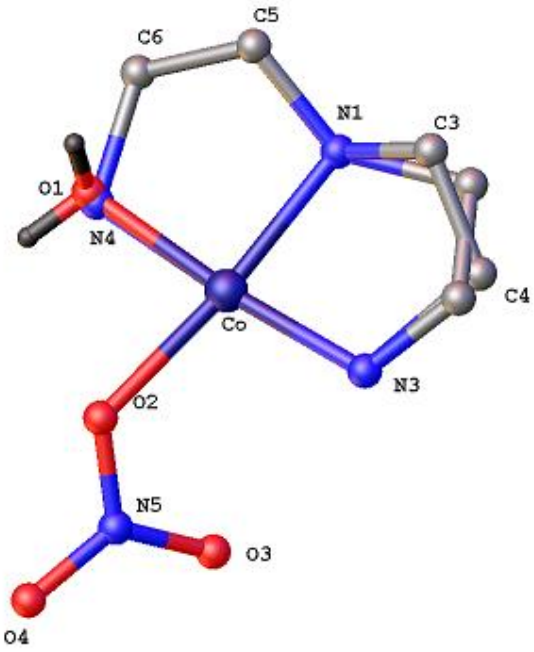

Figure 3-30 The asymmetric unit of complex **3.8** with two nitrate anions and hydrogen atoms omitted for clarity. The chelate ring of the tren is disordered over two different conformations, and the other chelate ring is disordered with water

The molecular structure of **3.8** is shown in **Figure 3-29.** The molecule is disordered in the asymmetric unit which generates disorder by symmetry in the whole molecule. The asymmetric unit of the molecule is shown in **Figure 3-30**.

The NMR data for complex **3.8** are consistent with the crystal structure. The four signals at 62.21, 60.62, 43.93 and 43.60 ppm are assigned to four kinds of carbon atoms of the tren ligand. The peaks at m/z 266.06, 203.07 and 102.03 in the mass spectrum, corresponding to $[Co(tren)(ONO_2)\text{-}H^+]^+$, $[Co(tren)\text{-}2H^+]^+$ and $[Co(tren)(ONO_2)\text{-}2H^+]^{2+}$, were also observed.

The product, $[(tren)Co(\mu\text{-}OH)_2Pt(chda)]^{3+}$ (**3.7**), came in the third band from the column with 0.3 M eluent. The fraction was desalted firstly by methanol and acetone extraction and secondly by size exclusion column chromatography on Sephadex G10. The complex was characterised by NMR and mass spectrometry techniques. The isotope pattern at m/z 273.08 can be assigned to $[(tren)Co(\mu\text{-}OH)_2Pt(chda)\text{-}H^+)]^{2+}$ (**Figure 3-31**)

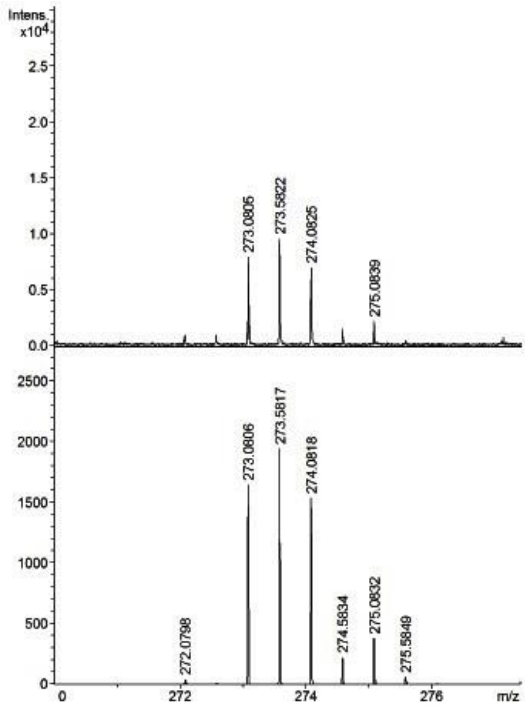

Figure 3-31 Experimental (top) and simulated isotope patterns (bottom) for the highest abundance mass peak of $[(tren)Co(\mu\text{-}OH)_2Pt(chda)\text{-}H^+]^{2+}$ ion

The ^{1}H and ^{13}C NMR Spectra of **3.7** are assigned using COSY and HSQC techniques (**Figures 3-32**, **3-33**, **3-34** and **3-35**).

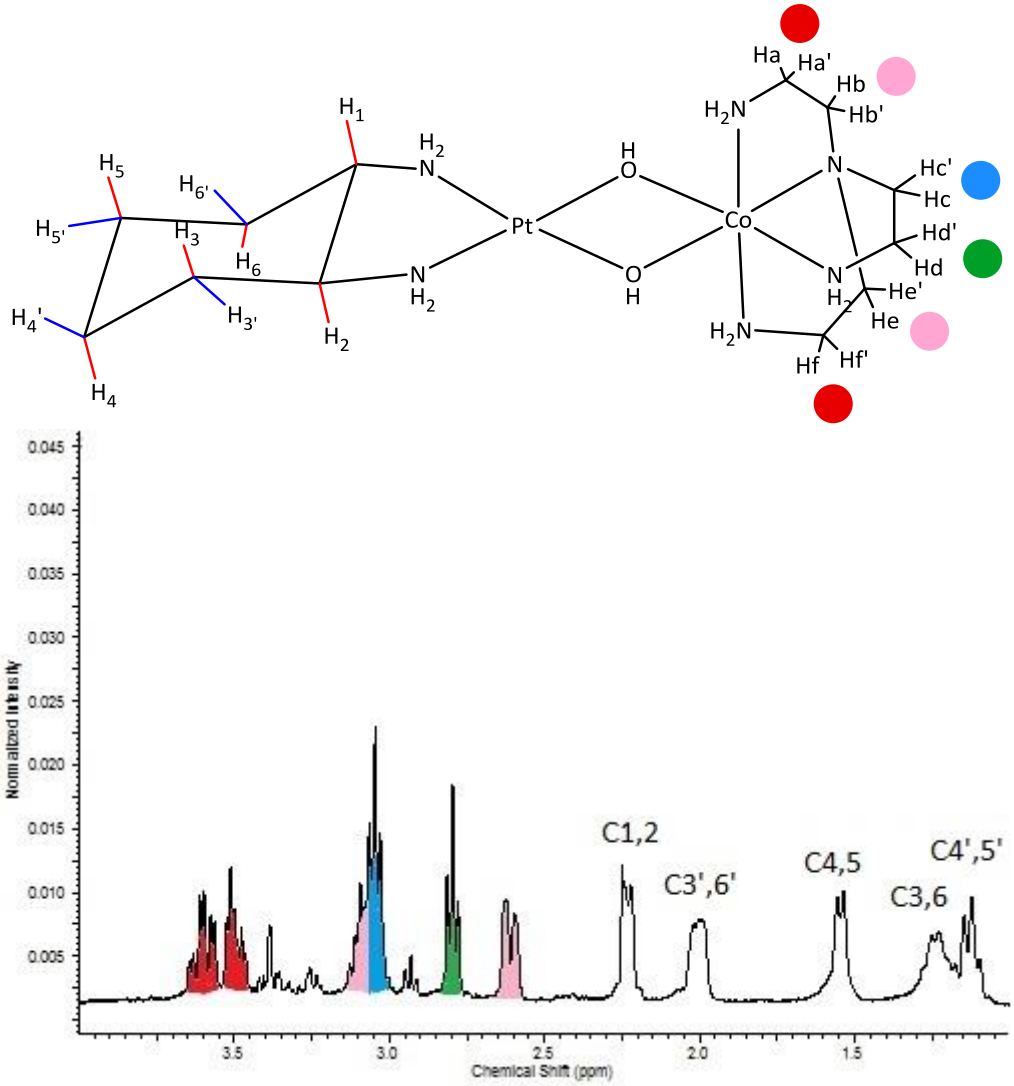

Figure 3-32 The ^{1}H NMR spectrum of **3.7** on D_2O**.** The signals marked by red colour are assigned to Ha,a',f,f'. The signals marked by pink colour are assigned to Hb,b',e,e'. The signal marked by blue colour is assigned to Hc,c' and the signal marked by green colour is assigned to Hd,d'. The cyclohexane hydrogen atoms are assigned by numbers.

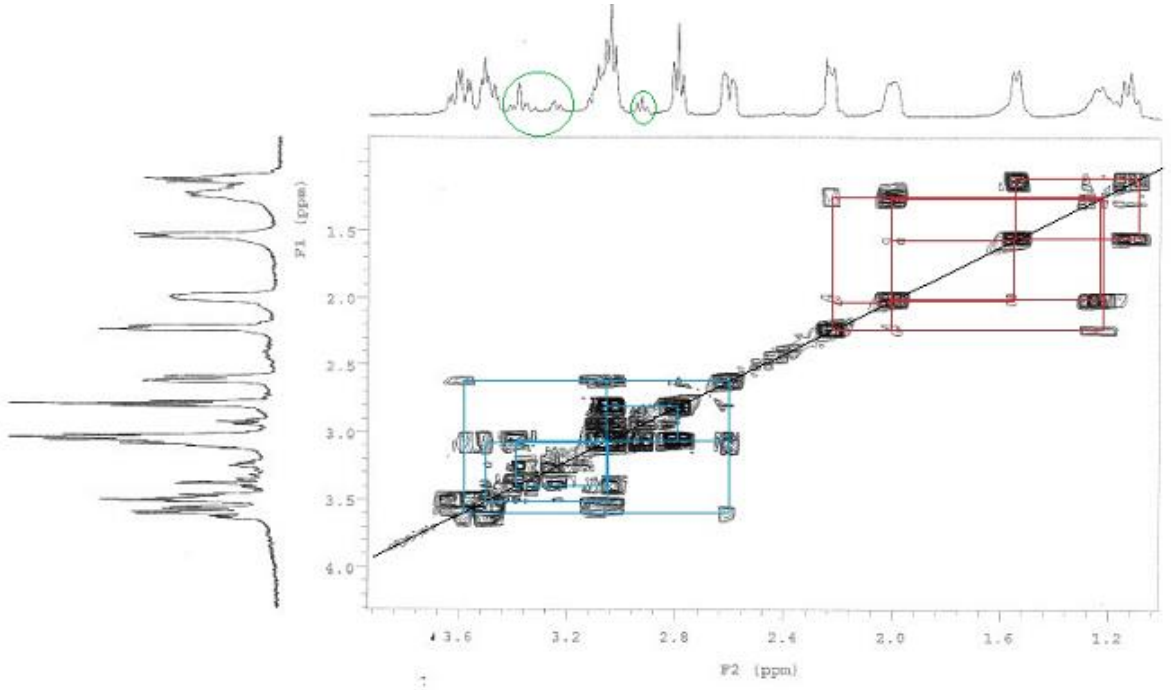

Figure 3-33 The ^{1}H-^{1}H COSY spectrum of **3.7** in D_2O**.** The squares drawn by blue colour show the correlations between tren protons on cobalt and those marked by red colour show the correlation of protons of chda ligand on platinum. The signals marked by green circles are impurities.

In the ^{13}C NMR spectrum, the four peaks at 62.22, 61.89, 44.5 and 44.27 ppm are assigned to four kinds of carbon atoms of tren ligand on Co (**Figure 3-34**). The three peaks at 62.22, 31.69 and 24.02 ppm are assigned to the three kinds of carbon atom present in the cyclohexane ring.

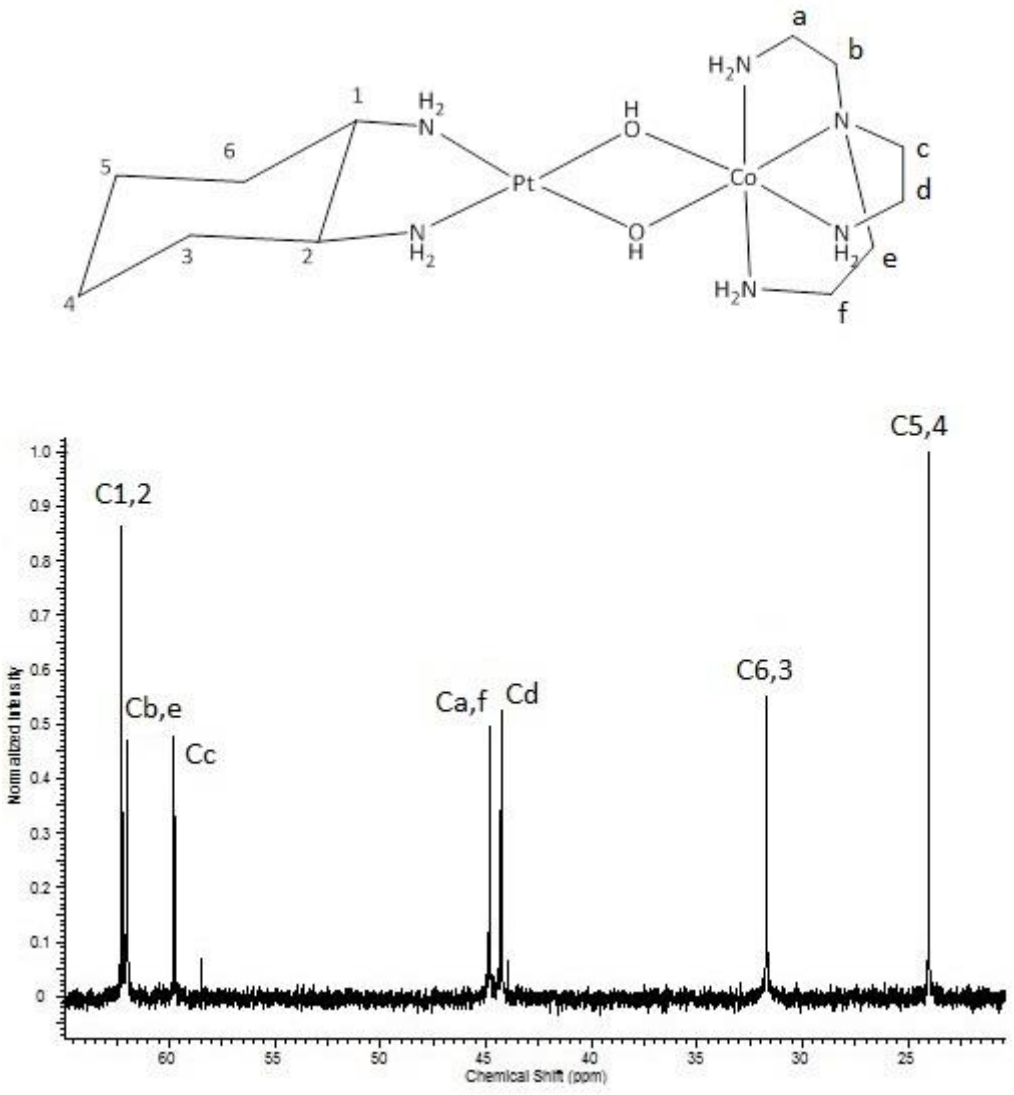

Figure 3-34 The ^{13}C NMR spectrum of **3.7** in D_2O. The cyclohexane carbon atoms are assigned by numbers; and the tren carbon atoms are assigned by letters.

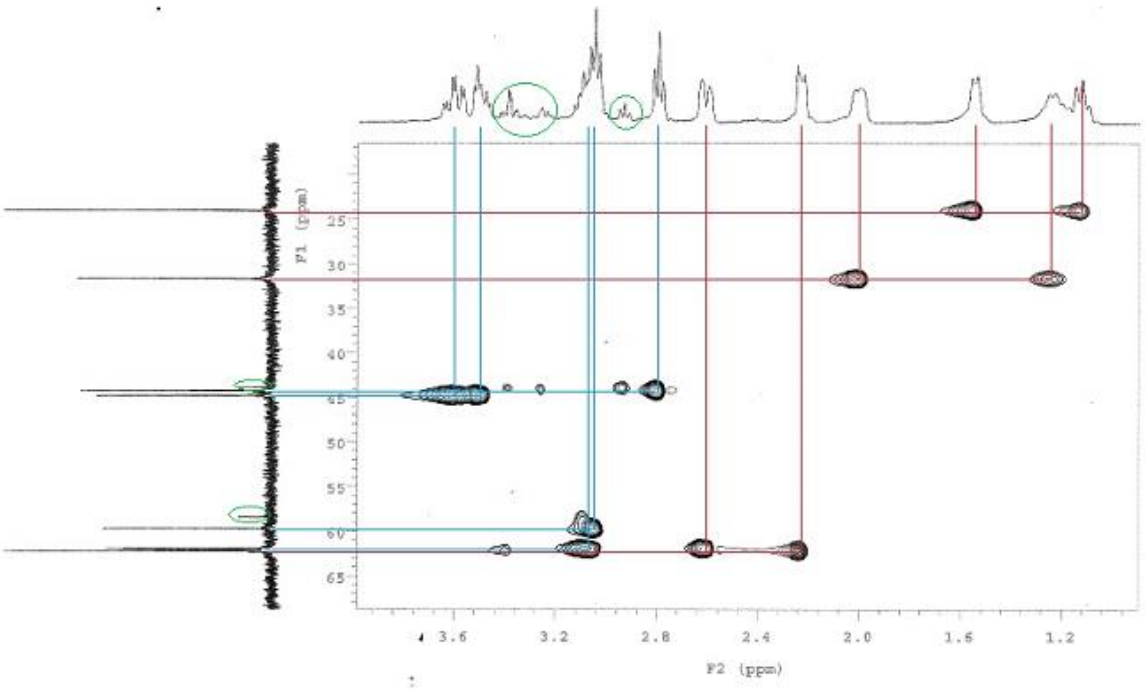

Figure 3-35 The ^{1}H-^{13}C HSQC spectrum of **3.7** in D_2O. The blue and red lines show the correlation between hydrogen and carbon atoms of tren ligand on Co and chda ligand on platinum respectively. The signals marked by green circles are impurities

3.3 Overview on cobalt-platinum chemistry

The isolation and purification of [Co(μ-OH)$_2$Pt] complexes from the reactions was quite challenging. Different methods such as recrystallisation and solvent extraction have been used in attempts to isolate the compounds but they did not work. Eventually, the use of ion exchange column chromatography came closest to achieving purification although this still did not give pure complexes. Purification of $[(en)_2Co(\mu\text{-}OH)_2Pt(chda)]^{3+}$ and $[(tren)Co(\mu\text{-}OH)_2Pt(chda)]^{3+}$ complexes were attempted on CM and SP Sephadex columns, and CM Sephadex gave better isolation. An SP column did not separate the bands completely and each fraction contained a huge number of impurities.

Purification of complexes by CM sephadex was associated with some problems. First of all the fractions did not elute as separate bands except the first band; but generally the separation of bands was better in CM Sephadex in comparison with SP Sephadex. Secondly,

the isolation had to be done as quickly as possible (which is difficult because water flow through the column is always slow), otherwise, the Co precursor would react with carboxylate groups of the column. Lastly, the majority of the last fraction stuck to the column presumably due to complexation with the carboxylate groups of the Sephadex.

Purification of $[(en)_2Co(\mu\text{-}OH)_2Pt(NH_3)_2]^{3+}$ and $[(tren)Co(\mu\text{-}OH)_2Pt(NH_3)_2]^{3+}$ complexes were attempted on size exclusion column chromatography on Sephadex G10. This column worked better for $[(tren)Co(\mu\text{-}OH)_2Pt(NH_3)_2]^{3+}$ and gave 3 bands.

Despite the fact that ion exchange chromatography can be used to obtain samples of dinuclear complexes that are relatively pure, there is also clear evidence that these complexes decompose while on the column and, on occasion, during evaporation of the eluates. The crystal structure of **3.4** might be good evidence describing the chemistry happening at least in the purification process of $[(en)_2Co(\mu\text{-}OH)_2Pt(chda)]^{2+}$ which may be very similar for other dinuclear $[Co(OH)_2Pt]$ complexes. Having $[Co(\mu\text{-}OH)_2Pt]$, a second platinum could coordinate to this platinum and the substitution chemistry results in the trinuclear compound which is shown in crystal structure (**3.4**) and eventually either platinum or cobalt (in a reaction with the carboxylate group of the column) leaves. If Co leaves, closing of the bridging ligand gives a diplatinum complex which its mass peak was found in mass spectrum. If platinum leaves, we may end up with a Co(μ-OH)Pt complex. Some evidence in support of this proposal is the occasional precipitation of yellowish powder from early fractions eluted from the column. The powder was later confirmed to be Pt(chda) by NMR with an unknown counter-ion. The ^1H NMR spectrum of the yellow powder is presented in **Figure 3-36.**

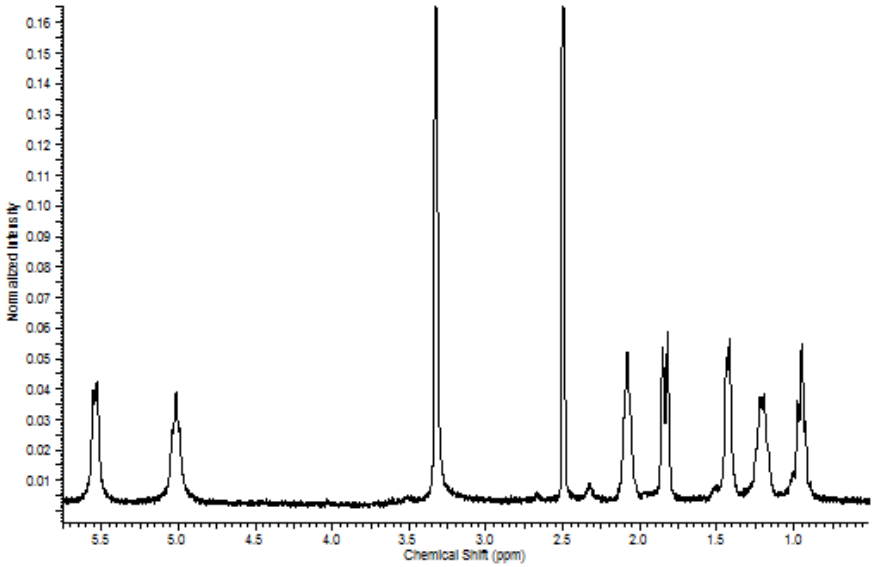

Figure 3-36 The ^{1}H NMR spectrum of yellow precipitation from third fraction in d^{6} DMSO

The intense red colour that remained on the columns necessarily means that the yield of the reactions cannot be high.

3.4 Conclusion

The key conclusion of this study is that dinuclear Co(μ-OH)$_2$Pt complexes can be made, but we have been unable to isolate them in pure form. The synthesis of dinuclear Co(μ-OH)Pt complexes has been proven by perfectly matched isotopic patterns in mass spectrometry and NMR studies. The crystals gained from this experiment (**3.4**) are trinuclear, suggested the lability of the Co(μ-OH)Pt complexes.

Attempts at purufying these complexes by using cation exchange chromatography on CM Sephadex and size exclusion column chromatography on Sephadex G10 were not succesful. None of these methods give the pure compounds in good yields.

The yield of the reactions are not high due to the side products produced and also based on the intense red colour remaining on the resin.

Chapter 4

Synthesis and Characterisation of Neutral Cobalt(III)-Platinum(II) Complexes

Chapter 4. Synthesis and Characterisation of Cobalt(III)-Platinum(II) Complexes

4.1 Introduction

The goal of our study is to prepare a series of $Co(\mu\text{-}OH)_2Pt$ complexes which may have potential to be anticancer drugs. Our initial efforts to synthesise dinuclear complexes containing Co(III)-amine systems resulted in mixtures of several other complexes with the dinuclear complexes we sought. Separations and isolation of the dinuclear complexes from these systems proved to be very challenging and were ultimately only partially successful.

Many of the Platinum(II) complexes whose isolation has been reported in the literature have no overall charge. Therefore, we attempted to synthesise neutral dinuclear complexes. Nitrilotriacetate (nta), as a L^{3-} ligand, was chosen for coordination to the Co(III) centre, and with two hydroxido bridging ligands between the Co(III) and platinum(II) ions, the overall charge of the resulting complex will come to zero, providing the remaining ligands on the platinum(II) centre are neutral.

Nitrilotriacetate normally acts as a tetradentate ligand, binding through the nitrogen atom and three carboxylate oxygen atoms to a metal ion[130]. The first attempt to synthesise a Co(III) complex of nta was reported by Mori et al.[131], but the chemistry is complicated by a dimerisation reaction[132]. Mori prepared a blue-coloured Co-nta complex by addition of $CoCl_2{\cdot}6H_2O$ and nta in potassium bicarbonate solution (2.5 M) and oxidising it by addition of hydrogen peroxide. This blue complex was formulated as $\alpha\text{-}K_2[Co(nta)(H_2O)(OH)]{\cdot}2H_2O$ (**Figure 4-1**). The filtrate of the reaction mixture was then acidified and reddish violet crystals were obtained. This reddish complex was formulated as β-

$K_2[Co(nta)(H_2O)(OH)]\cdot 2H_2O$ (**Figure 4-1**). The α and β complexes were postulated to differ only in the location of the aqua proton (see **Figure 4-1**). The aqua-hydroxido isomerism is possible in the solid state but is unlikely in solution since rapid proton exchange would be expected to render the suggested α and β forms indistinguishable, particularly in aqueous solution.

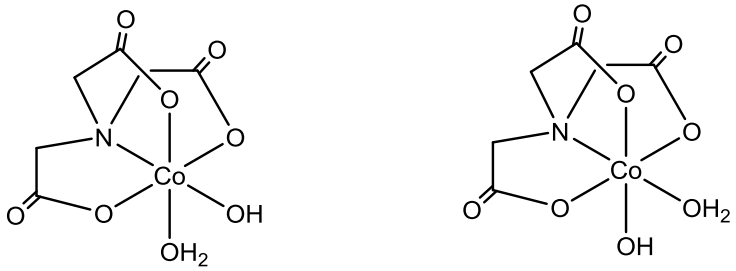

α-$[Co(nta)(H_2O)(OH)]^{2-}$ β-$[Co(nta)(H_2O)(OH)]^{2-}$

Figure 4-1 Structures of α- $[Co(nta)(H_2O)(OH)]^-$ and β-$[Co(nta)(H_2O)(OH)]^-$ proposed by Mori[131]

These formulations were based on elemental analyses and the bonding of an aqua and a hydroxide ligand was predicted for the remaining two bonding sites around the cobalt ion based on matching the analysis. Another study however proved the formulation was wrong[132]. A crystal structure determination of the so-called blue α-$K[Co(nta)(H_2O)(OH)]\cdot 2H_2O$ with the only difference being the presence of Cs^+ cations, proved to be $Cs_2[Co_2(nta)_2(\mu\text{-}OH)_2]\cdot 4H_2O$, containing a dinuclear cobalt complex (**Figure 4-2**).

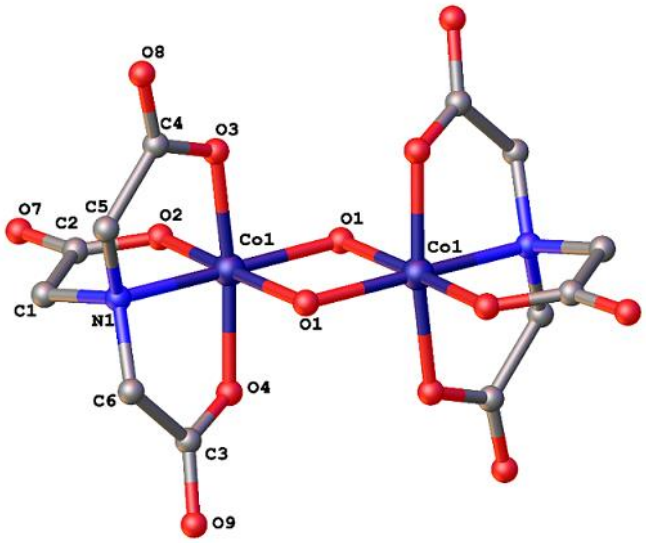

Figure 4-2 The crystal structure of anion of $Cs_2[Co_2(nta)_2(\mu\text{-}OH)_2]\cdot 4H_2O$[132]

A UV-Vis spectral study of the different Co-nta complexes present at different pH values led to the conclusion that the following reactions were occurring[132]:

$$[Co_2(nta)_2(\mu\text{-}OH)_2]^{2-} \underset{}{\overset{H^+}{\rightleftharpoons}} 2[Co(nta)(H_2O)_2] \underset{H^+}{\overset{OH^-}{\rightleftharpoons}} 2[Co(nta)(H_2O)(OH)]^-$$

The hydroxide bridges can be broken in a reversible protonation step to form the diaqua complex, $[Co(nta)(H_2O)_2]$. The diaqua complex forms the aqua-hydroxo complex, $[Co(nta)(H_2O)(OH)]^-$, with the addition of base in a reversible step.

4.2 Results and Discussion

4.2.1 Failure of the literature method to produce $[Co(nta)(H_2O)_2]$

$[Co(nta)(OH_2)_2]$ was synthesised using a different method to that described in the literature[131], as the literature method did not work for us, despite numerous attempts.

Our very first effort to synthesise $[Co(nta)(OH_2)_2]$ (**4.1**) complex was based on the Mori procedure, and gave a dinuclear complex of the formula of $K_2[Co_2(nta)_2(\mu\text{-}OH)_2]\cdot 6H_2O$ (**4.2**) in the first step; and $[Co(nta)(OH_2)_2]$ should have been obtained by acidifying the filtrate of the dinuclear complex. Although, we did not end up with the desired complex (**4.1**) by following this method, we did obtain some blue square crystals by slow evaporation of solvent, and these proved to be $K_2[Co_2(nta)_2(\mu\text{-}OH)_2]\cdot 6H_2O$ (**4.2**).

X-ray crystallography determined the structure of the $K_2[Co_2(nta)_2(\mu\text{-}OH)_2]\cdot 6H_2O$ to be that shown in **Figure 4-3**. This compound crystallised with half formula units in the asymmetric unit. Co1 is octahedrally coordinated to one N atom, three O atoms of the nta ligand and two bridging O atoms.

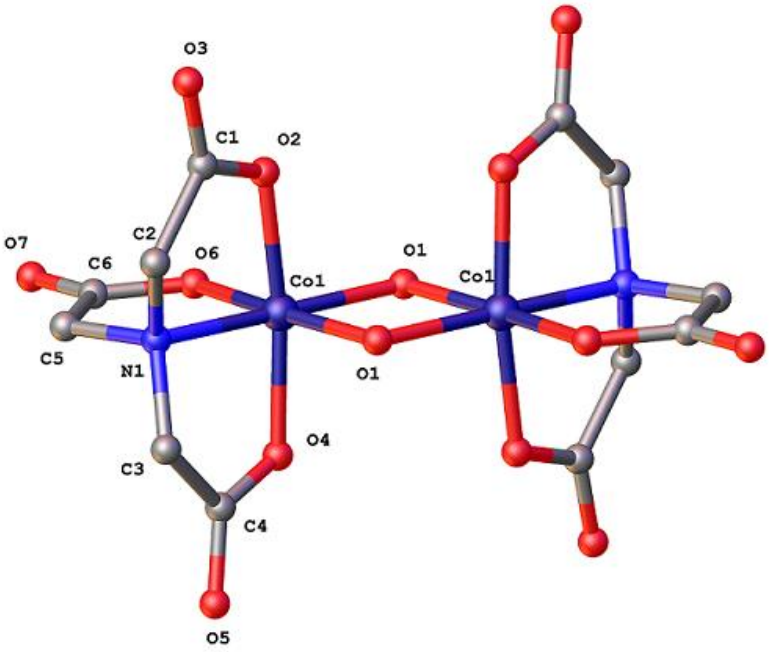

Figure 4-3 The crystal structure of the anion of **4.2**. Water molecules and hydrogen atoms are also omitted for clarity

As mentioned above, the crystal structure of $Cs_2[Co_2(nta)_2(\mu\text{-}OH)_2]$ has already been published. Our crystals, with potassium counter-ions, had a different unit cell and space

group to that of the cesium salt. The crystal data for our crystal and those of the published structure are compared in **Table 4-1**.

$Cs_2[Co_2(nta)_2(\mu\text{-}OH)_2]\cdot 4H_2O$	$K_2[Co_2(nta)_2(\mu\text{-}OH)_2]\cdot 6H_2O$
a = 19.640(2)	a = 12.6044(13)
b = 19.640(2)	b = 9.2309(7)
c = 12.581(2)	c = 13.0780(11)
Tetragonal, $I4_1/a$	Monoclinic, $P2_1/c$
α = 90	α = 90
β = 90	β = 110.233(11)°
γ = 90	γ = 90

Table 4-1 Crystal data comparison of $Cs_2[Co_2(nta)_2(\mu\text{-}OH)_2]\cdot 4H_2O$ and $K_2[Co_2(nta)_2(\mu\text{-}OH)_2]\cdot 6H_2O$

The dinuclear anion of **4.2** and the published structure both crystallised with half formula units in the asymmetric unit. The cobalt centres are octahedrally coordinated to the tetradentate nta ligand and two hydroxido bridging ligands.

4.3 Results from unsuccessful attempts to synthesise $[Co(nta)(H_2O)_2]$

Our attempts to synthesise $[Co(nta)(OH)_2]$ by different methods resulted in the isolation of other complexes, as shown in **Schemes 4-1**, **4-2**, and **4-3.** Crystals of **4.3**, **4.4** and **4.5** were obtained. The structures of these compounds are also shown in the schemes.

Cobalt is octahedrally attached to a tetradentate nta ligand and two carboxylate oxygen atoms of two other nta ligands in crystals of **4.3**.

In the crystal structure of **4.4**, Co1 is octahedrally attached to a tetradentate nta ligand and one carboxylate oxygen atom of another nta and one water molecule.

The crystal structure of **4.4** shows that cobalt is octahedrally coordinated to a nta ligand through two arms, three water molecules and one carboxylate oxygen atom.

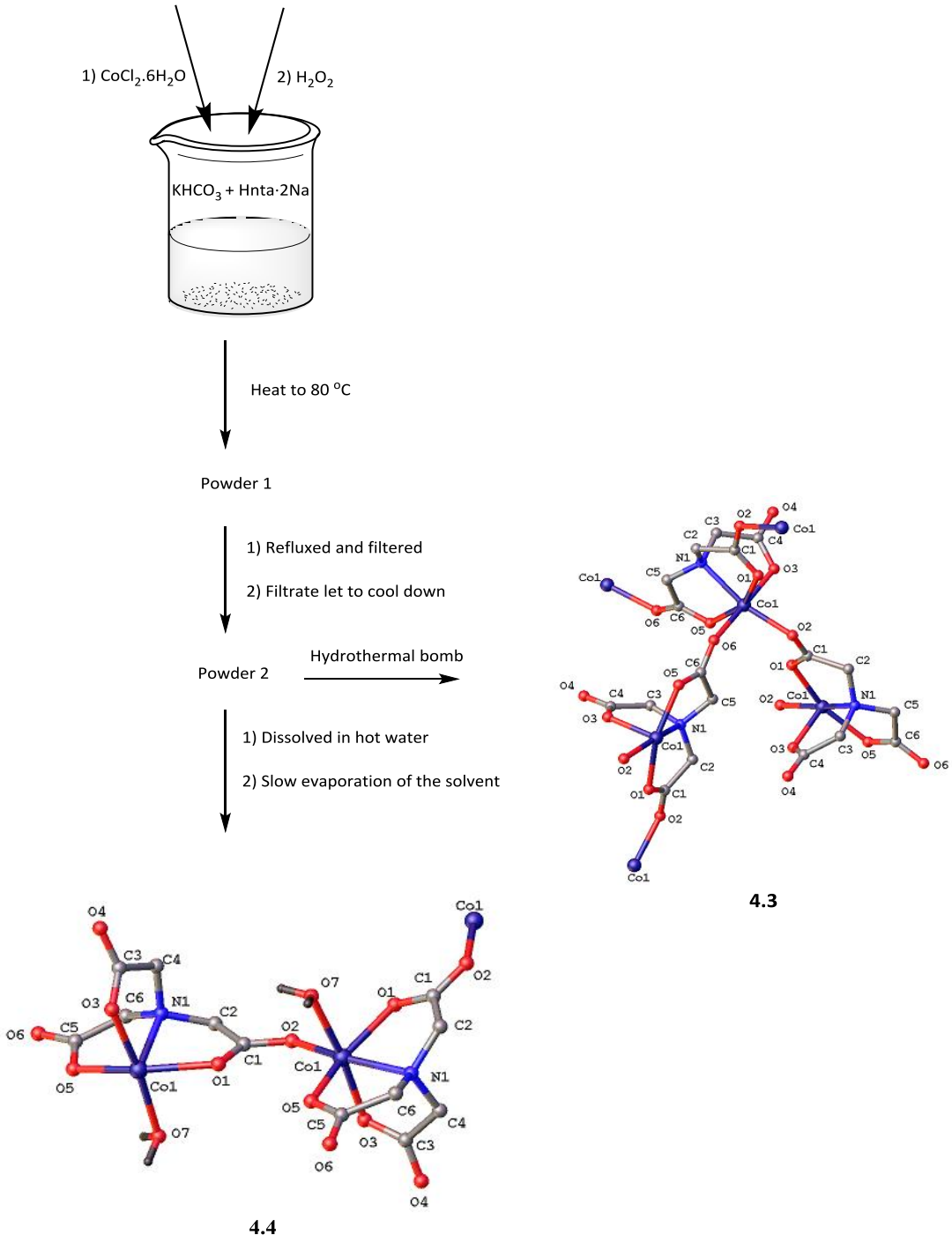

Scheme 4-1 Procedure to obtain crystals of **4.3** and **4.4**

Crystals of **4.3** have been reported, with two different preparation methods, in the literature[133],[134]. In one method, a mixture of $Co(NO_3)_2$, $NaHPO_4$ and nta was stirred at room temperature and then the reaction mixture was transferred to a sealed Teflon-lined stainless steel autoclave at 160 °C. The crystals of **4.3** formed after 4 days[133]. In the other method, a mixture of nta, $Co(CH_3COO)_2{\cdot}4H_2O$ and water was stirred, and then NaOH solution was added to adjust the pH to 5–6. Three weeks later, purple crystals of **4.3** were obtained[134].

In a new synthetic method, the disodium salt of Hnta and $KHCO_3$ were stirred at 80 °C in water and then $CoCl_2{\cdot}6H_2O$ and H_2O_2 were added. The formed powder was filtered and the powder suspended in water refluxed for two hours and then was filtered. The Powder 2 formed in the filtrate on cooling. Crystals of **4.3** were obtained by hydrothermal recrystallisation of Powder 2 at 60 °C.

Crystals of **4.4** have also been reported in literature, and were obtained by the following procedure[135]. The nta ligand was dissolved in water at 80 °C and the pH was adjusted to 6 by addition of NaOH solution. $Co(CH_3COO)_2{\cdot}4H_2O$ was then added to the reaction mixture. The reaction was filtered and crystals were obtained upon standing the filtrate for two months.

We obtained crystals of **4.4** by dissolving Powder 2 in water and allowing it to evaporate slowly.

In order to check that the single crystals that were analysed are representative of the bulk, the X-ray powder diffraction (PXRD) patterns were recorded. As shown in **Figure 4-4**, the peak positions in the experimentally determined patterns are in good agreement with those

calculated from the solution to the single crystal studies[133],[134]. The peak positions found for Powder 2 are a good match with the powder pattern of crystal **4.3**.

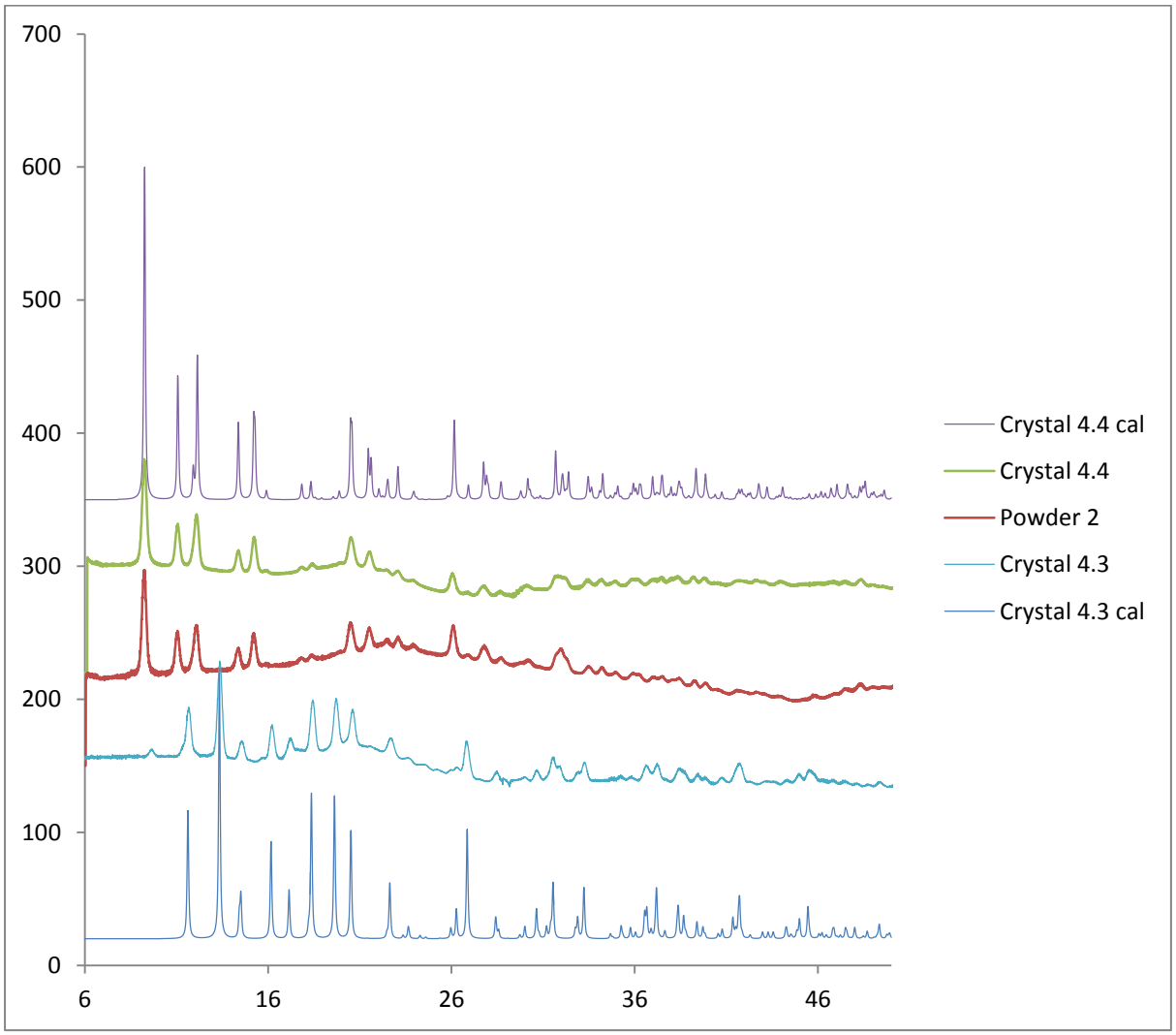

Figure 4-4 Experimental and Calculated PXRD patterns for crystal **4.3**, **4.4** and Powder 2

Thus, the methods shown in **Scheme 4-1** produce crystalline polymeric Co-nta complexes that have been previously synthesised by different but related methods.

Crystals of **4.5** were prepared by the method shown in **Scheme 4-2**. The disodium salt of nta was suspended in water and the pH was adjusted to 7.3 by addition of a solution of NaOH. $Co(NO_3)_2$ was added and the reaction was heated at 80 °C. The Powder 3 was collected and

heated at 70 °C in water and then filtered. Powder 4 formed in the filtrate and was collected and transferred to a hydrothermal bomb at 50 °C in water. The crystals formed, in this hot solution after a week.

A single crystal X-ray analysis revealed that these crystals of **4.5** were the same as those reported in the literature, which were obtained through slow evaporation of an equimolar mixture of $CoSO_4 \cdot 7H_2O$ and $nta \cdot K_2$ in water (both commercial grade)[136].

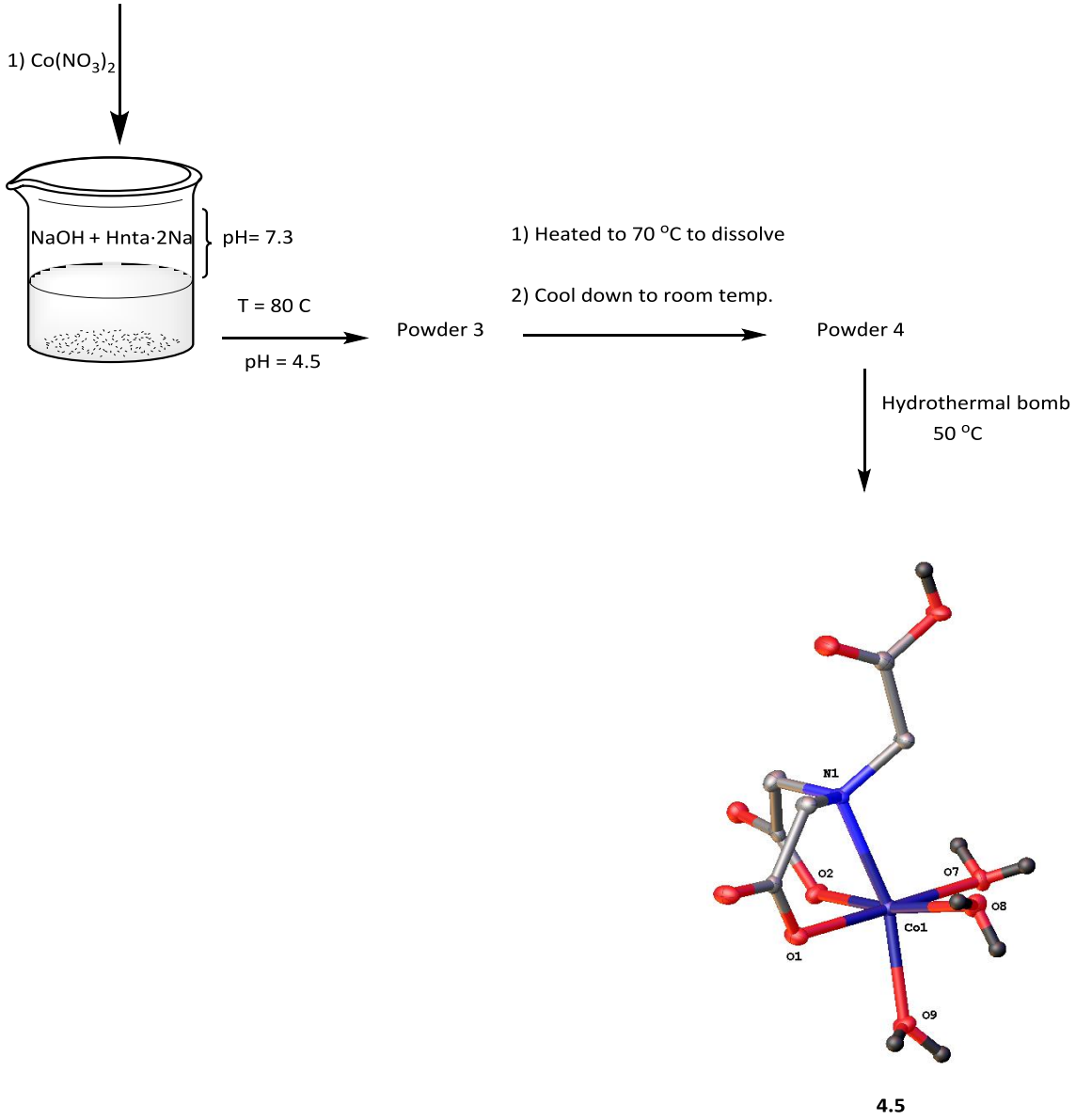

Scheme 4-2 Procedure to obtain crystal **4.5**

In order to check that the single crystals that were analysed are representative of the bulk, the X-ray powder diffraction (PXRD) patterns were recorded. As shown in **Figure 4-5**, the peak positions in the experimentally determined pattern are mostly in agreement with that calculated from the solution to the single crystal study.

The PXRD pattern of Powder 4 is mostly in agreement with the crystalline material but extra peaks are also observed, indicating that something else is also present in the powder.

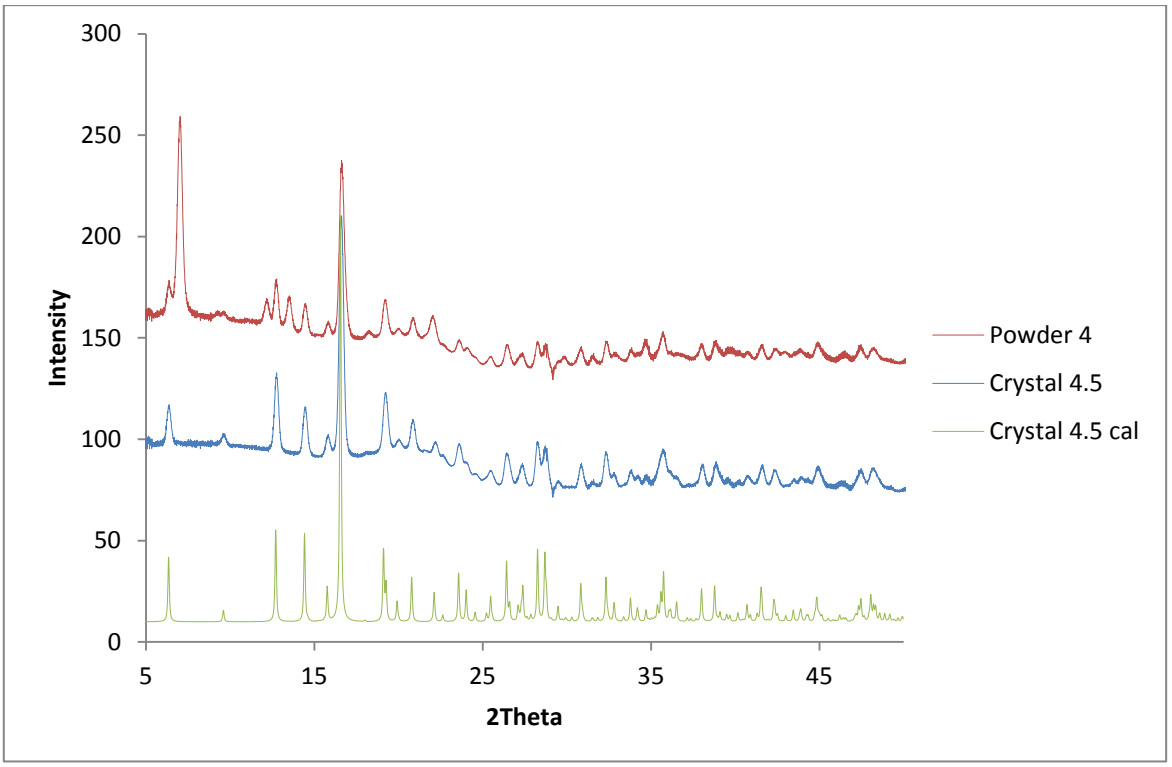

Figure 4-5 Experimental and simulated PXRD patterns for crystal **4.5** and powder 4

A different crystalline material was obtained using the procedure shown on **Scheme 4-3**.

The ligand was suspended in water and NaOH was added until the pH was approximately 7. $Co(NO_3)_2$ was added to reaction mixture. The pH of the reaction dropped to 4.2. The reaction was stirred at room temperature and after a while a pink precipitate formed. The precipitate was filtered and then suspended in water. 1 mL H_2O_2 50% was added and the

reaction was heated to 90 °C. The solution was left for some days and product formed as pink crystals (**4.6**).

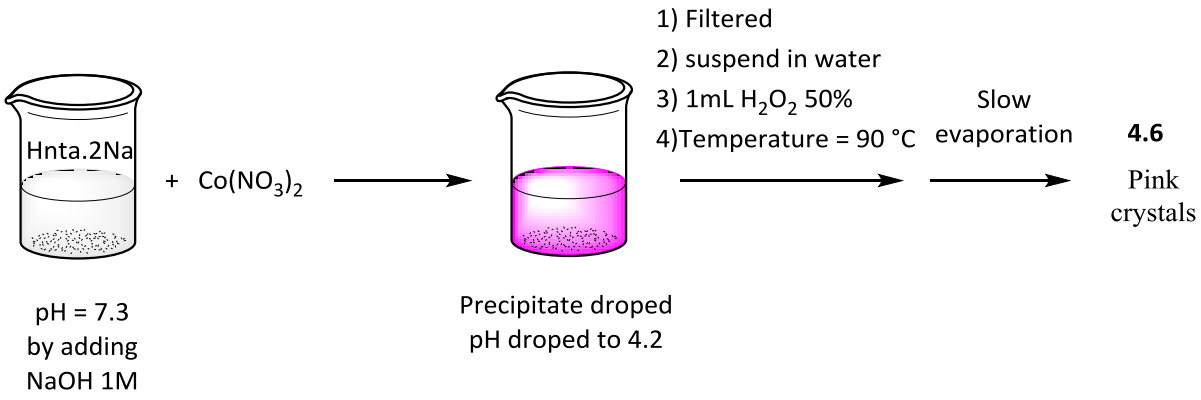

Scheme 4-3 Synthetic route to obtain crystals of **4.6**

The structure of the crystals $(C_{12}H_{29.8}Co_{2.5}N_2O_{21.4})_\infty$ (**4.6**) was determined by X-ray diffraction to be that of a polymer (**Figure 4-6**). The repeating unit has the formula $[C_{12}H_{21}N_2O_{17}Co_{2.5}]$. The crystal **4.6** contains three kinds of cobalt centres. Co1 is octahedrally coordinated to two nta ligands through two arms of each. It means Co1 is coordinated to four carboxylate oxygen atoms and two nitrogen atoms of two nta ligand. The non-coordinated arm of the nta ligand to Co1, chelates to two Co2 centres through O9 and O10. Another non-coordinated arm of the nta ligand to Co1, coordinated to Co3 monodentately through O15. Co2 unit is a dinuclear complex formed through O13. Co2 is coordinated to bridging oxygen atoms (O13), two water molecules (O11 and O12) and two carboxylate oxygen atoms of the nta ligand. Co3 is coordinated to four water molecules and two carboxylate oxygen atoms of the nta ligand. Selected bond lengths and bond angles of **4.6** are given in **Tables 4-2** and **4-3**.

The polymer is generated by CO_2 being in a centrosymmetric dimer and the coordination sphere around C3 being generated by a centre of symmetry. The packing diagram of **4.6** is shown by different colours in **Figure 4-7**.

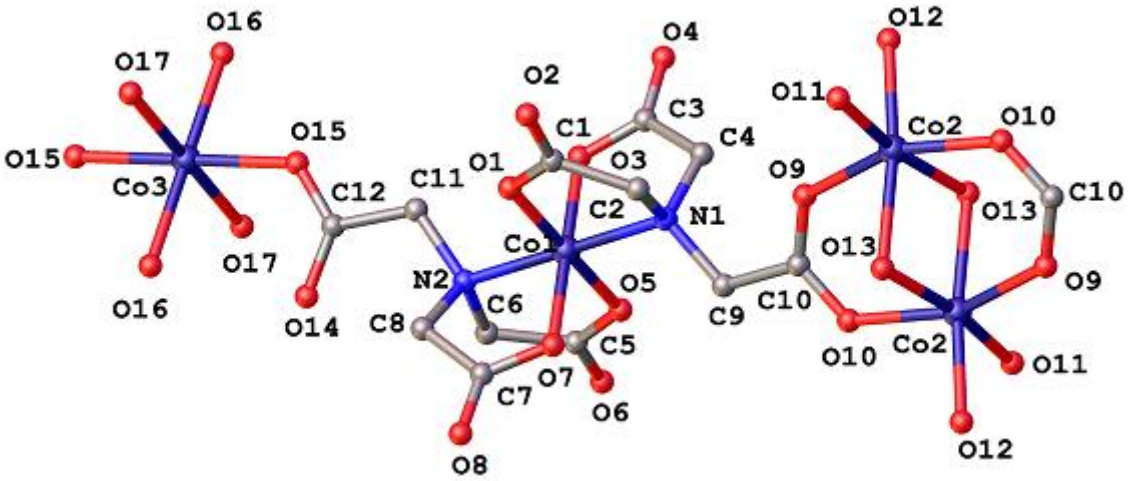

Figure 4-6 The crystal structure of **4.6.** The water molecules and hydrogen atoms are omitted for clarity

Bond length [Å]			
Co1-O1	1.889(2)	Co2-O13	2.062(2)
Co1-O5	1.883(2)	Co2-O12	2.062(2)
Co1-O3	1.889(2)	Co2-O11	2.037(3)
Co1-O7	1.892(2)	Co3-O15	2.115(2)
Co1-N2	1.975(3)	Co3-O16	2.087(2)
Co1-N1	1.986(3)	Co3-O17	2.090(3)
Co2-O10	2.067(2)	Co2-O9	2.070(2)

Table 4-2 Selected bond lengths for **4.6**

Bond angle [°]			
O1-Co1-O3	89.21(12)	C10-O10-Co2	124.5(2)
O1-Co1-O7	91.90(12)	C12-O15-Co3	125.4(2)
O1-Co1-N2	90.99(11)	C1-O1-Co1	115.2(2)
O1-Co1-N1	87.28(11)	C5-O5-Co1	115.2(2)
O5-Co1-O1	177.78(11)	C3-O3-Co1	115.4(2)
O5-Co1-O3	88.87(11)	C7-O7-Co1	114.2(2)
O5-Co1-O7	90.01(11)	C8-N2-Co1	103.2(2)
O5-Co1-N2	88.02(10)	C8-N2-C11	110.6(3)
O5-Co1-N1	93.75(10)	C8-N2-C6	111.3(3)
O3-Co1-O7	178.73(12)	C11-N2-Co1	112.00(19)
O3-Co1-N2	93.66(10)	C6-N2-Co1	106.44(19)
O3-Co1-N1	87.37(10)	C6-N2-C11	112.8(3)
O7-Co1-N2	85.70(10)	C9-N1-Co1	114.41(19)
O7-Co1-N1	93.30(10)	C9-N1-C2	110.1(3)
N2-Co1-N1	177.97(11)	C9-N1-C4	110.6(3)
O10-Co2-O13	83.45(9)	C2-N1-Co1	104.1(2)
O11-Co2-O10	89.23(10)	C4-N1-Co1	105.1(2)
O11-Co2-O13	171.39(9)	C4-N1-C2	112.3(3)
O11-Co2-O12	88.70(11)	O16-Co3-O15	89.47(9)
O12-Co2-O10	101.01(9)	O16-Co3-O17	90.49(10)
O12-Co2-O13	88.25(10)	O17-Co3-O15	92.98(10)

Table 4-3 Selected bond angles for **4.6**

The X-ray diffraction study showed complex **4.6** formed a mixed valence polymeric structure, based on the bond lengths. The Co3–O and Co2-O distances are in the range 2.062–2.205 A˚, comparable to the corresponding values found in Co(II) complexes[137],[136],. The Co(1)–O distances 1.889 A˚ and the Co(1)–N distance is 1.986 and 1.975 A˚, comparable to the corresponding values found in other Co(III) complexes. The packing structure of **4.6** is shown in **Figure 4-7**.

The ^{1}H NMR spectrum of **4.6** is shown in **Figure 4-8**. There are three sets of peaks, but they are broad, which may be consistent with its formulation as a mixed valence complex.

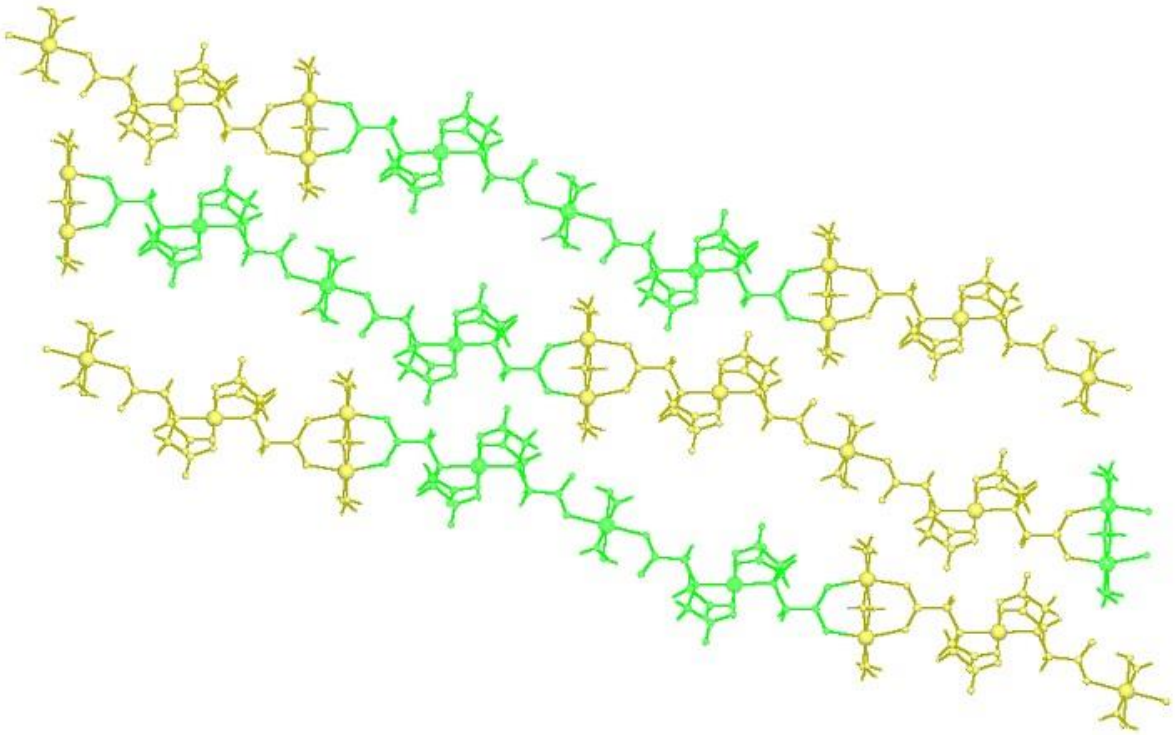

Figure 4-7 A packing diagram within the crystal structure of **4.6**.

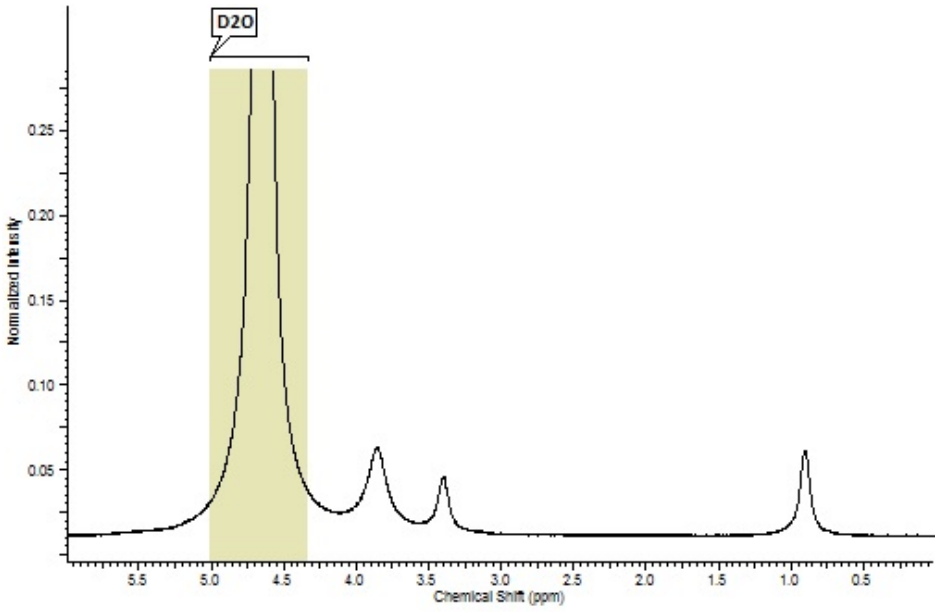

Figure 4-8 The ^{1}H NMR spectrum of **4.6** in D_2O

4.3.1 Synthesis and characterisation of [Co(nta)$(OH_2)_2$]

We synthesised [Co(nta)$(OH_2)_2$] in a straight-forward manner by addition of a lesser amount of potassium bicarbonate in comparison with Mori's method, giving an acidic medium (pH~3) for the reaction between $CoCl_2$ and the disodium salt of the nta ligand with hydrogen peroxide as the oxidant. Although we ultimately synthesised pure [Co(nta)$(OH_2)_2$] complex, the yield of the reaction (22%) is lower than the literature (40%).

The geminal hydrogen atoms are indicated in red and blue in **Figure 4-9.** The ^{1}H NMR spectrum of [Co(nta)$(H_2O)_2$] contains an AB multiplet and a singlet peak (**Figure 4-10).** These hydrogen atoms are inequivalent and couple to each other, leading to the AB system. The hydrogen atoms indicated in black are equivalent and they appear as a singlet in the ^{1}H NMR spectrum.

The ^{13}C NMR spectrum of [Co(nta)$(OH_2)_2$], contains four signals (**Figure 4-11**). The peaks at 178 and 168 ppm are assigned to the two equivalent axial carboxylic carbon atoms, and one equatorial carboxylic carbon atom, respectively, based on the fact that the signal at 178 ppm has twice the intensity of that at 168 ppm. Two other signals at 66.92 and 62.69 ppm are assigned to the two equivalent axial methylene carbon atoms and one equatorial methylene carbon atom, respectively, on the same basis.

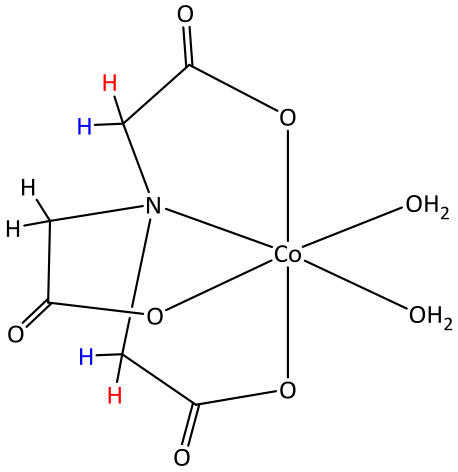

Figure 4-9 Structure of $[Co(nta)(H_2O)_2]$ (**4.1**)

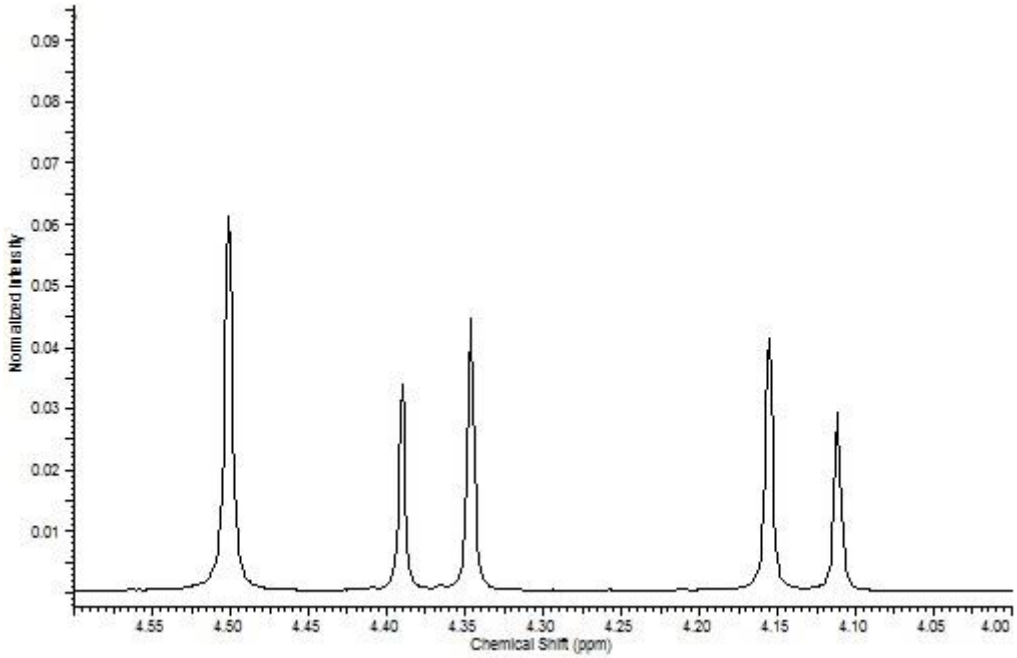

Figure 4-10 The ^{1}H NMR spectrum of $[Co(nta)(OH_2)_2]$ (**4.1**) in D_2O

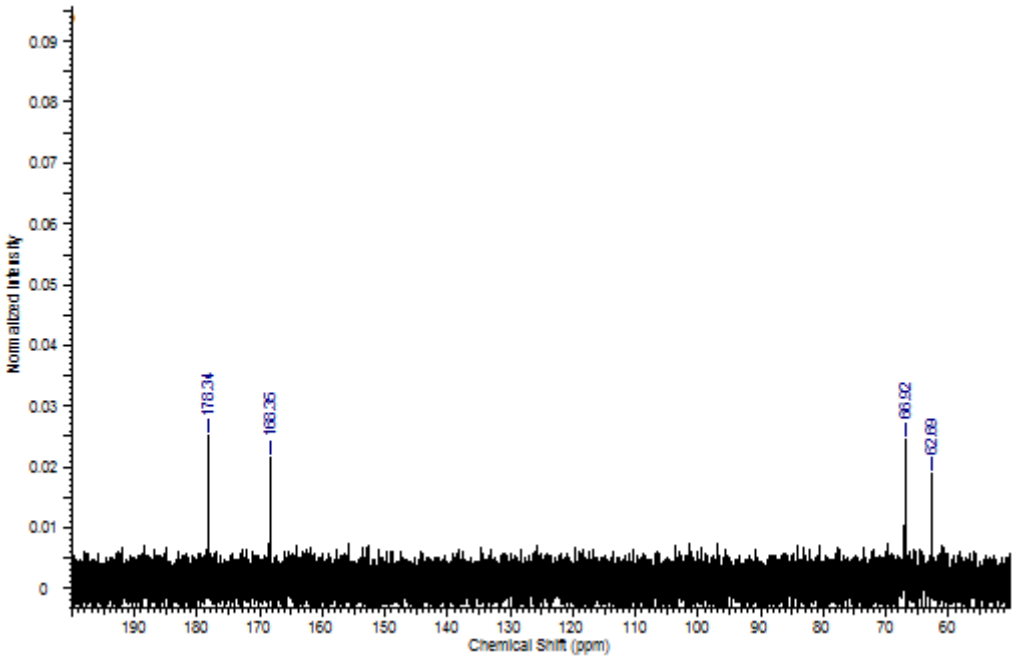

Figure 4-11 The ^{13}C NMR spectrum of $[Co(nta)(H_2O)_2]$ (**4.1**) in d^6 DMSO

4.4 Preparation and Characterisation of Neutral $[Co(\mu\text{-}OH)_2Pt]$ Complexes

A general overview of the synthesis of complexes of the general form $[(nta)Co(\mu\text{-}OH)_2Pt(L)]$ (L = chda, en, $(NH_3)_2$) is presented below, in **Scheme 4-4**. $[Pt(L)Cl_2]$ was treated with silver nitrate to displace halide ligands[125]. The silver halide precipitate was centrifuged and the pH of the supernatant was adjusted to 5 to match that of the solution of $[Co(nta)(OH_2)_2]$ in water. The supernatant was added to a solution of $[Co(nta)(OH_2)_2]$ (pH=5). The reaction mixture was stirred. The products (**4.7**, **4.12** and **4.16**) precipitated from the reaction mixture as pink powders.

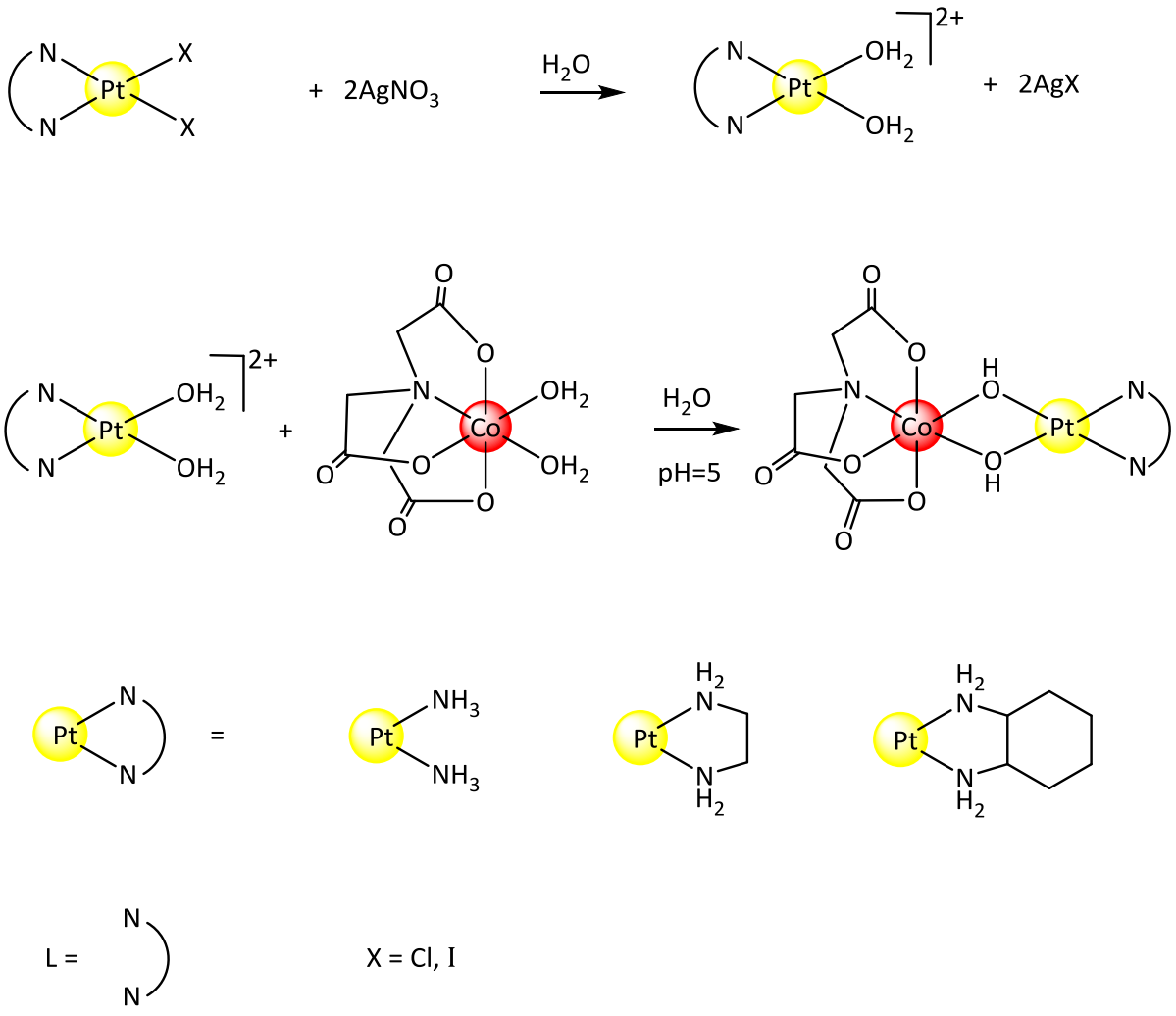

Scheme 4-4 General synthetic route to produce complexes of the general formula of [(nta)Co(μ-OH)$_2$Pt(L)] (L = chda, en, (NH$_3$)$_2$)

The elemental analysis results are consistent with the formula of [Co(nta)(μ-OH)$_2$Pt(L)]·2H$_2$O for the complexes. The characterisation of these complexes is limited due to their very low solubility in most solvents.

The IR spectra of the synthesised complexes are shown in **Figure 4-13.** The IR spectra of the three dinuclear complexes look very similar, as expected. There are significant differences between the spectra in the fingerprint region, presumably due to the different ligands being

bound to the platinum centre. The carbonyl stretching frequency of **4.7**, **4.12** and **4.16** are observed at 1621, 1614 and 1621 cm^{-1} respectively.

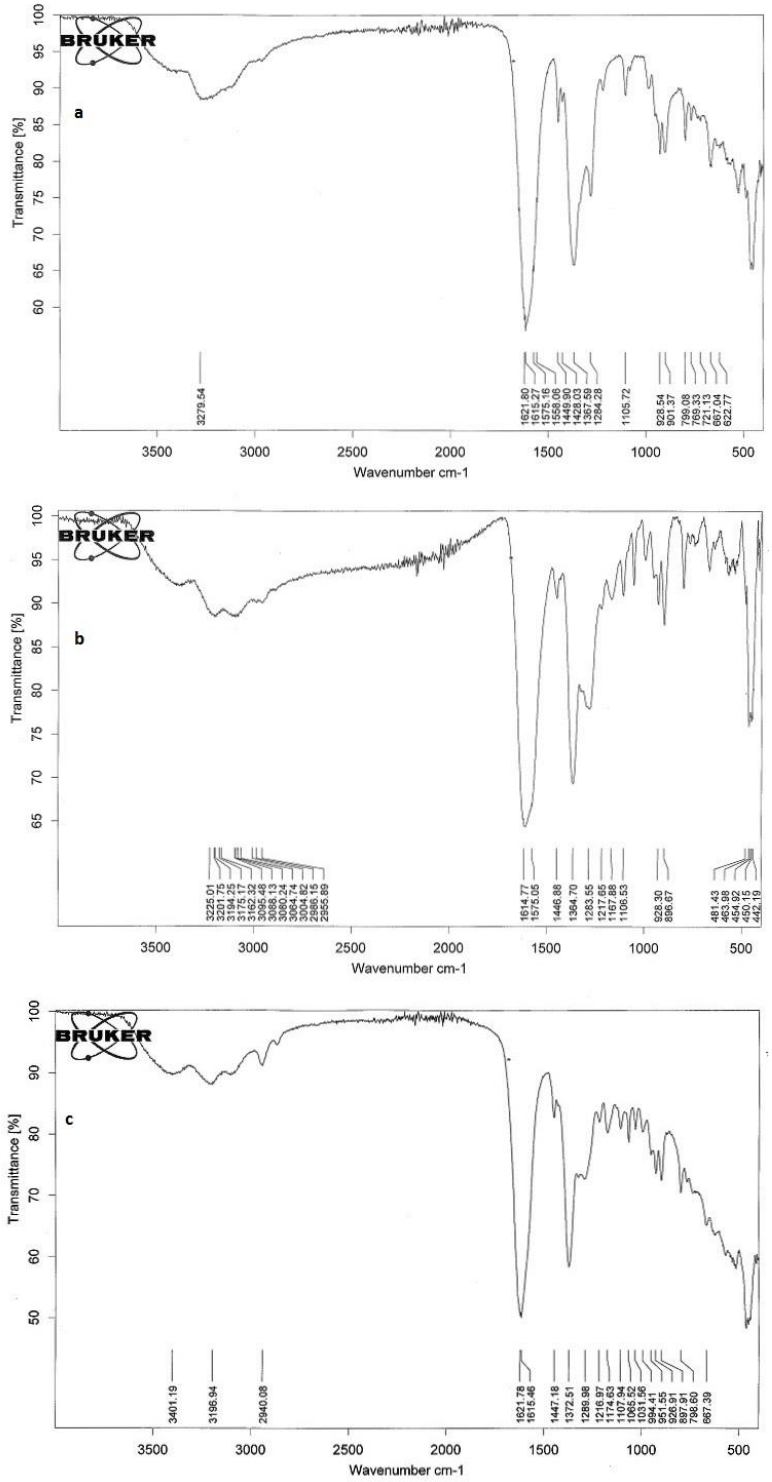

Figure 4-12 The IR spectra of **a)** [(nta)Co(μ-OH)$_2$Pt(NH$_3$)$_2$] (**4.16**), **b)** [(nta)Co(μ-OH)$_2$Pt(en)] (**4.12**) and **c)** [(nta)Co(μ-OH)$_2$Pt(chda)] (**4.7**)

4.4.1 NMR studies

4.4.1.1 NMR studies of [(nta)Co(μ-OH)$_2$Pt(chda)] in DMSO, 4.7

[Co(nta)(μ-OH)$_2$Pt(chda)] (**4.7**), shown in **Figure 4-13**, is insoluble in most of the common solvents except for some solubility in DMSO. The ^{1}H NMR spectrum of [Co(nta)(μ-OH)$_2$Pt(chda)] in d^6 DMSO is shown in **Figure 4-14**.

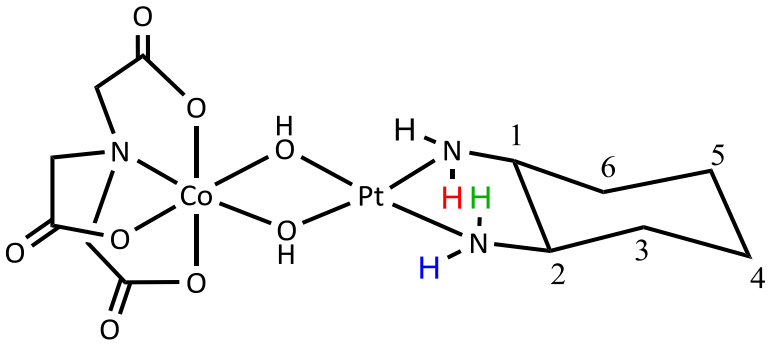

Figure 4-13 Arrangement of the hydrogen atoms on amine groups

The key point about **4.7** is the asymmetry of the molecule due to the amine chirality. One amine is *trans* to equatorial oxygen atom of nta and another amine is *trans* to the nitrogen atom of the nta. It means all hydrogen and carbon atoms on chda are inequivalent. Moreover, the axial arms of the nta ligand are not equivalent anymore. We expect to see 10 sets of signals for the cyclohexane hydrogen atoms, 4 signals for four different hydrogen atoms on the amine, two sets of AB systems for the methylene hydrogen atoms on the axial arms of the nta ligand and a singlet for the equatorial hydrogen atoms.

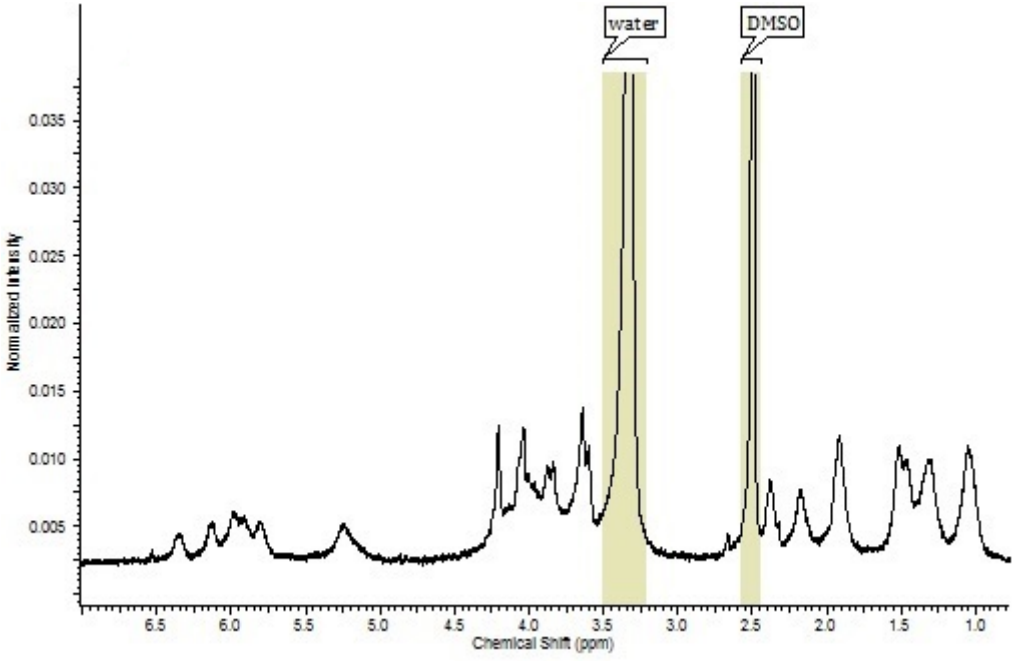

Figure 4-14 The ^{1}H NMR spectrum of **4.7** in d^{6} DMSO at 25 °C

The ^{1}H NMR spectrum of **4.7** in d^{6} DMSO at 25 °C showed 6 sets of signals from 1 to 2.5 ppm (**Figure 4-14**). This is the region that signals assigned to the chda ligand are observed, based on studies described in earlier chapters. The appearance of this part of the spectrum is also similar to other chda spectra discussed in earlier chapters. We have 10 different hydrogen atoms on carbon atoms in the chda ligand on platinum. Eight of the hydrogen atoms may coincidentally overlap each other and appeared as four sets of signals and two other hydrogen atoms appeared as two sets of signals with smaller integrations in the ^{1}H NMR spectrum (Figure **4-14**). The signals from 3.5 to 4.7 ppm belong to nta ligand, however it is not clear which signals belong to which protons within the ligand. This is largely due to of peak broadening and overlapping peaks. The rest of the signals from 5 to 6.5 are assigned to amine hydrogen atoms. The number of signals for the nta region shows there are more than one Co(nta) complex present in the solution. We speculate that this mixture of complexes is formed by reaction of **4.7** with DMSO.

In order to explore the reactivity of the complex with DMSO, another ^{1}H NMR spectrum was taken at high temperature (80 °C, **Figure 4-15 b**). The ^{1}H NMR spectrum (80 °C) showed five sets of signals in the chda region. The region assigned to the nta ligand contains three AB multiplets and two singlets.

There are also four broad signals from 5.6 to 6.4 ppm assigned to four amine hydrogen atoms. The signals assigned to the amine protons at 5.2 ppm disappeared (**Figure 4-15 b**). This may mean at least one of the OH bridging ligands is replaced by DMSO. The ^{1}H NMR spectra presented in the literature indicate that $[Pt(en)Cl_2]$ has a resonance at 5.31 ppm which is assigned to the equivalent amine protons. For $[PtCl(en)(dmso)]^{+}$, amine protons have sets of resonances at 6.31 and 6.06 ppm due to inequivalent amine protons[138]. Based on this result[138], we may infer the spectrum shown in **Figure 4-15 a** is a mixture of the dinuclear complex and the complex reacted to DMSO. The peak at 5.25 ppm may also be assigned to the amine protons of the dinuclear complex (**4.7**) and the peaks between 6 and 6.5 ppm may pertain to amine protons after having DMSO as a ligand attached to platinum. In other words, we think the dissolution of the complex is tied to the reaction with the solvent.

The NMR tube containing the sample was left for some hours at room temperature, and then a ^{1}H NMR spectrum was taken again (**Figure 4-15c**). This spectrum is very similar with the one obtained at 80 °C but lower in clarity.

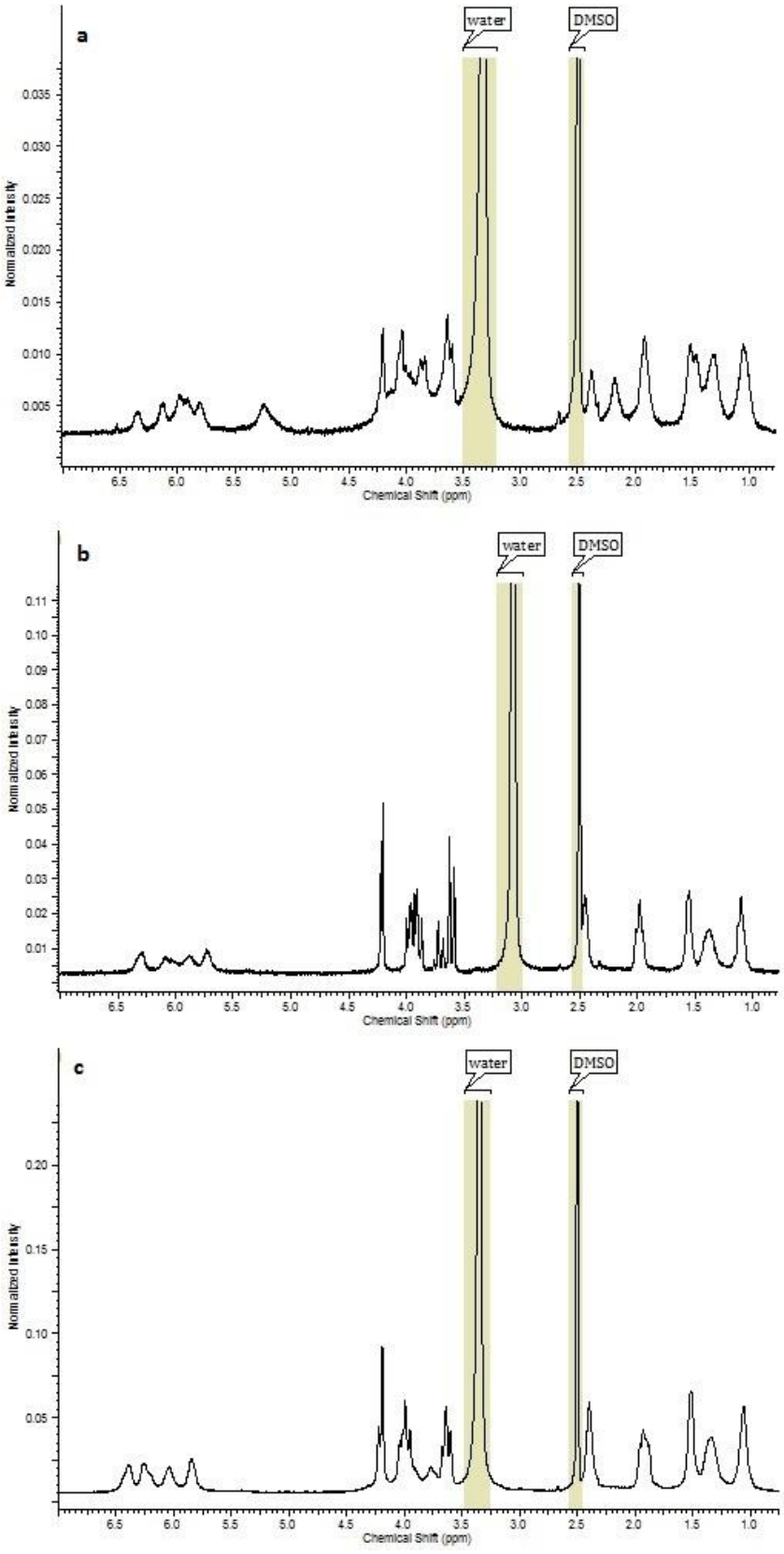

Figure 4-15 The ^{1}H NMR spectrum of [Co(nta)(μ-OH)$_2$Pt(chda)](**4.7**) **a)** at 25 °C; **b)** at 80 °C; **c)** after cooling down, at 25 °C in d^{6} DMSO

The ^{1}H-^{1}H COSY spectrum showed a cross peak between H1 and H2 of the chda ligand and the amine protons. The chemical shifts of the amine protons show they are *trans* to DMSO. The broad signal at 5.25 ppm possibly belongs to the amine hydrogen atoms of the dinuclear complex (**4.7)**. As this signal disappeared in the spectrum at high temperature, it may suggest that most of **4.7** reacted with DMSO.

The ^{13}C NMR spectrum was taken once in 80 °C and again at 25 °C after cooling down the sample (**Figure 4-16**)

We observed 6 signals for the cyclohexane ring, as we expected for **4.7,** since all of the carbon atoms of the cyclohexane ring become inequivalent after binding of platinum to Co(nta) (**Figure 4-16a**). The existence of at least four signals in the carboxylate carbon region and four signals in the methylene region would mean having more than one complex. The ^{1}H NMR spectrum already supported cleavage of one of the hydroxido bridging ligands by DMSO. The number of signals may suggests two compounds are present. We speculate **4.8** and **4.9** are present at the same time. If we have complexes **4.8** and **4.9**, we still expect to see 6 signals for chda, since the chda ligand may not be affected by the difference between having water or DMSO attached to cobalt; but more than one set of signals should be seen for nta ligand on cobalt.

The ^{13}C NMR spectrum taken at 25 °C, after cooling down is not very different from the one taken at 80 °C (**Figure 4-16b**). This means the reaction between complex **4.7** and DMSO is irreversible.

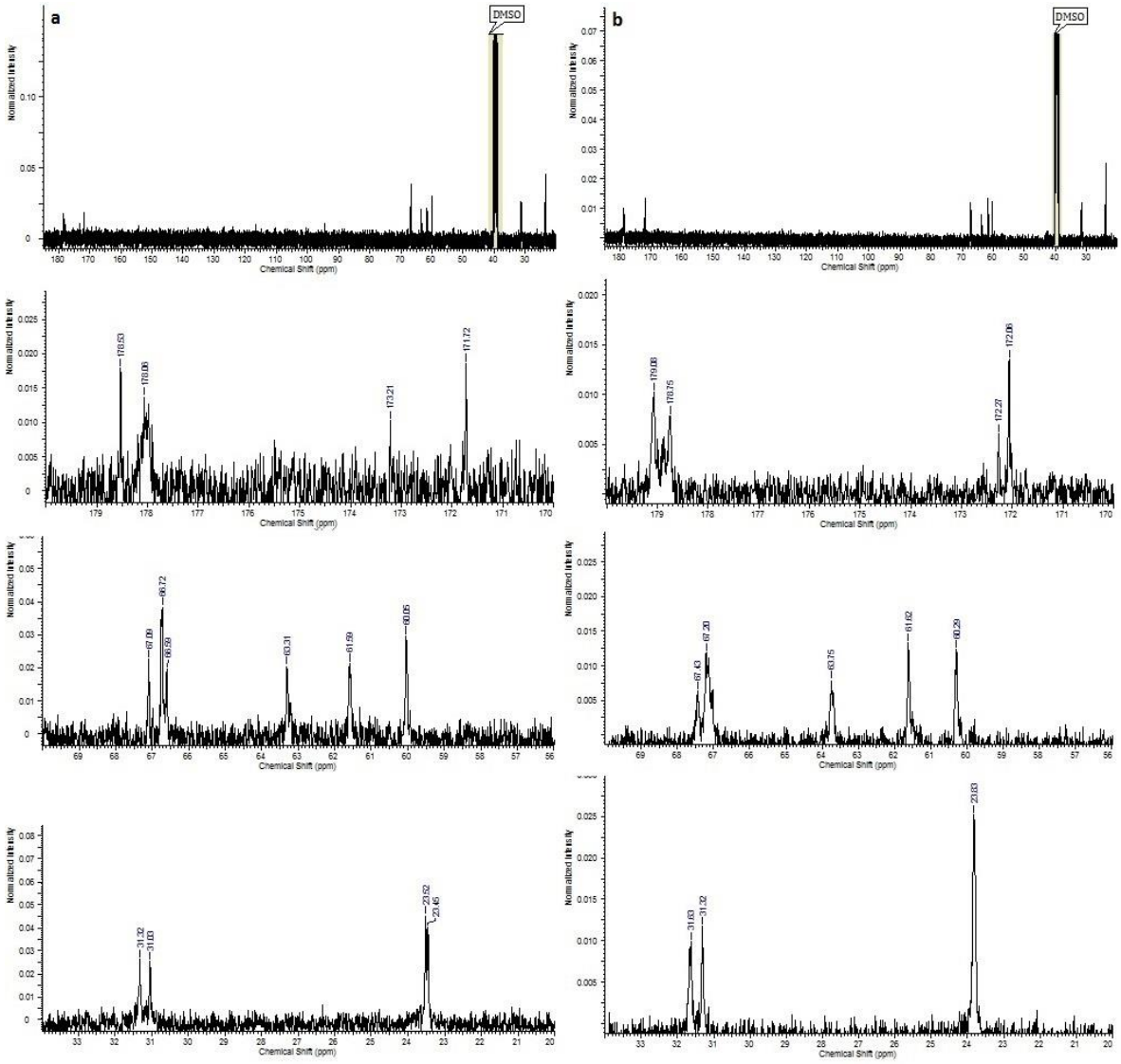

Figure 4-16 ^{13}C NMR spectrum of [Co(nta)(μ-OH)2Pt(chda)] **a)** at 80 °C and **b)** after cooling down to 25 °C. The enlargement of each spectrum is shown underneath of each spectrum

Using the suggested mechanism shown in **Scheme 4-5** helps to explain the NMR spectra. The spectrum in **Figure 4-16a** may represent having a mixture of **4.7**, **4.8** and **4.9**.

Square planar platinum complexes (16e$^-$, d^8) usually undergo associative ligand substitution[139]. In the associative mechanism, the M-Nu bond is formed before the M-X bond breaks. Crystal structures in the literature demonstrate that the coordination of DMSO

to platinum is usually through sulfur[140].The substitution of DMSO onto platinum should therefore be through sulfur, since platinum is a soft Lewis acid. Dissociative ligand substitution is most favored in coordinatively saturated 18e$^-$ complexes (e.g. d^6 octahedral Co(III) complexes)[141]. In the dissociative mechanism, the M-X bond is fully broken before the M-Nu bond forms, thereby avoiding an energetically unfavorable 20e$^-$ intermediate. As Co(III) is a hard Lewis acid, coordination of DMSO is expected to be from oxygen, and this is seen in the literature [142],[143].

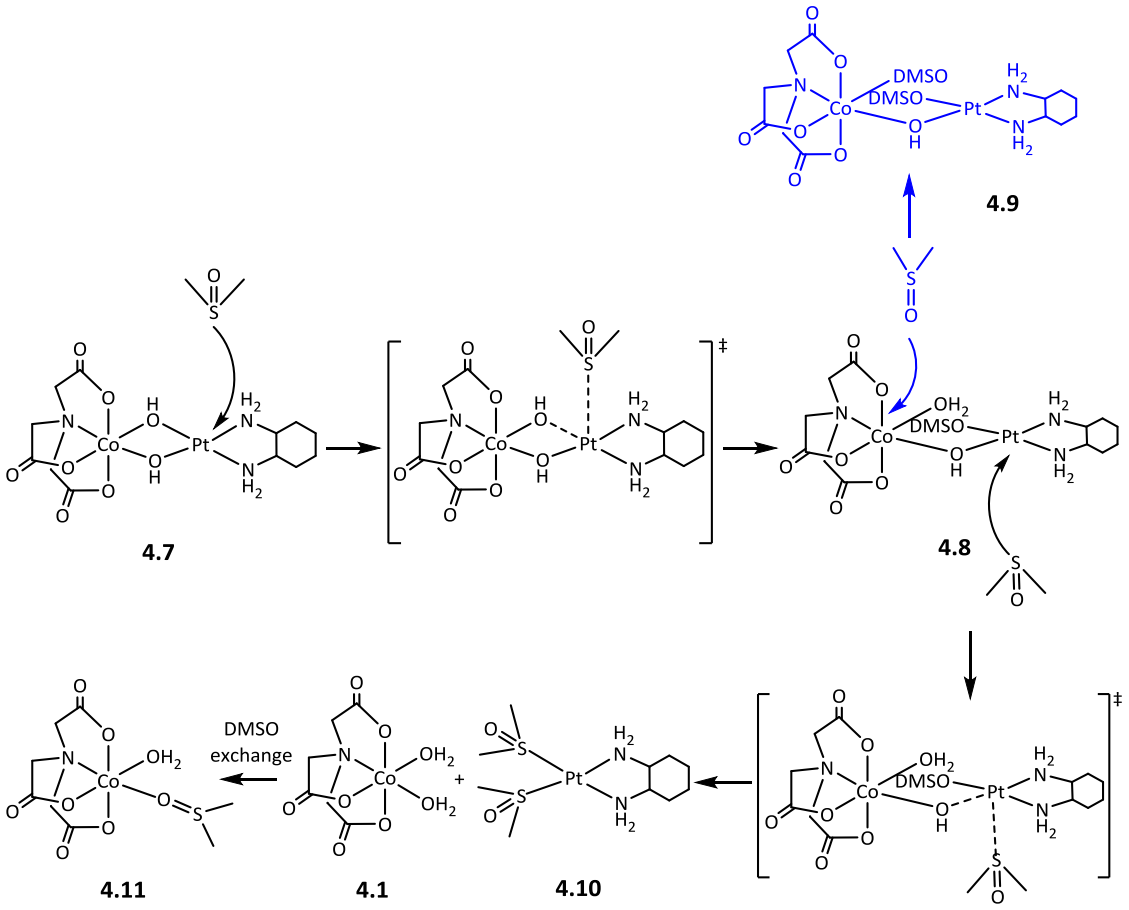

Scheme 4-5 Suggested mechanism for the substitution of hydroxido bridging ligand by DMSO

4.4.1.2 NMR studies of [(nta)Co(μ-OH)$_2$Pt(en)], 4.12

The complex (**4.12**) is insoluble in d^6 DMSO at 25 °C, and we could not record the ^{1}H NMR spectrum at room temperature. Therefore, the NMR spectrum was taken in 80 °C (**Figure 4-17a)**.

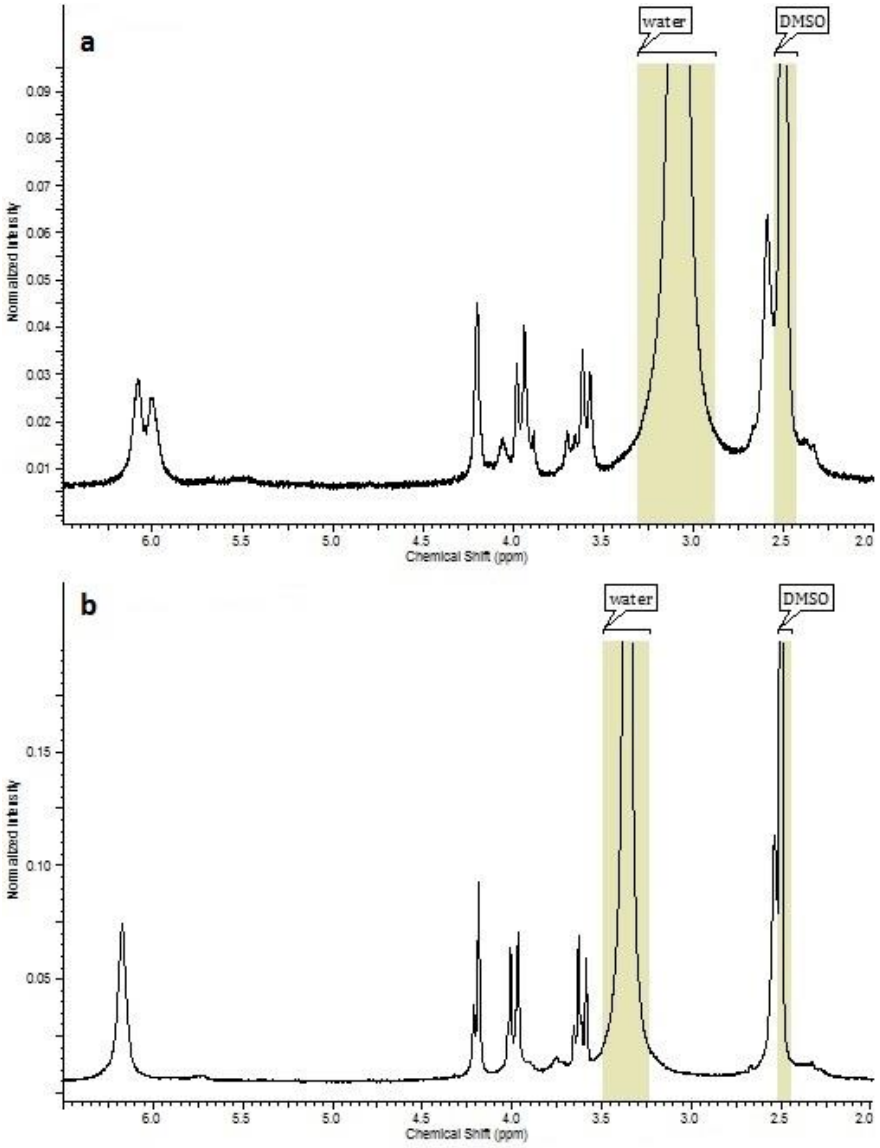

Figure 4-17 a) The ^{1}H NMR spectrum of [Co(nta)(μ-OH)$_2$Pt(en)] in d^6 DMSO at 80 °C **b)** The ^{1}H NMR spectrum of [Co(nta)(μ-OH)$_2$Pt(en)], 3 h after cooling down to 25 °C

We expected to see one set of AB mutiplets and a singlet for the nta ligand on the cobalt component and one singlet for the en ligand and another singlet for hydrogen on the amine

group on the platinum component. But the observation from the ^{1}H NMR at 80 °C showed two sets of AB multiplets and two singlet peaks for the nta ligand (**Figure 4-17a**). There are also two peaks at 6.25 and 6.19 ppm and one peak at 2.00 ppm which are assigned to hydrogen atoms on the amine groups and a methylene group of the en ligand that is attached to platinum, respectively. The COSY spectrum showed there is another peak underneath the DMSO peak which is also assigned to the en ligand on platinum (**Figure 4-18**).

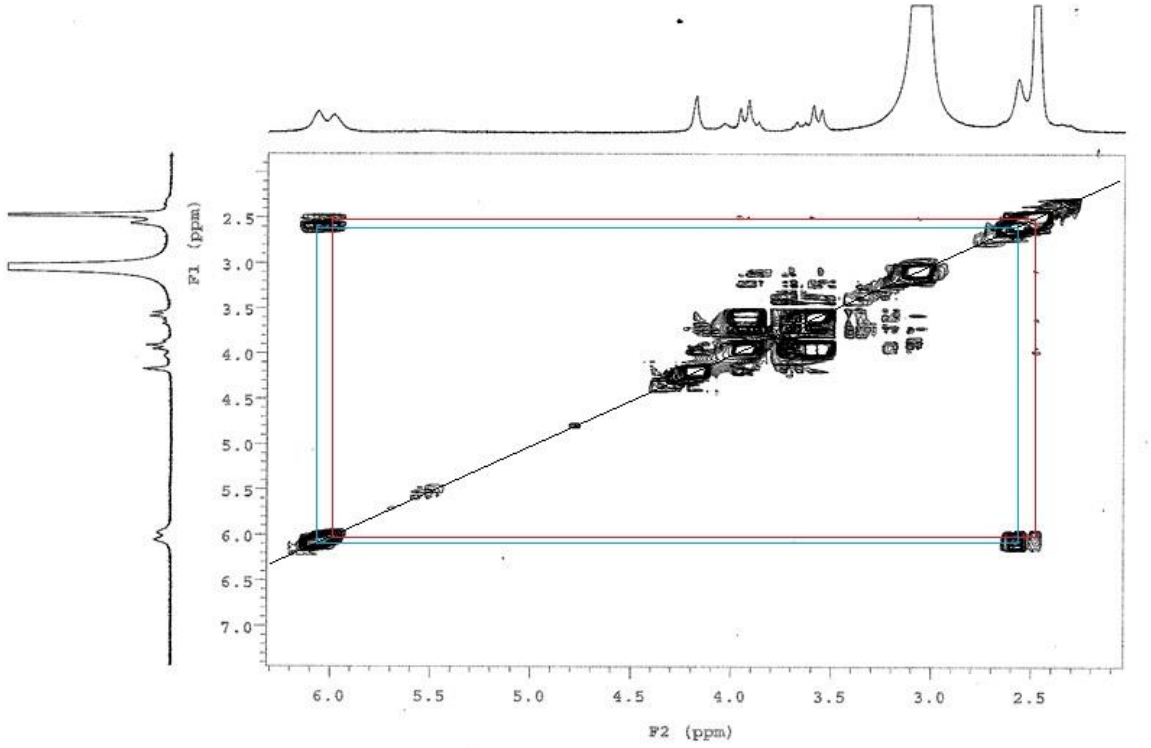

Figure 4-18 The ^{1}H-^{1}H COSY spectrum of [(nta)Co(μ-OH)$_2$Pt(en)](**4.12**) in d^6 DMSO at 80 °C

The two peaks at 2.5 and 2.59 ppm assigned to en ligand have a cross peak with the amine protons at 6.00 and 6.08 ppm respectively. This means the en protons on platinum are *trans* to different ligands. The cross peaks between 3.5 and 4.3 ppm are related to the nta ligand on cobalt. Insolubility of **4.12** in DMSO at room temperature and its partial solubility at 80 °C may lead to the inference that the heating causes reaction of the insoluble complex to

produce different, more soluble complexes. It may mean DMSO becomes a ligand on the Pt component and the NMR results are consistent with having a mixture of the **4.13** and **4.14**.

The NMR tube containing the sample was left for some hours at room temperature, and then the ^{1}H NMR spectrum was taken again (**Figure 4-17b**). The ^{1}H NMR spectrum contains two sets of signal for the nta ligand and one set of signals for the en ligand. ^{1}H NMR spectra described in the literature indicate that [Pt(en)Cl_2] has a resonance at 5.31 ppm for equivalent amine protons, and [Pt(en)(dmso)Cl]$^{+}$, has a set of resonances at 6.31 and 6.06 ppm due to inequivalent amine protons. The chemical shift the amine hydrogens appeared at is also consistent with coordination of DMSO to platinum[138]. The results may suggest the substitution of two DMSO ligands on to platinum (**4.15**) as there is only one signal for hydrogen atoms of the amine groups. On the other hand, two sets of signals for nta may represent having the mixture of **4.1** and **4.11** at the same time. Dissolution of the NMR sample in DMSO after cooling down to room temperature demonstrates that the complex actually reacted with DMSO.

The ^{13}C NMR spectrum of **4.12** in d^{6} DMSO at high temperature measured in a short experiment time was very noisy and we were unable to get any information out of it. Therefore, another ^{13}C NMR was taken 6 hours after cooling down the sample tube for a longer time (**Figure 4-19**).

There are three peaks for axial carboxylate carbon atoms at about 180 ppm and two peaks for equatorial. As the number of carbon signals for equatorial and axial carbon atoms should be equal and one of the carbon signals is taller (in 172.08 ppm), there may be a another signal underneath the signals at about 172 ppm. There are also three signals for the axial methylene carbon atoms at about 67 ppm and two signals for the equatorial methylene

carbon atoms. There should be one signal underneath because of the same reason brought for equatorial carboxylate carbon atoms. The ^{13}C NMR is a very good indicator that **4.12** has reacted with DMSO.

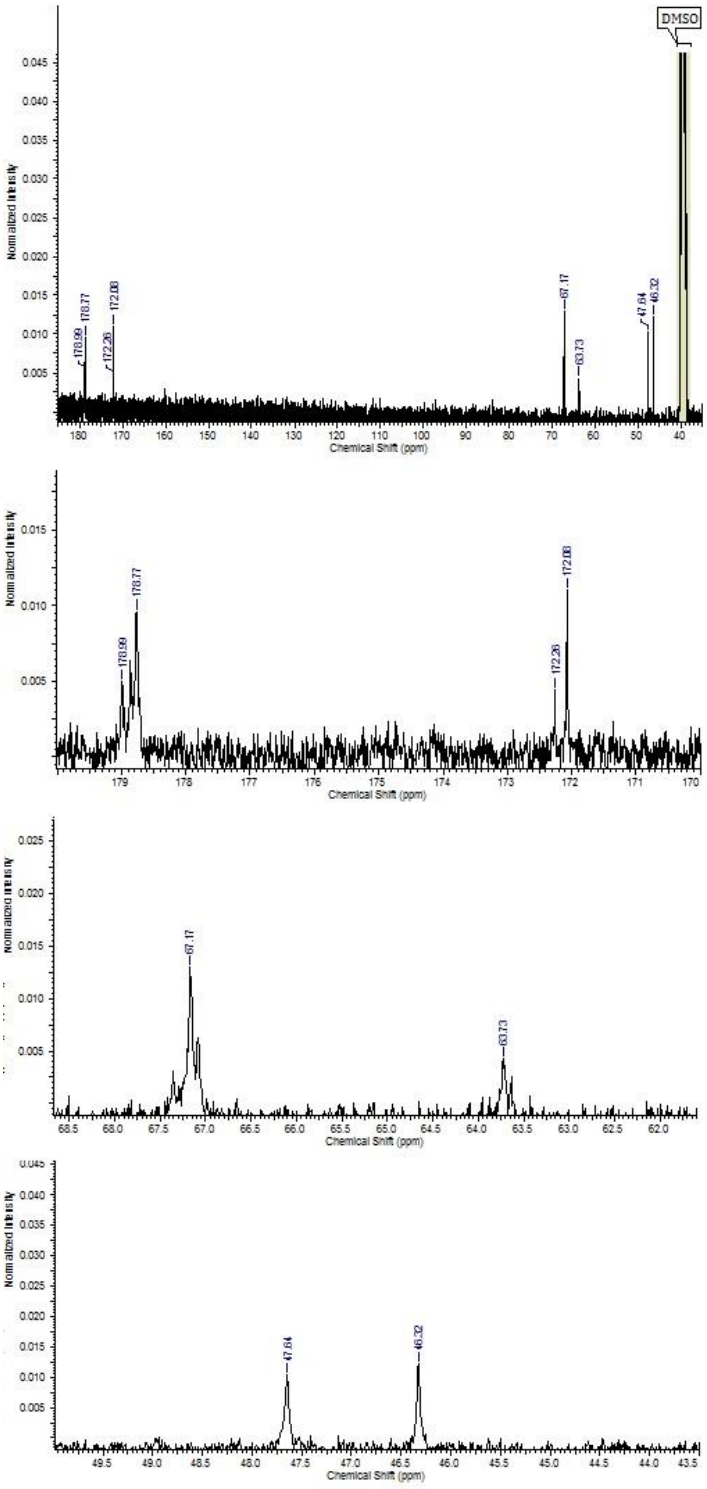

Figure 4-19 The ^{13}C NMR spectrum of [Co(nta)(μ-OH)$_2$Pt(en)] in d^6 DMSO after cooling down at 25 °C

The number of signals for en ligand and nta are consistent with having both complexes **4.13** and **4.14** present in solution (**Scheme 4-6**). In this way, we expect to see two sets of signals for the nta ligand on cobalt and two signals for en.

The suggested mechanism for the substitution of DMSO by hydroxido bridging ligand is demonstrated in **Scheme 4-6**. This mechanism is analogous to that of suggested for the reaction of [(chda)Pt(μ-OH)$_2$Co(nta)] with DMSO.

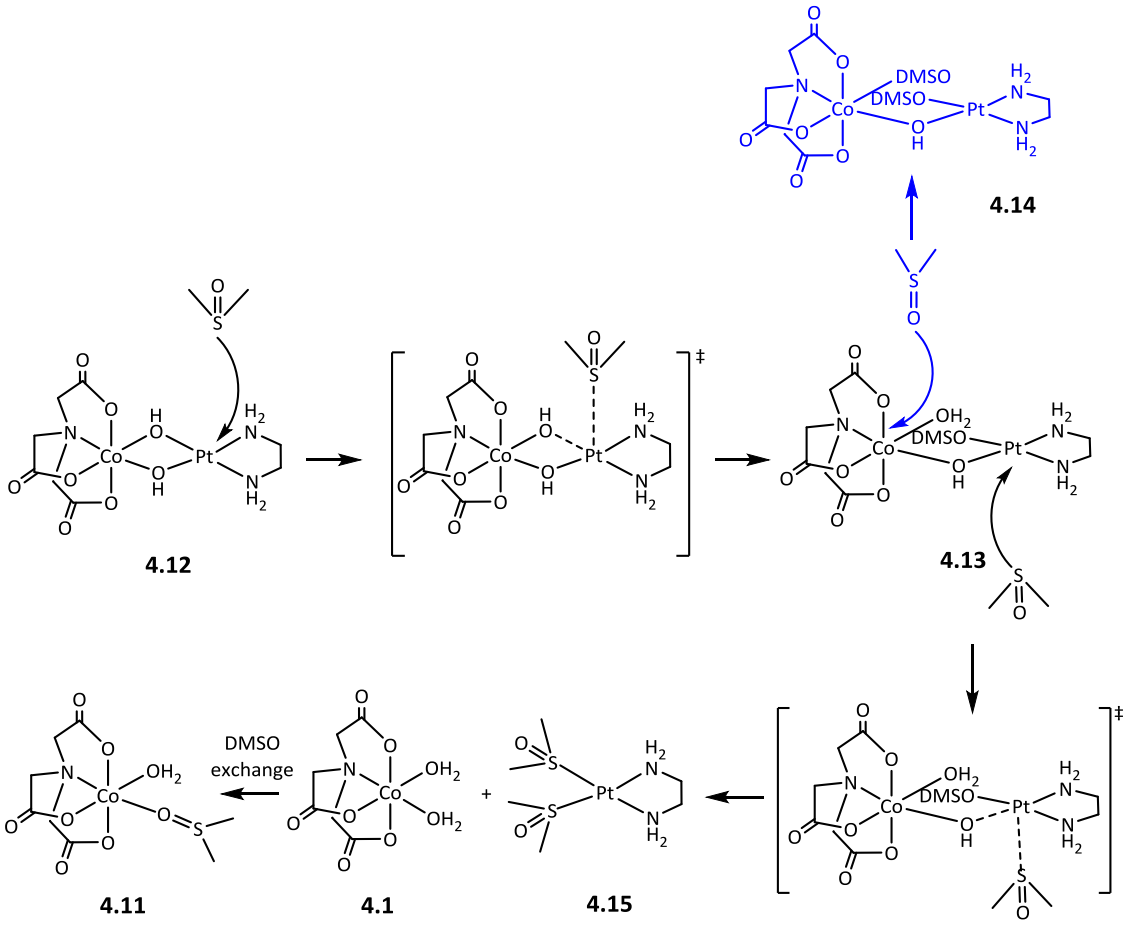

Scheme 4-6 Suggested mechanism for the substitution of hydroxido bridging ligand by DMSO

4.4.1.3 [(nta)Co (μ-OH)$_2$Pt(NH_3)$_2$], 4.16

The title complex has a mirror plane containing the axial arm of the nta attached to the cobalt, the bridging hyroxido ligands and platinum with the amine ligands. The amine ligands on platinum are different because one is *trans* to the equatorial O and another is *trans* to the equatorial N atom of the nta ligand. But they might not be affected by this difference in NMR since they are too far from nta ligand. We expect to see one set of AB system multiplets and a singlet for the nta ligand on cobalt and a signal for amine protons on platinum in the ^{1}H NMR spectrum of [(nta)Co(μ-OH)$_2$Pt(NH_3)$_2$] (**4.16**).

Compound **4.16** was slightly soluble in DMSO. The ^{1}H NMR spectrum taken at 25 °C is shown in **Figure 4-20a**. This NMR spectrum is noisy, but more than one set of signals for the nta ligand on cobalt is observable. In order to explore the extra signals and the peak broadening that occur due to a reaction with DMSO, another NMR spectrum was taken at 80 °C (**Figure 4-20b**). There are two sets of signals for the nta ligand on cobalt and two sets of signals for amine ligands on platinum which indicate that more than one compound is there. The number of signals suggests we either have a mixture of **4.16** and **4.19** or **4.17** and **4.18 (Scheme 4-7)**. However, having **4.16** seems less likely, since most of the compound, unlike the starting materal remains soluble in DMSO after cooling down. It means that the apparent solubility of **4.16** is due to reaction with DMSO. Evidence from ^{1}H NMR studies of cisplatin is consistent with DMSO reacting with **4.16**. The chemical shift for amine protons of cisplatin is 3.92 ppm. The NMR tube containing cisplatin in DMSO was left for half an hour and another ^{1}H NMR spectrum was taken (**Figure 4-21**). A new signal appearing at 4.69 ppm represents that DMSO reacted with platinum. Chemical shifts of amine protons observed for **4.16** dissolved in DMSO are close to the chemical shift of the amine protons of cisplatin

reacted with DMSO. Therefore, having **4.17** and **4.18** present in solution seems more likely than **4.16** and **4.19**.

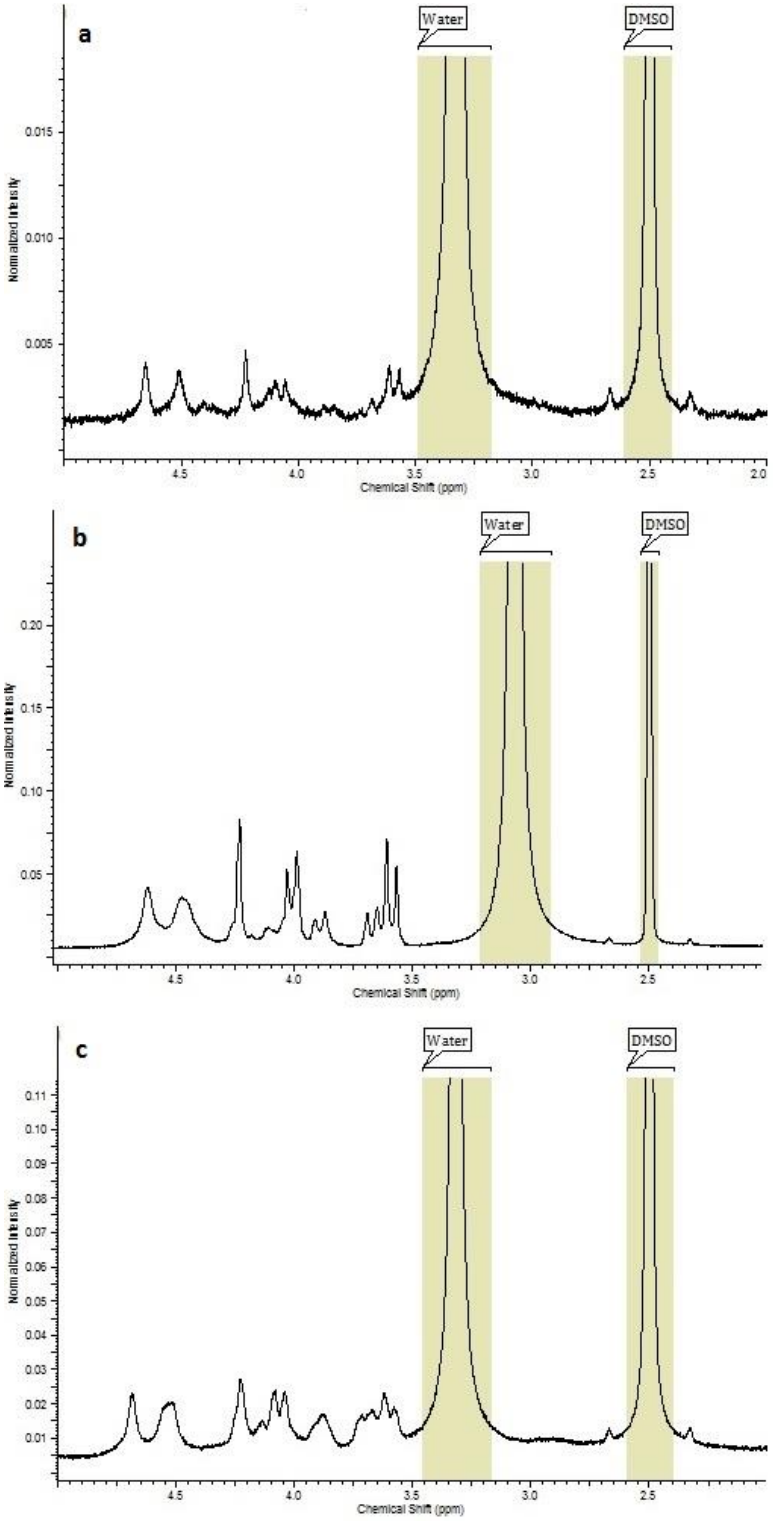

Figure 4-20 a) The ^{1}H NMR spectrum of [(nta)Co(μ-OH)$_2$Pt(NH$_3$)$_2$](**4.16**) in d^6 DMSO at 25 °C **b)** The ^{1}H NMR spectrum of **4.16** in DMSO at 80 °C **c)** The ^{1}H NMR spectrum of **4.16**, 3 h after cooling down in 25 °C

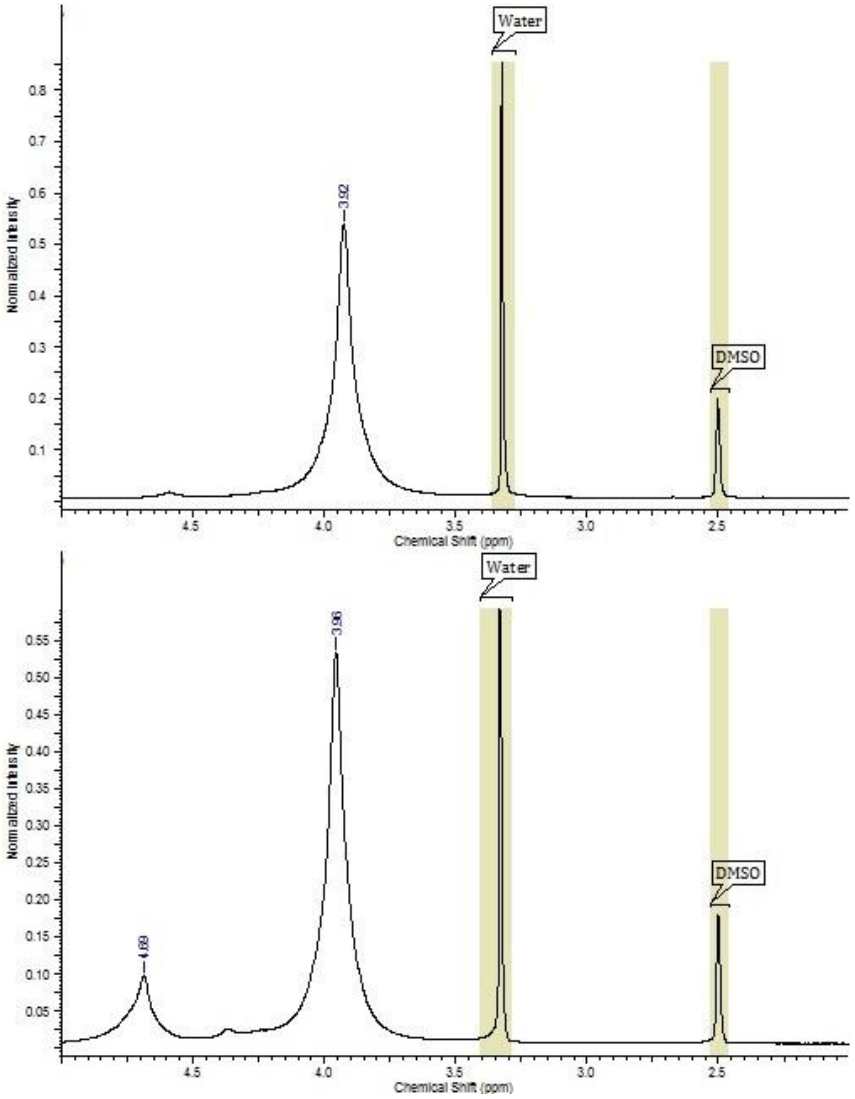

Figure 4-21 a) The ^{1}H NMR spectrum of cisplatin instantly after dissolving in d^{6} DMSO **b)** 30 min after dissolving in d^{6} DMSO

The suggested mechanism for substitution of DMSO onto **4.12** is shown in **Scheme 4-7**.

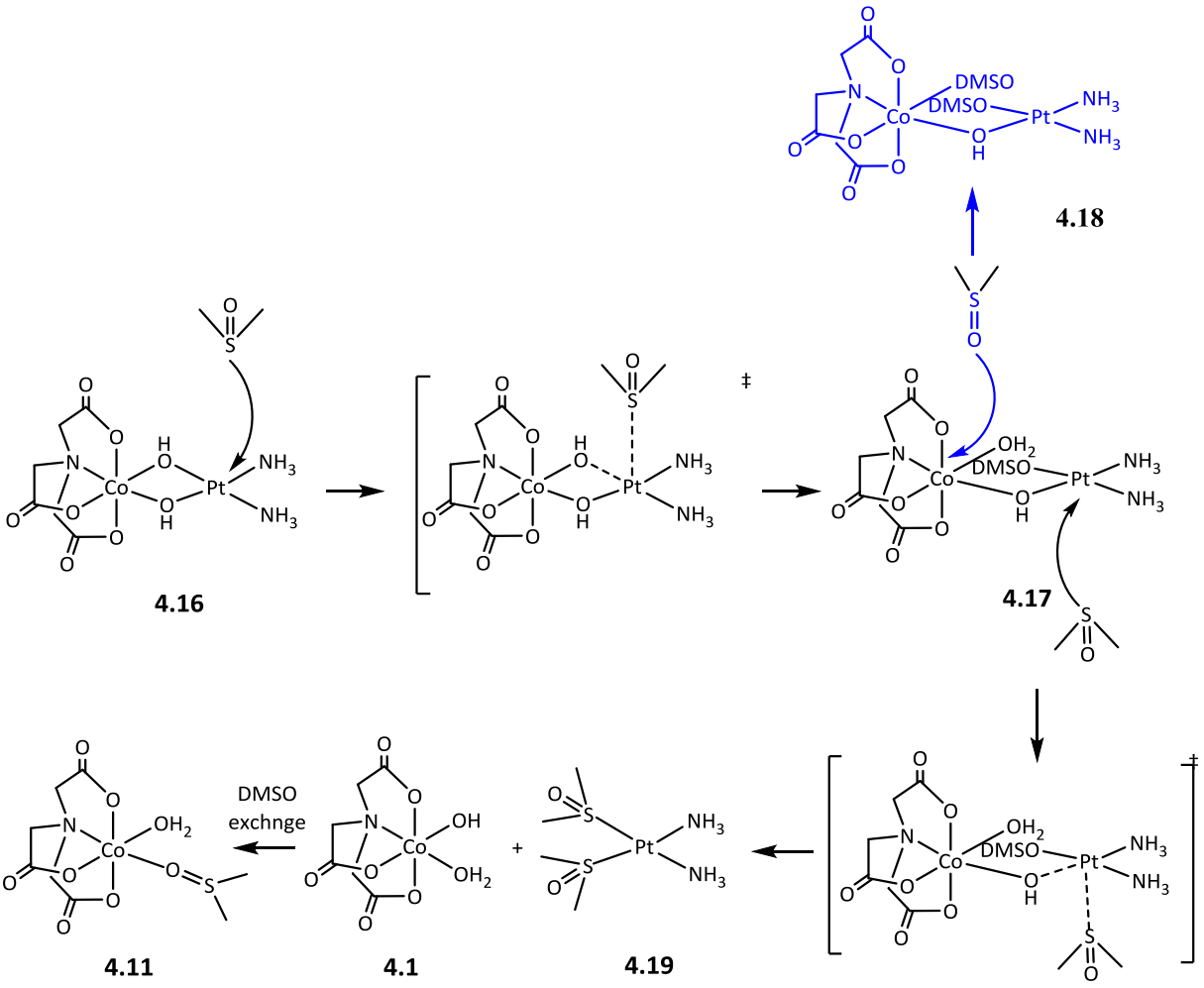

Scheme 4-7 Suggested mechanism for the substitution of hydroxido bridging ligand by DMSO

4.5 Antitumour activity study

Complexes **4.7**, **4.12** and **4.16** were screened in preliminary studies of *in vitro* anti-tumour activity against a human colon cell line (DLD-1). The solubility of all three complexes was very low in DMSO and they precipitated in the cell line media. Reporting the IC50 values without the entire complexes being dissolved has no real meaning, other than providing a lower limit for the toxicity of a complex.

Despite the precipitation, an IC50 value of the **4.7** was found to be in the range of 2-7 μM in DLD-1 cells, though it is likely that it would be lower if the entire sample of the complex was in solution. The other complexes had no activity at the concentrations studied.

4.6 Synthesis and crystal structure of $[Co(PMIDA)(OH_2)_2]\cdot H_2O$ (4.20)

In an effort to synthesise nta-analogus neutral complexes with better solubility, N-(phosphonomethyl)iminodiacetic acid (PMIDA), has been used as a ligand to coordinate to cobalt. By manipulating the pH, the phosphonate group can be protonated or deprotonated and change the charge of the complex. A brief synthetic procedure to prepare $[Co(PMIDA)(OH)_2]$ is shown in Scheme **4-8**.

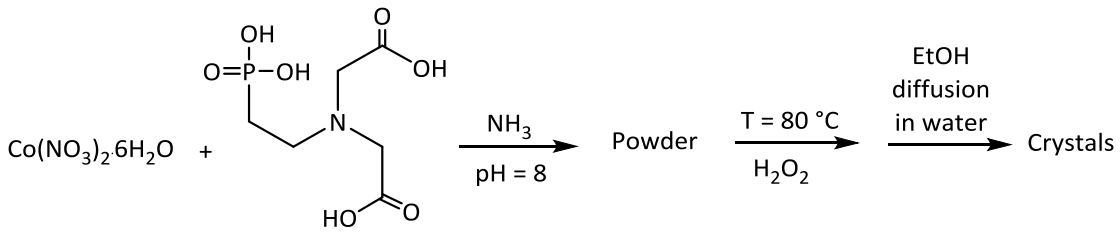

Scheme 4-8 Synthetic procedure to obtain compound **4.20**

After reaction for 2 hours, the volume of the reaction was decreased with rotatory evaporator and the reaction mixture was left overnight in the fridge. A precipitate came out after one day. The precipitate was suspended in water and the temperature was increased to 80 °C. H_2O_2 was added and the reaction was heated for two hours. The reaction mixture was cooled down. The crystals were obtained from diffusion of ethanol into the reaction mixture. We could not record NMR data for **4.20** presumably because the complex did not oxidise and the complex is Co(II). The reaction did not bubble after addition of H_2O_2. It might

be because the H_2O_2 was not new and possibly decomposed. After addition of H_2O_2 from a new bottle, the reaction mixture foamed, but no solid could be collected.

The crystal structure of **4.20** is shown in **Figure 4-24**. This compound crystallises in a monoclinic crystal system with $P2_1/c$ space group. Co is octahedrally coordinated to the two arms of the tetradentate PMIDA ligand (O2, O6 and N1) and two water molecules (O8, O9) and the oxygen atom of another PMIDA ligand (O7). This leads to formation of a coordination polymer and the repeating unit is $C_5O_9NPH_2Co$.

The packing structure of **4.20** is presented in **Figure 4-25**. There is a hydrogen bonding interaction between the non-coordinated water molecule and the hydrogen atom on O8 shown in the packing structure (**Figure 4-25**). Selected bond lengths and angles are shown in **Tables 4-4** and **4-5**. The bond lengths of Co-O2, Co-O6, Co-O7 and Co-N1 are 2.10, 2.13, 2.08 and 2.23 Å respectively, which is suggestive of a Co(II) complex.

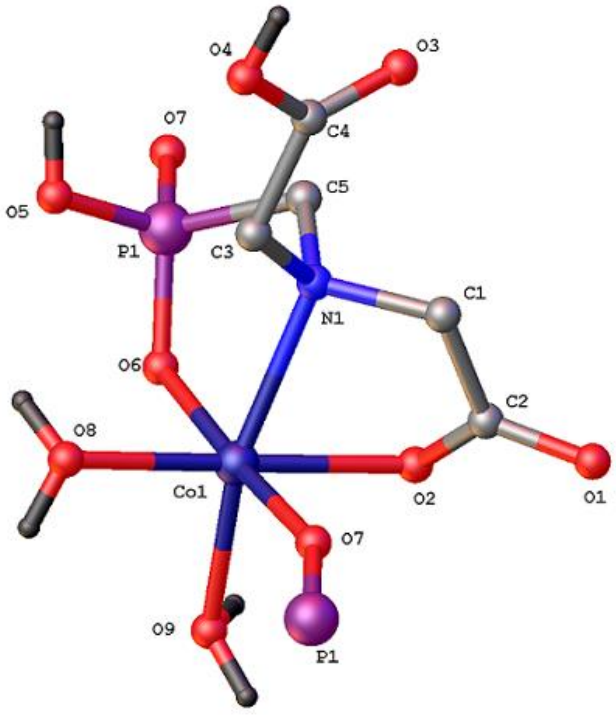

Figure 4-22 Crystal structure of **4.20** with hydrogen atoms and one water molecule omitted for clarity

Bond length [Å]			
Co1-O6	2.137(6)	O1-C2	1.271(9)
Co1-O8	2.099(6)	O3-C4	1.207(10)
Co1-O2	2.103(6)	O4-C4	1.309(10)
Co1-O9	2.071(6)	O2-C2	1.271(9)
Co1-O7	2.080(6)	N1-C1	1.482(10)
Co1-N1	2.236(6)	N1-C3	1.452(10)
P1-O5	1.557(7)	N1-C5	1.500(10)
P1-O6	1.522(6)	C4-C3	1.517(10)
P1-O7	1.499(6)	P1-C5	1.812(8)

Table 4-4 Selected bond length for **4.20**

Bond angles [°]	
O6-Co1-N1	85.9(2)
O8-Co1-O6	90.0(2)
O8-Co1-O2	174.7(2)
O8-Co1-N1	101.2(2)
O2-Co1-O6	94.3(2)
O2-Co1-N1	76.0(2)
O9-Co1-O6	91.7(2)
O9-Co1-O8	95.3(2)
O9-Co1-O2	87.8(2)
O9-Co1-O7	93.0(2)
O9-Co1-N1	163.3(3)
O7-Co1-O6	175.4(2)
O7-Co1-O8	89.7(2)
O7-Co1-O2	85.7(2)
O7-Co1-N1	89.7 (1)

Table 4-5 Selected bond angles for **4.20**

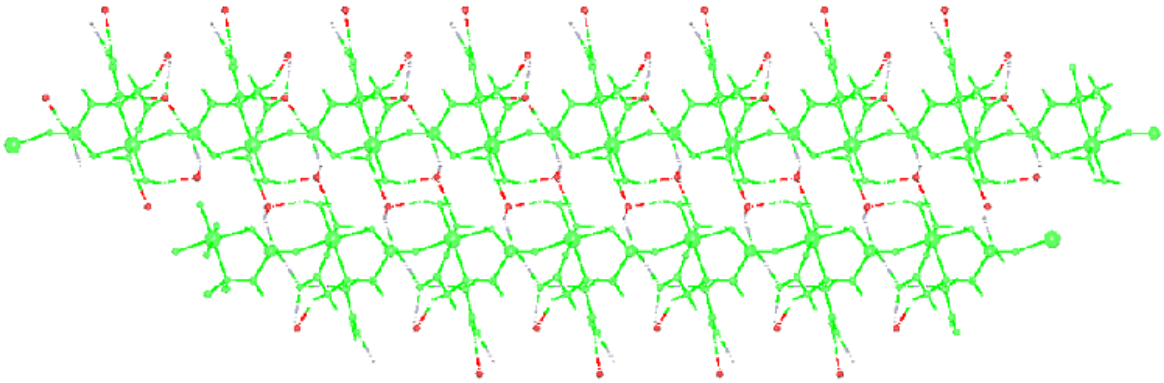

Figure 4-23 A packing diagrams and hydrogen bonding interactions within the crystal structure of **4.20**

4.7 Conclusion

The complexes (**4.7**, **4.12** and **4.16**) precipitate out from the addition of two solutions of $[Co(nta)(OH)(OH_2)]^-$ and $[Pt(L)(OH)_2]^{2+}$. Formation of powder inside the reaction is due to the formation of neutral dinuclear complexes. Among synthesised complexes, [(nta)Co(μ-$OH)_2$Pt(chda)] formed immediately after addition of the two precursors. The low solubility of the complexes increases the chances of them actually being pure.

The dinuclear complexes, **4.7**, **4.12** and **4.16**, were insoluble in most common solvents. This limited our ability to characterise the complexes. All complexes were almost insoluble in DMSO. In order to obtain NMR data, the temperature was increased to 80 °C. NMR spectra for the complexes showed more signals than expected. A key observation is the fact that the material stayed dissolved when the mixture is cooled. It means the materials that stayed dissolved inside the NMR tubes have different properties and so may well be different complexes. These different compounds possibly were formed by reaction with DMSO. The

chemical shifts that appeared for amine groups are also in agreement with having at least one DMSO attached to platinum.

Chapter 5

Conclusions and Future Prospect

Chapter 5. Conclusions and Future Prospects

5.1 Conclusion

The main goal of this project is to synthesise smart targeted drug delivery systems that deliver drugs to cancer cells with better efficacy and lower toxicity levels. As part of this goal, this thesis has described synthetic routes to achieve novel heterodinuclear [Co(μ-OH)Pt] metal complexes.

In chapter 2, formation of [{Co(μ-OH)$_n$-M}$_m$] complexes (M =metal ions) complexes by the reaction between [Co(en)$_2$(OH)(OH$_2$)] and different metal ions was studied using ^{13}C NMR spectroscopy. The conclusion of this study was that the equilibrium between the *cis* and *trans* isomers of the Co complex shifts toward the *cis* isomer after addition of diamagnetic metal ions. In addition, the elimination of *cis* peaks in the ^{13}C NMR after the addition of paramagnetic metal ions, showed preferential association of those metal ions with the *cis* isomer of the Co complex.

The ^{13}C NMR studies show that the reaction of [Co(en)$_2$(OH)(OH$_2$)]$^{2+}$ complex with Pt^{2+} and Pd^{2+} species produces several other complexes in addition to the dinuclear complexes observed in the solid state[116].

Chapter 3 focused on the synthesis and characterisation of [Co(μ-OH)$_2$Pt] complexes. Formation of [Co(μ-OH)$_2$Pt] complexes has been characterised, following separations on ion exchange resins. However, reaction of [Co(en)$_2$(OH)(OH$_2$)]$^{2+}$ and [Co(tren)(OH)(OH$_2$)]$^{2+}$ complexes with platinum species are associated with side products.

Separation of products using CM sephadex columns was better than other techniques, but high purity Co(μ-OH)$_2$Pt complexes could not be obtained. However, we believe that the formation of this class of complexes has been confirmed by a combination of good isotopic pattern matches with results from mass spectrometry experiments, and an accumulation of NMR evidence.

In addition to the dinuclear complexes reported in this chapter, the novel crystal structure of **3.4** shows that more complicated structures are also formed, either in the reaction mixture or *via* subsequent reactions of the dinuclear complexes. The crystal structure of **3.4** is presented again in **Figure 5-1**.

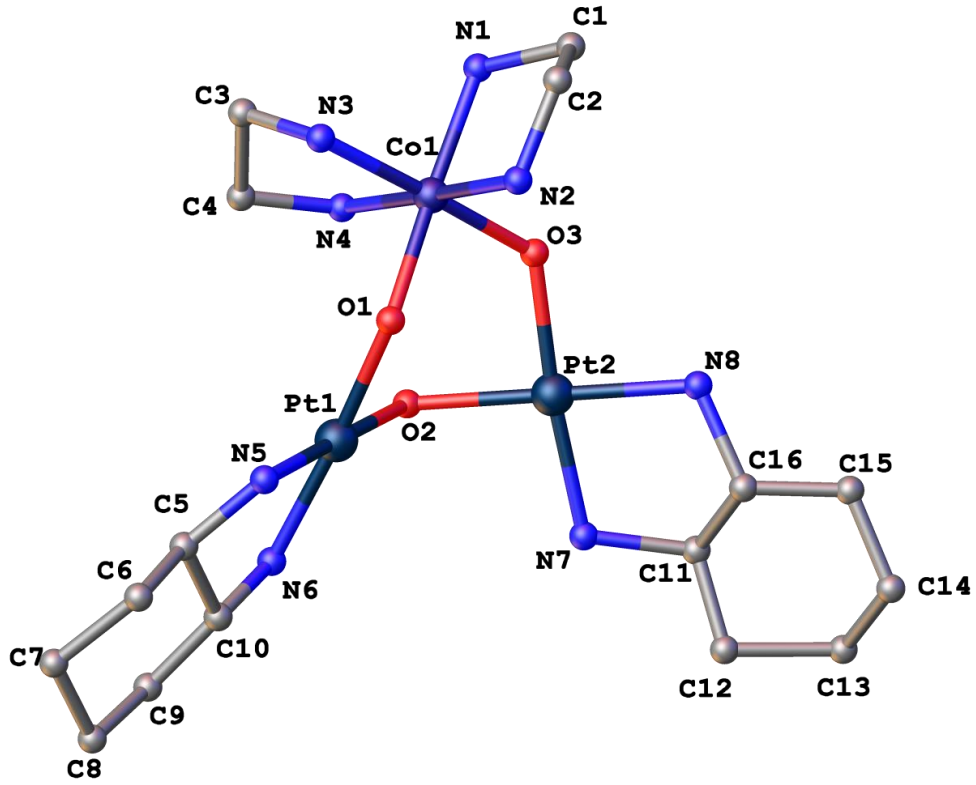

Figure 5-1 Crystal structure of **3.4**

An important result of this study is that the ^{1}H NMR spectrum of the crystalline material (**3.4**) was different from the bulk material from which the crystals were obtained (third band of the column (**3.2**)). The integration ratios derived from the ^{1}H NMR spectrum of the crystals show 2:1 molar ratios of en ligand vs chda ligand from which a ratio of two Pt *vs* one Co is inferred. But ^{1}H NMR spectra of the complete band (**3.2**) show 1:1 molar ratios of en ligand *vs* chda ligand, from which a ratio of one cobalt *vs* one platinum is inferred.

The occasional observation of formation of a yellow powder, either on the column or in eluates, is indicative of further reactions occurring. The yellow powder is presumed to be some form of Pt(chda) complex, based on NMR studies. Mass spectrometry results gave isotopic patterns that were a good match for [Pt(μ-OH)$_2$Pt] complexes. This evidence and other observations suggest the [Co(μ-OH)$_2$Pt] complexes are rather labile, which limited our ability to isolate them as pure compounds. The solubility of these complexes appears to be reasonably high in water, which maybe why our various efforts to crystallise them did not prove successful.

The problems associated with the synthesis of [Co(μ-OH)$_2$Pt] complexes in chapter 3 suggested to attempt to synthesise neutral dinuclear complexes. Nitrilotriacetate (nta), as a L^{3-} ligand, was chosen for coordination to the Co(III) centre, and with two hydroxido bridging ligands between the Co(III) and Pt(II) ions, the overall charge of the resulting complex will come to zero, providing the remaining ligands on the Pt(II) centre are neutral. In the synthetic method used, dinuclear complexes precipitated out of the reaction. The low solubility increases the chances of the [Co(μ-OH)$_2$Pt] complexes actually being pure. The elemental analysis results are consistent with the formula of [(nta)Co(μ-OH)$_2$Pt(L)]·2H$_2$O (L = chda, en, (NH$_3$)$_2$ for the complexes. The characterisation of these complexes is limited due to their very low solubility in most solvents. All these complexes were essentially insoluble in

most common solvents, except for some solubility in DMSO, and even that seemed to be due to reaction with the solvent rather than to simple dissolution. NMR studies done at 25 °C, were unsatisfactory due to the small amounts of the complexes that were present. Therefore, the NMR spectra were recorded at 80 °C. The NMR data are consistent with the reactivity of [Co(μ-OH)$_2$Pt] complexes with DMSO. This is consistent with the observation that the complexes remained dissolved in the DMSO after cooling down to room temperature.

Overalls, results obtained from chapter 3 and 4 are in agreement that [Co(μ-OH)$_2$Pt] complexes do form but they are also rather labile, and their solubility profiles were rather inconvenient. This lead us to begin attempts to synthesise complexes in which we may be able to control the solubility by manipulating the pH, and to design other [Co(μ-OH)$_2$Pt] complexes that may have higher stability. These ideas will be elaborated in the future work section, below.

5.2 Future work

The future work for this project can be taken in two different directions.

5.2.1 Manipulating the solubility by changing pH

We may be able to make dinuclear [Co(μ-OH)$_2$Pt] complexes with better control on solubility by changing pH. N-(Phosphonomethyl)iminodiacetic acid (PMIDA), shown in **Figure 5-2**, is a ligand analogous to nta, which may be able to coordinate to Co. By manipulating the pH, the phosphonate group can be protonated or deprotonated and change the charge of the complex. One of our preliminary efforts to synthesise [Co(PMIDA)(OH$_2$)$_2$] is reported in chapter 4. There are numerous reports of the coordination of PMIDA on Co. But all of them

reported Co(II) complexes of PMIDA ligand[144],[145],[146],[147],[148],[149]. A method for oxidising should be established, possibly by addition of hydrogen peroxide or aeration. Subsequent reactions might then be undertaken, using approaches similar to those used for nta complexes.

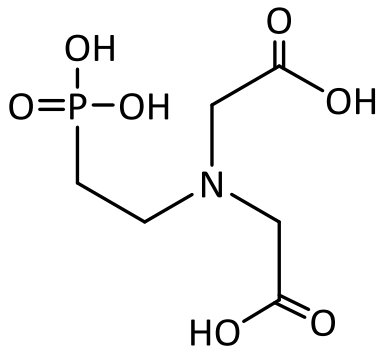

Figure 5-2 Structure of N-(phosphonomethyl)iminodiacetic acid (PMIDA)

5.2.2 Changing the lability of [Co(μ-OH)$_2$Pt] complexes

A method for preparation of dinuclear [Co(μ-OH)$_2$Pt] complexes, is proposed in **Scheme 5-1**. By following this method, hopefully, the ligand exchange on platinum can be avoided by introducing a bulky substitution to the ligand on Co, to block either sides of the platinum. 1,8-Naphthalimide is the proposed blocking group as it is planar and easily prepared from primary amines.

3,6,9,12-Tetraazatetradecane-1,14-diamine, is commercially available. The dinitro cobalt complex can be prepared by air oxidation of $Co(NO_3)_2 \cdot 6H_2O$ with a stoichiometric quantity of the ligand and $NaNO_2$[150]. The diaqua compound can be prepared by a method used for a similar complex[151].

The difficulty with the suggested reaction would be the fact that the association of the platinum species with cobalt might be harder due the blocking groups. Another point to

mention about the suggested [Co(μ-OH)$_2$Pt] complex, is that the 3+ charge of the complex might make the synthesis more complicated, but perhaps the hydrophobic blocking groups would favourably affect the solubility of the complex. We also suggest addition of an anionic substituent on the bulky groups to produce neutral complexes.

Once hetero-dinuclear [Co(μ-OH)$_2$Pt] complexes of this kind have been made, in the future, then the platinum drug release upon bio-reduction in hypoxic cell will be studied. **Scheme 5-2** proposed the mechanism of action of [Co(μ-OH)$_2$Pt] complexes in the hypoxic region of solid tumours which was widely discussed in chapter 1.

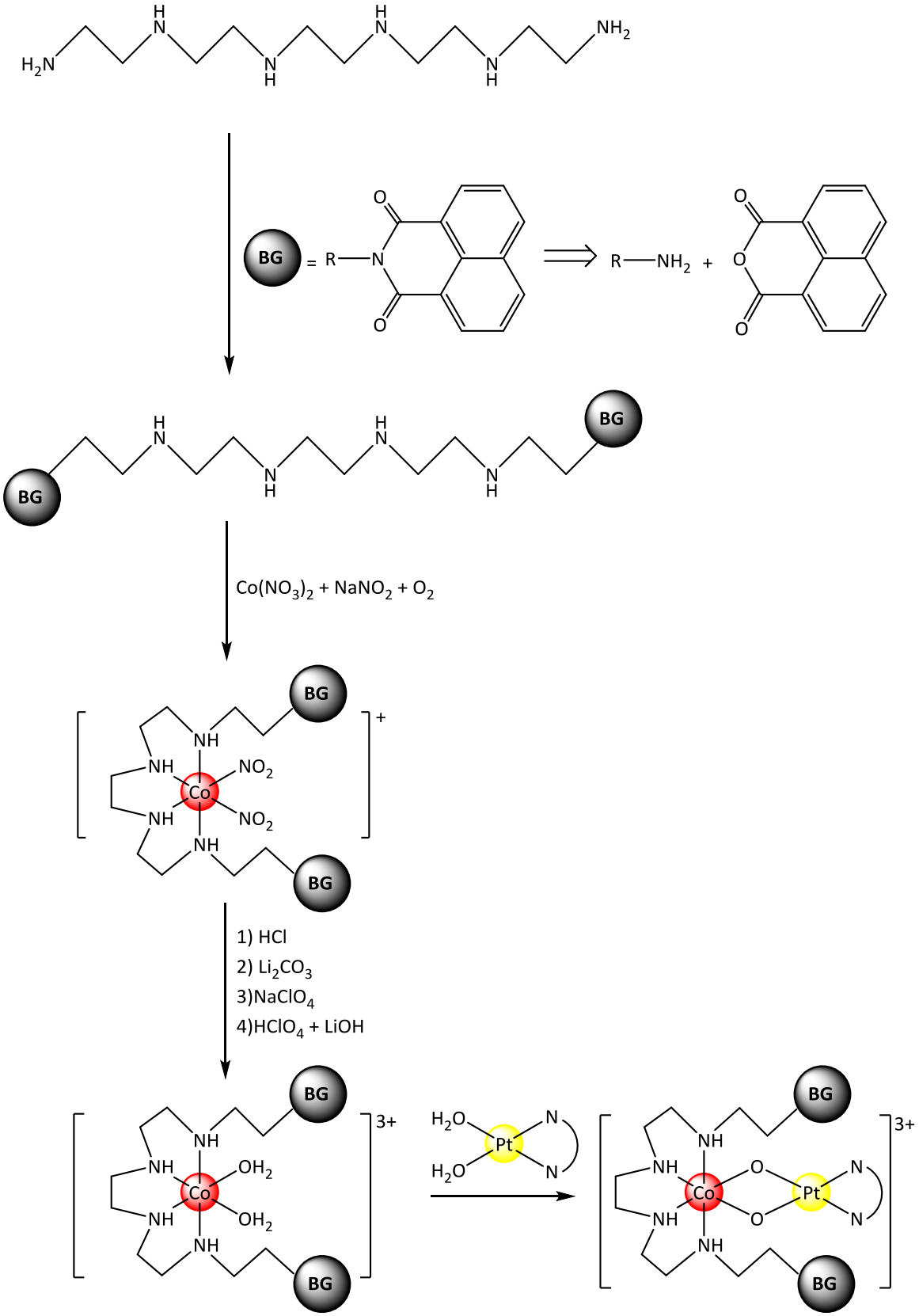

Scheme 5-1 Proposed mechanism to produce stable [Co(μ-OH)$_2$Pt] complexes. The long chain amine is represented as R-NH$_2$ for clarity

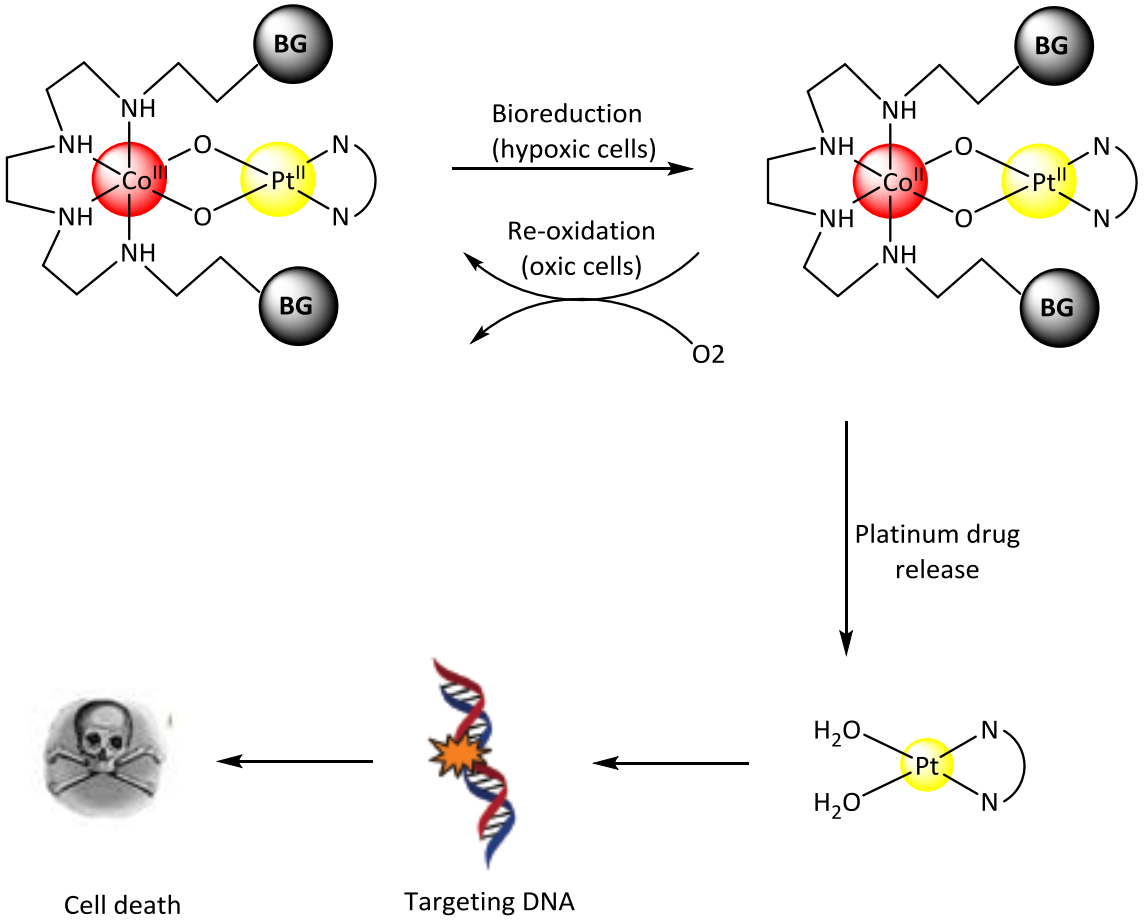

Scheme 5-2 Proposed mechanism of action of [Co(μ-OH)$_2$Pt] complexes in hypoxic region

Chapter 6

Terpyridine-derived Organotin Complexes

Chapter 6. Terpyrine-derived Organotin Complexes

6.1 Introduction

Organotin(IV) compounds have received considerable attention in recent years. This interest has been due to the remarkable structural diversity present, such as monomers, dimers, tetramers, ladders, cubes, butterflies and hexameric drums. Based on the type of organic ligands, tin-R groups, tin coordination geometry preferences and metal-to-ligand molar ratios, these various organotin derivatives have been constructed.[152],[153],[154],[155],[156],[157]

Another reason for this interest is due to their significantly important biological activities: bactericidal, fungicidal, biocidal and pesticidal. Furthermore, varieties of di- and tri-organotin species have shown potential as anticancer and anti-tuberculosis agents[158],[159],[157],[160],[161].

Cisplatin could bind to DNA with an intra-strand or inter-strand cross-link, while organotin(IV) compounds bind either to DNA bases or phosphate-oxygens of the DNA helix[162]. Different mechanisms of action of organotin compounds lead to alternative therapeutic protocols showing advantage in terms of lower toxicity and platinum induced resistance[163],[164],[165].

Gielen has demonstrated the effects of tin-based antitumour compounds and found that the *in vitro* antitumour activities of some di-n-butyltin, di-t-butyltin and diphenyltin 2,6-pyridinedicarboxylates were better than that of cisplatin against WiDr (a colon carcinoma) and MCF-7 cell lines (mammary tumour)[166],[167]. The variation of organic moieties and

donor ligands coordinated to the metal have resulted in several diorganotin(IV) and triorganotin(IV) compounds with high *in vitro* activity[168]. Generally, both diorganotin(IV) and triorganotin(IV) compounds could be active, but the activity of triorganotin(IV) compounds with a higher partition coefficient value is generally higher than the di- and monoanalogues, following the order $R_3SnL > R_2SnL_2 > RSnL_3$[169],[170]. Activity of organotin(IV) compounds was dependent on the R group, and decreased in the order: n-Bu > Ph and Et > Me as R[171]. The anti-cancer activity of several organotin compounds against WiDr and MCF-7 cells by Gielen have demonstrated that the R groups play more important roles than ligands, but the ligands (L) also play an important role in the bioactivity[166],[167]. Moreover, the studies on structure–activity correlation of organotin(IV) compounds by Huber[172] demonstrated that antitumour active organotin compounds should possess available coordination positions on the tin atom and also have low hydrolytic cleavage of the Sn-alkyl (or Sn-aryl) bonds. However, a necessary balance between lipophilic and hydrophilic properties is needed to cross the cell membrane and to demonstrate activity in an aqueous environment. It has been established that organotin(IV) compounds are very important in cancer chemotherapy because of their apoptosis inducing character[173],[174]. The exact mechanism by which organotin compounds exert their anticancer effect is not fully understood, but it has been suggested that organotin(IV) compounds could bring about numerous cellular effects; inhibition of macromolecular synthesis (DNA and protein synthesis), apoptosis by increasing intracellular Ca^{2+} concentration, followed by reactive oxygen species formation and cytochrome-c release from mitochondria, caspase activation and finally DNA fragmentation have been implicated in organotin-induced cytotoxicity[175],[176],[177].

Organotin compounds are famous for their versatile coordination chemistry that involves various coordination modes. The coordination number of tin(IV) varies from 4 to 6 in most cases[178]. The coordination number can be as high as 8 if appropriate chelating ligands are introduced[179].

2,2’:6’,2’’-Terpyridine derivatives are remarkable ligands for almost all the transition metal ions through the {N, N, N} coordination mode; some of their complexes have even evaluated as antitumour drugs[180].

This study is based on the ligands synthesised by a graduated PhD student of our research group, Gurpreet Kaur. Kaur synthesised terpyridine-amine based polydentate ligands and consequently synthesised a range of mono-, di-, and polynuclear complexes derived from them[181].

We will discuss the synthesis and characterisation of organotin complexes with 4'-(2"'-toluyl)-2,2':6',2"-terpyridine (ottp) and 4'-(4"'-toluyl)-2,2':6',2"-terpyridine (pttp) ligands.

6.2 Results and discussion

6.2.1 Synthesis and characterisation of terpyridine derived organotin complexes

6.2.1.1 [$Sn(CH_3)_2Cl_2$(pttp)]

The synthesis of the ottp ligand using a ‘one pot method’ has been reported in Kaur’s thesis[181]. The pttp ligand was synthesised by a similar method.

The synthesis of [$Sn(CH_3)_2Cl_2$(pttp)] (**6.1**) is presented in **Scheme 6-1**.

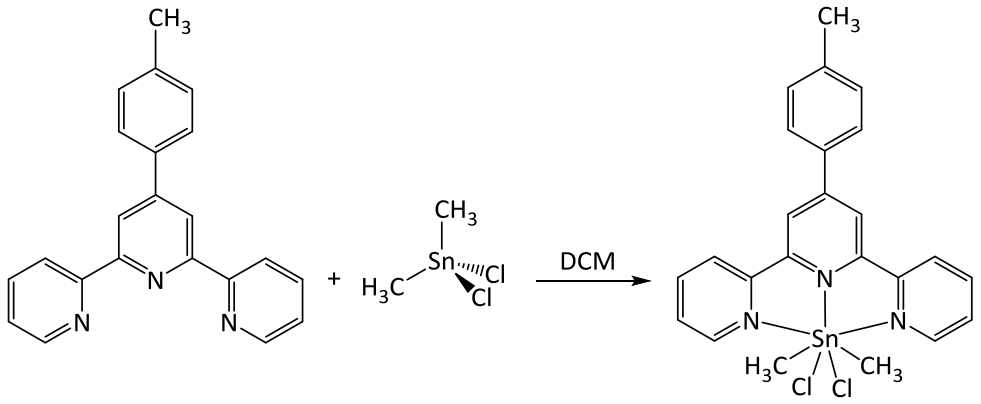

pttp **6.1**

Scheme 6-1 Brief description of synthesis of **6.1**

The ^{1}H NMR spectrum of **6.1,** shown in **Figure 6-1,** was recorded in d^{6} DMSO. The integrations of the protons on the methyl ligands on Sn, protons on pttp and the aromatic ring protons are 6, 3 and 14 respectively. The integrations are consistent with 1:1 metal to pttp coordination. The singlet peak at 1.02 ppm is assigned to the methyl protons attached to Sn (**Figure 6-1**). The methyl group signals carry satellites due to coupling of hydrogen atoms with ^{117}Sn and ^{119}Sn nuclei which have abundances of 7.68% and 8.59% respectively (**Figure 6-2**). The signals of the aromatic region were fully assigned (**Figure 6-1b**) using the ^{1}H NMR, ^{13}C NMR, ^{1}H-^{1}H COSY, ^{1}H-^{13}C HSQCD, ^{1}H-^{13}C HMBC and DEPT technique (**Figure 6-3**).

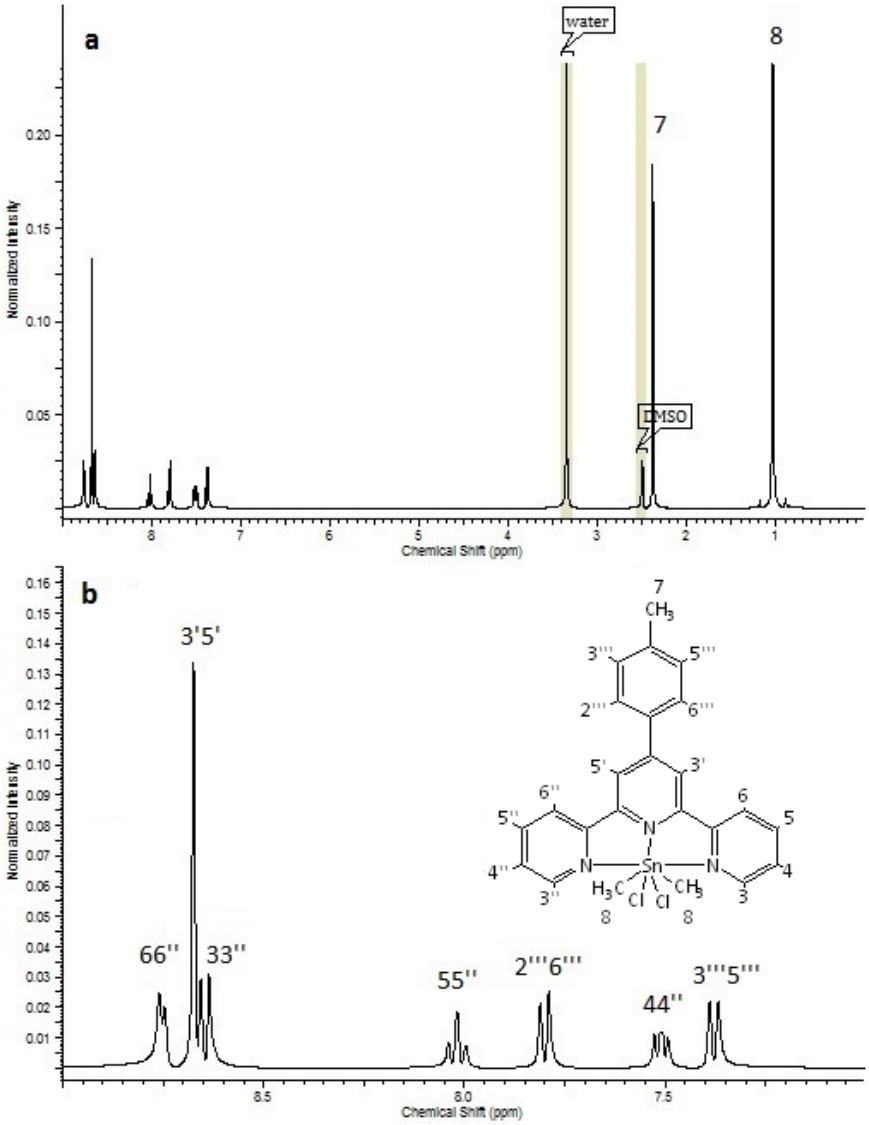

Figure 6-1 a) The ^{1}H NMR spectrum of **6.1** in d^{6} DMSO**. b)** An enlargement of the aromatic region

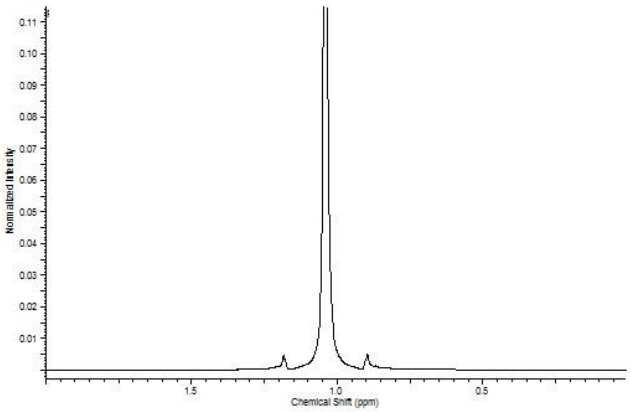

Figure 6-2 An enlargement of the methyl group signal and its Sn satellites

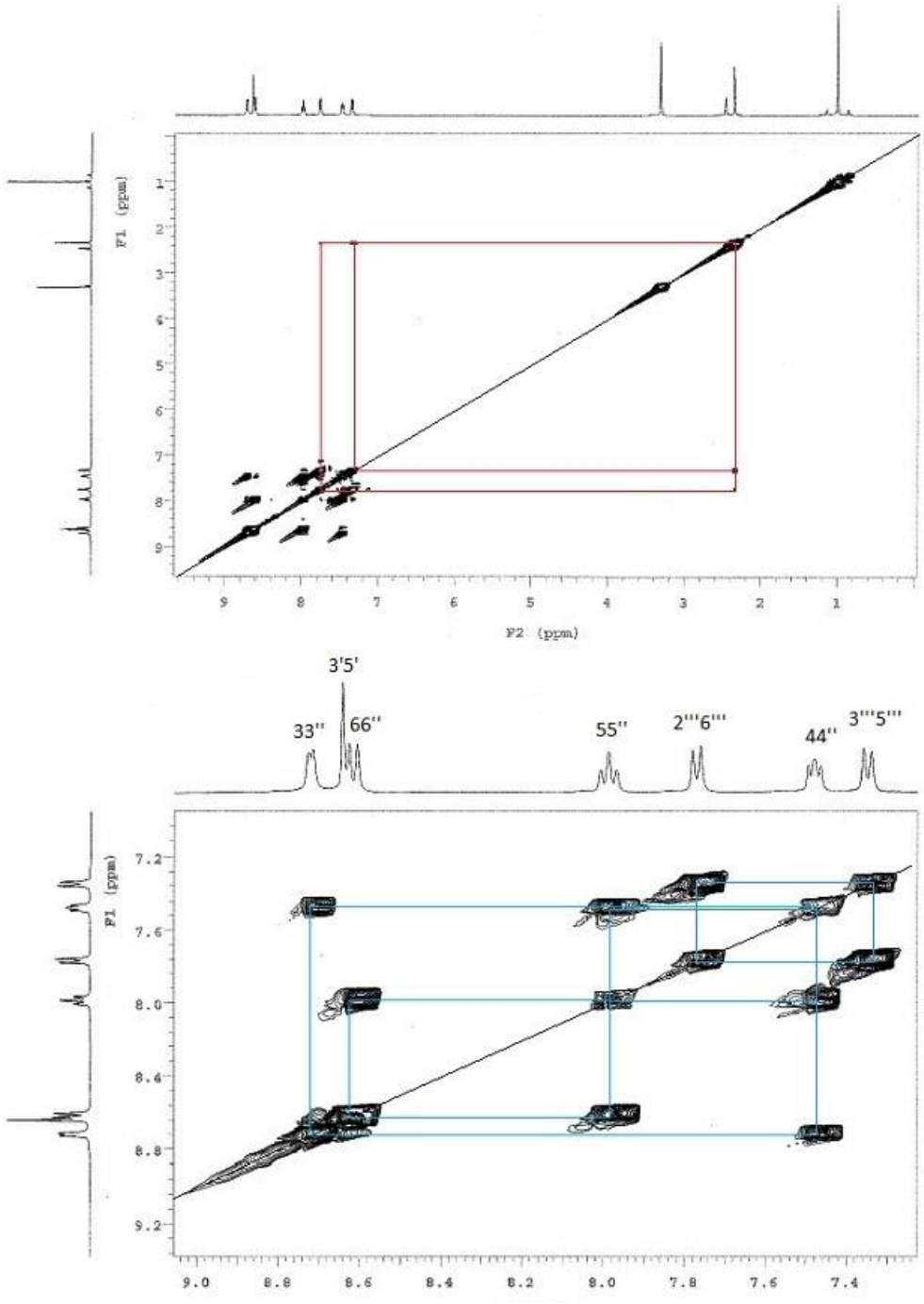

Figure 6-3 The ^{1}H-^{1}H COSY spectrum of **6.1** (Top), The enlargement of the aromatic region (bottom)

The ^{13}C NMR spectrum of **6.1**, in d^{6} DMSO, contains 1 signal at 20.84, 1 signal at 22.74 and 11 signals between 117.63 and 155.63 ppm, which we have assigned to the methyl carbon atoms on the ligand, methyl carbon atoms on tin and the aromatic rings carbon atoms of the complex (**Figure 6-4**).

There are 12 kinds of carbon atoms (7 tertiary and 5 quaternary) in complex **6.1** but 11 signals appeared. Only 4 quaternary carbon signals appeared while there are 5 of them in pttp ligand. The DEPT spectrum demonstrated that one of the quaternary signals is buried underneath one other signal at 149.34 ppm (**Figure 6-5**).

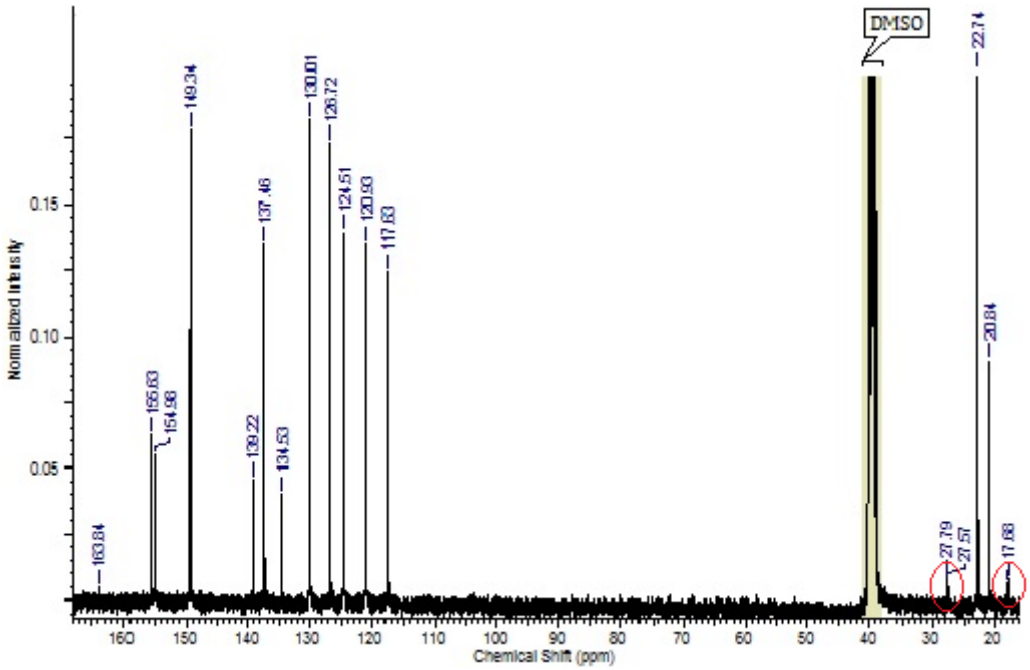

Figure 6-4 The ^{13}C NMR spectrum of **6.1.** Satellites of the methyl ligand on Sn are marked by red circles

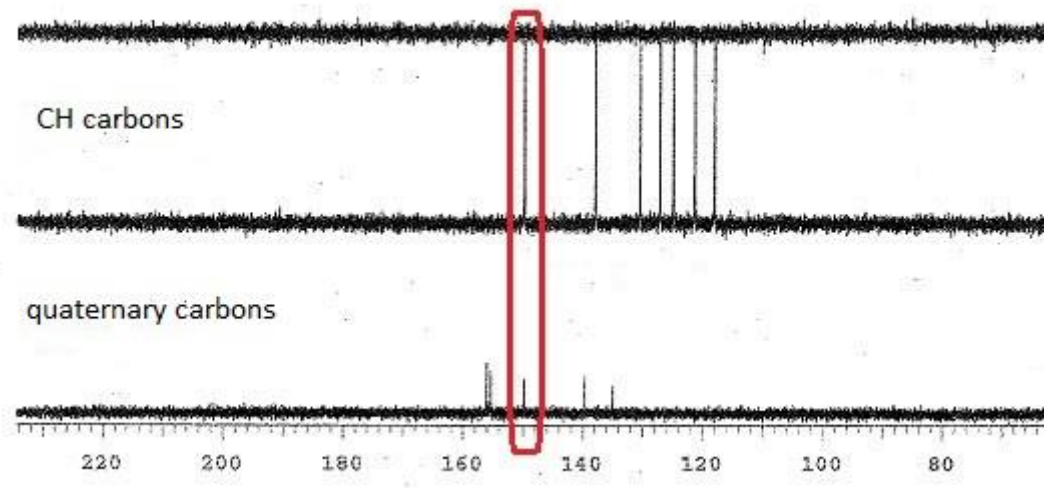

Figure 6-5 The DEPT spectrum of **6.1**. The red highlight identifies a quaternary carbon atom appeared at the same chemical shift as a tertiary carbon atom

Cross peaks in the COSY spectrum show that H3,3'' (t) couple to H4,4'' (d), H4,4'' couple to H5,5'' (d), and H5,5'' couples to H6.6'' (t). There is also a coupling between H3''',5''' (d) and H2''',6''' (d). The HMBC spectrum shows that there is a coupling between C3''',5''' and methyl group of pttp ligand. Another coupling to the methyl group is seen for C2''', C6'''. C1''' or C4''' couples to H3''', 5'''; and C4''' or C1''' couples to H2''', 6''' in the HMBC spectrum. The quaternary signal at 134.53 ppm is assigned to C1''' as it couples to H3',5'.

C3',5' couple in the HSQCD spectrum to the singlet assigned to H3', 5'. H6,6'' and H5.5''couple to C1,1'' in the HMBC spectrum. C1,1'' couple to H3,3'' and H3'5' in the HMBC spectrum. The full assignment is presented in **Figures 6-6** and **6-7**.

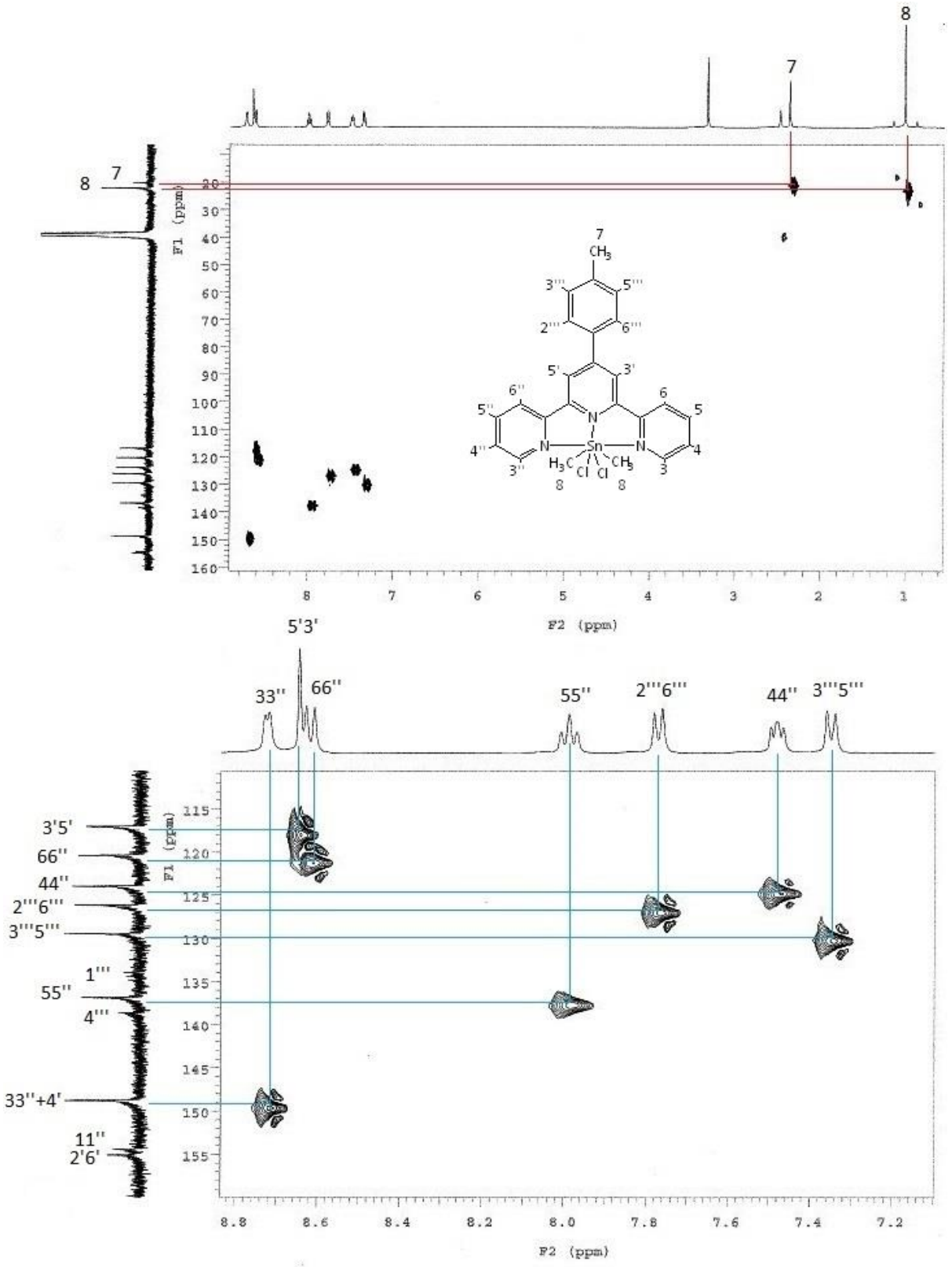

Figure 6-6 Top: The ^{1}H-^{13}C HSQCD spectrum of **6.1.** Bottom: An enlargement of the aromatic region

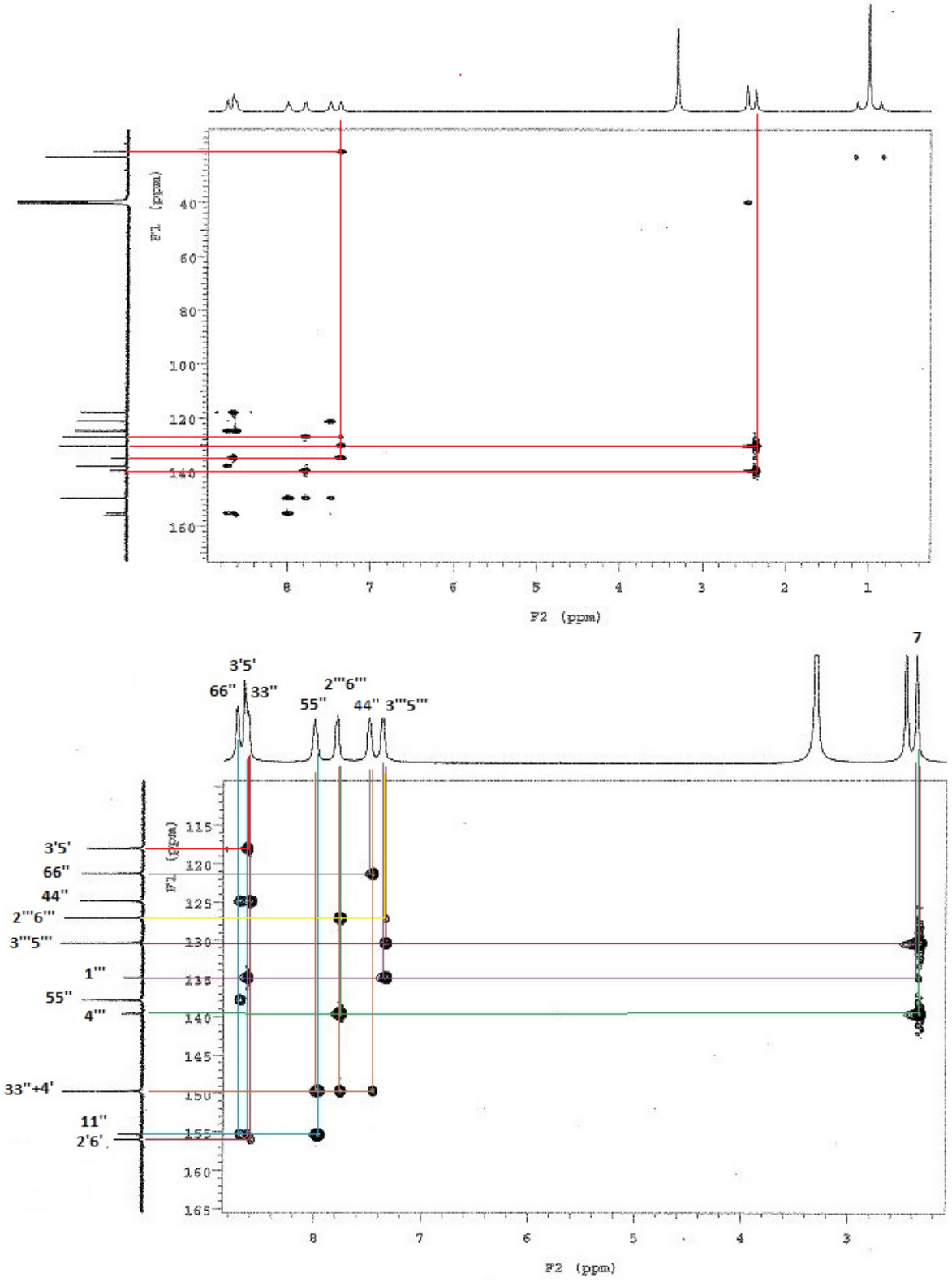

Figure 6-7 Top: The HMBC spectrum of **6.1.** Bottom: An enlargement of the aromatic region

The correlation between C-Sn-C angle and $^{1}J(^{13}C\text{-}^{119}Sn)$ is a useful method for providing information about the coordination environment of the tin(IV) nucleus[182]. In particular, the magnitude of $^{1}J(^{13}C\text{-}^{119}Sn)$ in solution has been related to the Sn coordination number.

The coupling constants $^{1}J(^{13}C–^{119}Sn)$ = 1033 Hz in **6.1** are consistent with a seven-coordinated methyltin complex[182].

The Lockhart and Manders equation given below correlates the C-Sn-C bond angle with the coupling constant $^{1}J(^{119}Sn\text{-}^{13}C_{\alpha})$[183]:

$\theta = 0.0877\ ^{1}J(^{119}Sn\text{-}^{13}C_{\alpha}) + 76.7543$

The magnitude of θ calculated from this equation (166˚) for compound **6.1** is comparable to that obtained from the X-ray crystallographic data (θ = 164.39°).

A few X-ray quality crystals, ($[Sn(CH_3)_2Cl(pttp)]\cdot 0.5[Sn(CH_3)_2Cl_4].CH_2Cl_2$, (**6.2**) were obtained by slow evaporation of a dichloromethane solution of crude **6.1**. The crystal structure of **6.2** is shown in **Figure 6-8**. This compound crystallised with one formula unit in the asymmetric unit. Sn(IV) is octahedrally coordinated to three N atoms of the pttp ligand, two methyl ligands and one chloride ligand. Selected bond length and selected bond angles are presented in **Tables 6-1** and **6-2**.

A $[Sn(CH_3)_2Cl_4]^{2-}$ ion is present as a counter ion and half of this moiety is present in the asymmetric unit. As the oxidation state of tin is IV, the methyl group is considered to be a −1 ligand. The charge of the $[Sn(CH_3)_2Cl(pttp)]$ moiety is +1. The packing diagram of **6.2** is presented in **Figure 6-9**.

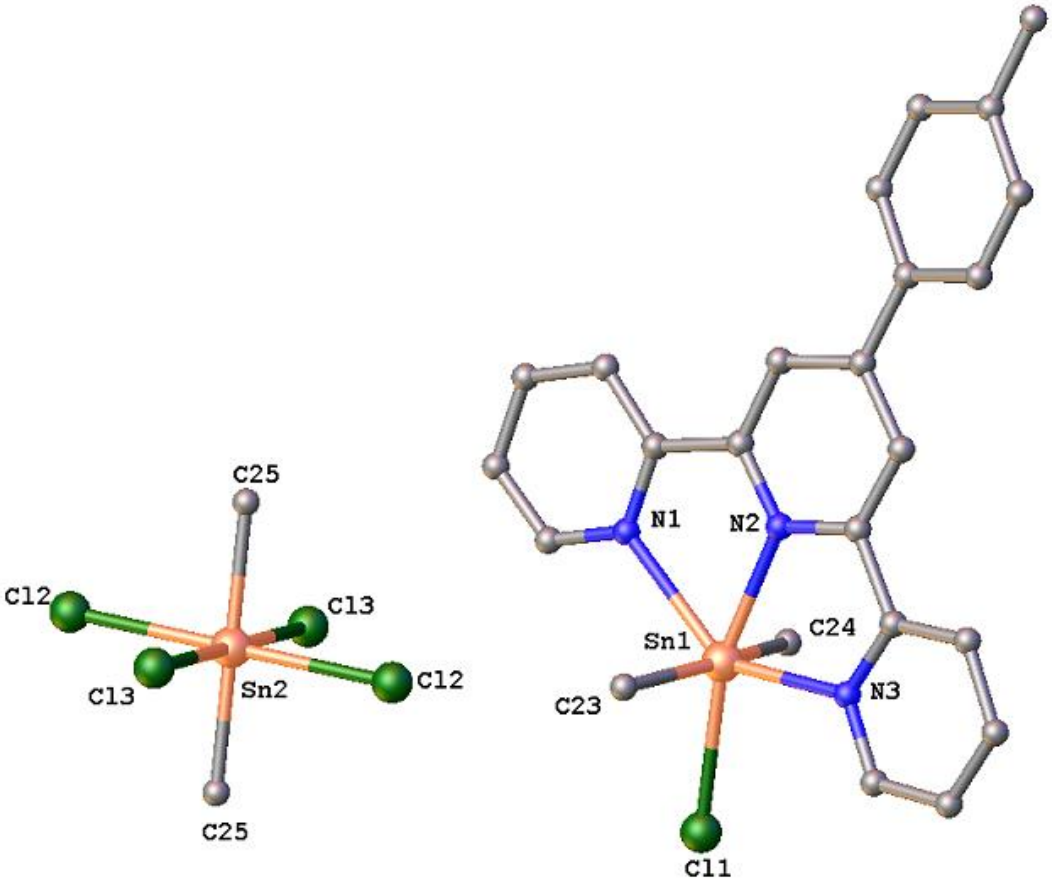

Figure 6-8 The crystal structure of $[Sn(CH_3)_2Cl(pttp)]\cdot 0.5[Sn(CH_3)_2Cl_4].CH_2Cl_2$ (**6.2**), with hydrogen atoms and one DCM molecule omitted for clarity

Selected bond length	
Sn2-Cl3	2.6238(11)
Sn2-Cl2	2.5924(11)
Sn2-C25	2.132(4)
Sn1-Cl1	2.6010(12)
Sn1-N2	2.276(4)
Sn1-N3	2.253(4)
Sn1-N1	2.412(4)
Sn1-C23	2.125(4)
Sn1-C24	2.087(5)

Table 6-1. Selected bond lengths for the structure of $[Sn(CH_3)_2Cl(pttp)]\cdot 0.5[Sn(CH_3)_2Cl_4].CH_2Cl_2$ **(6.2)**

Selected bond angles [°]			
Cl2-Sn2-Cl3	89.86(4)	C24-Sn1-Cl1	84.98(15)
C25-Sn2-Cl3	89.27(14)	C24-Sn1-N2	92.81(18)
C25-Sn2-Cl2	92.27(14)	C24-Sn1-N3	98.93(18)
N2-Sn1-Cl1	164.37(11)	C24-Sn1-N1	85.78(18)
N2-Sn1-N1	68.92(15)	C24-Sn1-C23	164.4(2)
N3-Sn1-Cl1	93.43(11)	C6-N2-Sn1	122.2(3)
N3-Sn1-N2	71.59(15)	C16-N2-Sn1	118.7(3)
N3-Sn1-N1	140.41(15)	C16-N2-C6	119.0(4)
N1-Sn1-Cl1	126.16(11)	C17-N3-Sn1	118.3(3)
C23-Sn1-Cl1	88.50(15)	C21-N3-Sn1	121.6(3)
C23-Sn1-N2	97.18(18)	C21-N3-C17	120.0(4)
C23-Sn1-N3	95.60(17)	C5-N1-Sn1	117.4(3)
C23-Sn1-N1	86.66(17)	C1-N1-Sn1	123.2(3)

Table 6-2 Selected bond angles for structure of $[Sn(CH_3)_2Cl(pttp)]\cdot 0.5[Sn(CH_3)_2Cl_4].CH_2Cl_2$ **(6.2)**

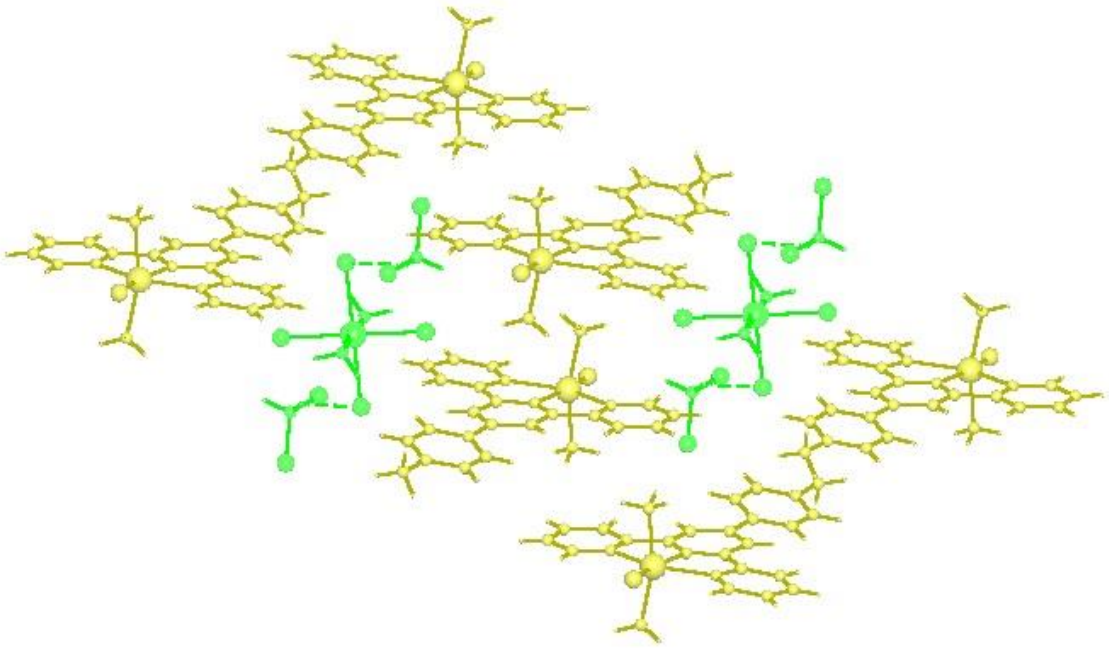

Figure 6-9 packing diagram of $[Sn(CH_3)_2Cl(pttp)]\cdot 0.5[Sn(CH_3)_2Cl_4].CH_2Cl_2$ **(6.2)**

In order to check that the single crystal is representative of the bulk sample, the X-ray powder diffraction (PXRD) patterns were recorded. As shown in **Figure 6-10**, the peak positions in the calculated and experimental patterns are not in good agreement with each other. This means the crystal structure is not representative of the bulk. Moreover, data

obtained by NMR confirm that the bulk material is largely different from that in the single crystal. The elemental analysis results are consistent with the formula of **6.1** being $[Sn(CH_3)_2Cl_2(pttp)]$.

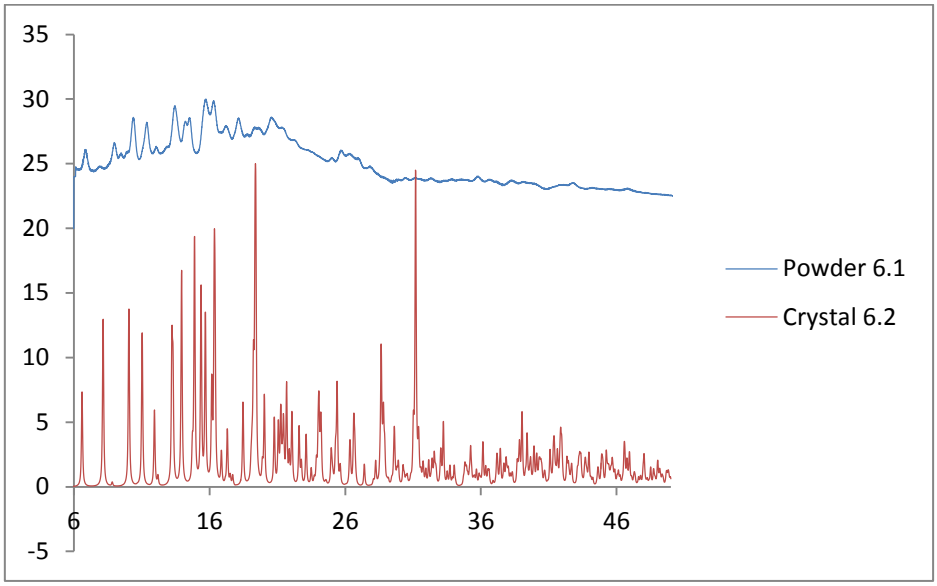

Figure 6-10 Calculated powder pattern from the single crystal structure solution, **6.2** (red), and Experimental PXRD pattern for the bulk sample, **6.1** (blue)

The mass spectrum of **6.1** contained peaks at m/z = 541.97 which can be assigned to the $[M\text{-}H^{+}]^{1-}$ ion (**Figure 6-11**).

In summary, mass spectrum and NMR data obtained from coupling constant ($^{1}J(^{13}C–^{119}Sn)$) are in agreement with having seven coordinated tin complex. However, the crystal structure of **6.2** showed a six coordinated tin complex with a six coordinated counter ion.

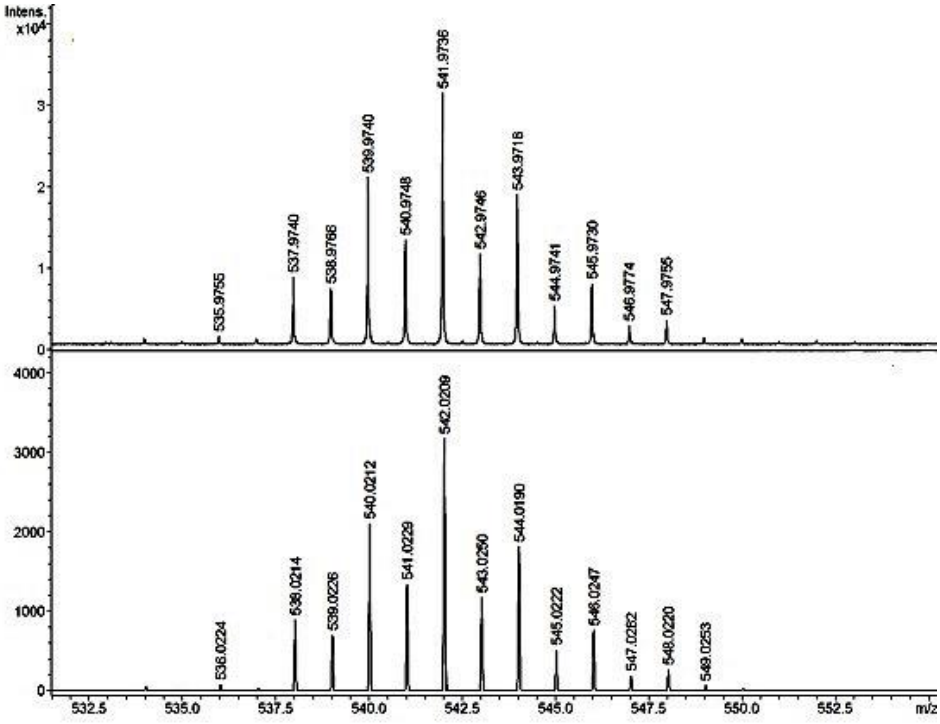

Figure 6-11 Experimental (top) and simulated isotope patterns for the highest abundance mass peak of $[M-H^+]^{1-}$ ion

$[Sn(CH_3)_2Cl(ottp)]Cl$ (6.3)

The synthesis of $[Sn(CH_3)_2Cl(ottp)]Cl$ (**6.3**) is presented below in **Scheme 6-2**.

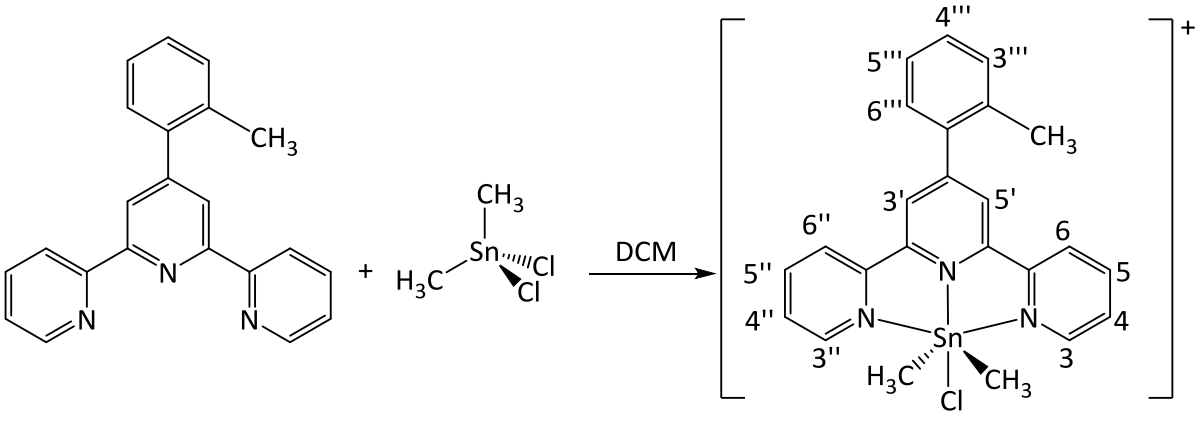

ottp **6.3**

Scheme 6-2 Brief description of synthesis of **6.3**

The ^{1}H NMR spectrum of $[Sn(CH_3)_2Cl(ottp)]^+$ (**6.3**) is shown in **Figure 6-12.**

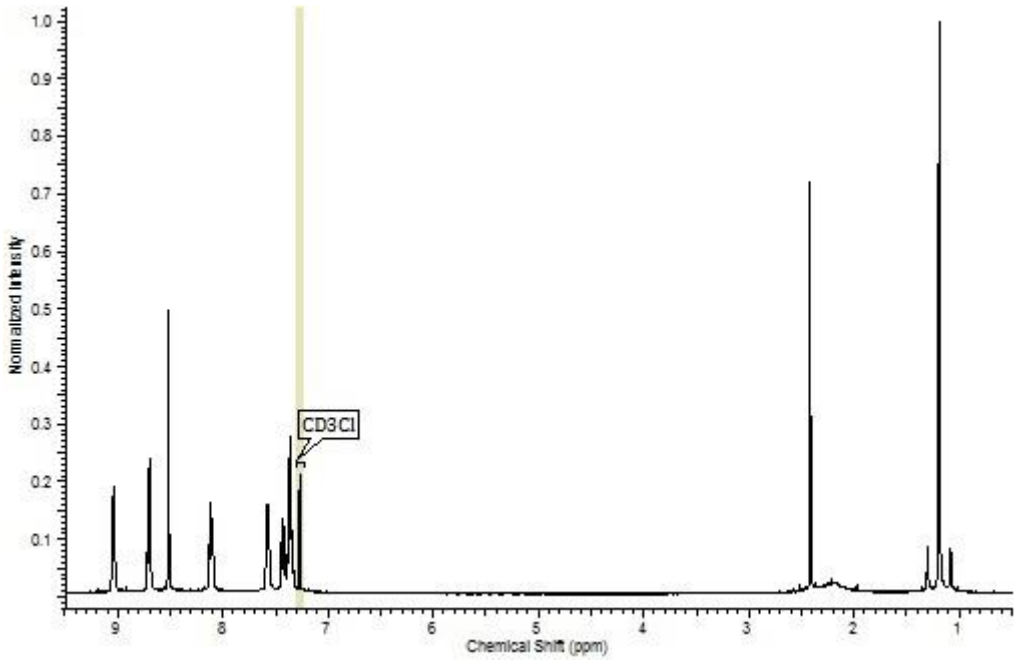

Figure 6-12 The ^{1}H NMR spectrum of **6.3** in $CDCl_3$

The integration ratios of the aromatic ring proton, methyl proton on ottp ligand and the protons on the methyl ligands are 12:3:6 representing coordination of 1 equivalent of ottp to 1 equivalent of Sn, and two methyl ligands on Sn.

The singlet peak at 1.19 ppm in the ^{1}H NMR spectrum of $[Sn(CH_3)_2Cl(ottp)]^+$ is assigned to the methyl protons attached to Sn. The methyl group signals carry satellites due to coupling of hydrogen atoms with ^{117}Sn and ^{119}Sn nuclei.

Some of the aromatic protons signals are readily assigned using the ^{1}H-^{1}H COSY spectrum (**Figure 6-13**). H3,3'' (d) couple to H4,4''(t); H4,4'' (t)couple to H5,5'' (t); and H5,5'' (t) couple to H6,6'' (d) in the COSY spectrum.

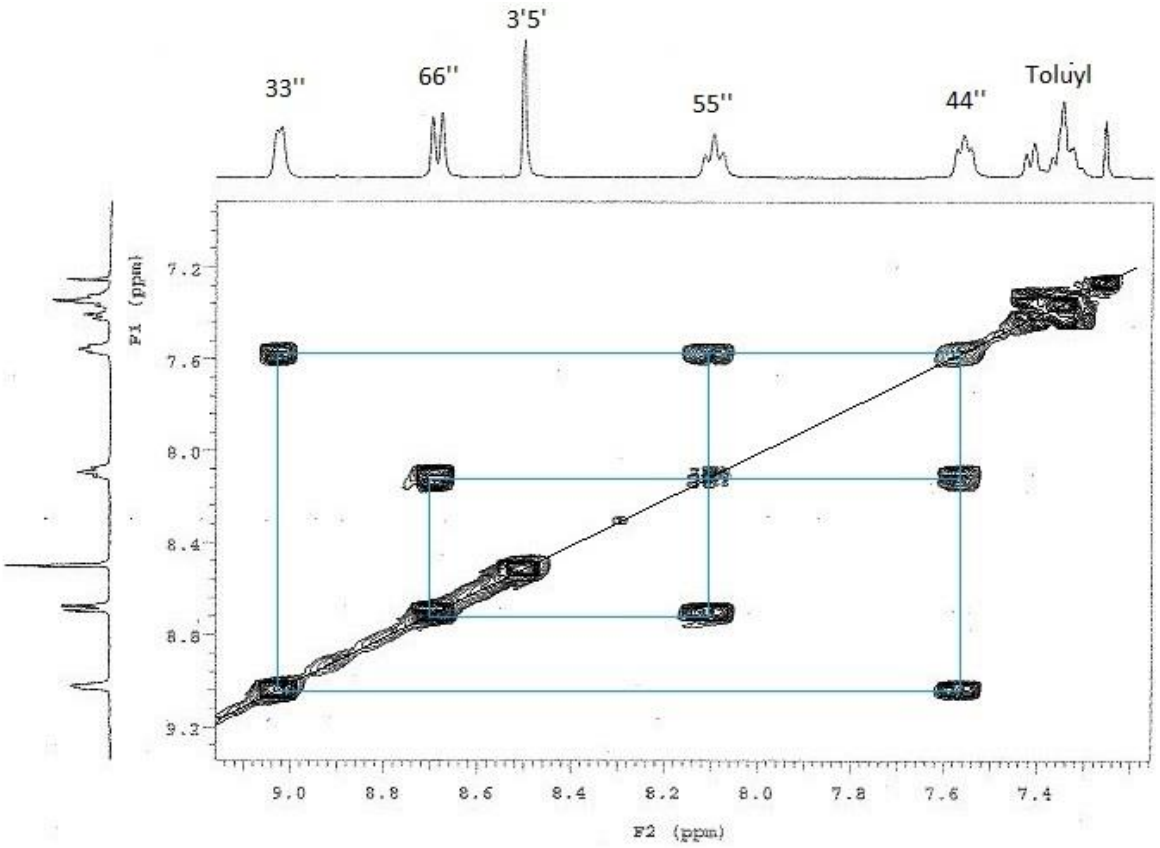

Figure 6-13 The ^{1}H-^{1}H COSY spectrum of **6.3**

The ^{13}C NMR spectrum of **6.3**, shown in **Figure 6-14**, is fully assigned using HSQCD, HMBC and DEPT NMR studies. The two peaks at 17.87 and 20.47 ppm are assigned to carbon atoms of methyl groups on Sn and the carbon atom of the methyl group in the ottp ligand, respectively.

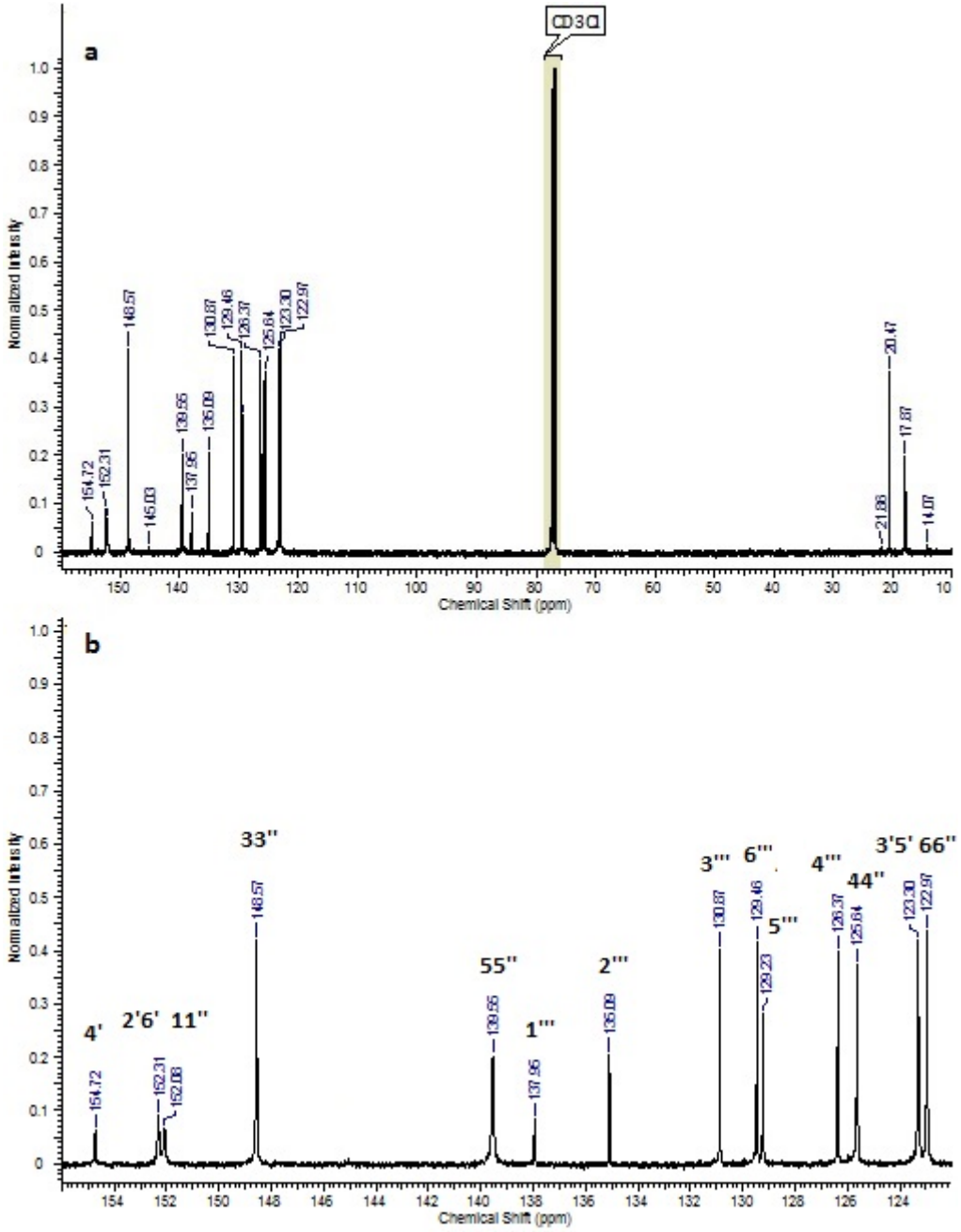

Figure 6-14 a) The ^{13}C NMR spectrum of **6.3** in $CDCl_3$ **b)** An enlargement of the aromatic region

Tertiary and quaternary carbon atoms were recognised by DEPT spectrum (**Figure 6-15**).

The tertiary carbon atoms, except those in the toluyl ring, were assigned by using HSQCD NMR spectrum (**Figure 6-16**).

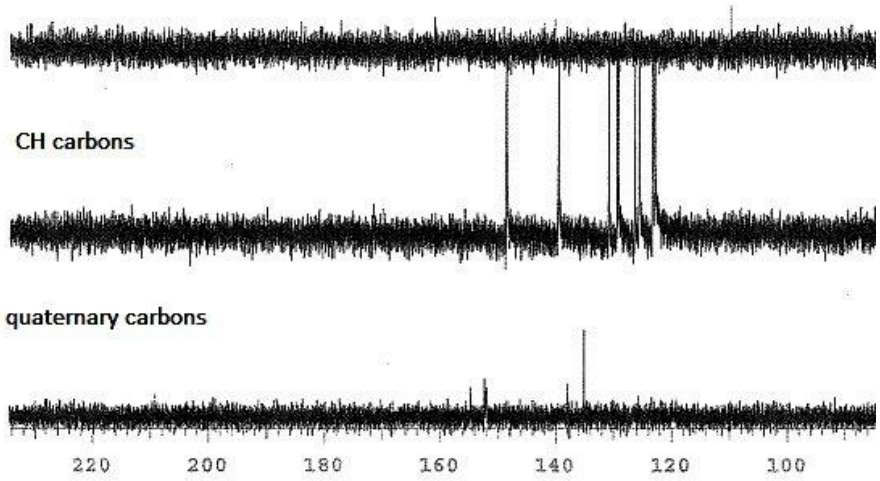

Figure 6-15 The DEPT spectrum of **6.3**

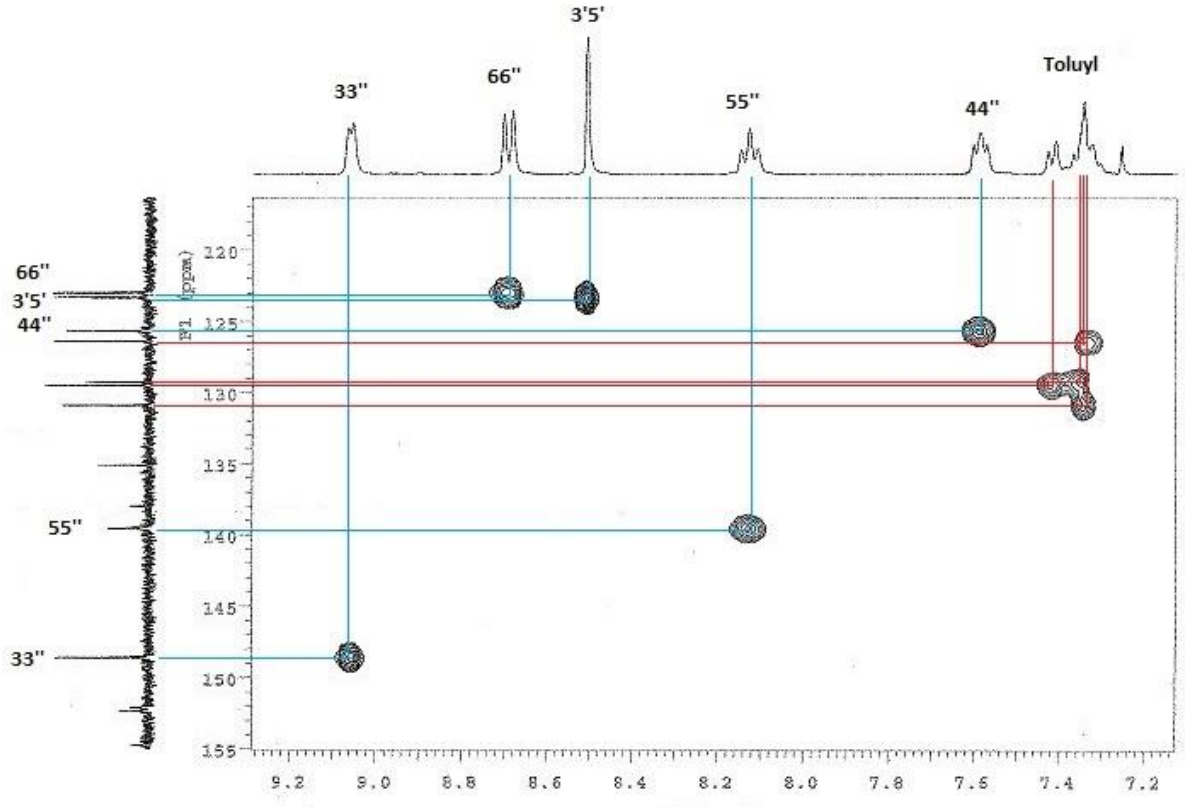

Figure 6-16 The ^{1}H-^{13}C HSQCD spectrum of **6.3**. The red lines show the coupling between ^{1}H and ^{13}C nuclei of the toluyl ring. The blue lines show the coupling for the rest of the ligand

The quaternary carbon atoms and the toluyl ring were assigned by using HMBC spectrum (**Figure 6-17**). The quaternary signal at 154.72 ppm has a cross peak with the doublet of a toluyl ring at 7.43 ppm. Therefore, the carbon signal at 154.72 ppm is assigned to 4’ and the

hydrogen signal at 7.43 ppm is assigned to 6’’’. The signal at 129.46 ppm is assigned to C6’’’ from the HSQCD spectrum. C1’’’ couples to H3’5’ and the multiplet of the toluyl ring. C2’’’ couples to the multiplet and the doublet of the toluyl ring as well as the methyl group in the HMBC spectrum. The signal at 129.23 ppm does not have any coupling with a methyl group; therefore it is expected to be C5’’’. The signal at 130.87 ppm is assigned to C3’’’ as it has a strong coupling with the methyl protons and the multiplet of the toluyl ring. The signal at 126.37 ppm is assigned to C4’’’ since the coupling with the methyl is much weaker.

The signal at 152.08 ppm is assigned to C1,1’’ as they have coupling with H3,3’’ and H 5,5’’ in HMBC spectrum. The signal at 152.31 ppm is assigned to C2’,6’ as they have coupling with H3’,5’ and H 6,6’’ in HMBC spectrum.

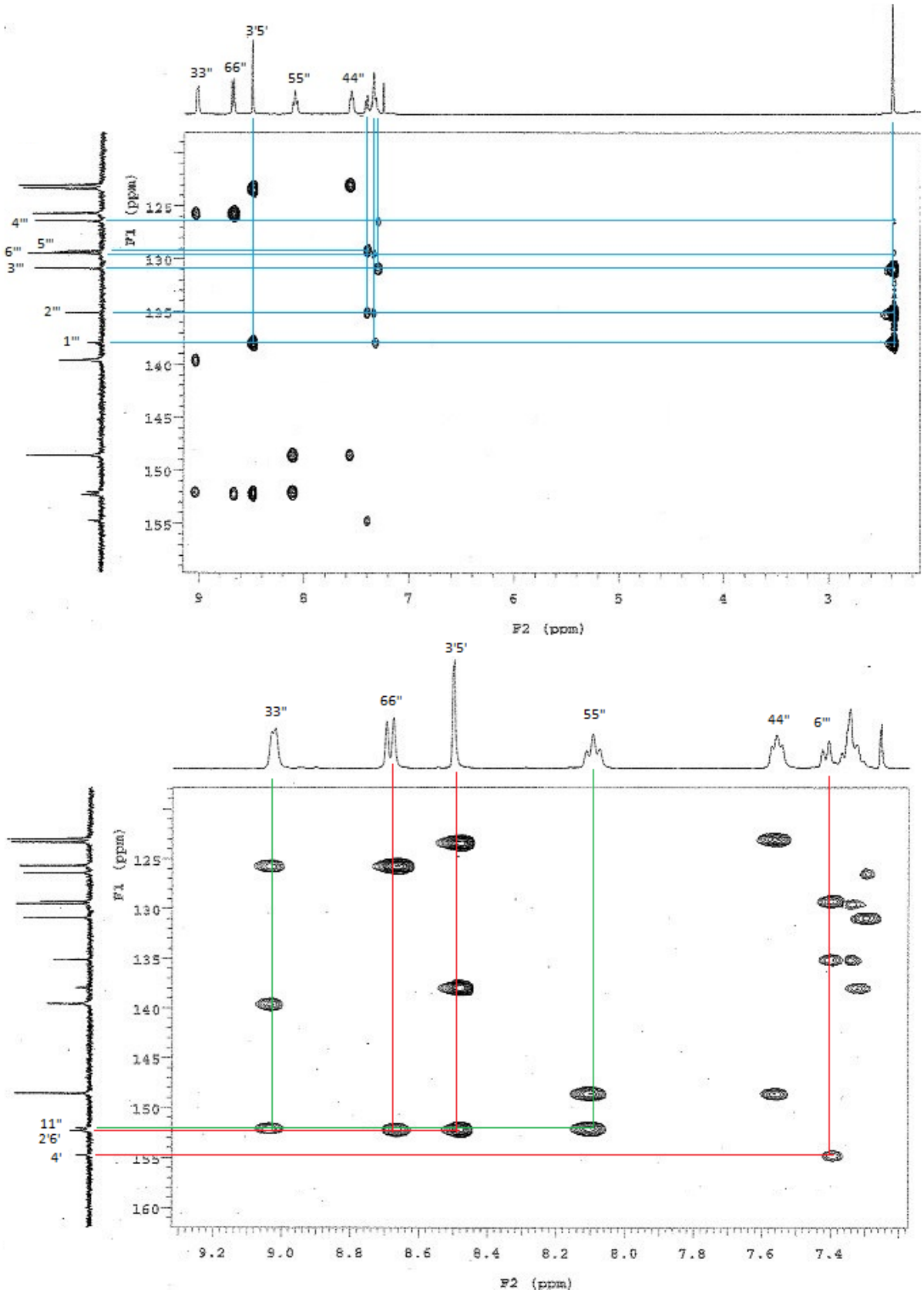

Figure 6-17 The ^{1}H-^{13}C HMBC spectrum of **6.3 (**top), and an enlargement of the aromatic region (bottom)

The coupling constants $^{1}J(^{13}C–^{119}Sn)$ = 801.86 Hz in **6.3** suggest a six-coordinated dimethyltin complex[182].

The Lockhart and Manders equation given below correlates the C-Sn-C bond angle with the coupling constant $^{1}J(^{119}Sn\text{-}^{13}C_{\alpha})$.

$\theta = 0.0877\ ^{1}J(^{119}Sn\text{-}^{13}C_{\alpha}) + 76.7543$

The magnitude of θ calculated from this equation is 147° for compound **6.3**.

Results from elemental analysis were consistent with the formula of $[Sn(CH_3)_2Cl(ottp)]Cl$. We considered one chloride attached to Sn and another as the counter-ion due to the coordination number of Sn found by NMR results.

The mass spectrum of **6.3** was taken in ethanol, and the whole molecular mass peak was not found. But the mass peak found in m/z 518.12 is a good match with the formula of $[Sn(CH_3)_2(OEt)(ottp)]^{1+}$ (**Figure 6-18**). Thus it appears that before or during the mass spectrometry experiment, the chloride ligand is replaced by ethanol which is presumably deprotonated later.

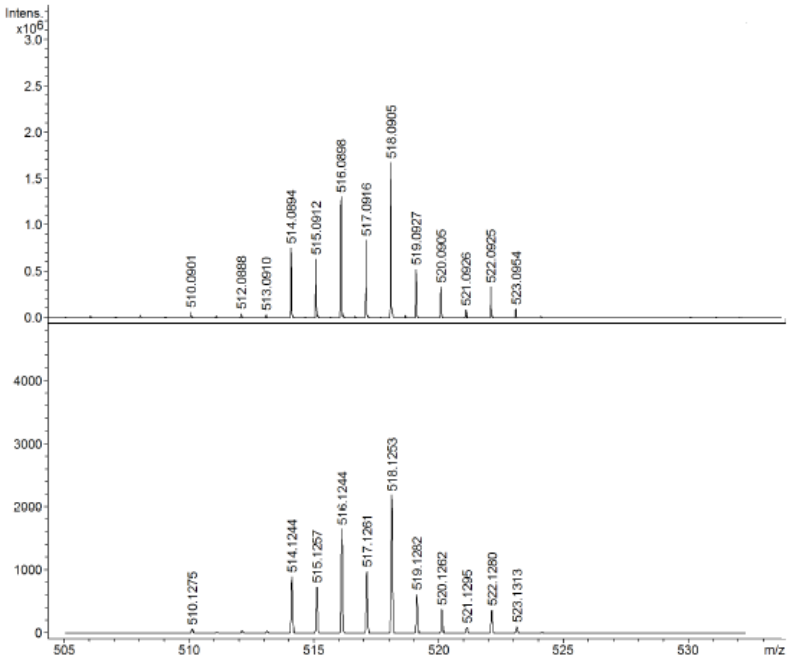

Figure 6-18 Experimental (top) and simulated isotope patterns for the mass peak of $[Sn(CH_3)_2(OEt)(ottp)]^{1+}$ion

6.2.1.2 $[SnCl_2(ottp)(Ph)][SnCl_2(Ph)_3]$

The synthesis of $[SnCl_2(Ph)(ottp)][SnCl_2(Ph)_3]$ (**6.4**) is presented below in **Scheme 6-3**.

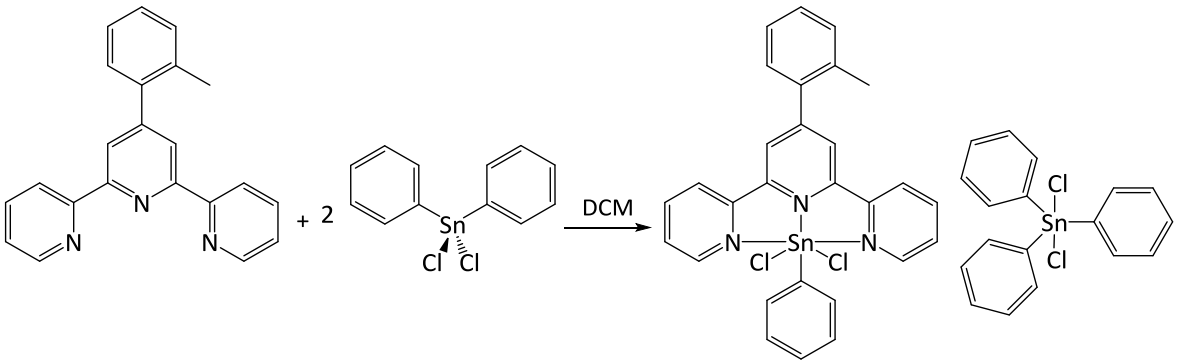

ottp **6.4**

Scheme 6-3 Brief description of the synthesis of $[SnCl_2(Ph)(pttp)][SnCl_2(Ph)_3]$ **(6.4)**

A pure sample of the titled complex was not isolated; however, the single crystal diffraction defined the structure as shown in Figure **6-19**. X-ray quality crystals were obtained by diffusion of diethyl ether into the dichloromethane solution of crude **6.4**.

There are only a few crystal of **6.4** obtained.

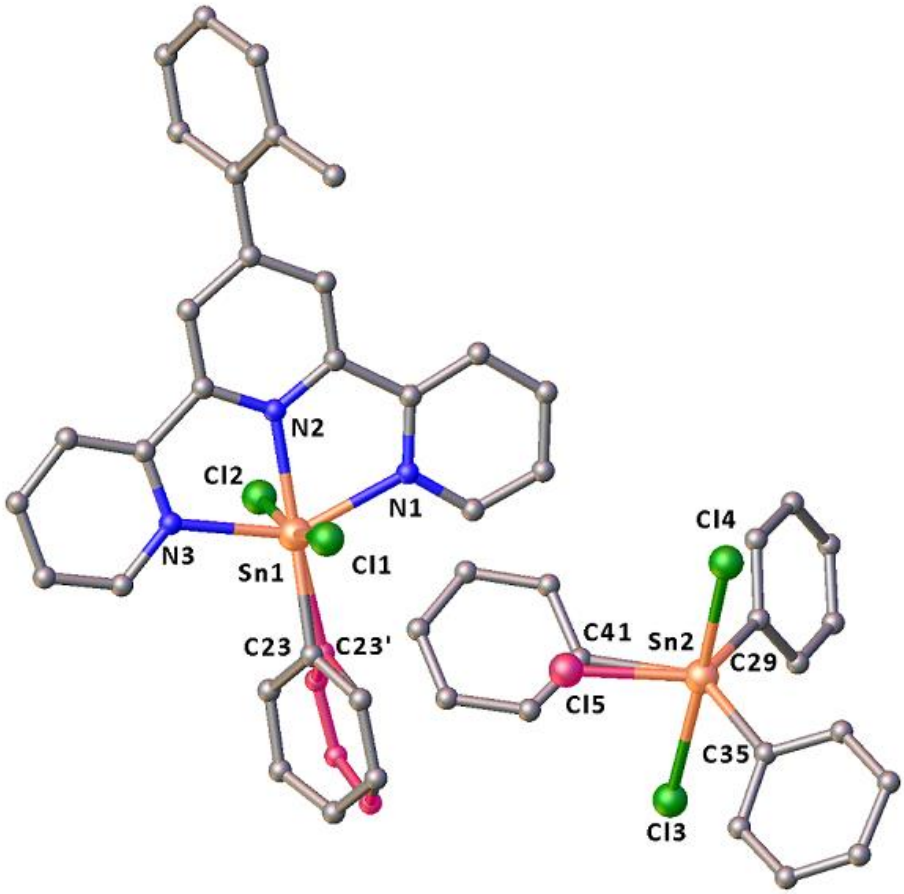

Figure 6-19 Crystal structure of **6.4**. The crystal is disordered based on coordination around Sn2 and the phenyl ring attached to Sn1. The phenyl ring attached to Sn2 showed disorder with 66% occupation and the chloride atom shown in pink occupied 33%. The occupation of the atoms shown in pink is 33%

Sn1 is octahedrally attached to three nitrogen atoms of the ottp ligand, two chloride ligands and a phenyl ring. This unit formed a +1 complex. The counter-ion of this complex is a five coordinate tin complex. The Coordination around Sn1 is disordered in which the ligands are either two chloride ions and three phenyl rings or three chloride ions and two phenyl rings.

The selected bond lengths and bond angles of 6.4 are shown in **Tables 6-3** and **6-4**. The packing diagram of 6.4 is presented in **Figure 6-20**.

Bond length [Å]	
Sn2-Cl4	2.516(2)
Sn2 Cl3	2.670(2)
Sn2-Cl5	2.348(13)
Sn2-C35	2.112(8)
Sn2-C29	2.152(8)
Sn2-C41	2.10(2)
Sn1 Cl2	2.435(3)
Sn1-Cl1	2.439(3)
Sn1-N2	2.186(6)
Sn1-N3	2.220(8)
Sn1-N1	2.218(8)
Sn1-C23	2.103(3)

Table 6-3 Selected bond lengths for **6.4**

Bond angle [°]	
N3-Sn1-N2	73.32(9)
N2-Sn1-N1	73.30(3)
Cl2-Sn1-Cl1	166.81(8)
Cl2-Sn1-C23	100.91(8)
Cl2-Sn1-C23’	89.21(5)
Cl-Sn1-C23	92.30(8)
Cl1-Sn1-C23’	103.818
Cl4-Sn2-Cl3	177.17(8)
Cl5-Sn2-Cl4	92.1(4)
Cl5-Sn2-Cl3	85.8(4)
C35-Sn2-Cl3	87.1(2)
C35-Sn2-C15	116.9(4)
C35-Sn2-C29	119.9(3)
C29-Sn2-C14	92.4(3)
C29-Sn2-C13	90.4(3)
C29-Sn2-C15	122.8(4)
C41-Sn2-C14	92.6(9)
C41-Sn2-C13	85.7(9)
C41-Sn2-C35	126.5(6)
C41-Sn2-C29	113.2(6)

Table 6-4 Selected bond angles for **6.4**

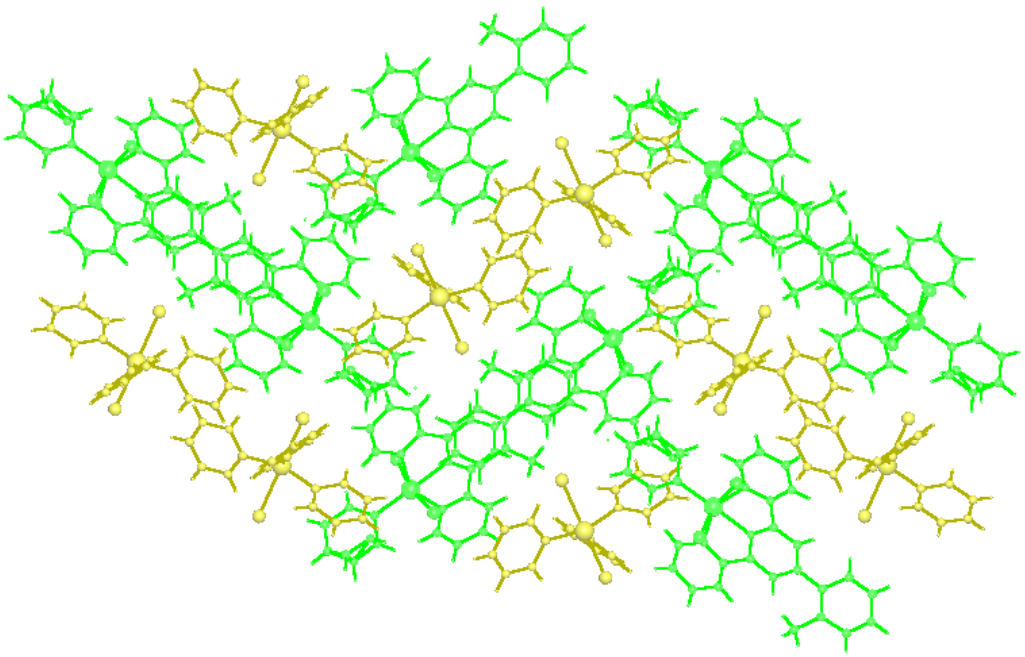

Figure 6-20 The packing diagram of **6.4**

6.2.1.3 $[SnCl_2(Ph)(pttp)][SnCl_2(ph)_3]$ (6.5)

The synthesis of $[SnCl_2(Ph)(pttp)][SnCl_2(Ph)_3]$ (**6.5**) is presented below in **Scheme 6-4**. Unfortunately, X-ray quality crystals could not be obtained. However, results from elemental analysis were consistent with the formula of $[Cl_2(ph)Sn(pttp)][(ph)_3SnCl_2]$ which is suggested to have a structure similar to **6.4**.

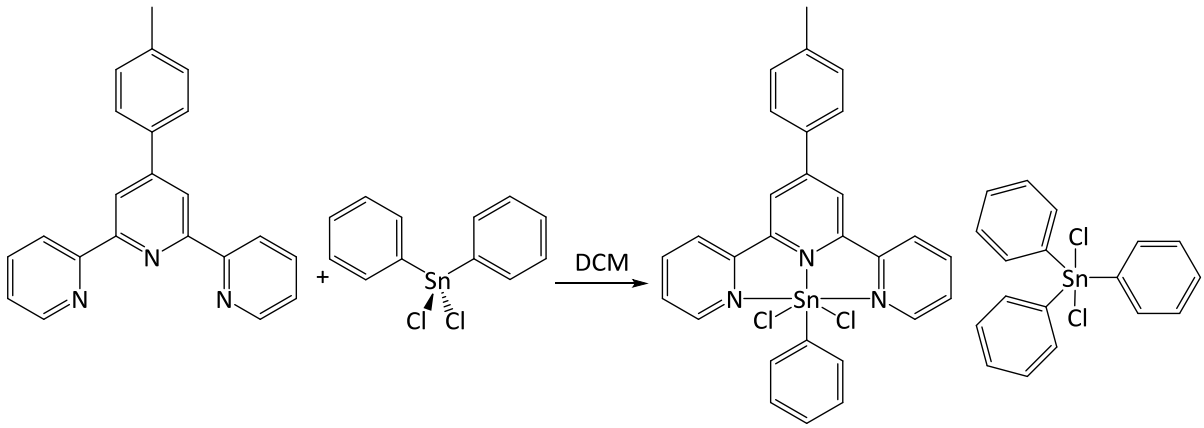

L6.1 **6.5**

Scheme 6-4 Brief description of synthesis of $[Cl_2(ph)_2Sn(pttp)][(ph)_3SnCl_3]$ **(6.5)**

The ^{1}H NMR spectrum of **6.5** is shown in Figure **6-18**. The integration ratio of the pttp ligand protons *vs* phenyl rings protons on Sn is 14 to 20, which is in agreement with the structure defined for **6.5**. The protons on the pttp ligand are assigned as shown in Figure **6-21**.

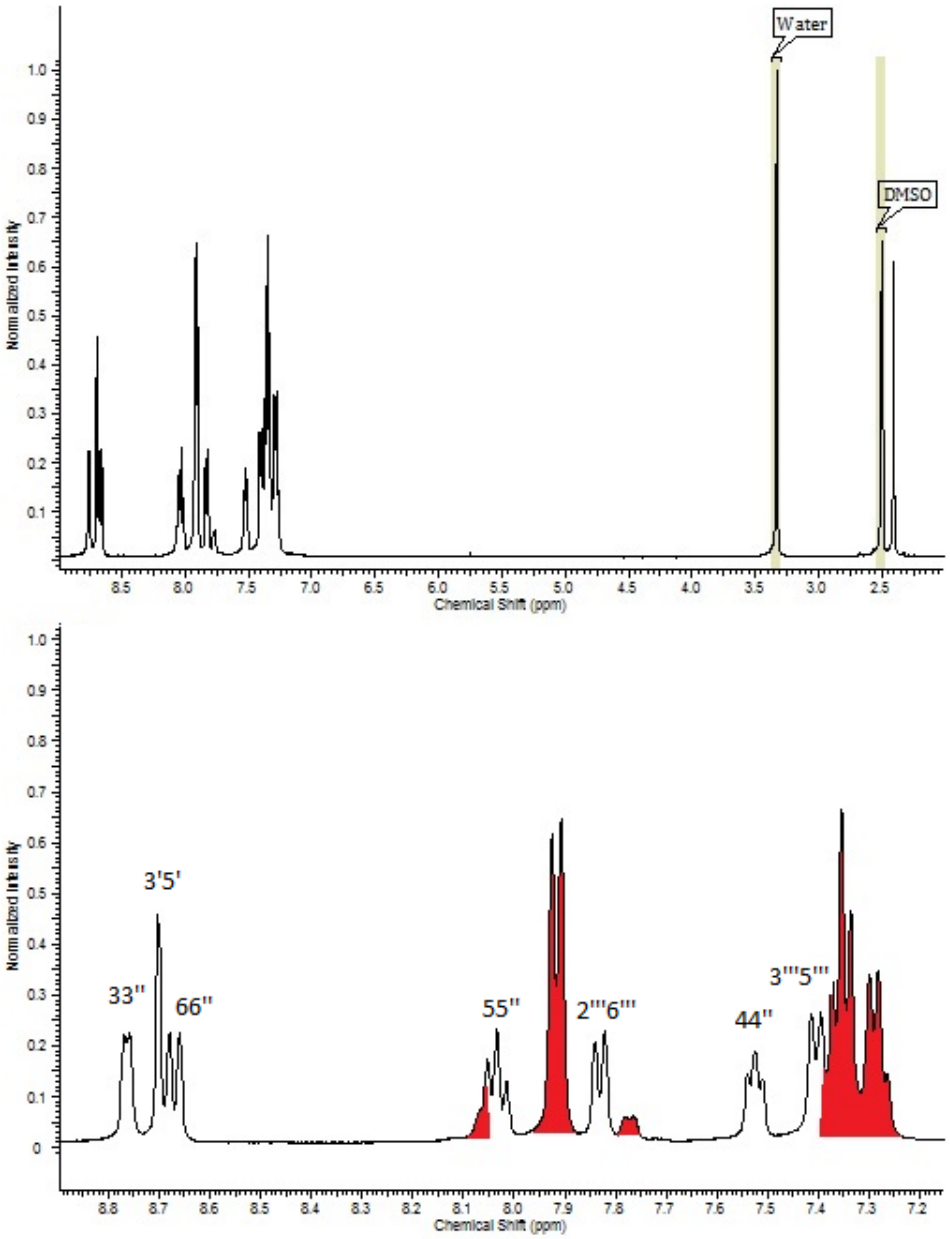

Figure 6-21top: The ^{1}H NMR spectrum of **6.5** (top) in DMSO, The enlargement of the aromatic region. The proton signals and the satellites of the phenyl ligand on Sn are marked by coloured by red (bottom).

The ^{13}C NMR spectrum of **6.5** is shown in **Figure 6-22.** The signal at 20.82 ppm is assigned to methyl carbon atom on pttp ligand. The aromatic region signals are assigned based on the assignments of **6.1**. The signals marked by stars are assigned to phenyl carbon atoms on Sn. There are 7 quaternary and 13 tertiary kinds of aromatic carbon atoms in **6.5**. There are 16 signals in the aromatic region. The DEPT spectrum showed there is a quaternary signal underneath the tertiary signal at 149.34 ppm (**Figure 6-23**). The DEPT spectrum shows 5 kind of quaternary signals while there are 7 of them in the proposed structure. The two signals at 154.99 and 155.65 ppm are twice as tall as other quaternary signals. Thus, we suspect that two other quaternary signals are underneath those two signals.

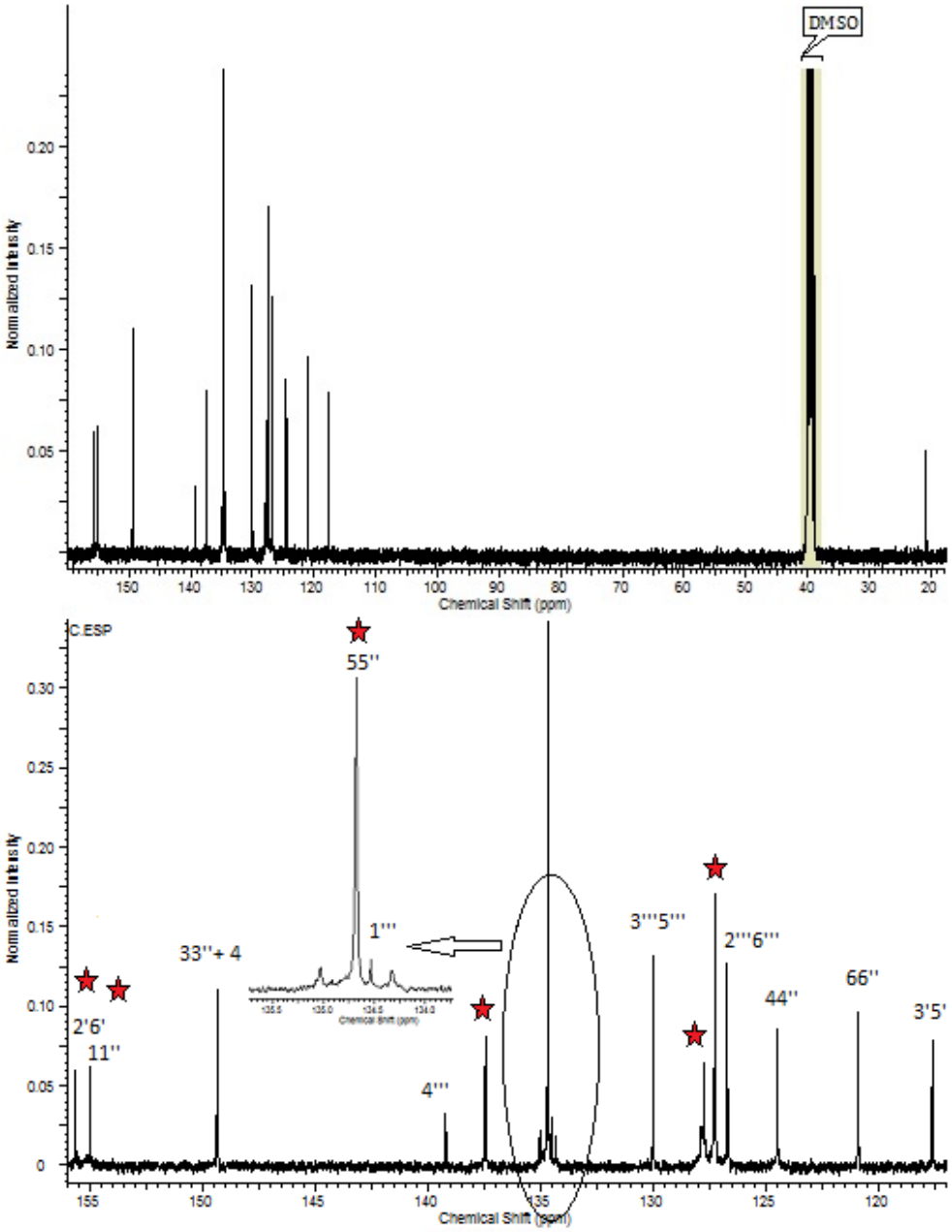

Figure 6-22 The ^{13}C NMR spectrum of **6.5** (Top). The enlargement of the aromatic region (bottom). The enlargement of peaks marked by circle is shown as well

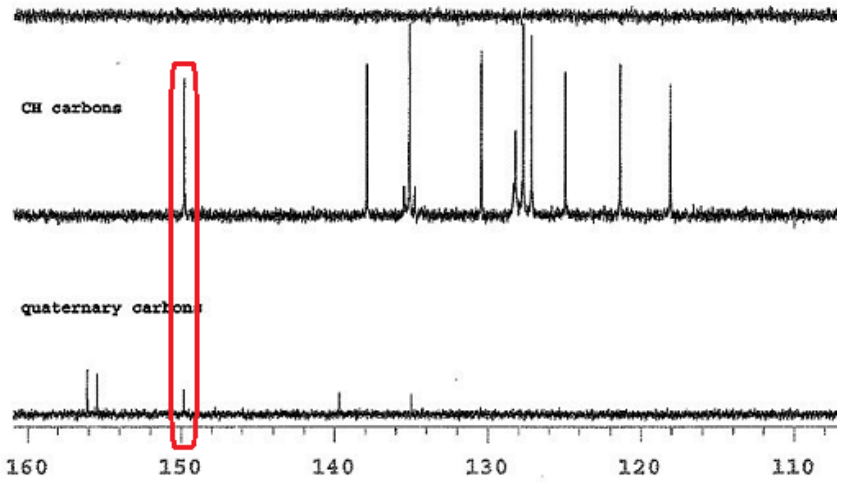

Figure 6-23 The DEPT NMR spectrum of **6.5**. the red highlight identifies a quaternary carbon atom appeared in same chemical shift with a tertiary carbon atom

The ^{1}H-^{13}C HSQCD NMR spectrum of **6.5** showed the signal at 134.68 ppm has a correlation with H5,5'' of the ligand and the protons of the phenyl ring on Sn (**Figure 6-24**). This represents two different kinds of signals appearing in a same place in 134.68 ppm.

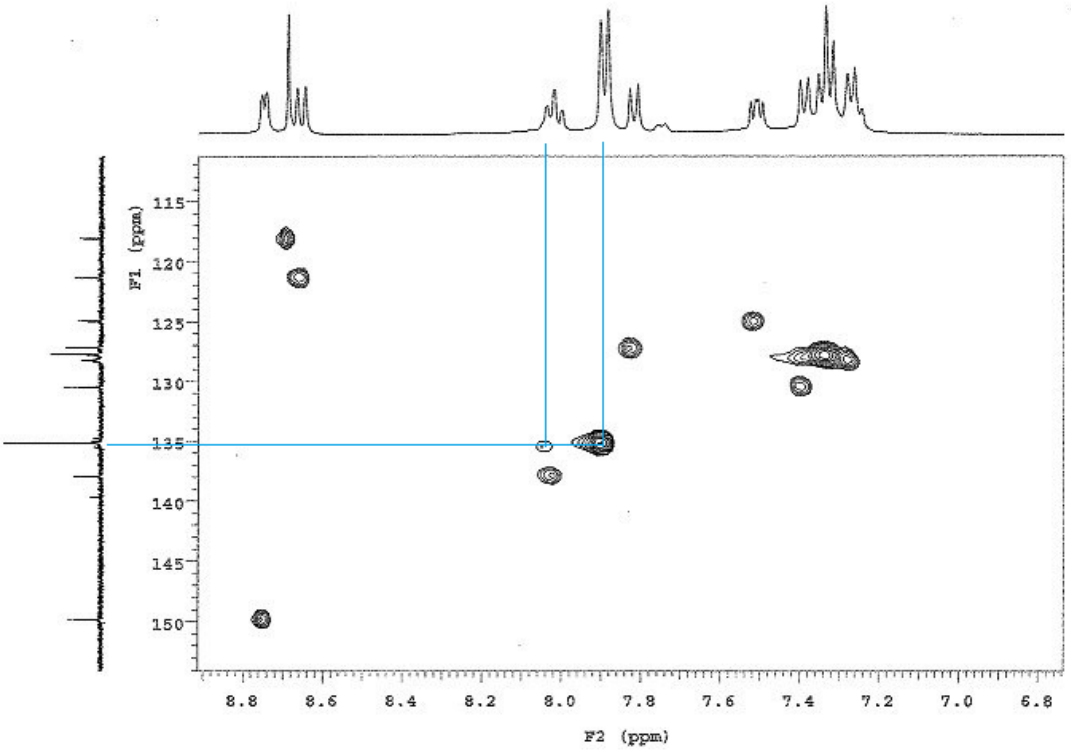

Figure 6-24 The ^{1}H-^{13}C NMR spectrum of **6.5**

The positive ion mass spectrum did not show any peaks matching with **6.5**. The negative ion mass spectrum of **6.5** is shown in **Figure 6-25**. The enlargement of the mass peaks at m/z: 378.85 and 420.91 and their simulations are shown in **Figure 6-26**.

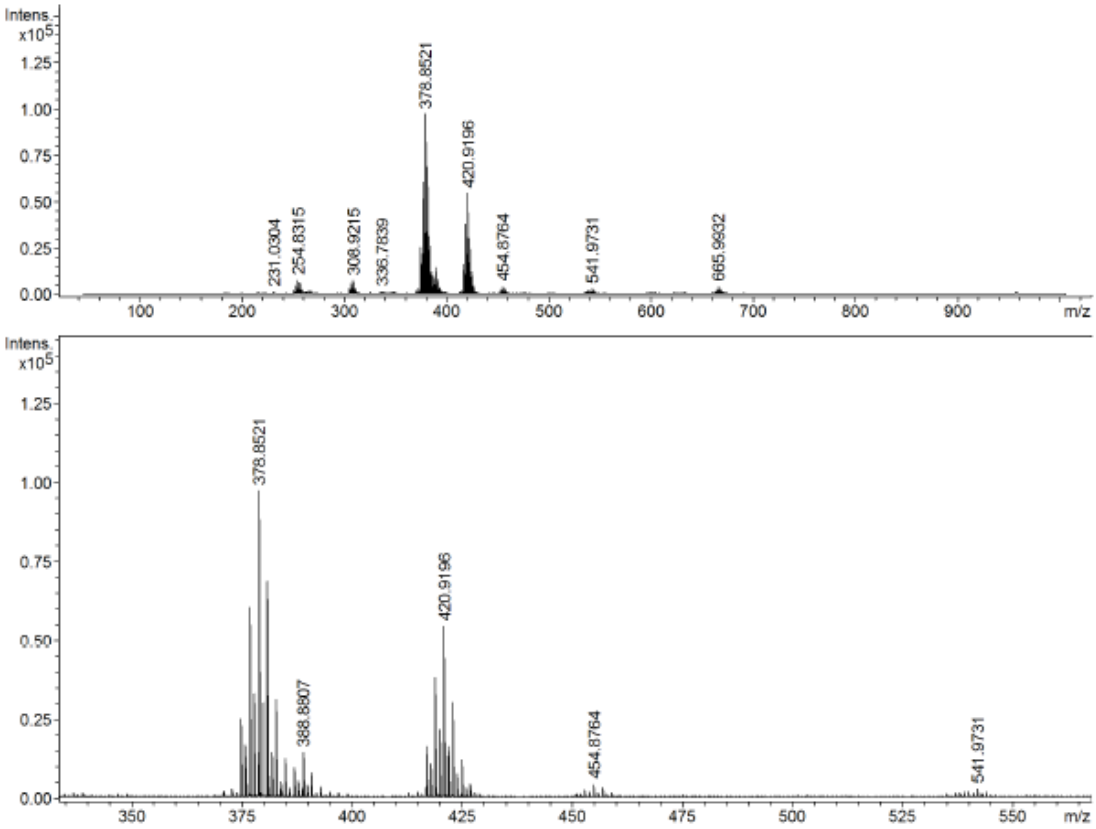

Figure 6-25 Mass spectrum of **6.5** and the enlargement of the main peaks (Top), and the enlargement (bottom)

The peaks at m/z = 378.85 and 420.91 are assigned to the $[Cl_3Sn(ph)_2]^{1-}$ and $[Cl_2Sn(ph)_3]^{1-}$ respectively.

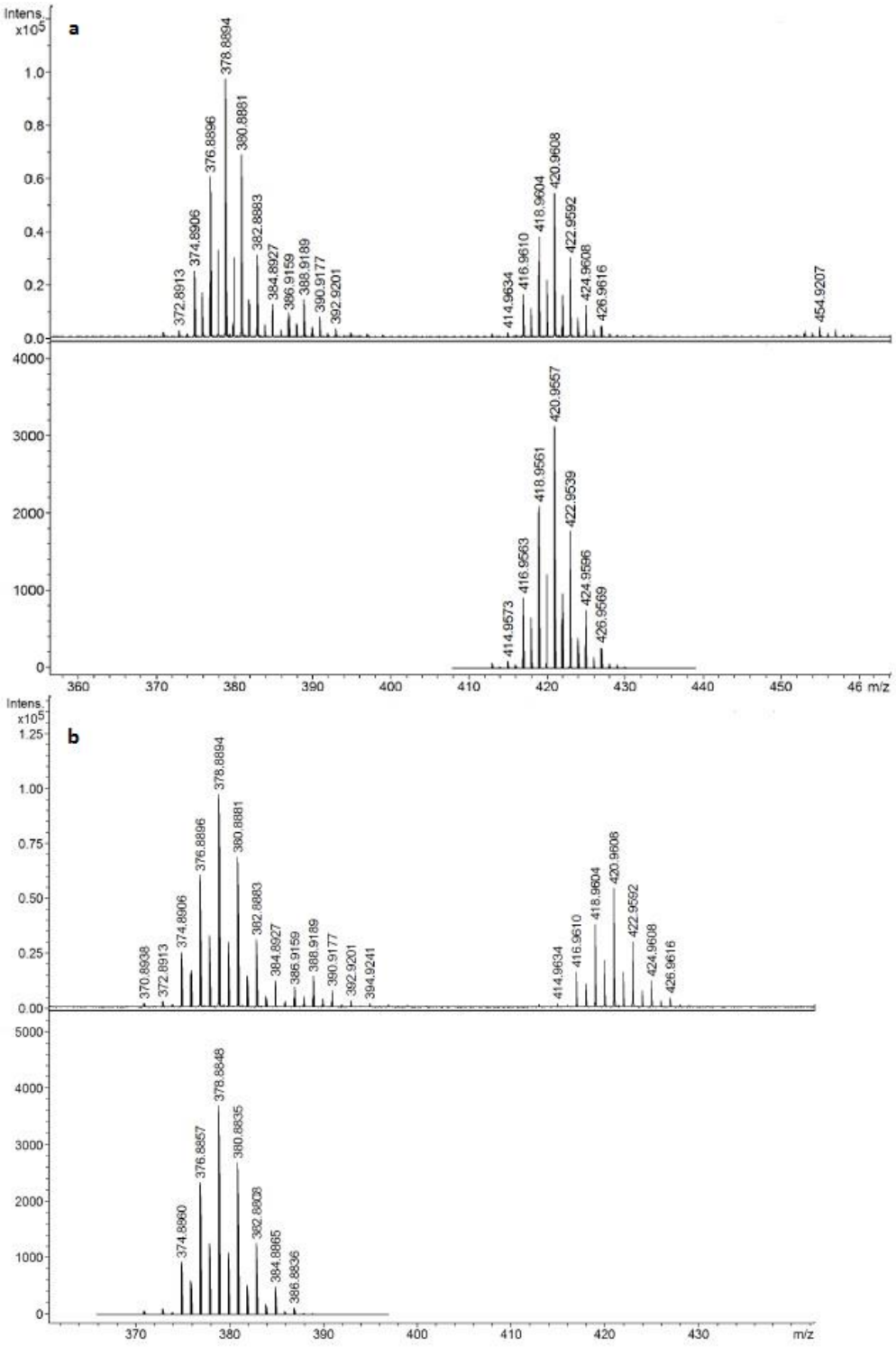

Figure 6-26 The enlargement of the main peaks in the mass spectrum of **6.5**. a) Experimental (top) and simulated isotope patterns for the mass peak of $[SnCl_3(ph)_2]^{1-}$ ion b) Experimental (top) and simulated isotope patterns for the mass peak of $[SnCl_2(ph)_3]^{1-}$ ion

6.3 Conclusion

In this chapter, the syntheses and characterisation of organotin complexes with terpyridine based ligands were discussed. The structure obtained from X-ray diffraction experiments on single crystals did not match with data obtained from NMR and mass spectra for **6.1**. NMR and mass studies are in agreement with having a 7-coordinated tin complex ($[Sn(CH_3)_2Cl_2(pttp)]$) while a crystal structure showed a 6-coordinated organotin complex with a six-coordinated organotin complex as a counter-ion $[Sn(CH_3)_2Cl(pttp)]$-$\cdot 0.5[Sn(CH_3)_2Cl_4].CH_2Cl_2$ (**6.2**).

We considered one of the chloride atoms as a counter-ion since data obtained from coupling constants in **6.3** led us to suggest a 6-coordinate organotin complex is formed. Moreover, the mass peak found in the mass spectrum of **6.3** was consistent with a 6-coordinated tin complex with the formula of $[(EtOH)(CH_3)_2Sn(pttp)]^+$. Presumably, the chloride was replaced by the sample solvent (ethanol).

The pure complex, $[SnCl_2(ph)(ottp)][SnCl_3(ph)_3]$, was not isolated from the reaction between $SnCl_2(ph)_2$ and ottp. However, the a crystal structure of a single crystal is shown in **Figure 6-27**.

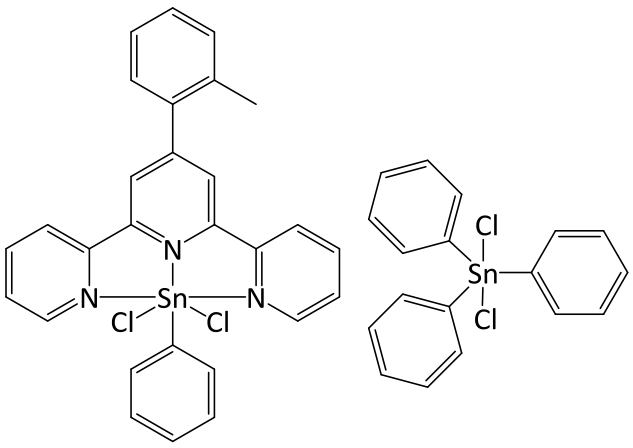

Figure 6-27 structure of **6.4**

We did not obtain a crystal of **6.5** for diffraction but elemental analysis and NMR data are in agreement with having a similar structure to that of **6.4**.

Chapter 7

Experimental

Chapter 7. Experimental

7.1 General Information

All solvents, reagents and starting materials were reagent grade, purchased from standard suppliers and used without purification. Solvents used for syntheses of complexes were analytical grade and used as received. Water was purified in-house by reverse osmosis. All anhydrous solvents used in reactions of moisture sensitive compounds were purified either in-house by passing over a sealed column of activated alumina or distilled from standard drying agents. Electro-thermal Melting Point Apparatus used to record melting points. Microanalyses were performed by Campbell Microanalytical Laboratory at the University of Otago, New Zealand.

Nuclear Magnetic Resonance

^{1}H and ^{13}C NMR spectra were recorded on Varian VNMR 500, or Agilent 400MR with Varian 7600-AS auto-sampler. Spectral chemical shifts were referenced to the residual solvent resonance or, in the case of D_2O, using TPMS or dioxane as an internal reference. 2D COSY, HSQCD, HMBC and DEPT experiments were performed to assign proton and carbon peaks where required, using standard Varian pulse sequence. All samples were prepared in commercially available deuterated solvents.

Mass Spectrometery

Mass spectra were recorded by Dr. Marie Squire and Dr. Amelia Albrett on a BrukerMaXis4G spectrometer. The instrument was operated in a high resolution positive and negative ions electron spray mode. Samples were prepared by dissolving and diluting to the required concentration in appropriate HPLC grade solvents.

Infrared Spectroscopy

Infrared spectra were recorded on a Bruker FTIR spectrometer equipped with Alpha's Platinum ATR single reflection diamond, and samples were placed directly on the diamond under clamp without any preparation (denoted neat). The abbreviations used are: s: strong, vs: very strong, m: medium, w: weak, sh: sharp.

X-Ray Crystallography

X-ray data were collected on an Oxford-Agilent Supernova instrument with a focused microsource Mo Kα [λ = 0.71073 Å] or Cu Kα [λ = 1.54184 Å] radiation and an ATLAS CCD area detector. CrysAlisPro 171.36.28 was used for the data collection and data processing. The crystals were mounted on nylon loop using a perfluorinated polyethylene glycol. The crystal was kept at 120.00(10) K during data collection. All structures were solved using direct methods with SHELXT and refined on *wF*2 using all data by full matrix least square procedures with SHELXL using OLEX-2 for visualisation. Graphical presentation of crystallographic data was prepared using OLEX-2 and the Graphical presentation of lattice and hydrogen bonding through the lattice was prepared using TOPOS.

Synthesis of precursors and ligands

The following compounds were prepared according to the literature procedures: $[Co(en)_2(OH)(OH_2)](ClO_4)_2$[184],[185], $[Co(tren)(OH)(OH_2)](ClO_4)_2$[185], $[PtCl_2(en)]$[186],[187], $[Pt(chda)I_2]$[187], pttp[181], ottp[181].

7.2 Experimental related to chapter 2

7.2.1 Study of reaction of $[Co(en)_2(OH)(OH_2)](ClO_4)_2$ with different diamagnetic metals

Each titration was carried out inside a 5 mm NMR tube, with $[Co(en)_2(OH)(OH_2)](ClO_4)_2$ (0.0860 g, 1 eq) and different molar equivalents of M (M= $Li(NO_3)$, $K(NO_3)$, $Mg(NO_3)_2$, $Ag(NO_3)$, $Zn(ClO_4)_2$, $Zn(NO_3)_2$, $Cd(NO_3)_2$, $K_2[PdCl_4]$ and $K_2[PtCl_4]$) in 1 ml D_2O). TMPS (3-(trimethylsilyl)-1-propanesulfonic acid) was added inside the tube as an internal reference. The ^{13}C-NMR spectrum was taken 30 minutes after addition of the M to cobalt complex solution.

7.2.2 Study of reaction of $[Co(en)_2(OH)(OH_2)](ClO_4)_2$ with different paramagnetic metals

Each titration was carried out inside a NMR tube between $[Co(en)_2(OH)(OH_2)](ClO_4)_2$ (0.0860 g, 1 eq) and different molar equivalents of M (M= $Cu(NO_3)_2$, $Ni(NO_3)_2$ and $Fe(NO_3)_3$ in 1 ml D_2O). 1,4-Dioxane was used as an internal reference to compare the integrations with. The ^{13}C-NMR spectrum was taken 30 minutes after addition of M to cobalt complex.

7.3 Synthesis of chapter 3 compounds

7.3.1 $[(en)_2Co(\mu\text{-}OH)_2Pt(chda)]^{3+}$, 3.2

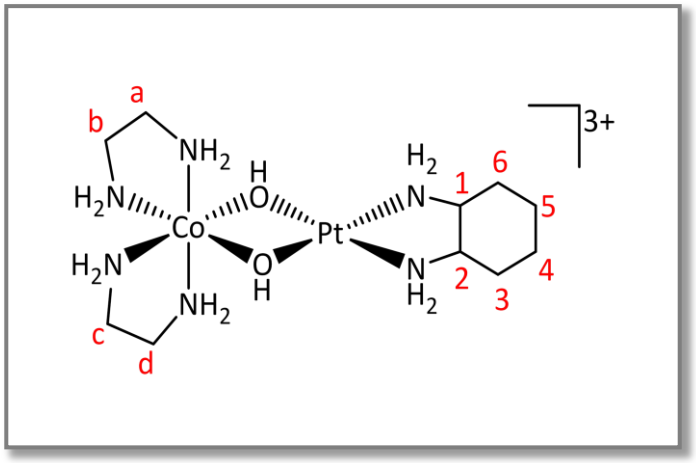

Silver nitrate (0.60 g, 3.54 mmol) was added to $[Pt(chda)I_2]$ (1.00 g, 1.77 mmol) in 5 ml water. The reaction mixture was stirred for 2 days in dark. Silver iodide precipitate was centrifuged and supernatant was added to $[Co(en)_2(OH)(OH_2)](ClO_4)_2$ (0.73 g, 1.77 mmol) in water. The reaction mixture was stirred for 3 days. The reaction mixture was filtered and the filtrate was evaporated to dryness to give reddish oil.

The crude compound was purified using cation exchange chromatography on CM Sephadex. The third band eluted with 0.4 M $NaNO_3$ solution was collected and evaporated to dryness. Most of the salt was removed by few methanolic extractions followed by G10 size exclusion column chromatography. Characterisation was done on red slurry obtained after solvent evaporation. Small amount of salt was remained, which limited the full characterisan. Due to remaining of some amount of salt determination of the yield was not possible.

^{1}H NMR: (400 MHz, D_2O), δ 3.17 (m, 2H, Ha,Hd), 3.03 (m, 2H, Ha',Hd'), 2.62 (m, 2H, Hb,Hc), 2.56 (m, 2H, Hb',Hc'), 3.17 (m, 2H, Ha,Hd), 2.26 (m, 2H, H1,H2), 2.05 (m, 2H, H6',H3'), 1.60 (m, 2H, H4,H5), 1.29 (m, 2H, H3,H6), 1.19 (m, 2H, Ha4',H5') **^{13}C NMR**: (400 MHz, D_2O), δ 62.08 (C1, C2), 44.69, 43.63 (C1, C2, C3, C4), 31.58 (C3, C6), 23.89 (C4, C5). **ESI-MS**: (water): *m/z* $([(en)_2Co(\mu\text{-}OH)_2Pt(chda)\text{-}2H^+]^{1+}$ 523.079

7.3.2 $[(en)_2Co(\mu\text{-}OH)_2Pt(NH_3)]^{3+}$, 3.5

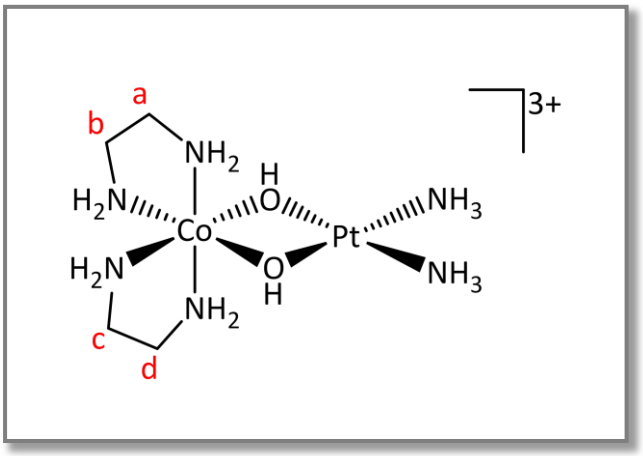

Silver nitrate (1.12 g, 6.66 mmol) was added to cisplatin (1.00 g, 3.33 mmol) in 5 ml water. The reaction mixture was stirred for 2 days in dark. Silver chloride precipitate was centrifuged and the supernatant was added to $[Co(en)_2(OH)(OH_2)]\ (ClO_4)_2$ (1.37 g, 3.33 mmol) in water. The reaction mixture was stirred for 3 days. The reaction mixture was attempted to be isolated by G10 size exclusion column chromatography but it did not work. The characterisation was done on the red slurry obtained after solvent evaporation of the reaction mixture.

^{1}HNMR: (400 MHz, D_2O), δ 3.00, 2.91, 2.60 (m, m, m, 4H, Ha,Hb,Hc,Hd). **^{13}C NMR**: (400 MHz, D_2O), δ 45.79, 43.71 (Ca, Cb, Cc, Cd), **ESI-MS**: (water): *m/z* $\{[(en)_2Co(\mu\text{-}OH)_2Pt(NH_3)_2]^{3+}\text{-}H^+\}^{2+}$ 220.54

7.3.3 $[(tren)Co(\mu\text{-}OH)_2Pt(NH_3)_2]^{3+}$, 3.6

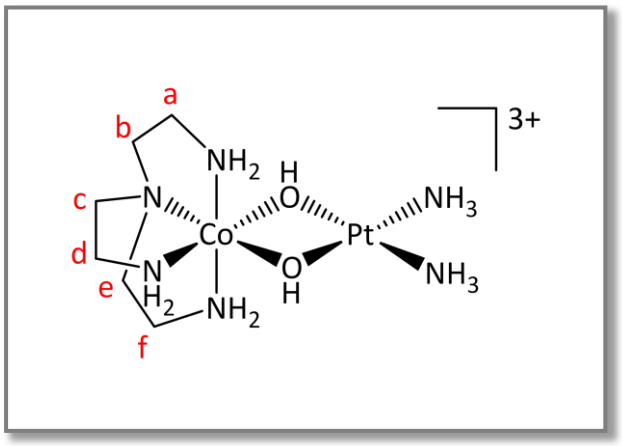

Silver nitrate (1.12 g, 6.66 mmol) was added to cisplatin (1 g, 3.33 mmol) in 5 ml water. The reaction mixture was stirred for 2 days in dark. Silver chloride precipitate was centrifuged and supernatant was added to $[Co(tren)(OH)(OH_2)](ClO_4)_2$ (1.45 g, 3.33 mmol) in water. The reaction mixture was heated for overall 2 hours in a microwave (450 W) with 90 sec intervals.

The reaction mixture was filtered and the filtrate was evaporated to dryness to give reddish oil. The crude material was diluted in minimum amount of water and the mixture separated using size exclusion column chromatography on Sephadex G10 resin (30×1.5). $[(en)_2Co(\mu\text{-}OH)_2Pt(NH_3)](NO_3)_3$ was collected from the second band and $[(en)_2Co(\mu\text{-}OH)_2Pt(NH_3)_2](ClO_4)_3$ was collected from the second band.

^{1}HNMR: (400 MHz, D_2O), δ 3.16, 3.04 (m, m, 4H, Ha,Ha',Hf,Hf'), 2.64, 2.18 (m, d, 4H, Hb,Hb',Hc,Hc'), 2.62 (t, 2H, Hc,Hc'), 2.35 (t, 2H, Hd, Hd'). **^{13}C NMR**: (400 MHz, D_2O), δ 60.40 (Cb,Ce), 58.31 (Cc), 43.99 (Ca, Cf), 43.02 (Cd). **ESI-MS**: (water): *m/z* $[(tren)Co(\mu\text{-}OH)_2Pt(NH_3)_2]^{3+}$ 156.03, $[(tren)Co(\mu\text{-}OH)_2Pt(NH_3)_2\text{-}H^+]^{2+}$ 233.54, $[(tren)Co(\mu\text{-}OH)_2Pt(NH_3)_2\text{-}2H^+]^+$ 466.09, $\{[(tren)Co(\mu\text{-}OH)_2Pt(NH_3)_2\text{-}H^+](NO_3)\}^+$ 529.08, $\{[(tren)Co(\mu\text{-}OH)_2Pt(NH_3)_2\text{-}H^+](ClO_4)\}^+$ 667.00

7.3.4 $[(tren)Co(\mu\text{-}OH)_2Pt(chda)]^{3+}$, 3.7

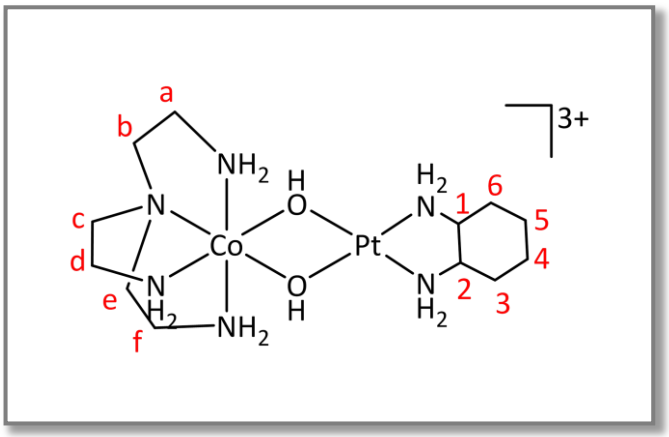

Silver nitrate (0.60 g, 3.54 mmol) was added to $[Pt(chda)I_2]$ (1.00 g, 1.77 mmol) in 5 ml water. The reaction mixture was stirred for 2 days in dark. Silver iodide precipitate was centrifuged and supernatant was added to $[Co(tren)(OH)(OH_2)](ClO_4)_2$ (0.77 g, 1.77 mmol) in water. The reaction mixture was heated for overall 2 hours in a microwave (450 W) with 90 sec intervals.

The crude compound was purified using cation exchange chromatography on CM Sephadex. The third band eluted with 0.4 M $NaNO_3$ solution was collected and evaporated to dryness.

Characterisation was done after removing the salt by methanolic extractions followed by G10 size exclusion column chromatography.

^{1}H NMR: (400 MHz, D_2O), δ 3.60, 3.51 (m, m, 4H, Ha,Ha',Hf,Hf'), 3.09, 2.61 (m, d, 4H, Hb,Hb',Hc,Hc'), 3.05 (t, 2H, Hc,Hc'), 2.80 (t, 2H, Hd,Hd'), 2.23 (m, 2H, H1,H2), 2.00 (m, 2H, H3',H6'), 1.55 (m, 2H, H4,H5), 1.24 (m, 2H, H3,H6), 1.12(m, 2H, H2',H5'). **^{13}C NMR**: (400 MHz, D_2O), δ 62.22 (C1, C2), 62.97 (Cb,Ce), 59.77 (Cc), 44.83 (Ca, Cf), 44.27 (Cd), 31.69 (C6, C3), 24.02 (C4, C5). **ESI-MS**: (water): *m/z* $[(tren)Co(\mu\text{-}OH)_2Pt(chda)\text{-}H^+)]^{2+}$ 273.08.

7.4 Synthesis of chapter 4 compounds

7.4.1 $[Co(nta)(OH_2)_2]$, 4.1

Cobalt(II) chloride hexahydrate (5 g, 38.5 mmol) was added to a solution of nitrilotriacetic acid (nta) (4.7 g, 38.5 mmol) in potassium bicarbonate (0.2 M, 25 mL). The reaction mixture was heated at 70˚ C for an hour. Hydrogen peroxide (50%, 1 mL) was added and the reaction was stirred for half an hour at 70˚ C. The mixture was left in the fridge overnight. The resulting precipitate was then filtered and washed with ethanol and diethyl ether. The product was obtained by recrystallisation of the powder from hot water. Yield: 22%.

^{1}H NMR: (500 MHz; solvent D_2O) δ 4.13 d(AB), 4.36 d(AB)

^{13}C NMR (500 MHz, DMSO-d^6) δ 178.34, 168.35, 66.92, 62.69.

7.4.2 [(nta)Co(OH)$_2$Pt(chda)], 4.7

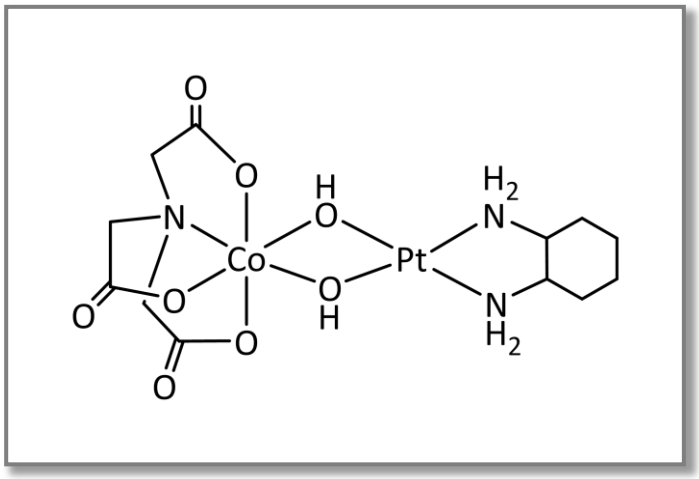

[Pt(chda)I$_2$] (597 mg, 1.06 mmol) was treated with silver nitrate (360 mg, 2.12 mmol) in 2 mL of water for two days. The silver iodide precipitate was centrifuged and the supernatant was separated. The pH of the supernatant was adjusted to 5 by addition of NaOH solution. [Co(nta)(OH$_2$)$_2$] (300 mg, 1.06 mmol) was suspended in 4 mL of water and the pH was adjusted to 5.15 by addition of NaOH solution. The platinum supernatant was added to cobalt solution. The reaction mixture was stirred for 18 h. The precipitate was collected and washed with ethanol and diethyl ether. Yield: 550 mg 90%, M.p: Stable over 250 °C

Elemental Analysis: Found C 23.28, H 4.45, N 6.58, Calcd. ([Co(nta)(OH)$_2$Pt(NH$_3$)$_2$]·2H$_2$O) (%): C 23.00, H 4.19, N 6.71. **IR:** υ_{max} 3401(w), 3196(w), 2940(w), 1621(vs), 1372(s), 951(m), 926(m), 490(m) cm^{-1}.

7.4.3 [Co(nta)(OH)$_2$Pt(en)], 4.12

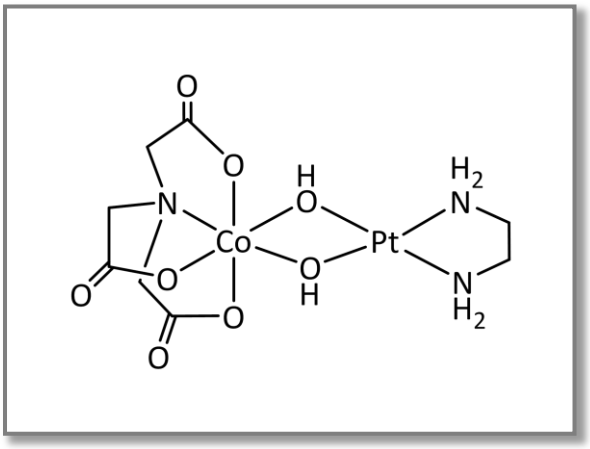

Dichlorido(ethane-1,2-diamine)platinum(II) ([PtCl$_2$(en)]) (345 mg, 1.06 mmol) was treated with silver nitrate (359 mg, 2.12 mmol) in 2 ml of water for two days. The silver chloride precipitate was centrifuged and the supernatant was separated. The pH of the supernatant was adjusted to 5 by addition of

NaOH solution. [Co(nta)$(OH_2)_2$] (300 mg, 1.06 mmol) was suspended in 4 ml of water and the pH was adjusted to 5.15 by addition of NaOH solution. The platinum supernatant was added to cobalt solution. The reaction mixture was stirred for 18 h. The precipitate was collected and washed with ethanol and diethyl ether. Yield: 473 mg 85%, M.p: Stable over 250 °C

Elemental analysis: Found C 16.87, H 3.28, N 7.06, Calcd. ([Co(nta)$(OH)_2$Pt(en)]**.**$2H_2O$) (%): C 16.78, H 3.52, N 7.34. **IR:** υ_{max} 3229(w), 3095(w), 2985(w), 1614(vs), 1446(w), 1364(s), 1217(m), 928(w), (896(w), 463(sh), 450(sh) cm^{-1}.

7.4.4 [(nta)Co$(OH)_2$Pt$(NH_3)_2$], 4.16

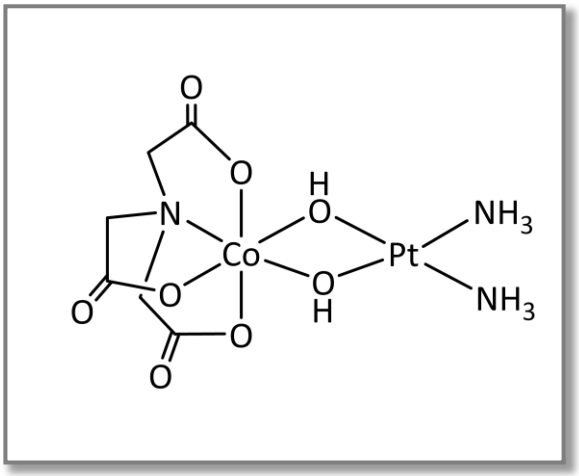

Cisplatin (318 mg, 1.06 mmol) was treated with silver nitrate (350 mg, 2.12 mmol) in 2 ml of water for two days. The silver chloride precipitate was centrifuged and the supernatant was separated. The pH of the supernatant was adjusted to 5 by addition of NaOH solution. [Co(nta)$(OH_2)_2$] (300 mg, 1.06 mmol) was suspended in 4 mL of water and the pH was adjusted to 5.15 using NaOH solution. The platinum supernatant was added to the cobalt solution. The reaction mixture was stirred for 18 h. The precipitate was collected and washed with ethanol and diethyl ether. Yield: 480 mg 93%, M.p: Stable over 250 °C

IR: υ_{max} 3279(m), 1621(vs), 1367(m), 1284(w), 928(w), 921(w), 490(m) cm^{-1}.

Elemental analysis: Found C 13.67, H 3.32, N 7.94, Calcd. ([Co(nta)$(OH)_2$Pt$(NH_3)_2$]**.**$2H_2O$) (%): C 13.19, H 3.32, N 7.69.

7.4.5 NMR study of [(nta)Co(OH)$_2$Pt(L)] complexes

The NMR samples of complexes **4.7**, **4.12** and **4.16** were prepared in d^6 DMSO. The complexes were almost non-soluble in DMSO in room temperature. The temperature of the NMR machine was increased to 80 °C to increase the solubility of the samples. Results obtained from NMR data showed the solubility of the complexes is due to a reaction with DMSO. The NMR results of these complexes are fully discussed in chapter 4.

7.5 Synthesis of chapter 6 compounds

7.5.1 [Sn(CH$_3$)$_2$Cl$_2$(pttp)], 6.1

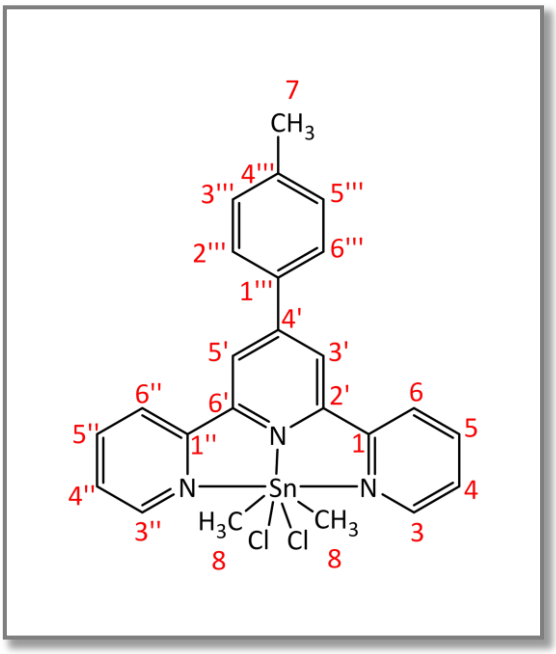

Dimethyltin dichloride (114 mg, 0.52 mmol) was added to a 100 mL round bottom flask containing pttp ligand (168 mg, 0.52 mmol) in 30 mL dry DCM while flushing under N_2. The reaction mixture was heated at reflux for 6 h. The solvent was removed by rotary evaporation. The compound was recrystallised from methanol. The crystals were filtered and washed with diethyl ether. Yield: 240 mg, 78%. M.p: 161 °C

^{1}H NMR (400 MHz; solvent d^6 DMSO): δ 8.75 (2H, d, H6, H6’’), 8.67 (2H, s, H3’, H5’), 8.65 (2H, d, H3, H3’’), 8.02 (2H, t, H5, H5’’), 7.80 (2H, d, H2’’’, H6’’’), 7.51 (2H, t, H4, H4’’), 7.38 (2H, d, H3’’’, H5’’’), 2.39 (3H, s, H7), 1.04 (6H, s, H8). **^{13}C NMR** (400 MHz; solvent d^6 DMSO):

δ 155.63 (2C, C2', C6'), 155.98 (2C, C1, C1''), 149.34 (3C, C3, C3'', C4'), 139.22 (1C, C4'''), 137.46 (2C, C5, C5''), 134.53 (1C, C1'''), 130.01 (2C, C3''', C5'''), 128.12 (2C, C2''', C6'''), 124.51 (2C, C4, C4''), 120.93 (2C, C6, C6''), 117.63 (2C, C3', C5'), 22.74 (1C, C7), 20.84 (C, C8). **ESI-Ms** (MeOH): *m/z* $[Cl_2(CH_3)_2Sn(pttp)\text{-}H^+]^-$ 541.97. **Elemental analysis:** Found (%) C 53.30, H 4.30, N 7.50, Calcd. $[Sn(CH_3)_2Cl_2(pttp)]$ (%): C 53.08, H 4.27, N 7.74. I**R:** υ_{max} 3056(w), 2915(w), 1601(m), 1582(m), 1465(m), 1427(m), 1252(w), 1194(w), 1017(m) 889(w), 788 (vs), 742(m), 725(m), 621.69(m) cm^{-1}.

7.5.2 $[Sn(CH_3)_2Cl(ottp)]Cl$, 6.3

Dimethyltin dichloride (114 mg, 0.52 mmol) was added to a 100 mL round bottom flask containg ottp ligand (168 mg, 0.52 mmol) in 30 mL dry DCM while flushing under N_2. The reaction mixture was heated at reflux for 6 h. The solvent was removed by rotary evaporation. The compound was recrystallised from methanol. The crystals were filtered and washed with diethyl ether.

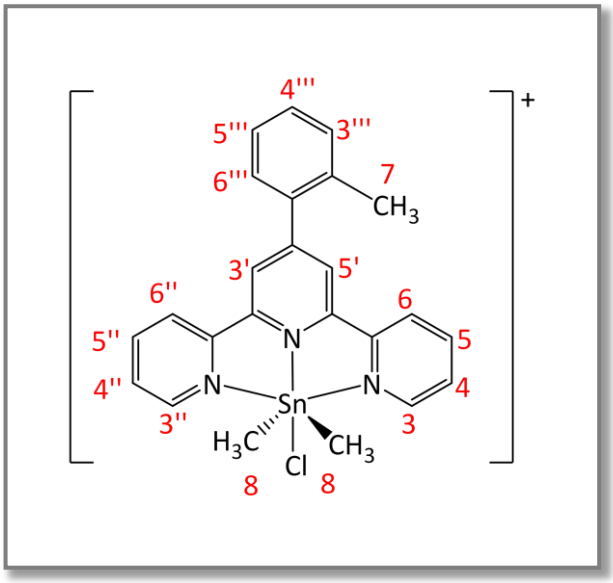

Yield: 190 mg, 70%. M.p: 139 °C

^{1}H NMR (400 MHz; solvent d^6 DMSO): δ 9.04 (2H, d, H3, H3''), 8.70 (2H, d, H6', H6'), 8.52 (2H, s, H3', H5'), 8.11 (2H, t, H5, H5''), 7.57 (2H, t, H4, H4''), 7.44-7.32 (4H, m, H3''', H4''', H5''', H6'''), 2.42 (3H, s, H7), 1.19 (6H, s, H8). **^{13}C NMR** (400 MHz; solvent d^6 DMSO): δ 154.72 (1C, C4'), 152.31 (2C, C2', C6'), 152.08 (2C, C1, C1''), 148.57 (2C, C3, C3''), 139.55 (2C,

C5, C4''), 137.95 (1C, C1'''), 135.09 (1C, C2'''), 130.87 (1C, C3'''), 129.46 (1C, C6'''), 129.23 (1C, C5'''), 126.37 (1C, C4'''), 125.64 (2C, C4, C''), 123.30 (2C, C3'. C5'), 122.97 (2C, C6, C6''), 20.47 (1C, C7), 17.87 (1C, C8). **ESI-Ms** (EtOH): *m/z* $[Sn(CH_3)_2(OEt)(ottp)]^+$ 541.97. **Elemental analysis:** Found (%) C 53.30, H 4.37, N 7.56, Calcd. $[Sn(CH_3)_2Cl(ottp)]Cl$ (%): C 53.08, H 4.27, N 7.74. **IR:** υ_{max} 3007(w), 2918(w), 1598(m), 1583(m), 1567(m), 1540(m), 1462(m), 1414(m), 1390(m), 1304(m), 1248(w), 1163(w), 1017(m), 990(w), 893(w), 787(vs), 770(vs), 741(vs), 728(vs), 688(sh), 657(sh), 645(m), 626(m) cm^{-1}.

7.5.3 $[Sn(ph)Cl_2(pttp)][Sn(ph)_3Cl_2]$, 6.5

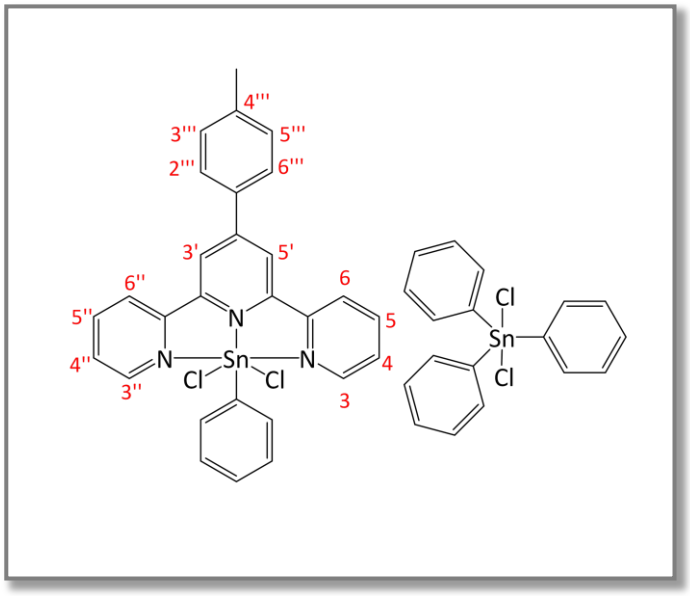

Diphenyltin dichloride (233 mg, 0.72 mmol) was added to a 100 mL round bottom flask containg pttp ligand (248 mg, 0.72 mmol) in 30 mL dry DCM while flushing under N_2. The reaction mixture was heated at reflux for 12 h. The solvent was removed by rotary evaporation. The compound was recrystallised from methanol. The crystals were filtered and washed with diethyl ether. Yield: 310 mg, 42%, M. p: 208 °C

^{1}H NMR (400 MHz; solvent d^6 DMSO): δ 8.77 (2H, d, H3, H3''), 8.70 (2H, s, H3', H5'), 8.67 (2H, d, H6, H6''), 8.06 (1H, d), 8.03 (2H, H5, H5'') 7.92 (6H, d), 7.83 (2H, d, H2''', H6'''), 7.77

(1H,d), 7.53 (2H, t, H4, H4’’), 7.40 (2H, d, H3’’’, H5’’’) 7.37-7.28 (12H, m) 2.40 (3H, s, H7), 1.19 **^{13}C NMR** (400 MHz; solvent d^{6} DMSO): δ 155.65 (3C, C2’, C6’, C_{ph}), 154.99 (3C, C1’, C1’’, C_{ph}), 149.34 (3C, C3, C3’’, C4), 139.21 (1C, C4’’’), 137.45 (C_{ph}), 134.68 (2C, C5, C5’’), 130.00 (2C, C3’’’, C5’’’), 127.77 (C_{ph}), 127.28 (C_{ph}), 126.72 (2C, C2’’’, C6’’’), 124.50 (2C, C4, C4’’), 120.91 (2C, C6’. C6’’), 117.63.97 (2C, C3’, C5’), 20.82 (1C, C7). **ESI-Ms** (MeOH): *m/z* $[SnCl_3(ph)_2]^-$ 420.96, $[SnCl_2(ph)_3]^-$ 378.88. **Elemental analysis:** Found C 54.79, H 3.75, N 4.24, Calcd. $[SnCl_2(ph)(pttp)][SnCl_2(ph)_3]$ (%): C 54.65, H 3.69, N 4.16. **IR:** υ_{max} 3048(w), 1599(vs), 1570(m), 1543(m), 1480(sh), 1430(sh), 1405(m), 1367(w), 1306(w), 1256(m), 1018(sh), 996(m), 891(w), 883(w), 845(sh), 789(vs), 770(vs), 739(sh), 729(vs), 694(vs), 658(m), 639(m), 623(m) cm^{-1}.

Appendices

Appendix 1

Two sets of data: A and B
A $\{A_1, A_2, A_3 \ldots A_{nA}\}$
B $\{B_1, B_2, B_3 \ldots B_{nB}\}$

Standard error:

$$\mathcal{E}_A = \frac{S_A}{\sqrt{n_A}} = \sqrt{\frac{\sum_{i=1}^{nA}(A_i - \bar{A})^2}{n_A^2}}$$

$$\mathcal{E}_B = \frac{S_B}{\sqrt{n_B}} = \sqrt{\frac{\sum_{i=1}^{nB}(B_i - \bar{B})^2}{n_B^2}}$$

Central limit theorem:
67% chance that true mean is within $\pm\mathcal{E}_A$ ✓
95% chance that true mean is within $\pm 2\mathcal{E}_A$
99.5% chance that true mean is within $\pm 3\mathcal{E}_A$

Reported value is:

$$< A > = \bar{A} \pm \mathcal{E}_A$$
$$< B > = \bar{B} \pm \mathcal{E}_B$$

Sum:

$$< S > = < A > \pm < B > = \bar{S} \pm \mathcal{E}_S$$
$$\bar{S} = \bar{A} \pm \bar{B}$$
$$\mathcal{E}_S = \sqrt{(\mathcal{E}_A)^2 + (\mathcal{E}_B)^2}$$

Product:

$$< P > = < A > \times < B > = \bar{P} \pm \mathcal{E}_P$$
$$\bar{P} = \bar{A} \times \bar{B}$$

$$\mathcal{E}_P = \bar{P}\sqrt{(\frac{\mathcal{E}_A}{A})^2 + (\frac{\mathcal{E}_B}{B})^2}$$

Ratio:

$$< R > = \frac{< A >}{< B >} = \bar{R} \pm \mathcal{E}_R$$
$$R = \frac{\bar{A}}{\bar{B}}$$
$$\mathcal{E}_R = \bar{R}\sqrt{(\frac{\mathcal{E}_A}{A})^2 + (\frac{\mathcal{E}_B}{B})^2}$$

Appendix 2. Crystallography Tables

A suitable crystal was selected and mounted on a SuperNova, Dual, Cu/Mo at zero, Atlas diffractometer. The crystal was kept at 120.01(10) K during data collection. Using Olex2, the structure was solved with the shleXT structure solution program using Direct Methods refined with the ShelXL refinement packing g Least Squares minimisation.

Crystal data and structure refinement for crystals in chapter 3			
Identification code	**3.3**	**3.4**	**3.8**
Empirical formula	$C_5H_{16}CoN_5O_6$	$C_{16}H_{44}CoN_{11}O_{14.9}Pt_2$	$C_8H_{22}CoN_8O_9$
Formula weight	301.16	1078.05	433.26
Temperature/K	120.00(10)	120.01(10)	120.00(10)
Crystal system	monoclinic	monoclinic	orthorhombic
Space group	$P2_1/c$	$P2_1/c$	Pnma
a/Å	11.3918(7)	15.6651(5)	25.6797(13)
b/Å	8.4058(5)	11.4383(3)	7.2533(3)
c/Å	23.4969(12)	21.0628(6)	7.8776(5)
α/°	90	90	90
β/°	96.826(5)	106.022(3)	90
γ/°	90	90	90
Volume/$Å^3$	2234.0(2)	3627.45(19)	1467.30(13)
Z	8	4	4
$\rho_{calc}g/cm^3$	1.791	1.974	1.961
μ/mm^{-1}	12.372	18.316	9.883
F(000)	1248.0	2077.0	900.0
Crystal size/mm^3	0.094 × 0.0143 × 0.0077	0.1152 × 0.0379 × 0.0137	0.1552 × 0.0302 × 0.0117
Radiation	CuKα (λ = 1.54184)	CuKα (λ = 1.54184)	CuKα (λ = 1.54184)
2Θ range for data collection/°	7.578 to 153.556	5.87 to 152.884	6.884 to 176.988
Index ranges	-11 ≤ h ≤ 13, -10 ≤ k ≤ 10, -29 ≤ l ≤ 29	-18 ≤ h ≤ 19, -14 ≤ k ≤ 14, -26 ≤ l ≤ 20	-32 ≤ h ≤ 27, -9 ≤ k ≤ 8, -9 ≤ l ≤ 4
Reflections collected	10974	19930	4109
Independent reflections	4525 [R_{int} = 0.0941, R_{sigma} = 0.1164]	7528 [R_{int} = 0.0656, R_{sigma} = 0.0721]	1581 [R_{int} = 0.0569, R_{sigma} = 0.0595]
Data/restraints/parameters	4525/0/307	7528/0/440	1581/0/136
Goodness-of-fit on F^2	1.220	1.161	1.076
Final R indexes [I>=2σ (I)]	R_1 = 0.0657, wR_2 = 0.1414	R_1 = 0.0668, wR_2 = 0.1751	R_1 = 0.0881, wR_2 = 0.2457
Final R indexes [all data]	R_1 = 0.1078, wR_2 = 0.1591	R_1 = 0.0847, wR_2 = 0.1938	R_1 = 0.0995, wR_2 = 0.2597
Largest diff. peak/hole / e $Å^{-3}$	0.77/-0.56	2.48/-1.84	0.81/-1.04

Crystal data and structure refinement for crystals in chapter 4			
Identification code	**4.2**	**4.6**	**4.20**
Empirical formula	$C_{12}H_{28}Co_2K_2N_2O_{27}$	$C_{12}H_{29.8}Co_{2.5}N_2O_{21.4}$	$C_5H_{15}CoNO_{10}P$
Formula weight	828.42	691.90	339.08
Temperature/K	120.01(10)	120.01(10)	120.01(10)
Crystal system	monoclinic	triclinic	monoclinic
Space group	$P2_1/c$	P-1	$P2_1/c$
a/Å	12.6044(13)	10.6545(9)	6.2817(6)
b/Å	9.2309(7)	11.7338(10)	28.711(2)
c/Å	13.0780(11)	11.7529(9)	6.3686(10)
α/°	90	72.100(7)	90
β/°	110.233(11)	69.880(7)	100.893(11)
γ/°	90	63.298(9)	90
Volume/Å^3	1427.7(2)	1211.9(2)	1127.9(2)
Z	2	2	4
ρ_{calc}g/cm^3	1.927	1.896	1.997
μ/mm^{-1}	12.783	14.267	1.713
F(000)	844.0	709.0	696.0
Crystal size/mm^3	0.148 × 0.0978 × 0.0139	0.1149 × 0.0601 × 0.0244	0.1113 × 0.0518 × 0.0091
Radiation	CuKα (λ = 1.54184)	CuKα (λ = 1.54184)	MoKα (λ = 0.71073)
2Θ range for data collection/°	7.474 to 152.726	8.148 to 146.766	5.676 to 61.746
Index ranges	-15 ≤ h ≤ 15, -11 ≤ k ≤ 10, -9 ≤ l ≤ 16	-13 ≤ h ≤ 13, -11 ≤ k ≤ 14, -9 ≤ l ≤ 14	-9 ≤ h ≤ 5, -38 ≤ k ≤ 11, -8 ≤ l ≤ 7
Reflections collected	6650	7713	3587
Independent reflections	2909 [R_{int} = 0.0651, R_{sigma} = 0.0759]	4615 [R_{int} = 0.0441, R_{sigma} = 0.0580]	2512 [R_{int} = 0.0918, R_{sigma} = 0.1274]
Data/restraints/parameters	2909/0/232	4615/28/442	2512/10/173
Goodness-of-fit on F^2	1.371	1.042	1.131
Final R indexes [I>=2σ (I)]	R_1 = 0.1386, wR_2 = 0.3448	R_1 = 0.0384, wR_2 = 0.0993	R_1 = 0.0910, wR_2 = 0.1905
Final R indexes [all data]	R_1 = 0.1674, wR_2 = 0.3804	R_1 = 0.0492, wR_2 = 0.1092	R_1 = 0.1317, wR_2 = 0.2157
Largest diff. peak/hole / e Å^{-3}	2.69/-1.25	0.61/-0.65	0.84/-1.16

Crystal data and structure refinement for crystals in chapter 6		
Identification code	**6.2**	**6.4**
Empirical formula	$C_{26}H_{28}Cl_5N_3Sn_{1.5}$	$C_{44}H_{36}Cl_{4.33}N_3Sn_2$
Formula weight	737.80	997.12
Temperature/K	120.01(10)	120.00(10)
Crystal system	triclinic	orthorhombic
Space group	P-1	$P2_12_12_1$
a/Å	9.3940(7)	9.0744(2)
b/Å	12.1283(9)	15.8444(3)
c/Å	14.1617(11)	28.4493(7)
α/°	70.950(7)	90.0
β/°	81.926(6)	90.0
γ/°	69.444(7)	90.0
Volume/$Å^3$	1427.4(2)	4089.62(17)
Z	2	4
$\rho_{calc}g/cm^3$	1.717	1.619
μ/mm^{-1}	14.989	12.589
F(000)	730.0	1977.0
Crystal size/mm^3	0.102 × 0.0505 × 0.0152	0.2275 × 0.1118 × 0.0858
Radiation	CuKα (λ = 1.54184)	Cu Kα (λ = 1.54184)
2Θ range for data collection/°	6.606 to 153.62	6.214 to 153.646
Index ranges	-11 ≤ h ≤ 11, -15 ≤ k ≤ 15, -17 ≤ l ≤ 13	-11 ≤ h ≤ 11, -14 ≤ k ≤ 19, -32 ≤ l ≤ 35
Reflections collected	13173	39629
Independent reflections	5925 [R_{int} = 0.0649, R_{sigma} = 0.0644]	[R_{int} = 0.0661, R_{sigma} = 0.0451]
Data/restraints/parameters	5925/1/326	8536/7/ 548
Goodness-of-fit on F^2	1.044	1.041
Final R indexes [I>=2σ (I)]	R_1 = 0.0552, wR_2 = 0.1463	R_1 = 0.0416, wR_2 = 0.1078
Final R indexes [all data]	R_1 = 0.0609, wR_2 = 0.1568	R_1 = 0.0463, wR_2 = 0.1125
Largest diff. peak/hole / e $Å^{-3}$	1.91/-1.57	1.34/-1.60

References

[1] Mortality 2012 online tables. . Wellington: Ministry of Health. **2015**.

[2] T. H. M., T. H. M. What is cancer? What forms does it take? How does it kill? Science. **1974**, *183*, 1068.

[3] Cancer Research UK: What is cancer, http://www.cancerresearchuk.org/about-cancer/what-is-cancer.

[4] National Cancer Institute: Treatment for cancer, http://www.cancer.gov/about-cancer/treatment.

[5] BREASTCANCER.ORG: How chemothrapy works, http://www.breastcancer.org/treatment/chemotherapy/how_it_works.

[6] Y. Shao, X. Lu, K. Li, Z. Zhao, X. Shi, D. Jin, et al. Theoretical insight into photo-induced intramolecular electron transfer in heterodinuclear Ru(II)-Co(III) complexes. Mater Chem Phys. **2015**, *162*, 6.

[7] S. Doldi. Michele Peyrone and his salt. Chimica e l'Industria (Milan). **1995**, *77*, 989.

[8] B. Rosenberg, C. L. Van, T. Krigas. Inhibition of cell division in Escherichia coli by electrolysis products from a platinum electrode. Nature (London, United Kingdom). **1965**, *205*, 698.

[9] D. J. Higby, H. J. Wallace, Jr., J. F. Holland. Cis-diamminedichloroplatinum (NSC-119875): a phase I study. Cancer chemotherapy reports Part 1. **1973**, *57*, 459.

[10] M. Galanski. Recent developments in the field of anticancer platinum complexes. Recent Pat Anticancer Drug Discov. **2006**, *1*, 285.

[11] D. Lebwohl, R. Canetta. Clinical development of platinum complexes in cancer therapy: an historical perspective and an update. Eur J Cancer. **1998**, *34*, 1522.

[12] R. M. Roat-malone. in *Bioinorganic Chemistry* **2002**, pp. 287-289 (Wiley-VCH: New Jersey).

[13] E. Cvitkovic, J. Spaulding, V. Bethune, J. Martin, W. F. Whitmore. Improvement of cis-dichlorodiammineplatinum (NSC 119875): therapeutic index in an animal model. Cancer (Philadelphia). **1977**, *39*, 1357.

[14] D. M. Hayes, E. Cvitkovic, R. B. Golbey, E. Scheiner, L. Helson, I. H. Krakoff. High dose cis-platinumdiamminedichloride. Amelioration of renal toxicity by mannitol diuresis. Cancer (Philadelphia). **1977**, *39*, 1372.

[15] D. D. Von Hoff, R. Schilsky, C. M. Reichert, R. L. Reddick, M. Rozencweig, R. C. Young, et al. Toxic effects of cis-dichlorodiammineplatinum(II) in man. Cancer Treat Rep. **1979**, *63*, 1527.

[16] E. I. Montero, S. Diaz, A. M. Gonzalez-Vadillo, J. M. Perez, C. Alonso, C. Navarro-Ranninger. Preparation and Characterization of Novel trans-[$PtCl_2$(amine)(isopropylamine)] Compounds: Cytotoxic Activity and Apoptosis Induction in ras-Transformed Cells. J Med Chem. **1999**, *42*, 4264.

[17] E. Pantoja, A. Alvarez-Valdes, J. M. Perez, C. Navarro-Ranninger, J. Reedijk. Synthesis and characterization of new cis-[PtCl2(isopropylamine)(amine')] compounds: cytotoxic activity and reactions with 5'-GMP compared with their trans-platinum isomers. Inorg Chim Acta. **2002**, *339*, 525.

[18] L. Kelland. The resurgence of platinum-based cancer chemotherapy. Nature Reviews Cancer. **2007**, *7*, 573.

[19] M. A. Jakupec, M. Galanski, B. K. Keppler. Tumour-inhibiting platinum complexes-state of the art and future perspectives. Rev Physiol, Biochem Pharmacol. **2003**, *146*, 1.

[20] M. J. Cleare, J. D. Hoeschele. **1972,** pp. 193-5 (Univ. Park Press).

[21] A. Eva, K. C. Robbins, P. R. Andersen, A. Srinivasan, S. R. Tronick, E. P. Reddy, et al. Cellular genes analogous to retroviral onc genes are transcribed in human tumor cells. Nature (London). **1982**, *295*, 116.

[22] A. H. Calvert, S. J. Harland, D. R. Newell, Z. H. Siddik, A. C. Jones, T. J. McElwain, et al. Early clinical studies with cis-diammine-1,1-cyclobutane dicarboxylate platinum II. Cancer Chemother Pharmacol. **1982**, *9*, 140.

[23] S. G. Allan, J. F. Smyth. Small intestinal mucosal toxicity of cis-platinum - comparison of toxicity with platinum analogs and dexamethasone. Br J Cancer. **1986**, *53*, 355.

[24] Y. Sasaki, T. Amano, M. Morita, T. Shinkai, K. Eguchi, T. Tamura, et al. Phase I study and pharmacological analysis of cis-diammine(glycolato)platinum (254-S; NSC 375101D) administered by 5-day continuous intravenous infusion. Cancer Res. **1991**, *51*, 1472.

[25] J. Lokich, N. Anderson. Carboplatin versus cisplatin in solid tumors: an analysis of the literature. Annals of oncology : official journal of the European Society for Medical Oncology / ESMO. **1998**, *9*, 13.

[26] R. J. Pelley. Oxaliplatin: a new agent for colorectal cancer. Current oncology reports. **2001**, *3*, 147.

[27] S. Mani, M. A. Graham, D. B. Bregman, P. Ivy, S. G. Chaney. Oxaliplatin: A review of evolving concepts. Cancer Investigation. **2002**, *20*, 246.

[28] J. L. Misset, H. Bleiberg, W. Sutherland, M. Bekradda, E. Cvitkovic. Oxaliplatin clinical activity: a review. Critical reviews in oncology/hematology. **2000**, *35*, 75.

[29] S. Dilruba, G. V. Kalayda. Platinum-based drugs: past, present and future. Cancer Chemother Pharmacol. **2016**, Ahead of Print.

[30] T. C. Johnstone, K. Suntharalingam, S. J. Lippard. The Next Generation of Platinum Drugs: Targeted Pt(II) Agents, Nanoparticle Delivery, and Pt(IV) Prodrugs. Chem Rev (Washington, DC, U S). **2016**, *116*, 3436.

[31] T. C. Johnstone, K. Suntharalingam, S. J. Lippard. Third row transition metals for the treatment of cancer. Philos Trans R Soc, A. **2015**, *373*, 1.

[32] L. Galluzzi, L. Senovilla, I. Vitale, J. Michels, I. Martins, O. Kepp, et al. Molecular mechanisms of cisplatin resistance. Oncogene. **2012**, *31*, 1869.

[33] D. P. Gately, S. B. Howell. Cellular accumulation of the anticancer agent cisplatin: A review. British Journal of Cancer. **1993**, *67*, 1171.

[34] G. V. Kalayda, C. H. Wagner, U. Jaehde. Relevance of copper transporter 1 for cisplatin resistance in human ovarian carcinoma cells. J Inorg Biochem. **2012**, *116*, 1.

[35] R. Safaei. Role of copper transporters in the uptake and efflux of platinum containing drugs. Cancer Lett (Amsterdam, Neth). **2006**, *234*, 34.

[36] G. Samimi, R. Safaei, K. Katano, A. K. Holzer, M. Rochdi, M. Tomioka, et al. Increased expression of the copper efflux transporter ATP7A mediates resistance to cisplatin, carboplatin, and oxaliplatin in ovarian cancer cells. Clin Cancer Res. **2004**, *10*, 4661.

[37] D. P. Gately, S. B. Howell. Cellular accumulation of the anticancer agent cisplatin: A review. Br J Cancer. **1993**, *67*, 1171.

[38] S. B. Howell, R. Safaei, C. A. Larson, M. J. Sailor. Copper transporters and the cellular pharmacology of the platinum-containing cancer drugs. Mol Pharmacol. **2010**, *77*, 887.

[39] P. Abada, S. B. Howell. Regulation of cisplatin cytotoxicity by Cu influx transporters. Met-Based Drugs. **2010**, 317581.

[40] S. Zhang, K. S. Lovejoy, J. E. Shima, L. L. Lagpacan, Y. Shu, A. Lapuk, et al. Organic Cation Transporters Are Determinants of Oxaliplatin Cytotoxicity. Cancer Res. **2006**, *66*, 8847.

[41] J. W. Reishus, D. S. Martin, Jr. cis-Dichlorodiammineplatinum (II). Acid hydrolysis and isotopic exchange of the chloride ligands. J Am Chem Soc. **1961**, *83*, 2457.

[42] M. P. Goren, R. K. Wright, M. E. Horowitz. Cumulative renal tubular damage associated with cisplatin nephrotoxicity. Cancer Chemother Pharmacol. **1986**, *18*, 69.

[43] S. Ishida, J. Lee, D. J. Thiele, I. Herskowitz. Uptake of the anticancer drug cisplatin mediated by the copper transporter Ctr1 in yeast and mammals. Proc Natl Acad Sci U S A. **2002**, *99*, 14298.

[44] X. Lin, T. Okuda, A. Holzer, S. B. Howell. The copper transporter CTR1 regulates cisplatin uptake in Saccharomyces cerevisiae. Mol Pharmacol. **2002**, *62*, 1154.

[45] P. A. Andrews, S. B. Howell. Cellular pharmacology of cisplatin: perspectives on mechanisms of acquired resistance. Cancer Cells. **1990**, *2*, 35.

[46] J. Reedijk. The relevance of hydrogen bonding in the mechanism of action of platinum antitumor compounds. Inorg Chim Acta. **1992**, *198-200*, 873.

[47] J. Reedijk. New clues for platinum antitumor chemistry: Kinetically controlled metal binding to DNA. Proc Natl Acad Sci U S A. **2003**, *100*, 3611.

[48] R. A. Alderden, M. D. Hall, T. W. Hambley. The discovery and development of cisplatin. Journal of Chemical Education. **2006**, *83*, 728.

[49] R. B. Martin. (Ed. Lippert B) **1999**, pp. 183–206 (Verlag Helvetica Chimica Acta: Zurich; Wiley-VCH: Weinheim, Germany: Zurich).

[50] J. Arpalahti. (Ed. Lippert B) **1999**, pp. 207–222 (Verlag Helvetica Chimica Acta: Zurich; Wiley-VCH: Weinheim, Germany).

[51] C. J. C. Legendre. F. (Ed. B L) **1999**, pp. 223–246 (Verlag Helvetica Chimica Acta: Zurich; Wiley-VCH: Weinheim, Germany).

[52] E. R. Jamieson, S. J. Lippard. Structure, recognition, and processing of cisplatin-DNA adducts. Chemical Reviews (Washington, D C). **1999**, *99*, 2467.

[53] T. W. Hambley. Platinum binding to DNA: structural controls and consequences. Journal of the Chemical Society, Dalton Transactions. **2001**, 2711.

[54] E. Reed, Y. Ostchega, S. M. Steinberg, S. H. Yuspa, R. C. Young, R. F. Ozols, et al. Evaluation of platinum-DNA adduct levels relative to known prognostic variables in a cohort of ovarian cancer patients. Cancer Res. **1990**, *50*, 2256.

[55] Y.-P. Ho, S. C. F. Au-Yeung, K. K. W. To. Platinum-based anticancer agents: innovative design strategies and biological perspectives. Med Res Rev. **2003**, *23*, 633.

[56] G. L. Cohen, J. A. Ledner, W. R. Bauer, H. M. Ushay, C. Caravana, S. J. Lippard. Sequence dependent binding of cis-dichlorodiammineplatinum(II) to DNA. Journal of the American Chemical Society. **1980**, *102*, 2487.

[57] Z. Guo, P. J. Sadler. Medicinal inorganic chemistry. Adv Inorg Chem. **2000**, *49*, 183.

[58] O. Tredan, C. M. Galmarini, K. Patel, I. F. Tannock. Drug resistance and the solid tumor microenvironment. J Natl Cancer Inst. **2007**, *99*, 1441.

[59] D. Hanahan, R. A. Weinberg. Hallmarks of cancer: the next generation. Cell (Cambridge, MA, U S). **2011**, *144*, 646.

[60] M. Egeblad, E. S. Nakasone, Z. Werb. Tumors as organs: Complex tissues that interface with the entire organism. Dev Cell. **2010**, *18*, 884.

[61] S. Aznavoorian, M. L. Stracke, H. Krutzsch, E. Schiffmann, L. A. Liotta. Signal transduction for chemotaxis and haptotaxis by matrix molecules in tumor cells. J Cell Biol. **1990**, *110*, 1427.

[62] A. I. Minchinton, I. F. Tannock. Drug penetration in solid tumours. Nat Rev Cancer. **2006**, *6*, 583.

[63] I. F. Tannock, D. Rotin. Acid pH in tumors and its potential for therapeutic exploitation. Cancer Res. **1989**, *49*, 4373.

[64] J. Zhou, T. Schmid, S. Schnitzer, B. Bruene. Tumor hypoxia and cancer progression. Cancer Lett (Amsterdam, Neth). **2006**, *237*, 10.

[65] J. L. Wike-Hooley, J. Haveman, H. S. Reinhold. The relevance of tumour pH to the treatment of malignant disease. Radiother Oncol. **1984**, *2*, 343.

[66] C. C. Caldwell, H. Kojima, D. Lukashev, J. Armstrong, M. Farber, S. G. Apasov, et al. Differential effects of physiologically relevant hypoxic conditions on T lymphocyte development and effector functions. J Immunol. **2001**, *167*, 6140.

[67] R. D. Braun, J. L. Lanzen, S. A. Snyder, M. W. Dewhirst. Comparison of tumor and normal tissue oxygen tension measurements using OxyLite or microelectrodes in rodents. Am J Physiol Heart Circ Physiol. **2001**, *280*, H2533.

[68] P. Vaupel, A. Mayer. Hypoxia in cancer: significance and impact on clinical outcome. Cancer Metastasis Rev. **2007**, *26*, 225.

[69] M. W. Dewhirst, Y. Cao, B. Moeller. Cycling hypoxia and free radicals regulate angiogenesis and radiotherapy response. Nat Rev Cancer. **2008**, *8*, 425.

[70] C. N. Coleman. Hypoxia in tumors: a paradigm for the approach to biochemical and physiologic heterogeneity. J Natl Cancer Inst. **1988**, *80*, 310.

[71] A. C. Sartorelli. Therapeutic attack of hypoxic cells of solid tumors: presidential address. Cancer Res. **1988**, *48*, 775.

[72] D. G. Hirst, J. Denekamp. Tumour cell proliferation in relation to the vasculature. Cell Tissue Kinet. **1979**, *12*, 31.

[73] J. M. Brown, A. J. Giaccia. The unique physiology of solid tumors: opportunities (and problems) for cancer therapy. Cancer Res. **1998**, *58*, 1408.

[74] N. S. Bryce, J. Z. Zhang, R. M. Whan, N. Yamamoto, T. W. Hambley. Accumulation of an anthraquinone and its platinum complexes in cancer cell spheroids: the effect of charge on drug distribution in solid tumour models. Chem Commun (Cambridge, U K). **2009**, 2673.

[75] W. R. Wilson, M. P. Hay. Targeting hypoxia in cancer therapy. Nat Rev Cancer. **2011**, *11*, 393.

[76] J. M. Brown, W. R. Wilson. Exploiting tumor hypoxia in cancer treatment. Nat Rev Cancer. **2004**, *4*, 437.

[77] C. R. Munteanu, K. Suntharalingam. Advances in cobalt complexes as anticancer agents. Dalton Trans. **2015**, *44*, 13796.

[78] B. G. Wouters, S. A. Weppler, M. Koritzinsky, W. Landuyt, S. Nuyts, J. Theys, et al. Hypoxia as a target for combined modality treatments. Eur J Cancer. **2002**, *38*, 240.

[79] P. Subarsky, R. P. Hill. The hypoxic tumour microenvironment and metastatic progression. Clin Exp Metastasis. **2003**, *20*, 237.

[80] P. Vaupel. Tumor microenvironmental physiology and its implications for radiation oncology. Semin Radiat Oncol. **2004**, *14*, 198.

[81] C. G. Wermuth, C. R. Ganellin, P. Lindberg, L. A. Mitscher. Glossary of terms used in medicinal chemistry (IUPAC recommendations 1998). Pure Appl Chem. **1998**, *70*, 1129.

[82] N. Graf, S. J. Lippard. Redox activation of metal-based prodrugs as a strategy for drug delivery. Adv Drug Delivery Rev. **2012**, *64*, 993.

[83] G. O. Ahn, K. J. Botting, A. V. Patterson, D. C. Ware, M. Tercel, W. R. Wilson. Radiolytic and cellular reduction of a novel hypoxia-activated cobalt(III) prodrug of a chloromethylbenzindoline DNA minor groove alkylator. Biochem Pharmacol. **2006**, *71*, 1683.

[84] Y. Chen, L. Hu. Design of anticancer prodrugs for reductive activation. Med Res Rev. **2009**, *29*, 29.

[85] W. A. Denny, W. R. Wilson, M. P. Hay. Recent developments in the design of bioreductive drugs. Br J Cancer, Suppl. **1996**, *74*, S32.

[86] A. V. Patterson, M. P. Saunders, E. C. Chinje, L. H. Patterson, I. J. Stratford. Enzymology of tirapazamine metabolism: a review. Anti-Cancer Drug Des. **1998**, *13*, 541.

[87] A. Gilman. The initial clinical trial of nitrogen mustard. Am J Surg. **1963**, *105*, 574.

[88] W. B. Mattes, J. A. Hartley, K. W. Kohn. DNA sequence selectivity of guanine-N7 alkylation by nitrogen mustards. Nucleic Acids Res. **1986**, *14*, 2971.

[89] D. C. Ware, P. J. Brothers, G. R. Clark, W. A. Denny, B. D. Palmer, W. R. Wilson. Synthesis, structures and hypoxia-selective cytotoxicity of cobalt(III) complexes containing tridentate amine and nitrogen mustard ligands. Dalton. **2000**, 925.

[90] D. C. Ware, W. R. Wilson, W. A. Denny, C. E. F. Richard. Design and synthesis of cobalt(III) nitrogen mustard complexes as hypoxia selective cytotoxins. The x-ray crystal structure of bis(3-chloropentane-2,4-dionato)(RS-N,N'-bis(2-chloroethyl)ethylenediamine)cobalt(III) perchlorate, [Co(Clacac)2(bce)]ClO4. J Chem Soc, Chem Commun. **1991**, 1171.

[91] B. A. Teicher, J. L. Jacobs, K. N. S. Cathcart, M. J. Abrams, J. F. Vollano, D. H. Picker. Some complexes of cobalt(III) and iron(III) are radiosensitizers of hypoxic EMT6 cells. Radiat Res. **1987**, *109*, 36.

[92] B. A. Teicher, M. J. Abrams, K. W. Rosbe, T. S. Herman. Cytotoxicity, radiosensitization, antitumor activity, and interaction with hyperthermia of a cobalt(III) mustard complex. Cancer Res. **1990**, *50*, 6971.

[93] D. C. Ware, B. G. Siim, K. G. Robinson, W. A. Denny, P. J. Brothers, G. R. Clark. Synthesis and characterization of aziridine complexes of cobalt(III) and chromium(III) designed as hypoxia-selective cytotoxins. X-ray crystal structure of trans-$[Co(Az)_4(NO_2)_2]Br{\cdot}2H_2O{\cdot}LiBr$. Inorg Chem. **1991**, *30*, 3750.

[94] D. C. Ware, B. D. Palmer, W. R. Wilson, W. A. Denny. Hypoxia-selective antitumor agents. 7. Metal complexes of aliphatic mustards as a new class of hypoxia-selective cytotoxins. Synthesis and evaluation of cobalt(III) complexes of bidentate mustards. J Med Chem. **1993**, *36*, 1839.

[95] D. C. Ware, W. A. Denny, G. R. Clark. [N,N-Bis(2-chloroethyl)-1,2-ethanediamine-N,N']bis(3-methyl-2,4-pentanedionato-O,O')cobalt(III) perchlorate: a potential hypoxia selective anticancer agent. Acta Crystallogr, Sect C: Cryst Struct Commun. **1997**, *C53*, 1058.

[96] D. C. Ware, H. R. Palmer, P. J. Brothers, C. E. F. Rickard, W. R. Wilson, W. A. Denny. Bis-tropolonato derivatives of cobalt(III) complexes of bidentate aliphatic nitrogen mustards as potential hypoxia-selective cytotoxins. J Inorg Biochem. **1997**, *68*, 215.

[97] P. R. Craig, P. J. Brothers, G. R. Clark, W. R. Wilson, W. A. Denny, D. C. Ware. Anionic carbonato and oxalato cobalt(III) nitrogen mustard complexes. Dalton Trans. **2004**, 611.

[98] B. R. Zetter. Angiogenesis and tumor metastasis. Annu Rev Med. **1998**, *49*, 407.

[99] T. W. Failes, C. Cullinane, C. I. Diakos, N. Yamamoto, J. G. Lyons, T. W. Hambley. Studies of a cobalt(III) complex of the MMP inhibitor marimastat: a potential hypoxia-activated prodrug. Chem - Eur J. **2007**, *13*, 2974.

[100] K. Nabeshima, T. Inoue, Y. Shimao, T. Sameshima. Matrix metalloproteinases in tumor invasion: role for cell migration. Pathol Int. **2002**, *52*, 255.

[101] L. M. Coussens, B. Fingleton, L. M. Matrisian. Cancer therapy: matrix metalloproteinase inhibitors and cancer: trials and tribulations. Science (Washington, DC, U S). **2002**, *295*, 2387.

[102] S. R. Bramhall, M. T. Hallissey, J. Whiting, J. Scholefield, G. Tierney, R. C. Stuart, et al. Marimastat as maintenance therapy for patients with advanced gastric cancer: a randomised trial. Br J Cancer. **2002**, *86*, 1864.

[103] T. W. Failes, T. W. Hambley. Models of hypoxia activated prodrugs: Co(III) complexes of hydroxamic acids. Dalton Trans. **2006**, 1895.

[104] P. D. Bonnitcha, B. J. Kim, R. K. Hocking, J. K. Clegg, P. Turner, S. M. Neville, et al. Cobalt complexes with tripodal ligands: implications for the design of drug chaperones. Dalton Trans. **2012**, *41*, 11293.

[105] G. O. Ahn, D. C. Ware, W. A. Denny, W. R. Wilson. Optimization of the auxiliary ligand shell of cobalt(III)(8-hydroxyquinoline) complexes as model hypoxia-selective radiation-activated prodrugs. Radiat Res. **2004**, *162*, 315.

[106] J. Y.-C. Chang, R. J. Stevenson, G.-L. Lu, P. J. Brothers, G. R. Clark, W. A. Denny, et al. Syntheses of 8-quinolinolatocobalt(III) complexes containing cyclen based auxiliary ligands as models for hypoxia-activated prodrugs. Dalton Trans. **2010**, *39*, 11535.

[107] J. B. J. Milbank, R. J. Stevenson, D. C. Ware, J. Y. C. Chang, M. Tercel, G. O. Ahn, et al. Synthesis and Evaluation of Stable Bidentate Transition Metal Complexes of 1-(Chloromethyl)-5-hydroxy-3-(5,6,7-trimethoxyindol-2-ylcarbonyl)-2,3-dihydro-1H-pyrrolo[3,2-f]quinoline (seco-6-azaCBI-TMI) as Hypoxia Selective Cytotoxins. J Med Chem. **2009**, *52*, 6822.

[108] G.-L. Lu, R. J. Stevenson, J. Y.-C. Chang, P. J. Brothers, D. C. Ware, W. R. Wilson, et al. N-alkylated cyclen cobalt(III) complexes of 1-(chloromethyl)-3-(5,6,7-trimethoxyindol-2-ylcarbonyl)-2,3-dihydro-1H-pyrrolo[3,2-f]quinolin-5-ol DNA alkylating agent as hypoxia-activated prodrugs. Bioorg Med Chem. **2011**, *19*, 4861.

[109] J. Y.-C. Chang, G.-L. Lu, R. J. Stevenson, P. J. Brothers, G. R. Clark, K. J. Botting, et al. Cross-Bridged Cyclen or Cyclam Co(III) Complexes Containing Cytotoxic Ligands as Hypoxia-Activated Prodrugs. Inorg Chem. **2013**, *52*, 7688.

[110] N. Cenas, Z. Anusevicius, D. Bironaite, G. I. Bachmanova, A. I. Archakov, K. Oelinger. The electron transfer reactions of NADPH:cytochrome P450 reductase with nonphysiological oxidants. Arch Biochem Biophys. **1994**, *315*, 400.

[111] S. Riedl, D. Zweytick, K. Lohner. Membrane-active host defense peptides - Challenges and perspectives for the development of novel anticancer drugs. Chemistry and Physics of Lipids. **2011**, *164*, 766.

[112] J. M. Brown. The hypoxic cell: a target for selective cancer therapy--eighteenth Bruce F. Cain Memorial Award lecture. Cancer research. **1999**, *59*, 5863.

[113] D. J. Hodgson, K. Michelsen, E. Pedersen, D. K. Towle. Novel tetranuclear mixed-metal complexes containing the heteronuclear ions $[M(II)[(OH)_2CrA_4]_3]^{5+}$ and $[M(II)[(OH)_2CoA_4]_3]^{5+}$ (A = amine ligand). J Chem Soc, Chem Commun. **1988**, 426.

[114] U. Thewalt, S. Mueller. Copper(2+), palladium(2+) and platinum(2+) complexes with $[(en)_2Co(OH)_2]^+$ ligands. Z Naturforsch, B: Chem Sci. **1989**, *44*, 1206.

[115] U. Thewalt, S. Mueller. Polynuclear mixed-metal complexes. Preparation and structure of $[MnIII((OH)_2CoIII(en)_2)_3](ClO_4)_4Cl_2{\cdot}4H_2O$. Chem Ber. **1988**, *121*, 2111.

[116] S. Mueller, U. Thewalt. Polynuclear mixed-metal complexes. Preparation and structures of complexes with the cations $[M(II)\{(OH)_2Co(III)(en)_2\}_3]^{5+}$, M = nickel, zinc, magnesium. Z Naturforsch, B: Chem Sci. **1989**, *44*, 257.

[117] S. M. Joergensen. To the constitution of the cobalt, chrome and Rhodium bases: Report X. Anhydro basic Tetramine diaquodiamine cobalt salt. [machine translation]. Z anorg Ch. **1898**, *16*, 184.

[118] A. Werner. Poly-nucleated Metal-amines. Ber Dtsch Chem Ges. **1907**, *40*, 2103.

[119] W. G. Jackson, J. A. McKeon, M. Zehnder, M. Neuberger, S. Fallab. The rediscovery of Alfred Werner's second hexol. Chem Commun (Cambridge, U K). **2004**, 2322.

[120] A. Werner, a. et. Polynuclear Metal-Ammonias. X. Justus Liebigs Ann Chem. **1910**, *375*, 1.

[121] U. Thewalt, S. Mueller. Copper(2+), palladium(2+) and platinum(2+) complexes with [(en)2Co(OH)2]+ ligands. Zeitschrift fuer Naturforschung, B: Chemical Sciences. **1989**, *44*, 1206.

[122] W. Kruse, H. Taube. Exchange and isomerization rates of complex ions of the aquobis(ethylenediamine)cobalt(III) series. J Am Chem Soc. **1961**, *83*, 1280.

[123] D. A. Buckingham, C. R. Clark, G. M. Miskelly. The anation by oxalate and isomerization of cis- and trans-$[Co(en)_2(OH_2)OH]_2$. Inorganic chemistry. **2000**, *39*, 6139.

[124] W. G. Jackson. Secondary Deuterium Kinetic Isotope Effect for Aquation, Solvolysis, and Isomerization Reactions of trans-$[Co(en)_2(OSMe_2)N_3]^{2+}$, and the Resolution of a Mechanistic Anomaly. Inorg Chem. **2004**, *43*, 2577.

[125] J. L. Butour, J. P. Macquet. Differentiation of DNA.platinum complexes by fluorescence. The use of an intercalating dye as a probe. Eur J Biochem. **1977**, *78*, 455.

[126] A. Hazell, J. Jepsen. (Carbonato-O,O')bis(1,2-ethanediamine-N,N')cobalt(III) nitrate monohydrate. Acta Crystallogr, Sect E: Struct Rep Online. **2001**, *57*, m239.

[127] J. P. Falkenhagen, C. Limberg, S. Demeshko, S. Horn, M. Haumann, B. Braun, et al. Iron-molybdenum-oxo complexes as initiators for olefin autoxidation with O2. Dalton Trans. **2014**, *43*, 806.

[128] C.-C. Wang, C. Yin. Crystal structure of catena-(trans-bis(1-(4-pyridyl)-2-(4-pyridinio)ethylene)dodecaoxocyclotetravanadato(V)cobalt(II)), $Co(C_{12}H_{11})2(V_4O_{12})$. Z Kristallogr - New Cryst Struct. **2008**, *223*, 13.

[129] A. Khutia, P. J. S. Miguel, B. Lippert. Influence of PtII and PdII coordination on the equilibrium of 2,2'-dipyridylketone (dpk) with its hydrated gem-diol form (dpk·H_2O). Inorg Chim Acta. **2010**, *363*, 3048.

[130] H. G. Visser, J. K. Clegg. Bis(tetraphenylarsonium) di-μ-hydroxido-bis[(nitrilotriacetato)cobalt(III)] octahydrate. Acta Crystallogr, Sect E: Struct Rep Online. **2010**, *66*, m1401.

[131] M. Mori, M. Shibata, E. Kyuno, Y. Okubo. Synthesis of metal complexes. IV. Cobalt(III) complexes of nitrilotriacetic acid. Bull Chem Soc Jpn. **1958**, *31*, 940.

[132] H. G. Visser, W. Purcell, S. S. Basson, Q. Claassen. The syntheses and crystal structures of $Cs_2[Co_2(nta)_2(\mu\text{-}OH)_2]\cdot 4H_2O$ and $(C_{10}H_{10}N_3)_2[CoCl_4]$. Polyhedron. **1997**, *16*, 2851.

[133] Z.-M. Dai, Z. Shi, G.-H. Li, W.-S. Fu, W. Xu, S.-H. Feng. Hydrothermal syntheses, crystal structures and magnetic properties of Na[M(nta)].H_2O (M = Co, Ni; nta = nitrilotriacetate). Gaodeng Xuexiao Huaxue Xuebao. **2003**, *24*, 1950.

[134] Q.-Z. Zhang, C.-Z. Lu, W.-B. Yang. Synthesis and structures of two cobalt complexes [NaCoII(NTA)(H_2O)]n and NH_4[CoIII($IDA)_2$]·$2H_2O$. J Coord Chem. **2006**, *59*, 837.

[135] M.-L. Hu, J.-J. Lin, Q. Miao, Y. Xiong. A nitrilotriacetate bridged heteronuclear Co(II)-Na(I) polymer: {[CoNa(NTA)($H_2O)_3$]·$2H_2O$}n. Chin J Chem. **2002**, *20*, 235.

[136] I. N. Polyakova, A. L. Poznyak, O. A. Egorova. Crystal structure of monoprotonated cobalt(II) nitrilotriacetate tetrahydrate Co(HNta).$4H_2O$. Russ J Coord Chem. **2001**, *27*, 852.

[137] L. P. Battaglia, A. Corradi Bonamartini, M. E. Vidoni Tani. Crystal and molecular structure of potassium monoaquamono(nitrilotriacetato)cobaltate(II) dihydrate (K[Co($C_6H_6NO_6$) (OH_2)].$2H_2O$). Acta Crystallogr, Sect B. **1975**, *B31*, 1160.

[138] H. C. Fry, C. Deal, E. Barr, S. D. Cummings. Photoactivation of dichloro(ethylenediamine)platinum(II). J Photochem Photobiol, A. **2002**, *150*, 37.

[139] R. Handerson. in *The mechanisms of reactions at transition metal sites* **1993**, pp. 16 (Oxford University Press).

[140] C. J. L. Lock, R. A. Speranzini, G. Turner, J. Powell. Molecular structure of μ-(9-methyladenine-N1,N7)-bis(di-isopropyl sulfoxide-S)-trans-dichloroplatinum(II). J Am Chem Soc. **1976**, *98*, 7865.

[141] R. Handeson. in *The mechanisms of reactions at transition metak sites* **1993**, pp. 26 (Oxford University Press).

[142] S. Kaenket, P. Phuengphai, C. Pakawatchai, S. Youngme. Poly[tris(μ-4,4'-bipyridine-κ2N:N')bis(dimethyl sulfoxide-κO)tetrakis(thiocyanato-κN)dicobalt(II)]. Acta Crystallogr, Sect E: Struct Rep Online. **2014**, *70*, m265.

[143] E. Viola, M. P. Donzello, S. Ciattini, G. Portalone, C. Ercolani. Redox Chemistry of Tetrakis[5,6-di(2-pyridyl)-2,3-pyrazino]porphyrazinatocobalt(II): Isolation and Characterization of Solid Pure CoI, CoII, and CoIII Complexes. Eur J Inorg Chem. **2009**, 1600.

[144] S. O. H. Gutschke, D. I. Price, A. K. Powell, P. T. Wood. Solvothermal synthesis of the canted antiferromagnet [K_2[$CoO_3PCH_2N(CH_2CO_2)_2$]]6.xH_2O. Angew Chem, Int Ed. **1999**, *38*, 1088.

[145] J.-G. Mao, A. Clearfield. Metal Carboxylate-Phosphonate Hybrid Layered Compounds: Synthesis and Single Crystal Structures of Novel Divalent Metal Complexes with N-(Phosphonomethyl)iminodiacetic Acid. Inorg Chem. **2002**, *41*, 2319.

[146] Y. Fan, G. Li, W. Jian, M. Yu, L. Wang, Z. Tian, et al. Solvothermal synthesis, crystal structure, magnetic and luminescent properties of ($H_3O)_6$·[$Co_4(H_2O)_4$($HPMIDA)_2$($PMIDA)_2$]·$2H_2O$. J Solid State Chem. **2005**, *178*, 2267.

[147] F.-N. Shi, F. A. Almeida Paz, P. I. Girginova, L. Mafra, V. S. Amaral, J. Rocha, et al. Hydrothermal synthesis, structural characterisation and magnetic behaviour of hybrid complexes of N-(phosphonomethyl)iminodiacetate. J Mol Struct. **2005**, *754*, 51.

[148] Z.-G. Gu, S. C. Sevov. Syntheses, structures, and magnetic properties of heterometallic coordination polymers with carboxyphosphonate linkers. J Mater Chem. **2009**, *19*, 8442.

[149] Z.-G. Gu, S. C. Sevov. Isolated Co15 Clusters and Their Assembly into a 3D Network: Conformation-Directed Synthesis. Inorg Chem. **2009**, *48*, 8066.

[150] M. McClure. Synthesis and symmetry of two cobalt (III) complexes with tetradentate ligands. An advanced inorganic chemistry experiment. J Chem Educ. **2008**, *85*, 420.

[151] C. B. Storm, P. Ellsworth. cis-β-Hydroxyaquo(triethylenetetramine)cobalt(III) perchlorate. Biochem Prep. **1971**, *13*, 59.

[152] R. R. Holmes. Organotin cluster chemistry. Accounts of Chemical Research. **1989**, *22*, 190.

[153] Q. Li, F. Wang, R. Zhang, J. Cui, C. Ma. Syntheses and characterization of organostannoxanes derived from 2-chloroisonicotinic acid: Tetranuclear and hexanuclear. Polyhedron. **2015**, *85*, 361.

[154] T. J. Boyle, T. M. Alam, M. A. Rodriguez, C. A. Zechmann. Hydrolysis of Tin(II) Neo-pentoxide: Syntheses, Characterization, and X-ray Structures of $[Sn(ONep)_2]_\infty$, $Sn_5(\mu_3\text{-}O)_2(\mu\text{-}ONep)_6$, and $Sn_6(\mu_3\text{-}O)_4(\mu\text{-}ONep)_4$ Where ONep = OCH_2CMe_3. Inorganic Chemistry. **2002**, *41*, 2574.

[155] R. R. Holmes, K. C. K. Swamy, C. G. Schmid, R. O. Day. Organotin clusters. 4. Cubic, butterfly, and oxygen-capped clusters of n-butyloxotin phosphinates. A new class of organotin compounds. Journal of the American Chemical Society. **1988**, *110*, 7060.

[156] G. Prabusankar, R. Murugavel. Hexameric Organotincarboxylates with Cyclic and Drum Structures. Organometallics. **2004**, *23*, 5644.

[157] V. Chandrasekhar, S. Nagendran, V. Baskar. Organotin assemblies containing Sn-O bonds. Coord Chem Rev. **2002**, *235*, 1.

[158] X. Shang, X. Meng, E. C. B. A. Alegria, Q. Li, M. F. C. Guedes da Silva, M. L. Kuznetsov, et al. Syntheses, Molecular Structures, Electrochemical Behavior, Theoretical Study, and Antitumor Activities of Organotin(IV) Complexes Containing 1-(4-Chlorophenyl)-1-cyclopentanecarboxylato Ligands. Inorganic Chemistry. **2011**, *50*, 8158.

[159] M. Sirajuddin, S. Ali, V. McKee, M. Sohail, H. Pasha. Potentially bioactive organotin(IV) compounds: Synthesis, characterization, in vitro bioactivities and interaction with SS-DNA. Eur J Med Chem. **2014**, *84*, 343.

[160] D. B. Shpakovsky, C. N. Banti, E. M. Mukhatova, Y. A. Gracheva, V. P. Osipova, N. T. Berberova, et al. Synthesis, antiradical activity and in vitro cytotoxicity of novel organotin

complexes based on 2,6-di-tert-butyl-4-mercaptophenol. Dalton Transactions. **2014**, *43*, 6880.

[161] M. Nath, P. K. Saini. Chemistry and applications of organotin(iv) complexes of Schiff bases. Dalton Trans. **2011**, *40*, 7077.

[162] L. Y. Kuo, M. G. Kanatzidis, M. Sabat, A. L. Tipton, T. J. Marks. Metallocene antitumor agents. Solution and solid-state molybdenocene coordination chemistry of DNA constituents. Journal of the American Chemical Society. **1991**, *113*, 9027.

[163] A. Alama, B. Tasso, F. Novelli, F. Sparatore. Organometallic compounds in oncology: implications of novel organotins as antitumor agents. Drug Discovery Today. **2009**, *14*, 500.

[164] M. Gielen. Organotin compounds and their therapeutic potential: a report from the organometallic chemistry department of the Free University of Brussels. Appl Organomet Chem. **2002**, *16*, 481.

[165] L. Ghys, M. Biesemans, M. Gielen, A. Garoufis, N. Hadjiliadis, R. Willem, et al. Multinuclear 1D and 2D NMR investigations on the interaction between the pyrimidic nucleotides 5'-CMP, 5'-dCMP, and 5'-UMP and diethyltin dichloride in aqueous medium. Eur J Inorg Chem. **2000**, 513.

[166] M. Gielen. Tin-based antitumor drugs. Coord Chem Rev. **1996**, *151*, 41.

[167] M. Gielen. An overview of forty years organotin chemistry developed at the Free Universities of Brussels ULB and VUB. J Braz Chem Soc. **2003**, *14*, 870.

[168] M. Gielen. *Metallotherapeutic Drugs and Metal–based Diagnostic Agents. The Use of Metals in Medicine* **2005** (J Wiley & Sons,).

[169] M. Ashfaq. Synthesis of novel bioactive phthalimido-4-methyl pentanoateorganotin(IV) esters with spectroscopic investigation. Journal of Organometallic Chemistry. **2006**, *691*, 1803.

[170] M. Parvez, S. Ali, M. Mazhar, M. H. Bhatti, M. A. Choudhary. (N-Maleoylmethioninato)trimethyltin(IV). Acta Crystallogr, Sect C: Cryst Struct Commun. **1999**, *C55*, 1429.

[171] S. K. Hadjikakou, N. Hadjiliadis. Antiproliferative and anti-tumor activity of organotin compounds. Coordination Chemistry Reviews. **2009**, *253*, 235.

[172] A. K. Saxena, F. Huber. Organotin compounds and cancer chemotherapy. Coordination Chemistry Reviews. **1989**, *95*, 109.

[173] S. Tabassum, C. Pettinari. Chemical and biotechnological developments in organotin cancer chemotherapy. Journal of Organometallic Chemistry. **2006**, *691*, 1761.

[174] C. Pellerito, P. D'Agati, T. Fiore, C. Mansueto, V. Mansueto, G. Stocco, et al. Synthesis, structural investigations on organotin(IV) chlorin-e6 complexes, their effect on sea urchin embryonic development and induced apoptosis. Journal of Inorganic Biochemistry. **2005**, *99*, 1294.

[175] M. F. Powers, A. D. Beavis. Triorganotins inhibit the mitochondrial inner membrane anion channel. Journal of Biological Chemistry. **1991**, *266*, 17250.

[176] Y. Yamabe, A. Hoshino, N. Imura, T. Suzuki, S. Himeno. Enhancement of Androgen-Dependent Transcription and Cell Proliferation by Tributyltin and Triphenyltin in Human Prostate Cancer Cells. Toxicology and Applied Pharmacology. **2000**, *169*, 177.

[177] A. Gennari, B. Viviani, C. L. Galli, M. Marinovich, R. Pieters, E. Corsini. Organotins Induce Apoptosis by Disturbance of [Ca^{2+}] and Mitochondrial Activity, Causing Oxidative Stress and Activation of Caspases in Rat Thymocytes. Toxicology and Applied Pharmacology. **2000**, *169*, 185.

[178] B. E. K. Barth, K. Harms, S. Dehnen. Attachment of Chelating Ligand Pockets to Tinorganyl Moieties. Eur J Inorg Chem. **2014**, *2014*, 2406.

[179] A. Sousa-Pedrares, M. I. Casanova, J. A. Garcia-Vazquez, M. L. Duran, J. Romero, A. Sousa, et al. Synthesis and X-ray structures of tin(IV) and lead(II) complexes with heterocyclic thiones. Eur J Inorg Chem. **2003**, 678.

[180] A. W. U.S. Schubert, G.R. Newkome,. in *Optoelectronic and Life Science Applications* **2011,** (WILEY-VCH Verlag GmbH & Co. KGaA: Weinheim).

[181] G. Kaur. Structure and reactivity of dinuclear and polynuclear metal complexes. PhD Thesis, University of Canterbury, Christchurch, New Zealand. **2014**.

[182] A. Ramirez-Jimenez, E. Gomez, S. Hernandez. Penta- and heptacoordinated tin(IV) compounds derived from pyridine Schiff bases and 2-pyridine carboxylate: Synthesis and structural characterization. J Organomet Chem. **2009**, *694*, 2965.

[183] T. P. Lockhart, W. F. Manders, J. J. Zuckerman. Structural investigations by solid-state carbon-13 NMR. Dependence of $|^{1}J(^{119}Sn,^{13}C)|$ on the methyl-tin-methyl angle in methyltin(IV)s. J Am Chem Soc. **1985**, *107*, 4546.

[184] J. Springbørg, C. E. Schäffer, J. M. Preston, B. Douglas. in *Inorganic Syntheses* **2007**, pp. 63-77 (John Wiley & Sons, Inc.).

[185] E. Kimura, S. Young, J. P. Collman. Cleavage of amino acid esters and peptides with hydroxoaquo(2,2',2''-triaminotriethylamine)cobalt(III) ion. Inorg Chem. **1970**, *9*, 1183.

[186] M. D. Zivkovic, D. P. Asanin, S. Rajkovic, M. I. Djuran. Hydrolysis of the amide bond in N-acetylated L-methionylglycine catalyzed by various platinum(II) complexes under physiologically relevant conditions. Polyhedron. **2011**, *30*, 947.

[187] S. C. Dkhara. Rapid method for the synthesis of cis[$Pt(NH_3)_2Cl_2$]. Indian J Chem. **1970**, *8*, 193.